

Novel Calcium Complexes Applied to Intramolecular Hydroamination Catalysis

by
James S. Wixey MChem (Hons.)



Thesis submitted to the University of Cardiff, Wales,
for the degree of Doctor of Philosophy, July 2012.

Abstract

This Thesis discusses the synthesis, characterisation, and reactivity studies of a range of new chiral calcium complexes supported by various polydentate N-donor ligands and their suitability as catalysts for intramolecular hydroamination.

Chapter One outlines the case for developing organocalcium complexes, including a general overview of their current application to a variety of heterofunctionalisation reactions.

Chapter Two introduces the chiral ethylene diamines which are extensively used as calcium supporting ligands and later as precursors for the synthesis of bisimidazoline and potential imoxazoline ligands. Chapter Two provides details of the diamine synthesis and includes studies related to racemisation concerns of the chiral centre.

Chapter Three discusses novel calcium complexes supported by the chiral ethylene diamine analogues presented in Chapter Two. Complex synthesis, characterisation, and catalytic performance in intramolecular hydroamination is probed and discussed.

Chapter Four details a range of new bisimidazoline ligands and their employment as supporting ligands on calcium. The catalytic performance of the resulting complexes in intramolecular hydroamination is subsequently analysed and discussed.

Chapter Five investigates the attempted development of a total synthetic pathway to a new class of imoxazoline ligand and related issues.

Chapter Six contains all experimental procedures, characterising data pertaining to all new compounds and complexes presented in this Thesis.

Appendices A-K contain additional catalytic figures and tables of crystallographic data for all new crystallographically characterised compounds. Summary sheets of every literature and new compound presented mentioned in this Thesis are also included, along with copies of both printed publications resulting from this Thesis at the time of submission.

Acknowledgements

Firstly I must express my deepest gratitude to my supervisor Dr. Benjamin Ward. I will never forget the first time I stepped into your office to discuss a PhD position within your group nor shall I forget your boundless help, advice, and optimism, which truly are virtues that I greatly admire and look up to.

I would like to thank the Ward group members both past and present. The last few years working with and alongside each of you in the laboratory has left me with many fond memories. In no particular order: Stacey Bennett for your help and kindness with so many aspects during my studies. Tom O'Brien for your humour and excellent company, which was especially welcomed on the many occasions when working late. I must also thank Angelica Orsi, Fred Seeley, David Collis, Kate Smith, Matt Craig, Matt O'Brien, Scott Board and Victoria Hallhead for all your individual contributions when assisting me on the challenging synthetic side of my work. To Dr. Andy Hallett and Dr. Tracy Nixon, thank you both for your time and advice.

I would not have made it through the past three years without the support and friendship of Wei Ye Lu, Steven Robert Hughes, Benjamin Palmer, Andreas Schneeman, Daniel Russell, Dominic Caswell, Chris Mackay, Wilson Fung, Joanna Ha, Iris Cheung, Diane Chung and Mark Stevenson. I am especially grateful to Kim MacPhee, for her endless encouragement.

Throughout my doctoral studies I have had the pleasure of knowing Dr. Sanka Meenakshisundaram, Dr. Yulia Rogan, Dr. Barry Dean, Dr. Tanya Kotionova and Piotr Rutkowski. I have very much enjoyed the time spent with you all, although this group would not be complete without mention of Ewa Nowicka; of whom I am thankful for the many discussions on the delights of the continent with.

Particular thanks must go to Dr. Robert Jenkins for his help, patience, and advice related to the NMR spectroscopy that constitutes such a large proportion of this Thesis. I would also like to convey my appreciation to Dr. Benson Kariuki for assistance in obtaining the crystallographic data presented in this Thesis. I extend my thanks to Robin Hicks and Dave Walker for their sterling work with respect to the Mass Spectrometry analysis that accompanies this Thesis. I am also ever appreciative of Ricky Fearn's glassblowing expertise that without many of my experiments would not have been possible.

To Dr. Huw Tallis, Dr. Angelo Amoroso, Dr. James Knight, Dr. Paul Newman, Dr. Ian Morgan, Dr. Tom Tatchell and Dr. Anthony Thompson; I am indebted to each of you for the time you spent with me discussing my work, my frustrations, or my future aspirations.

The ladies and gentlemen of the Chemical Stores, Technical Services and Administrative Staff: Gary Coleman, Jamie Cross, Sham Ali, John Cavanagh, Alun Davies, Steven Morris, Terrie Dumelow, Matthew James and Alison Rowlands; It has been a pleasure to know you all during my post-graduate years at Cardiff and I am ever thankful to each of you for the help and backing you have given me during this time.

I would especially like to say to Malcolm Bryant that it has been an enjoyment to work with you and to have known you during the last three years. I am in your debt for the support you have rendered.

I never anticipated taking on a part time job during my final year of research, however the year I spent working at the Barocco Bar in Cardiff's Highstreet will not easily be forgotten. The hard work, the good times, nor the friends I made; Caroline Venter, Carl Rowlands, Gareth Rees, Vanessa Brown, James Moinet, Arnaud Ritter, Rhys Littlejohns, Josh Windsor, Chris Mcilquham, Vikki Paskell, Sam Spierling, Gemma Dick, Jess Magness, Tori Cowley, Dan Busby and Yusef Canning.

Finally I wish to thank my family, Mum and Dad, Andy, Lind, and Catherine for your unwavering support. You have all offered your help to me over the many years, which has not gone amiss.

I am grateful to the EPSRC and Leverhulme Trust for providing the funding which allowed me to accomplish the work described within this Thesis.

Thank you all.

Abbreviations

General

Å	Angstrom
Ac	acetate group, [CH ₃ COO] ⁻
acac	acetylacetonate
AE	Alkaline Earth
Ar	aryl
BBL	β-butyrolactone
BINOL	1,1'-bi-2-naphthol
BDI	β-diketimidato
Boc	<i>tert</i> -butyloxycarbonyl
BOX	bisoxazoline
^t Bu	<i>tert</i> -butyl
°C	degrees Celsius
<i>ca.</i>	<i>circa</i> , about
cf.	compared with
ε-CL	ε-caprolactone
COD	cyclooctadiene
Cp*	cyclopentadiene anion
d	day(s)
DIPEA	diisopropylethylamine
DMAP	N,N-dimethylaminopyridine
DMAT	2-N(CH ₃) ₂ -α-Si(CH ₃) ₃ -CH(C ₆ H ₅)
DME	1,2-dimethoxyethane
DPE	1,1-diphenylethylene
Dpp	diphenylphosphinyl group
e.e	enantiomeric excess
E.I.	Electron Impact
Et	ethyl
g	gram
h	hour(s)
HBCat	Catecholborane, (1,3,2-Benzodioxaborole)

HBPin	pinacolborane, (4,4,5,5-tetramethyl-1,3,2-dioxaborolane)
HMDS	hexamethyldisilazane, $[\text{N}(\text{Si}(\text{Me}_3)_2)]^-$
HMPA	Hexamethylphosphoramide, $(\text{Me}_3\text{N})_3\text{PO}$
HNN ^R	ethylene 1,2-diamine
iBCF	<i>iso</i> -butylchloroformate
IMOX	imoxazoline
<i>ipso</i> -	<i>ipso</i> substituted
L ₂	mono-anionic supporting ligand
LA	lactide
Ln	lanthanide
M	metal atom
<i>m</i> -	<i>meta</i> substituted
Me	methyl
MS	Mass Spectrometry
min	minute(s)
NMM	N-methylmorpholine
<i>o</i> -	<i>ortho</i> substituted
OTf	triflate group, $[\text{CF}_3\text{SO}_3]^-$
<i>p</i> -	<i>para</i> substituted
PDI	Polymer Dispercity Indices
Ph	phenyl
Pht	phthalic anhydride moiety
PPN ⁺	μ -nitrido-bis(triphenylphosphine) ¹⁺
ⁱ Pr	<i>iso</i> -propyl
py	pyridine
py-Box	pyridinebisoxazoline
<i>R</i>	rectus enantiomer
<i>R</i>	alkyl or aryl group
R-BIM	bisimidazoline
R-MIM	mono-imidazoline imoxazoline precursor
ROP	Ring-Opening Polymerisation
<i>S</i>	sinister enantiomer
sec	second(s)

ST	styrene
TBTU	<i>O</i> -(benzotriazol-1-yl)- <i>N,N,N',N'</i> -tetramethyluronium tetrafluoroborate
^t Bu	<i>tert</i> -Butyl
TFPB	tetrakis(3,5-bis(trifluoromethyl)phenyl)borate
THF	tetrahydrofuran
TMC	trimethylenecarbonate
TMS	trimethylsilane
Tpm	HC(3,5-dimethylpyrazole) ₃
Ts	tosyl group, (CH ₃ C ₆ H ₄ SO ₂)
<i>vs.</i>	Versus
<i>Viz.</i>	<i>videlicet</i> , that is to say
X ¹	mono-anionic σ-bound substituent

Nuclear Magnetic Resonance Spectroscopic Data

app.	apparent
br.	broad
¹³ C- ¹ H}	proton-decoupled ¹³ C
COSY	Correlation SpectroscopY
d	doublet
δ	chemical shift in ppm
J	coupling constant
HMBC	Heteronuclear Multiple Bond Connectivity
HSQC	Heteronuclear Multiple Quantum Coherence
Hz	Hertz
m	multiplet
MHz	Megahertz
NMR	Nuclear Magnetic Resonance
nOe	nuclear Overhauser effect
ppm	parts per million
q	quartet
quin.	quintet

s	singlet
sept.	septet
t	triplet

Infrared Spectroscopic Data

br	broad
cm ⁻¹	wave number
IR	Infrared
m	medium
v	frequency
s	strong
w	weak

Notes about numbering of literature compounds described in this Thesis

Literature compounds described in this Thesis are sequentially numbered **1.X**, **2.X**, **3.X**, **4.X**, and **5.X**, according to the Chapter in which they are first presented. The new compounds expressed in this Thesis are numbered **1-16**.

Contents

Chapter One – Organocalcium Catalysis

1.1	The Case for Calcium	2
1.1.1	Taming Calcium	4
1.2	Calcium in Catalysis	5
1.2.1	Hydroamination	6
1.2.1.1	Intermolecular Hydroamination	13
1.2.1.2	Asymmetric Hydroamination of Alkenes	16
1.2.1.3	Intermolecular Hydroamination of Isocyanates and Carbodiimides	21
1.2.2	Hydrosilylation	26
1.2.2.1	Asymmetric Hydrosilylation of Alkenes	32
1.2.3	Hydrophosphination	33
1.2.3.1	Hydrophosphination of Carbodiimides	38
1.2.4	Hydrogenation	41
1.2.5	Hydroboration of Alkenes	43
1.3	References	47

Chapter Two – Chiral Ethylene Diamine Synthesis

2.1	Introduction	54
2.2	Route One – Acid Anhydride Intermediate	57
2.2.1	Amino Acid Protection	57
2.2.2	Amidation of <i>N</i> -phthaloyl valine via an Acid Anhydride Route	58
2.3	Route Two – Aziridine Intermediate	60
2.3.1	Catalysed Aziridine Ring-Opening	61
2.4	Route Three – Acid Chloride Intermediate	62
2.4.1	Amidation via an Acid Chloride	64
2.4.2	Removal of Phthalamide Protecting Group	66
2.4.3	Amide Reduction	68

2.5	Racemisation of the Chiral Centre	72
2.6	References	77

Chapter Three – Calcium Complexes Supported by Diamine Ligands

3.1	Introduction	80
3.2	Preparation of Calcium Complexes Supported by Diamine Ligands	82
3.3	Spectroscopic Characterisation	83
3.4	DFT	88
3.5	Intramolecular Hydroamination Catalysis	90
	3.5.1 Catalytic Performance and Enantioselectivity	94
3.6	References	100

Chapter Four – Chiral Bisimidazoline Supported Calcium Complexes

4.1	Introduction	103
4.2	Ligand Synthesis and Characterisation	108
	4.2.1 Ligand Bridge Component	109
	4.2.2 Structural Tautomers and Evidence of Diastereoisomerism	112
4.3	Chiral Calcium Complexes Supported by Bisimidazolines	113
	4.3.1 Complex Synthesis	113
	4.3.2 Complex Characterisation	115
4.4	Complex Redistribution	118
4.5	DFT	124
4.6	Catalytic Performance	126
	4.6.1 Enantiomeric Excess Determination	127
	4.6.2 Kinetics of Catalysis	127
	4.6.3 Catalyst Performance Analysis	130
4.7	References	136

Chapter Five – A Potential New Class of Ligand - Imoxazolines

5.1	Introduction	140
5.2	Ligand Precursor Synthesis and Characterisation	141
5.2.1	Ethyl 2-Cyanoacetimidate Hydrochloride Synthesis	142
5.2.2	Mono-imidazoline IMOX Precursors	145
5.2.2.1	R-MIM Molecular Structures	147
5.3	Attempted IMOX Ligand Synthesis	151
5.4	References	155

Chapter Six – Experimental and Characterisation Data

6.1	General Methods and Instrumentation	157
6.2	Experimental and Characterising Data for Chapter Two	158
6.3	Experimental and Characterising Data for Chapter Three	174
6.4	Experimental and Characterising Data for Chapter Four	183
6.5	Experimental and Characterising Data for Chapter Five	209
6.6	References	216

Appendices

A.	Product Conversion Curves for Chapter Three	218
B.	Product Conversion Curves for Chapter Four	224
C.	X-ray Structure Analysis of [1]	232
D.	X-ray Structure Analysis of [13a]	235
E.	X-ray Structure Analysis of [13b]	238
F.	X-ray Structure Analysis of [13c]	243
G.	X-ray Structure Analysis of [13f]	247
H.	X-ray Structure Analysis of [15]	250
I.	Summary Sheet of Literature Compounds Included in this Thesis	252
J.	Summary Sheet of Novel Compounds Presented in this Thesis	257
K.	Publications Resulting from This Thesis	265

Chapter One

Organocalcium Catalysis

1.1 The Case for Calcium

In recent years there has been a renaissance in coordination and catalytic chemistry involving the Alkaline Earth (AE) metals; magnesium (Mg), calcium (Ca), strontium (Sr), and barium (Ba). Of the heavier AE metals Ca, Sr, and Ba the progress of organocalcium literature is beginning to gain momentum. This is expressed by the flurry of publications from the area over recent years.

Of the AE metals the exploitation of magnesium is probably most familiar in the form of the eponymous Grignard reagents (RMgX),¹ with the other heavier elements of the group remaining far less developed. Obstruction of inroads to this area is likely to have stemmed from the initial limited availability of suitable synthetic precursors. These problems were compounded by the early perception that the heavier AE metals presented no real advantage over magnesium.

Preparation of AE metal organometallics has proved troublesome in the past; however the barriers to their utilisation are slowly being eroded. New methods to fulfil the steric demands of the metal by judicious use of bulky ligands, the importance of stabilising with agostic interactions, and insights into control of ligand redistribution have all allowed advance in this promising area.^{2,3}

Thus far, the field of organometallic catalysis has been monopolised by the d-block Transition metals, particularly the precious metals (Ru, Rh, Pd, Os, Ir, and Pt), where they have experienced unparalleled success. In the last decade, three of the Nobel prizes for chemistry have been related to Transition-metal-based organometallic complexes and their subsequent utilisation in catalysis (Knowles, Noyori, and Sharpless 2001; Chauvin, Grubbs, and Schrock 2005; Heck, Negishi, and Suzuki 2010). In spite of such success, contemporary research has been driven by the necessity for the future generation of alternative, sustainable technology, commonly referred to as “Green Chemistry”.

Green Chemistry is defined by 12 principles focusing on atom economy and employing chemicals of reduced hazard and/or toxicity from sustainable feedstocks. It requires products of these reactions to be safer than current alternatives and that reactions yield minimal waste.⁴ In lieu of this, the field of organometallic catalysis is in pursuit of alternatives to meet these criteria. When selecting potential catalyst replacements one is able to strongly advocate the case for calcium for several excellent reasons.

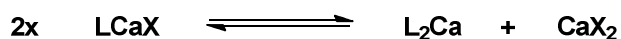
Calcium has been identified as a possible ‘cheap metal for noble tasks’ in the quest for alternative catalysts to the ubiquitous precious metals.^{5, 6} Calcium is the fifth most abundant element in the Earth’s crust with aluminium and iron being the only metals that occur more readily.^{7, 8} Its global abundance is reflected in the price of the raw metal when compared to that of the precious metals. Current prices for 100 g of raw calcium metal sit within affordability at approximately £22. In stark contrast precious metals such as platinum and palladium currently cost in the region of £100 for 1 g. Such a dramatic difference already highlights a large potential for cost reductions, typically when catalyst recovery is often troublesome in already expensive chemical processes.

Calcium is fundamentally important in nature, present in minerals, habitats like coral reefs, and is vital for flora development. In mammals and humans it is utilised in the body’s nervous system, blood clotting mechanism and bone structure. The profuse application of calcium in nature highlights the environmentally benign nature of the element. Thus the impact upon the environment and living systems from its use in organometallic catalysis is expected to be greatly reduced compared to more harmful alternatives.

These benefits are notwithstanding the enticing academic prospects such chemistry presents. This once dormant metal is now finding its way into the limelight of catalysis through its application to an ever-growing range of reactions. This introduction will focus upon the current catalytic applications of calcium in regards to the heterofunctionalisation of unsaturated organic molecules. There has also been a significant amount of interest in the polymerisation of styrene⁹⁻¹² and cyclic esters,¹³⁻²⁹ Lewis acid catalysis,³⁰⁻³⁴ and other organic transformations.³⁵⁻⁴³ These areas along with a detailed discussion of the coordination chemistry of calcium and the AE metals^{2, 44-47} lies beyond the scope of this Chapter and the reader is therefore directed to the noted references for further information.

1.1.1 Taming Calcium

As Group 2 of the periodic table is descended the metals become larger and more ionic in nature. This results in decreasing M-L bond strength and complex reactivity increases.^{3, 44} The accompanying side-effect is the increased inclination of the larger AE metals to undergo ligand redistribution (Scheme 1) as well as aggregation. Strategies to improve complex resistance to redistribution and aggregation typically utilise sterically demanding polydentate ligands and co-ligands to help saturate the coordination sphere around the metal centre.



Scheme 1 Ligand redistribution also known as Schlenk-type equilibrium

(L = mono-anionic supporting ligand; X = mono-anionic substituent).

Many of the early examples of bulky ligands relied on the β -diketimidato (BDI) **1.1**, and tri(pyrazolylborate) **1.2** ligands reported by Chisholm *et al.* (Fig. 1). Whilst they have become popular supporting scaffolds the presence of dimeric species and/or products of ligand redistribution in solution have been reported.¹⁶

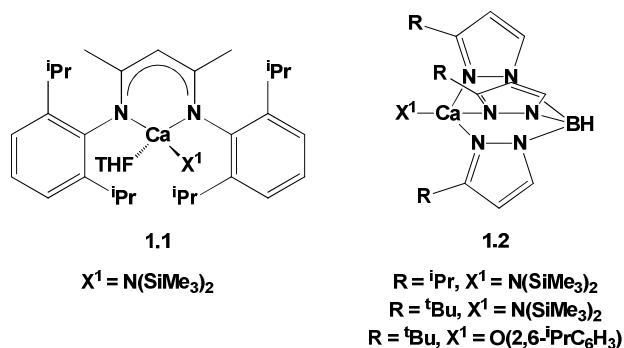


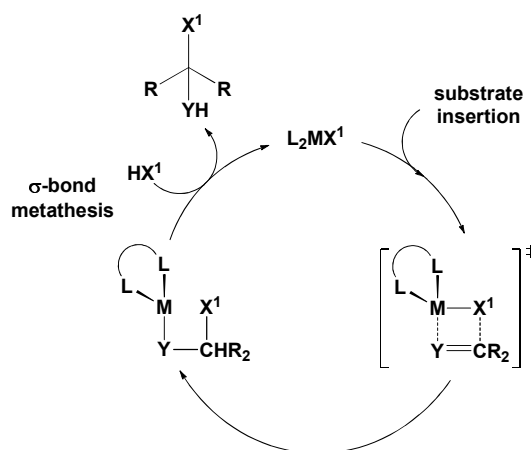
Fig. 1 Well-defined calcium β -diketimidato (**1.1**) and tri(pyrazolylborate) (**1.2**) complexes reported by Chisholm *et al.*.

The most common stabilising anion used is bis(trimethylsilyl)amide ($[\text{N}(\text{SiMe}_3)_2]^-$) or a derivative thereof.⁴⁷⁻⁵² Bulky silylalkyls, typically of the form $[\text{C}(\text{SiR}_2\text{H})]^-$ have also been exploited.⁵³⁻⁵⁹ Addition of such supporting ligands also eases the AE metals' notoriously poor solubility.

The problem of ligand redistribution arguably provides the greatest challenge to the development of AE metal catalysts. It is important to overcome since redistribution from the generally active heteroleptic species LCaX (X = alkyl or amide co-ligand), gives rise to normally unreactive L_2Ca , and reactive but unselective CaX_2 . Thus any redistribution is likely to result in loss of the active catalytic species and accompanying ligand effects upon substrates. The loss of ligand influence is particularly detrimental to asymmetric catalysis where stereodirecting influence is often due to the supporting ligand.

1.2 Calcium in Catalysis

The heavy AE metals often have parallels drawn between them and lanthanides due to their highly ionic, non-directional metal-ligand bond interactions.^{60, 61} In the case of trivalent lanthanides work by Hong and Marks has shown that $\text{L}_2\text{M}(\text{X}^1)_2$ ($\text{M} = \text{Ln}^{3+}$, L_2 = bidentate anionic ligand, X^1 = anionic σ -bound species) systems are able to undertake two types of fundamental reactivity.⁶² The first being σ -bond metathesis and the second, the insertion of unsaturated C-C or C-E (E = heteroatom) bonds into a $\text{M}-\text{X}^1$ σ -bond. It is often the case that these two modes of reactivity can be exploited together (Scheme 2). The utilisation of this feature with lanthanides led to the development of catalysts successful in hydroamination,⁶³⁻⁶⁹ hydrophosphination,^{70, 71} hydrosilylation,^{72, 73} hydrogenation,^{74, 75} and hydroboration⁷⁶⁻⁷⁸ of unsaturated C=C bonds.



Scheme 2 σ -bond metathesis and unsaturated bond insertion into $\text{M}-\text{X}^1$ bond as part of a catalytic heterofunctionalisation cycle (L_2 = bidentate anionic ligand; $\text{M} = \text{Ca}$; X^1 = anionic σ -bound species, for example $[\text{N}(\text{SiMe}_3)_2]^-$ or $[\text{C}(\text{SiMe}_3)_3]^-$).

When presented with the bonding similarities of both the heavier AE metals and trivalent lanthanides, with respect to their non-directional ionic M-L bonds, it poses the question of whether the heavy AE metals could be applied in a similar manner as lanthanides to heterofunctionalisation catalysis involving insertion and subsequent σ -bond metathesis.

Whilst a great deal of work was undertaken with lanthanides in heterofunctionalisation catalysis during the 1990s it has taken nearly a decade for the above question to be probed with the AE metals; primarily as a consequence of the less-developed nature of the coordination chemistry of these metals. Studies over the past 7 years have validated the aforesaid hypothesis, leading to AE catalyst application to all of the above heterofunctionalisation reactions including ring-opening polymerisation (ROP) of lactides, styrene polymerisation, and various Lewis-acid catalysed organic transformations. The development and use of organocalcium complexes over a variety of heterofunctionalisation reactions is now discussed.

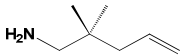
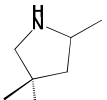
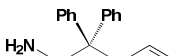
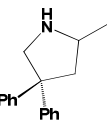
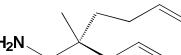
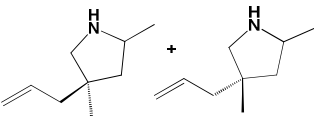
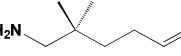
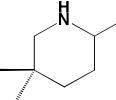
1.2.1 Hydroamination

Hydroamination is defined as the formal addition of an N-H bond across an unsaturated bond, and presents itself as a very attractive means to prepare a wide range of nitrogen containing compounds via a 100% atom-efficient route. Whilst the unsaturated moiety is typically C=C or C \equiv C, C=O and C=N functionalities have also been hydroaminated (*vide infra*). Successful exploitation of hydroamination has the potential to ease the synthesis of chiral amines and azacycles starting from readily available alkenes and primary amines, which are useful in the preparation of pharmaceuticals, industrial feedstocks, and fine chemicals.

Whilst hydroamination is a thermodynamically allowed exothermic process, electrostatic repulsion between the amine lone pair of electrons and the unsaturated C-C bond results in a high activation barrier. The overall negative entropy of the reaction means that heating the reaction to overcome the activation energy renders the reaction less favourable. Due to these circumstances the intervention of a catalyst is requisite (unless the precursors contain activated, electron deficient unsaturated C-C bonds).^{51, 79}

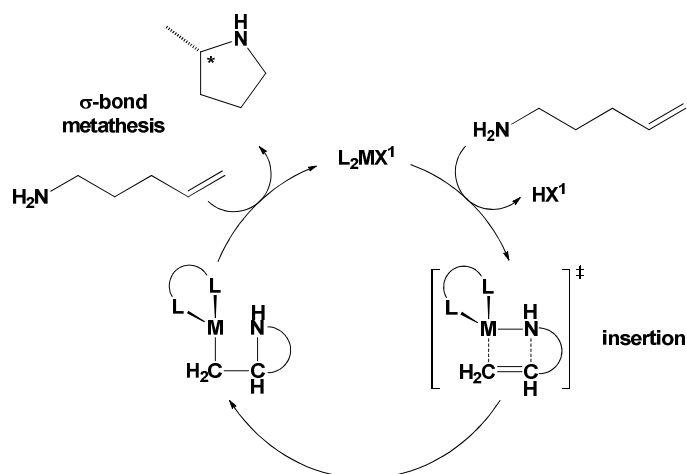
The first example of intramolecular hydroamination mediated by calcium was reported by Hill *et al.* in 2005 where the authors utilised Chisholm's BDI supported calcium complex **1.1**.⁵¹ The study was later expanded to include a more extensive range of aminoalkenes in 2009.⁸⁰ A summary of results from their first endeavour is contained in Table 1. The results demonstrate that for a range of simple aminoalkenes near quantitative conversion to the cyclic amines was achieved.

Table 1 Results of hydroaminated aminoalkenes mediated by calcium complex **1.1**.

Entry ^a	Aminoalkene	Product(s)	Time (h)	Temp. (°C)	Conv.% ^b
1			0.25	25	>99
2			0.25	25	>99
3			0.25	25	>99
4			6	60	86

^a Entries 1-3 used 10 mol% catalyst loading, entry 4, 20 mol% catalyst (10 mol% required 72 h to yield 85% conversion). ^b Determined by ¹H NMR in C₆D₆.

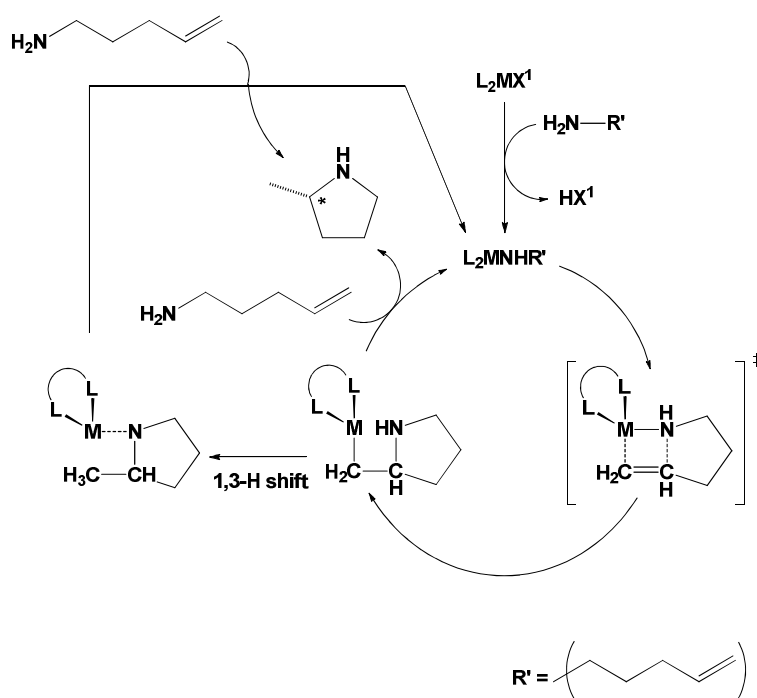
Whilst the formation of pyrrolidines (generally from 2,2-dialkyl-4-penten-1-amine derivatives, Table 1) was found to be relatively facile. Larger heterocycles (6-membered piperidines or 7-membered hexahydroazepines) are more difficult to form (as predicted by Baldwin's rules)⁸¹ and required forcing conditions, i.e. elevated temperatures (up to 80°C) for extended periods of 24-72 hours, or with increased catalyst loadings. The authors note the magnesium analogue of **1.1** was successful when applied to the same reaction, albeit over 5.5 days at 80°C to give 88% of the expected hexahydroazepine product (entry 4, Table 1). The reasoning as to why magnesium was more successful was put down to the higher stability of the magnesium catalyst at elevated temperatures during long reaction durations.^{51, 80} This proof of concept report served to pioneer further research in the area, with notable contributions from Harder,⁴⁹ Roesky,⁸²⁻⁸⁴ Sadov,⁸⁵ and Hill.⁸⁶⁻⁹¹



Scheme 3 Intramolecular hydroamination (L_2 = bidentate anionic ligand; $M = Ca$; X^1 = anionic σ -bound species, for example $[N(SiMe_3)_2]^-$ or $[C(SiMe_3)_3]^-$).

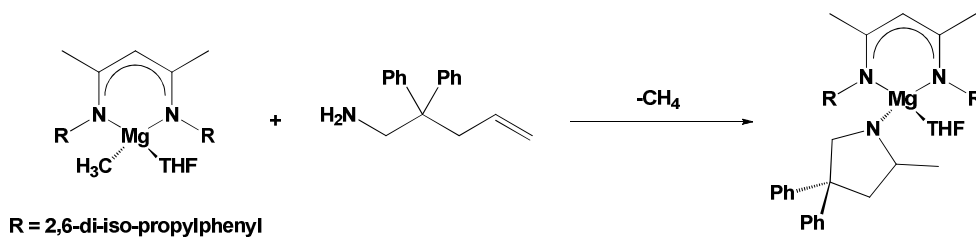
The mechanism by which intramolecular hydroamination occurs, is akin to many of the heterofunctionalisation reactions presented in this chapter, and is derived from the lanthanides (Scheme 3). The first step is the sigma-bond metathesis between the amine moiety of the incoming aminoalkene and the anionic donor ligand X^1 bound to the calcium complex (step 1, Scheme 3). Depending on the nature of X^1 , i.e. its basicity, this step is fast. When the protio by-product HX^1 displays a similar acidity to that of the aminoalkene substrate this reaction is known to exist in equilibrium.³ The nucleophilic attack from the electron rich $C=C$ upon the electropositive calcium centre results in the $C=C$ bond insertion between the $Ca-N$ σ -bond.

Calcium complexes are unable to insert into isolated $C=C$ double bonds in intermolecular reactions and so substrates are typically activated by way of conjugation e.g. styrene or 1,3-butadiene. Intramolecular hydroamination can proceed without activated substrates since the loss in entropy ($-\Delta S$) is less for a single aminoalkene molecule when compared to that of the two reactive moieties combining from separate molecules.

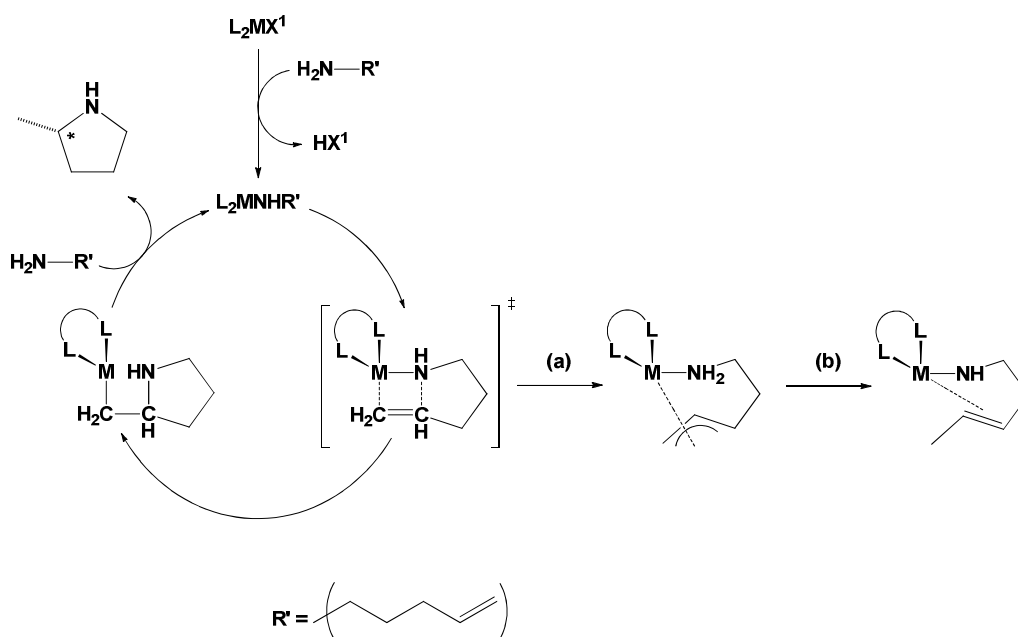


Scheme 4 Intramolecular 1-3-hydrogen shift during intramolecular hydroamination (L_2 = bidentate anionic ligand; $M = \text{Ca}$; X^1 = anionic σ -bound ligand, for example $[\text{N}(\text{SiMe}_3)_2]^-$ or $[\text{C}(\text{SiMe}_3)_3]^-$).

Evidence to support the proposed mechanism in the form of isolated and characterised intermediates has remained elusive for AE mediated hydroamination. One experiment involving the deuterium labeling of the aminoalkene amine moiety has however been investigated,⁸⁰ wherein isolation of the cyclic product bearing a CH_2D moiety at the *exo*-cyclic methyl position is consistent with the lanthanide mechanism (since monodeuteration would occur at the σ -bond metathesis in step 3, Scheme 3). It has been suggested that an intramolecular 1,3-hydrogen shift could also be possible during the course of the reaction and should not be discounted (Scheme 4). An example complex bearing an isolation secondary cyclic amine bound to the metal centre has been reported, albeit with magnesium (Scheme 5).⁸⁰



Scheme 5 Reaction of the Mg analogue of **1.1** with 1-amino-2,2-diphenyl-4-pentene.

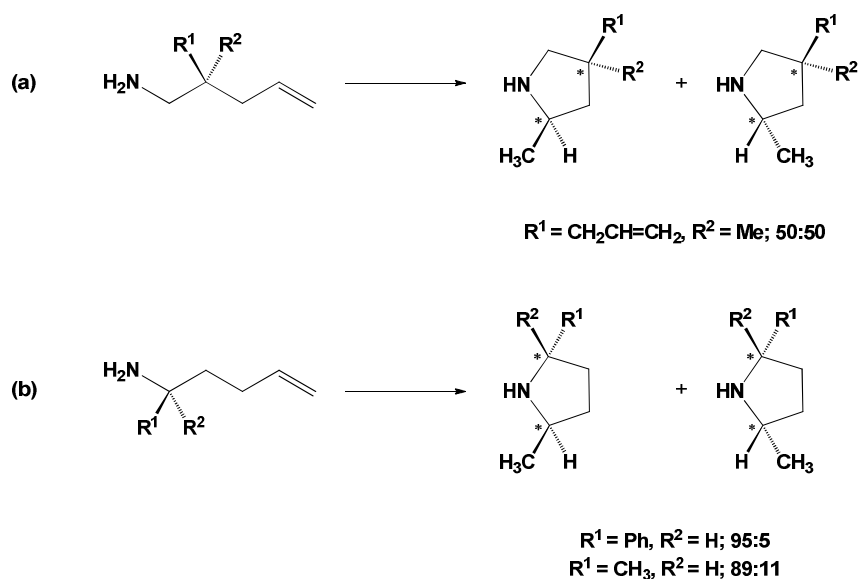


Scheme 6 Alkene isomerisation during intramolecular hydroamination (L_2 = bidentate anionic ligand; $M = \text{Ca}$; X^1 = anionic σ -bound species, for example $[\text{N}(\text{SiMe}_3)_2]^-$ or $[\text{C}(\text{SiMe}_3)_3]^-$).

Occasional observations of alkene isomerisation have been noted by Hill and co-workers when intramolecular deprotonation occurs at the alkene $\text{HC}=\text{CH}_2$ resulting in protonation of the amine moiety (step a, Scheme 6). This is followed by the subsequent protonation at the terminal carbon of the aminoalkene chain giving the overall effect of a new position of the alkene functionality from its original terminal position (step b, Scheme 6).

So far investigation of aminoalkenes has been restricted to primary and secondary amines bearing $\text{C}=\text{C}$ unsaturation at the terminal position. Substrates often contain geminal substitution at the mid-point of the alkyl chain. The inclusion of geminal substitution is a feature of the more reactive substrates and is owed to the Thorpe-Ingold effect (the compression of internal bond angles caused by the mutual repulsion of the gem-substituents promoting cyclisation and reduction in possible molecule conformations).⁹² Favoured reactivity of larger geminal substituents has been noted in alternative hydroamination systems and is not only restricted to the heavier AE metals.^{61, 93}

Examples of aminoalkenes containing multiple C=C double bonds have been reported in intramolecular hydroamination,^{42, 86} as well as aminoalkenes bearing monomethyl or dimethyl substitution at the terminal methylene group of the C=C.⁸⁰ Substitution at the terminal alkene ($\text{RHC}=\text{CR}^1_2$) results in the complete arrest of cyclisation. Methyl substitution at the methylene position ($\text{RR}^1\text{C}=\text{CH}_2$) resulted in elongated reaction times before full conversion was attained. The increased steric presence imposed by alkyl-substitution around the terminal alkene is likely to interfere with the ease of insertion of the alkene, since this is generally accepted as the rate determining step (step 1, Scheme 3).⁸⁹



Scheme 7 Intramolecular hydroamination resulting in diastereomeric products depending upon position of alkylchain substitution mediated by **1.1** ($\text{R} = \text{alkyl}, \text{R}^1 = \text{Ph}, \text{CH}_3, \text{R}^2 = \text{H}$).

When investigating regioselectivity with the intramolecular hydroamination of aminoalkenes bearing two pro-chiral centres, it was found that variations in substitution along the alkyl chain could also dramatically influence the regioselectivity of the resulting cyclic amine. Using the typical 2,2-dialkyl-4-penten-1-amine derivatives (where both alkyl groups are inequivalent) to illustrate this point, substitution at the β -position of the amine had no effect upon the diastereoselectivity of the reaction, however substitution at the α -position to the amine gave diastereoselective intramolecular hydroamination (Scheme 7).⁸⁰ Whilst substitution at the α -position to the amine displayed intriguing diastereoselectivities, reaction rates and yields were comparable to similar substrates

bearing no substitution at this position, unlike the aforesaid terminal alkene substitution effect.

The largest diastereomeric excesses are observed in the products bearing inequivalent substitution at the α -position in favour of *trans*-conformers. Diastereoselectivities of up to 95% were observed when mediated by **1.1**. The magnesium analogue of **1.1** gave marginally higher selectivities for identical substrates. The preferred *trans*-conformation can be explained by consideration of the most favourable transition state conformation during the insertion step. Of the possible conformations, those which place the most sterically demanding R-substituent where it causes the least amount of steric impingement upon the metal centre and supporting ligand are the most favourable. A conformation which sees R group impingement upon the steric sphere of the metal centre and its supporting ligand is likely to be less favoured since competing steric interactions are liable to raise the energy barrier to reaction. Such interactions are not so prevalent when the aminoalkene has substitution at the β -position to the amine, hence less drastic preference for a particular isomer is induced. Enantioselectivity when applied to intramolecular hydroamination has also been investigated and is discussed in greater detail at the end of this section.

Within the last year Roesky *et al.* have combined the reactivity of calcium and zirconium in a single system that was then applied to intramolecular hydroamination of primary and secondary aminoalkenes.⁹⁴ The stoichiometric reaction of $[\text{Cp}^*_2(\text{CH}_3)\text{Zr}(\text{OH})]$ with $[\text{Ca}\{\text{N}(\text{SiMe}_3)_2\}_2(\text{THF})_2]$ results in a new class of catalyst **1.3**, containing both Lewis acidic centres bridged by an oxygen atom (Fig. 2). The calcium centre adopts a trigonal-bipyramidal geometry typical in 5-coordinate systems, whereas the zirconium centre conforms to distorted tetrahedral geometry. The Zr-O-Ca bond is almost linear at 177° .

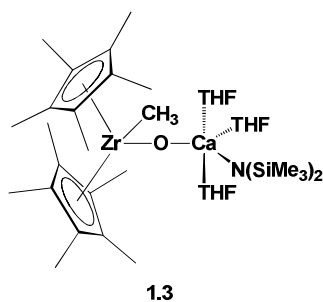
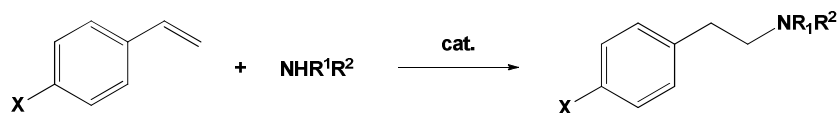


Fig. 2 Bimetallic catalyst system comprised of Zr and Ca for intramolecular hydroamination (**1.3**).

Application of **1.3** to the intramolecular hydroamination of primary aminoalkenes gave good yields (80-99%), however reaction times were notably slower when compared to **1.1** and $[\text{Ca}\{\text{N}(\text{SiMe}_3)_2\}_2(\text{THF})_2]$ under similar reaction conditions. Application of 10 mol% of **1.3** to a range of secondary aminoalkenes required much higher reaction temperatures (110 °C) as well as the presence of an equimolar equivalent of activator $[\text{PhN}(\text{CH}_3)_2\text{H}][\text{B}(\text{C}_6\text{F}_5)_4]$. The activator was used to protonate a methyl from the zirconium (as methane) generating a cationic zirconium species *in-situ*. This is one of the few examples of a calcium catalyst used in the cyclisation of secondary aminoalkenes where good conversions were obtained, normally 96-99% over a period of 20-50 hours at 110 °C. This is comparable to literature precedence using **1.1**, albeit it at greatly elevated temperatures (110 °C vs. room temperature).⁸⁰ Mechanistic studies suggest that for primary aminoalkene substrates the zirconium centre does not participate in the activation of the aminoalkene, which still proceeds by coordinating to the calcium centre, liberating $\text{HN}(\text{SiMe}_3)_2$.

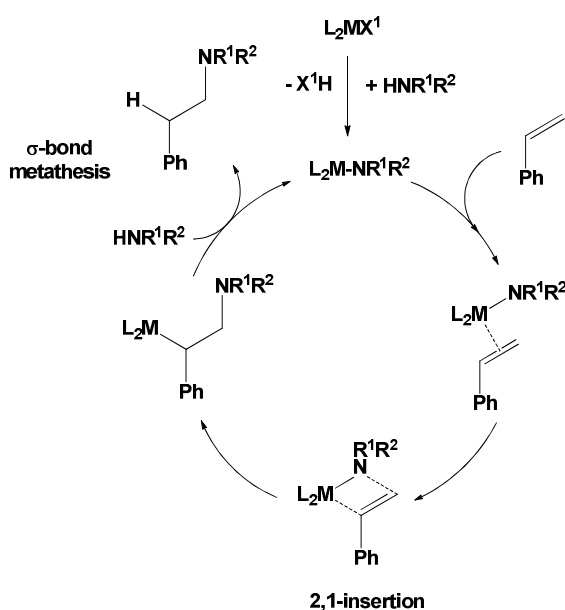
1.2.1.1 Intermolecular Hydroamination

Intermolecular hydroamination (Scheme 9) has been successful with catalyst **1.1**, $[\text{Ca}\{\text{N}(\text{SiMe}_3)_2\}_2]$, and $[\text{Ca}\{\text{CH}(\text{SiMe}_3)_2\}_2(\text{THF})_2]$ for a range of activated alkene substrates with various primary and secondary amines (Scheme 8).^{89, 90} Reactions progressed under solvent-free conditions at 60 °C for 2-168 hours yielding 17-95% product. The reaction was most successful when the X substituent was either H or Cl and the amine deployed was benzylamine (PhCH_2NH_2) or pyrrolidine ($\text{NH}(\text{CH}_2)_4$). The combination of these substrates gave yields of 92% and 95% respectively.

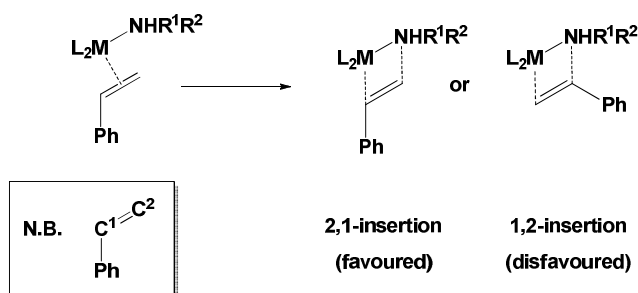


Scheme 8 Intermolecular hydroamination (X = H, CH₃, OCH₃, Cl; R¹=R² = -(CH₂)₄-, -(CH₂)₅-; R¹ = H, R² = (C₆H₅)CH₂-).

Intermolecular hydroamination gives products resulting from 2,1-insertion into the C=C bond, a phenomenon also observed in intermolecular hydrophosphination (Section 1.2.3), (Scheme 10). This occurs due to a favoured conformation during the transition state before N-C bond formation and because of factors that stabilise the developing anionic charge upon the adjacent carbon (C¹) to the calcium centre. A 2,1-insertion mechanism allows the adjacent phenyl group to C¹ to stabilise the anionic intermediate, lowering the transition state energy and consequently making it more favourable. A 1,2-insertion means the adjacent carbon to the metal centre, in this case C², would be devoid of such stabilising assistance rendering this conformation less favourable.



Scheme 9 Proposed mechanism for the organocalcium mediated intermolecular hydroamination (L_2 = bidentate mono-anionic ligand; $M = Ca$; X^1 = anionic σ -bound species, for example $[N(SiMe_3)_2]^-$ or $[C(SiMe_3)_3]^-$).



Scheme 10 Preferred 2,1-addition for styrene with calcium (L_2 = bidentate mono-anionic ligand; $M = \text{Ca}$; X^1 = anionic σ -bound species, for example $[\text{N}(\text{SiMe}_3)_2]^-$ or $[\text{C}(\text{SiMe}_3)_3]^-$).

The proposed mechanism for intermolecular hydroamination is taken from the mechanism postulated for the lanthanides (Scheme 9).^{62, 95} Calcium's predominantly ionic bonding denotes the reaction pathway is dominated by Coulomb interactions between catalyst and substrate. Initiation occurs with rapid reaction between the calcium complex and the incoming amine substrate, which causes the formation of a secondary-amine calcium complex and the protonation of the mono-anionic species X^1 to HX^1 . Alkene insertion into the Ca-N σ -bond is ascribed as the rate-determining step (as calculated from model complex studies involving ethylene and ammonia).⁸⁹ 2,1-insertion of the alkene occurs by way of a four-centre transition intermediate where significant electron density is located over the amine moiety and of the unsaturated carbon adjacent to the calcium centre (C^1 , Scheme 10). As electron density accrues over the adjacent unsaturated carbon (C^1), nearing the equivalent of one additional electron, electron density is withdrawn from N-Ca bond lobe and is dispersed into the newly forming N-C bond.

Hill and co-workers' calculations put the energy barrier to the initial deprotonation of the amine substrate to form the secondary-amine calcium complex at 36.0 kJ mol^{-1} and alkene insertion into the Ca-N bond at 69.9 kJ mol^{-1} . Eyring analysis of intermolecular hydroamination of styrene with piperidine catalysed by $[\text{Ca}\{\text{N}(\text{SiMe}_3)_2\}_2(\text{THF})_2]$ suggests $\Delta G^\ddagger = 100.8 \text{ kJ mol}^{-1}$ (although the authors suggest this value appears somewhat overestimated compared to calculations on the model system with ethylene and ammonia). The authors add that calcium provides the ideal balance between polarization and polarizability which assists the ease of alkene insertion.

In further mechanistic support evidence for the formation of calcium-alkene adducts of the type postulated during the mechanism has been provided by Schumann *et al.*⁹⁶ and Wiecko *et al.*⁹⁷ Although the latter case involved the barium analogue, complexes **1.4** and **1.5** were isolated (Fig. 3). Lanthanide variants of these types of complex are also known.⁹⁸

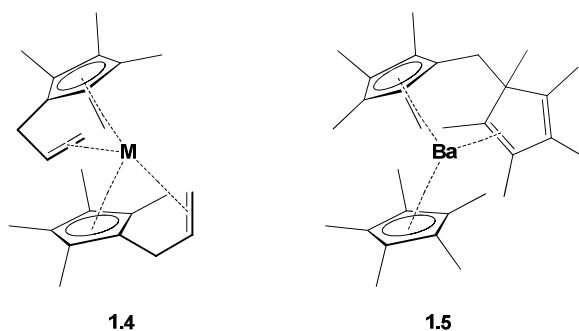
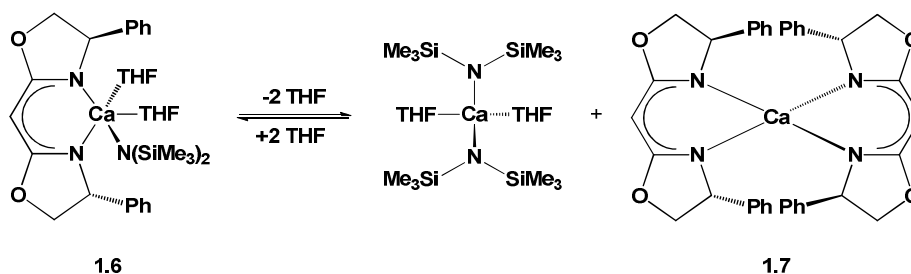


Fig. 3 Isolated alkaline earth metal complexes **1.4** and **1.5**, depicting metal-alkene bonds (M = Mg, Ca, Sr, and Ba).

1.2.1.2 Asymmetric Hydroamination of Alkenes

Prior to pioneering work with a chiral bisoxazoline (BOX) supported calcium complex by Buch and Harder in 2008,⁴⁹ application of calcium complexes to asymmetric inter-/intramolecular heterofunctionalisation catalysis was non-existent. Whilst efforts at the time were being made towards developing and understanding well-defined complexes, investigating exchange processes, and improving the library of calcium precursors, taking the step to tackle asymmetric catalysis could be regarded as appreciably ambitious. When Buch and Harder applied complex **1.6** (Scheme 11) to both hydroamination catalysis (and hydrosilylation as discussed in Section 1.2.2.1), selectivities were poor (*ca.* 4-10% ee).



Scheme 11 Redistribution of $[\text{Ca}(\text{BOX})\{\text{N}(\text{SiMe}_3)_2\}(\text{THF})_2]$ **1.6** to **1.7**.

The low enantiomeric excess was deemed a result of the prevalent Schlenk-type equilibrium already well-known to be operating in systems of this type (Section 1.1.1). The formation of the two homoleptic species reduces the quantity of active, stereodirecting heteroleptic complex L_2CaX^1 to its significantly less active, or even entirely inactive L_2Ca analogue. This is accompanied by the formation of the active, yet non-stereoselective CaX^1_2 compound that not only affects catalytic rate but also results in racemic product formation (Scheme 11). This truly highlights the importance of suppressing Schlenk-type equilibria in asymmetric catalysis systems in order to obtain more stereoselective catalysts.

To this end Buch and Harder probed the addition of further equivalents of unreactive homoleptic BOX complex (**1.7**, Scheme 11) to cause the equilibrium to shift in favour of the formation of active compound **1.6**. The addition of 1 equivalent of **1.7** to a solution of **1.6** resulted in a system largely free of $[Ca\{N(SiMe_3)_2\}_2(THF)_2]$. Buch and Harder also adopted this approach to their studies on hydroamination, though enantiomeric excesses only improved from 5% to 6% ee.

Alongside studies of **1.6** the use of chiral complex **1.8** (Fig. 4) was investigated in hydroamination (and hydrosilylation as set out in Section 1.2.2.1), but the authors report that it also underwent ligand redistribution in the same manner as **1.6**. However when **1.8** was applied to hydroamination a selectivity of 10% ee was recorded, a mild increase over that of **1.6**

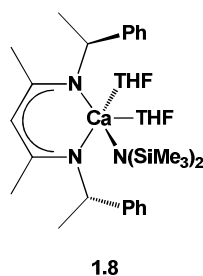


Fig. 4 Chiral calcium complex **1.8**.

Since 2008, exploits into asymmetric hydroamination have progressed and Sadow *et al.* have reported increased enantioselectivities in hydroamination with chiral tris(oxazolinyl)borato calcium complex **1.9** (Fig. 5).⁸⁵ When applied to intramolecular hydroamination of various typical substrates, e.g. 2,2-dimethyl-4-penten-1-amine and 2,2-diphenyl-4-penten-1-amine precursors (entries 1 and 2, Table 2), both substrates displayed complete product conversion in less than 5 minutes at room temperature.

Of the two substrates the gem-diphenyl pyrrolydine was racemic, however the gem-dimethyl substituted pyrrolidine product gave a calculated enantiomeric excess of 16%. An 18% ee was also noted for the cyclisation of 2-cyclohexyl-4-penten-1amine (entry 3).

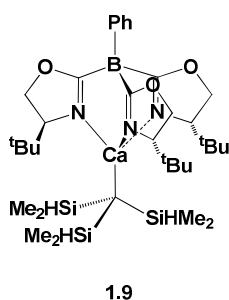


Fig. 5 Tris(oxazolonyl)borato calcium complex **1.9**.

Table 2 Hydroamination of aminoalkenes with calcium complex **1.9**.

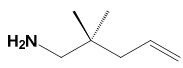
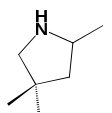
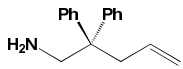
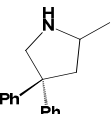
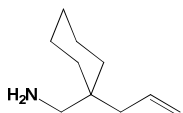
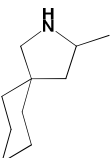
Entry ^a	Aminoalkene	Product(s)	Time	Temp. (°C)	Conv.% ^b	ee % ^b
1			5 min	25	>99	16
2			5 min	25	>99	0
3			5 min	25	>99	18
4			7 days	80	<10	-

^a Entries 1-3 10 mol% catalyst loading, entry 4 1 mol% catalyst.

^b Determined by ¹H NMR.

Sadow and co-workers also probed the intramolecular hydromamination of identical substrates with the magnesium analogue of **1.9**. When the magnesium complex was reacted with the substrates from entries 1-3 of Table 2, substantially lower activity was noted (Table 3). For reactions to proceed with magnesium elevated temperatures of up to 80 °C were necessary for longer durations (upwards of 24 hours) before comparable conversions of 80-93% were obtained. Although magnesium displayed lower activity than calcium the stereoselectivity was greatly enhanced. Entries 1 and 3 in Table 3 show calculated enantiomeric excesses of 27% and 36% respectively.

Table 3 Hydroamination of aminoalkenes with the magnesium analogue of complex **1.9**.

Entry ^a	Aminoalkene	Product(s)	Time	Temp. (°C)	Conv.% ^b	ee % ^b
1			5 days	80	80	27
2			12 h	60	>99	0
3			26 h	60	93	36

^a Entries 1-3 10 mol% catalyst loading. ^b Determined by ¹H NMR.

These results also showed improved enantioselectivity compared to previously reported magnesium mediated intramolecular hydroamination reactions, where Hultsch and co-workers implemented a diamidobinaphthyl supported magnesium catalyst **1.10** (Fig. 6) to attain 14% ee using the 2,2-diphenyl-4-penten-1-amine substrate.⁹⁹ Both results have been superseded as of 2012 where Hultsch *et al.* utilised the magnesium complex **1.11** (Fig. 7) in a wide variety of intramolecular hydroamination reactions where stereoselectivities were very favourable for a wide range of substrates, being recorded between 51-93% ee.¹⁰⁰

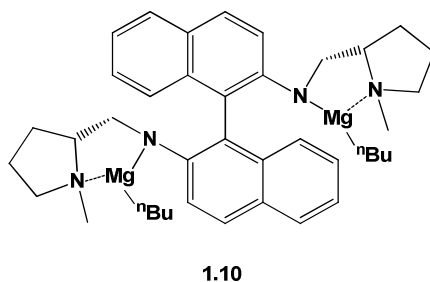


Fig. 6 Diamidobinaphthyl magnesium complex (**1.10**) achieved 14% ee in asymmetric intramolecular hydroamination.

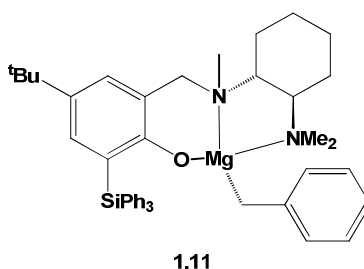


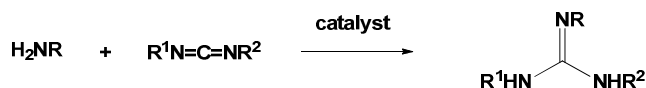
Fig. 7 Phenoxyamine magnesium complex (**1.11**) achieved 93% ee in asymmetric intramolecular hydroamination.

The above handful of examples goes to highlight the limited developments within AE metal mediated asymmetric heterofunctionalisation reactions, specifically that of heteroatom insertion into unsaturated bonds. Of the transformations examined hydroamination has been at the frontier of organocalcium driven asymmetric catalysis with only one example investigating asymmetric hydrosilylation (Section 1.2.2.1).

Induced enantioselectivity in asymmetric hydroamination from AE metal based catalysts is still generally lower than those experienced by the lanthanides or d-block metals, with more success arising from magnesium based complexes (having just accomplished 93% ee in intramolecular hydroamination).¹⁰⁰ Asymmetric hydroamination with calcium has experienced much slower growth compared to magnesium, but has seen improvement from 6% to 18% ee. It is in this context that the research presented in this Thesis aims to understand and develop chiral ligand systems in order to achieve increased levels of enantioselectivity with calcium complexes in the intramolecular hydroamination/cyclisation of aminoalkenes.

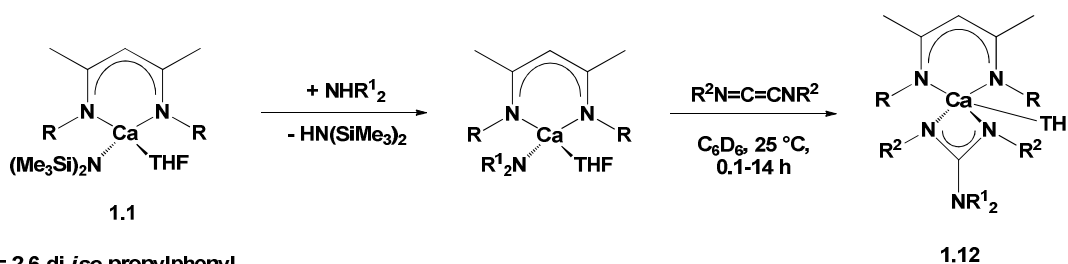
1.2.1.3 Intermolecular Hydroamination of Isocyanates and Carbodiimides

The majority of hydroamination literature has been confined to substrates bearing C=C or C≡C unsaturated bonds, however intermolecular hydroamination with complex **1.1** has also been expanded to that of carbodiimides (RN=C=NR) Scheme 12⁸⁸ and isocyanates (RN=C=O) Scheme 16.¹⁰¹



Scheme 12 Intermolecular hydroamination of carbodiimides mediated by calcium resulting in guanidine formation.

During discussion of the mechanisms for inter-/intramolecular hydroamination, the highly reactive nature of the intermediates was demonstrated by the difficulty experienced when trying to achieve their isolation. Conversely, the resulting product from insertion of a carbodiimide into the calcium-amine complex has been readily isolated. Hill *et al.* examined a selection of insertion products formed from **1.1** at room temperature in hydrocarbon solvents in their report.¹⁰¹ These results reveal a heteroleptic calcium complex with a BDI supporting ligand and 1,3-dialkylcarbodiimide bound to the metal centre (**1.12**). This also lends supporting evidence for the formation of this type of intermediate during catalysis (Scheme 13).¹⁰²

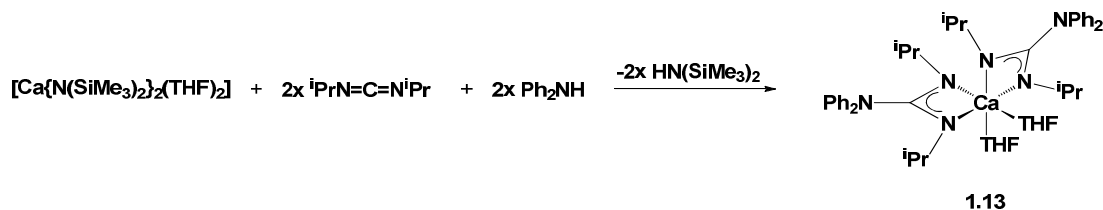


R = 2,6-di-*i*-propylphenyl
 NHR₁₂ = NH(CH₂)₂OCH₃, NPh₂, NHR
 R² = ^{*i*}Pr, Cy

Scheme 13 1,3-dialkylcarbodiimides insertion into the Ca-N bond to form complex **1.12**.

This was later elaborated upon with the isolation of homoleptic calcium complexes where the supporting ligands were both 1,3-dialkylcarbodiimides, proving that these “substrates” were indeed suitable ligands in their own right (Scheme 14). The stability of such calcium guanidinate complexes far outweighs other similar catalytic calcium

intermediates, with observations that some complexes remain stable in solution for a duration of 2 weeks or more under inert conditions.⁸⁸



Scheme 14 Homoleptic calcium complex **1.13** supported by two 1,3-dialkylcarbodiimides.

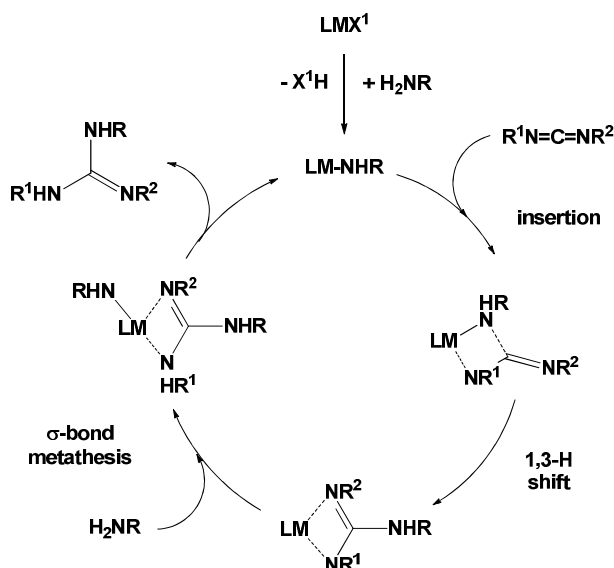
Feil and Harder have reported a homoleptic calcium bis(guanidinate) complex **1.13**, a result of reaction between calcium amide $[\text{Ca}\{\text{N}(\text{SiMe}_3)_2\}_2(\text{THF})_2]$ and two equivalents of 1,3-diisopropylcarbodiimide.¹⁰³ Complex **1.13** could also be formed in a typical manner via salt metathesis between the potassium salt of 1,3-diisopropylcarbodiimide with 0.5 equivalents of CaI_2 . Whilst the focus of this review is the application of organocalcium complexes to catalysis, several excellent reviews have been written discussing the synthesis of many of the AE metal precursors presented in this Chapter.^{2, 44-46}

Redistribution of complex **1.13** was mentioned and the authors note that the equilibrium, although favouring the heteroleptic complex **1.13**, can be shifted by an addition of an excess of homoleptic species, resulting in near quantitative formation of the heteroleptic species. Most recently Hill *et al.* have conducted similar investigations on a wider range of substrates to form both hetero- and homoleptic species upon the generality of insertion of 1,3-dialkylcarbodiimides (and isocyanates) into Ca-E bonds (E = N, P).¹⁰⁴

Use of **1.1** in hydroamination reactions involving 1,3-dialkylcarbodiimides was reported by Hill and co-workers as a follow up to their earlier studies concerning the calcium guanidinate complex **1.12** (Scheme 13)¹⁰² in 2008.⁸⁸ The authors comment upon the rapid reaction between the amine and 1,3-dialkylcarbodiimide with most reaching completion in 5 minutes or less, and with lower than normally observed catalyst loadings (2-4 mol%). The scope of their studies included both sterically demanding amines (e.g. 2,6-di-*iso*-propylaniline) and carbodiimides (e.g. 1,3-di-*tert*-butylcarbodiimide). Substrate limitation was remarked on by way of the facile nature by which this reaction progressed when the amine was an aniline analogue. The authors note that reactions using primary amines were unsuccessful.

For comparison reactions were carried out using $[\text{Ca}\{\text{N}(\text{SiMe}_3)_2\}_2(\text{THF})_2]$, which is also active. Yields from the employment of either catalyst gave good conversions (77-91%), however lower yields were noted for sterically demanding carbodiimides i.e. 1,3-di-*tert*-butylcarbodiimide and 1,3-di-cyclohexylcarbodiimide. In such instances isolated yields were reduced to 37-55%. These could be increased to 46-82% upon conducting the reaction at 80 °C as opposed to ambient conditions.

Reaction products from the aforesaid hydroamination of carbodiimides are reported to crystallise from reactions carried out in hexane where single-crystal X-ray diffraction techniques, coupled with multi-nuclear NMR spectroscopy have alluded to the guanidine products having undergone a 1,3-proton shift during the catalytic cycle (Scheme 15).



Scheme 15 Proposed mechanism for the organocalcium mediated hydroamination of carbodiimides. (L =BDI; M = Ca; X^1 = anionic σ -bound species, for example $[\text{N}(\text{SiMe}_3)_2]$).

During the catalytic cycle a homoleptic calcium guanidinate intermediate **1.14** is formed after insertion of the carbodiimide into the Ca-N bond of $[\text{L}_2\text{Ca-NHR}]$ and prior to protonolysis (Fig. 8). Complex **1.14** was also found to be a competent catalyst when applied to the substrates 1,3-di-*iso*-propylcarbodiimide and aniline. The authors suggested that whilst evidence indicates the calcium guanidinate species is dimeric in solution, the number of calcium centres in the active catalyst is likely to vary as a function of the substrate employed.

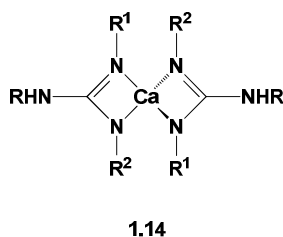
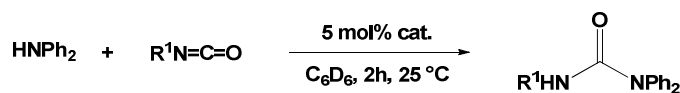


Fig. 8 Homoleptic calcium guanidinate complex **1.14**

suggested as the catalyst resting state.

A single publication from Hill *et al.* is current the only example of an organocalcium complex applied to the intermolecular hydroamination of isocyanates (Scheme 16).¹⁰¹ In this example 5 mol% of complex **1.1** or $[\text{Ca}\{\text{N}(\text{SiMe}_3)_2\}_2(\text{THF})_2]$ resulted in successful urea product in yields of 89% and 92% respectively, under mild conditions (25 °C, 2h).



R = 1-adamantyl, 2,6-di-*iso*-propylphenyl

Scheme 16 Intermolecular hydroamination of isocyanates resulting in urea formation.

Stoichiometric reaction between **1.1** and diphenylamine results in the calcium amide complex $[\text{Ca}\{\text{ArNC}(\text{CH}_3)\text{CHC}(\text{CH}_3)\text{NAr}\}(\text{NPh}_2)(\text{THF})]$ (Ar = 2,6-di-*iso*-propylphenyl). Addition of one equivalent of 1-adamantyl isocyanate results in the insertion of the aryl-isocyanate into the Ca-N bond, a reaction that occurs readily at room temperature in hydrocarbon solvents. The newly formed calcium ureido complex was subsequently isolated and crystallographically characterised (**1.15**, Fig. 9). A catalytic loading of 5 mol% of **1.15** was found to competently hydroaminate 2,6-di-*iso*-propylisocyanate and phenylamine (the constituents of which it was constructed) to 92% yield in 2 hours under ambient conditions. The proposed mechanism by which isocyanates are hydroaminated is presented in Scheme 17. The authors suggest that it is likely that the resulting urea product is able to act as a coordinating ligand which may interfere with the reaction by preventing substrate coordination and thus reaction.

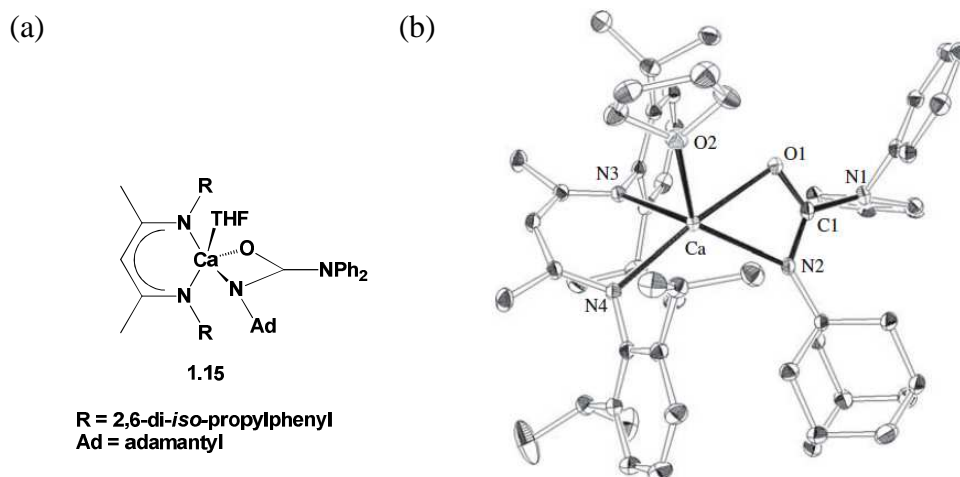
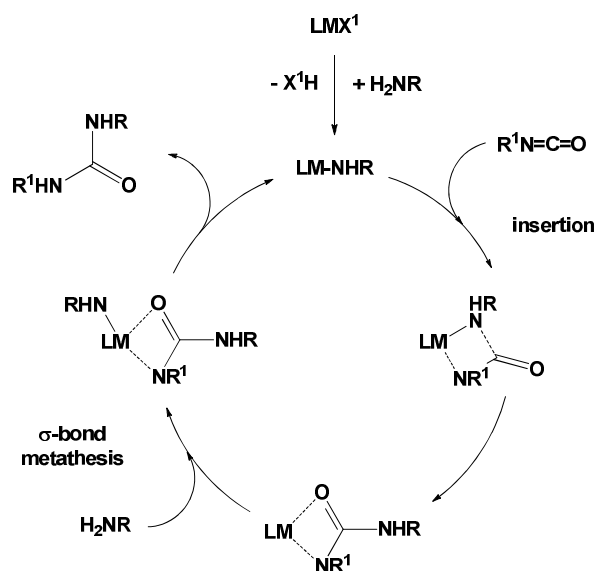


Fig. 9 (a) Calcium ureido complex **1.15** and (b) ORTEP representation of **1.15** thermal ellipsoids at 20% probability and H atoms omitted for clarity.¹⁰¹



Scheme 17 Proposed mechanism for the hydroamination of isocyanates.

(L =BDI; M = Ca; X¹ = anionic co-ligand, e.g. [N(SiMe₃)₂]).

Of the remaining heavier AE metal elements several examples of barium and strontium mediated hydroamination reactions have also been reported^{42, 82, 87, 88, 90, 101} and a general discussion concerning all heavier AE metals in hydroamination has been recently highlighted.⁹¹

1.2.2 Hydrosilylation

Hydrosilylation is the action of adding a polar Si-H bond to a multiple bond, most commonly C=C, C=O, or C=N. In the same manner as hydroamination, the process is a highly atom efficient route to incorporating silyl moieties into molecules. The addition of a silyl moiety to a vinyl group is a useful transformation however regio- and/or stereoselectivity can be troublesome due to unspecified insertion of the silyl group to either carbon of the C=C unsaturation. Two examples of calcium mediated hydrosilylation have so far been reported.^{49, 105}

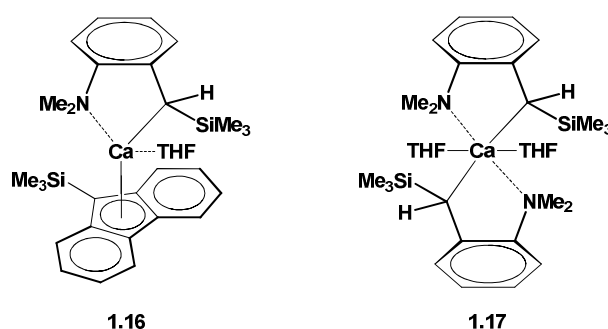


Fig. 10 The first examples of calcium complexes used in the execution of hydrosilylation, **1.16** and **1.17**.

Calcium benzyl complexes **1.16** and **1.17** (Fig. 10) were tested on a selection of substrates and the results are summarised in Table 4. The authors highlight that currently the range of substrates that AE metals can hydrosilylate remains limited to activated alkenes which carry the side-effect of being susceptible to polymerisation reactions.¹² This is the reason why the authors chose to investigate 1,1-diphenylethylene (DPE) as it fulfils the requirement of being an activated alkene whilst having sufficient steric bulk to resist polymerisation.

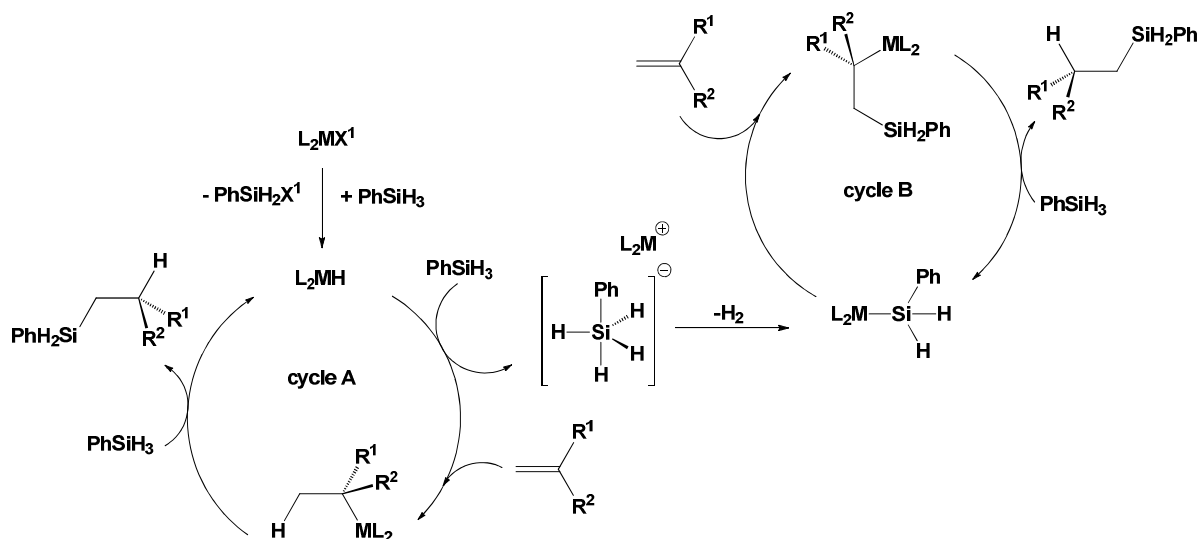
The homoleptic species **1.17** was the more reactive catalyst (entries 1 and 2 vs. 3 and 6) and in most examples product conversion was near quantitative. Reactions proceeded with low catalyst loadings (0.5-10 mol%) under moderately mild conditions of 50 °C for up to 24 hours or significantly less (entries 6, 8, and 9). In many studies solvent effects upon reaction performance have not been probed. In this study a change in preferred regioselectivity of the resulting product of reaction between PhSiH₃ and DPE was seen upon solvent exchange from benzene to THF (entries 3 and 4 vs. 10). Although solvent effects were not investigated further their study did bring to light a number of other points.

Table 4 Hydrosilylation activity of complexes **1.16** and **1.17** upon various alkenes.

Entry	Cat.	Cat. mol%	Substrates	Product	Time (h)	Temp. (°C)	Conv. (%)
1	1.16	5	DPE PhSiH ₃		16	50	10
2	1.16	5	Styrene Ph(CH ₃)SiH ₂		20	50	>98 ^a
3	1.17	2.5	DPE PhSiH ₃		16	50	>98
4	1.17	10	DPE PhSiH ₃		2	50	>98
5	1.17	2.5	Ph(CH ₃)C=CH ₂ PhSiH ₃		24	50	20
6	1.17	2.5	Styrene PhSiH ₃		<0.1	20	>98 ^a
7	1.17	0.5	Styrene PhSiH ₃		1.5	50	>98 ^a
8	1.17	2.5	Styrene Ph(CH ₃)SiH ₂		<0.1	20	>98 ^a
9	1.17	2.5	Cyclohexadiene PhSiH ₃		<0.1	20	>98
10 ^b	1.17	2.5	DPE PhSiH ₃		3	50	>98

^a Both diastereoisomers were obtained in an approximate 1:1 ratio. ^b Reaction in THF.

Reaction of catalysts **1.16** and **1.17** involving styrene resulted in the desired silane product rather than polystyrene. This suggests that alkene hydrosilylation occurs at a faster rate than polymerisation, since calcium benzyl complexes are known to polymerise styrene in the absence of a silane (*vide infra*). It was postulated that hydride-rich clusters form part of the reactive species responsible for hydrosilylation, although CaH_2 was found to lack catalytic activity when used directly as a hydrosilylation catalyst.



Scheme 18 Proposed mechanisms of intermolecular hydrosilylation concerning the heavier AE metals (L_2 = bidentate mono-anionic ligand; $\text{M} = \text{Ca}$; X^1 = anionic σ -bound species, for example $[\text{N}(\text{SiMe}_3)_2]^-$ or $[\text{C}(\text{SiMe}_3)_3]^-$).^{61, 105, 106}

The mechanism of this reaction is still under scrutiny although the favoured mechanisms are shown in Scheme 18. Detailed insight into the mechanisms of the heavier AE metals remains unclear due to the difficult nature of isolating the highly reactive reaction intermediates. In the case of hydrosilylation the proposed AE metal hydride intermediate $[\text{LCaH}]$, has remained unisolated and the known ease at which AE metal compounds undergoing Schlenk-type redistribution render this task significantly more difficult. Drawing parallels from lanthanide chemistry it is believed that the true catalytically active species involves a lanthanide hydride complex. This is generated as a result of an alkyl lanthanide compound reacting with a silane substrate.¹⁰⁷ The active hydride intermediate is referred to as “ L_2MH ” in Scheme 18, and after the formation of this reactive intermediate the lanthanide mechanism proceeds in a similar manner as denoted in

Scheme 2 with σ -bond metathesis resulting from the insertion of the unsaturated bond of the substrate. This is illustrated as “cycle A” in Scheme 18.

Cycle B of Scheme 18 involves the reaction proceeding through a silanide intermediate. It is suggested that the ion pairs $[\text{LM}]^+$ and $[\text{SiPhH}_4]^-$ decompose to form the metal silanide $[\text{LM}(\text{SiPhH}_2)]$ alongside the liberation of H_2 . This rationale is used to account for the observed variations in regiochemistry between polar and non-polar solvents. It has been suggested that the two transition states through which σ -bond metathesis occurs between LMX^1 and $\text{R}_n\text{SiH}_{4-n}$ (dictating product regioselectivity) likely have similar energetics and solvent interaction/non-interaction play a large part in dictating the reaction pathway.

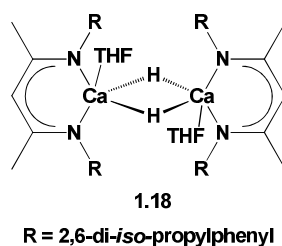
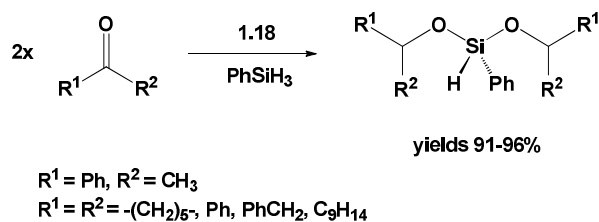


Fig. 11 Hydride containing calcium compound **1.18**.

Although the isolation of catalytic intermediates has so far proven fruitless, a dimeric calcium compound containing bridging calcium hydride bonds has been observed by Harder and Brettar, using complex **1.1** (Fig. 11). Nonetheless the isolation of dimeric **1.18** supports the possibility that such structures are feasible.

The dimeric complex **1.18** was also employed in the hydrosilylation of ketones (Scheme 19) the results of which are tabulated in Table 5. Hydrosilylation to form the desired silyl-ether ($\text{R}_3\text{SiOCHR}^1\text{R}^2$) was achieved using low catalyst loadings of 1.25 mol%, of **1.18** under relatively mild conditions (50 °C, 0.25-34 hours) resulting in commendable yields (91-96%). The well defined dibenzylcalcium catalyst **1.17** was also investigated and demonstrated comparable catalytic performance to **1.18**, albeit with slightly improved yields (95-98%) at the expense of elongated reaction times.¹⁰⁶



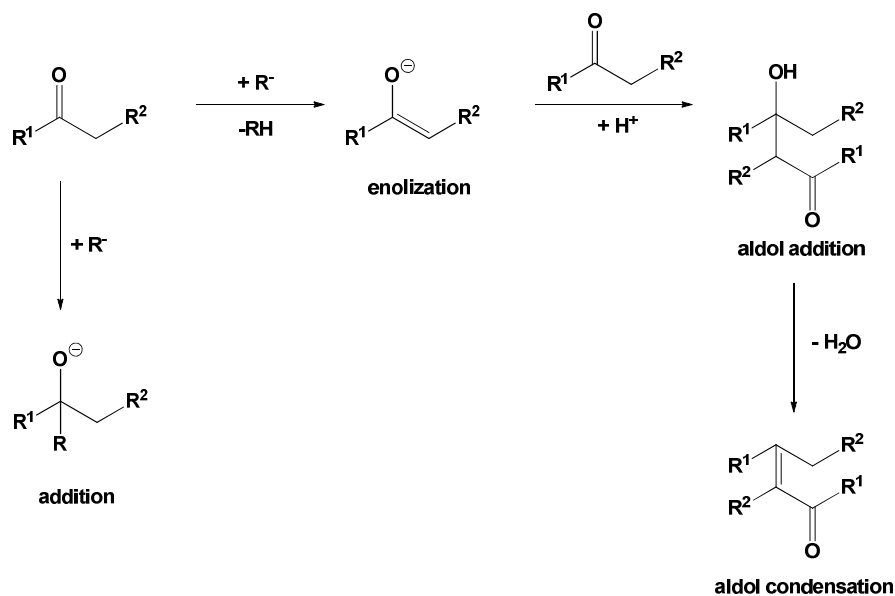
Scheme 19 Deployment of **1.18** to the hydrosilylation of ketones.

Table 5 Hydrosilylation of ketones using 1.25 mol% of **1.18** with PhH_3Si . Results for catalyst **1.17** are given in parentheses for comparison.

Entry	Ketone	Time (h)	$\text{PhHSi}(\text{CHOR}_1\text{R}_2)_2$ (%)
1	$\text{Ph}(\text{CO})\text{Ph}$	15 [15]	96 [96]
2	$\text{Ph}(\text{CO})\text{CH}_3$	34 [38]	95 [95]
3	cyclohexanone	3 [3]	91 [96]
4	$\text{PhCH}_2(\text{CO})\text{CH}_2\text{Ph}^{\text{a}}$	34 [54]	96 [95]
5	adamantone ^b	0.2 [1.5]	95 [98]

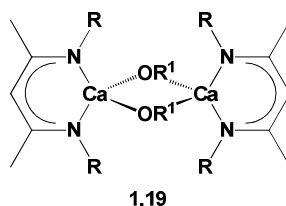
^a 5 mol% catalyst. ^b reaction conducted at 20 °C.

It is known that by-products resulting from competing carbonyl enolization and aldol condensation can occur (Scheme 20). Whilst the yields of hydrosilylation with **1.18** and **1.17** were high, the potential for side reactions was investigated further.



Scheme 20 Addition, enolization, and aldol condensation of ketones.

A staggered hydrosilylation reaction was undertaken between **1.18** and two equivalents of ketone, which resulted in the isolation of X-ray quality single crystals of a ketone bridged compound (**1.19**, Fig. 12). When R¹ was CH(Ph)₂ or adamantly **1.19** was obtained in yields of 73% and 67% respectively. All other examples showed significantly lower yields (9-25%). It was observed that all dimers were free of coordinated THF presumably due to the steric bulk of the more demanding alkoxide group saturating the coordination sphere of the metal centre.



1.19

R = 2,6-di-*iso*-propylphenyl

R¹ = CH(Ph)₂, CH(CH₃)(Ph), CH(CH₃)₂,
-(CH₂)₅-, CH(CH₂Ph), adamantyl

Fig. 12 Alkoxide bridged calcium compound **1.19** isolated by Harder *et al.*.

Once formed compound **1.19** went onto complete hydrosilylation upon the addition of trimethylsilyl chloride (Me₃SiCl). Table 6 summarises the results upon quenching with Me₃SiCl to form the addition product; the targeted silyl-ether (R₃SiOCHR¹R²). It shows that when the ketone is benzophenone or adamantone then the desired silyl-ether (addition product) is obtained in near-quantitative yields. All other examples exhibit low levels of enolization (15-35%) and still lower quantities of the aldol condensation by-product (<1-7%). When the ketone is acetone then none of the desired addition product is obtained and only enolization (76%) and aldol condensation (24%) by-products are observed. Probing the ratios of ketone:silane revealed an intriguing trend and showed that overall, regardless of the ketone:silane ratio the favoured reaction product is that of [PhSiH(OCHR¹R²)₂] (Scheme 19). This remains the major product even at elevated ratios of 1:2 ketone:silane. At low ketone:silane ratios low quantities of the trialkoxy silyl-ether [PhSi(OCHR¹R²)₃] are obtained.

Table 6 Hydrosilylation of ketones by **1.18** and proportions of by-products.

Entry	Ketone ^a	% Addition	% Enolization	% Aldol Cond.
1	Ph(CO)Ph	100	-	-
2	Ph(CO)CH ₃	85	15	<1
3	CH ₃ (CO)CH ₃	-	76	24
4	cyclohexanone	58	35	7
5	PhCH ₂ (CO)CH ₂ Ph	68	32	<1
6	adamantone	100	-	-

^a All reactions used catalyst **1.18** with the specified ketone for 16 hours at 20 °C before quenching with Me₃SiCl.

1.2.2.1 Asymmetric Hydrosilylation of Alkenes

In Section 1.2.1.2, compounds **1.6** and **1.8** (Scheme 11 and Fig. 4) were introduced as the first chiral calcium complexes to be applied to intramolecular hydroamination. These two complexes were also applied to the first and only example of asymmetric intermolecular hydrosilylation along with compound **1.17** (Fig. 10).⁴⁹ The results of their reaction with styrene and phenylsilane into PhCH(SiH₂Ph)CH₃ is tabulated in Table 7.

Table 7 Hydrosilylation of styrene and phenylsilane into PhCH(SiH₂Ph)CH₃.

Entry	Catalyst	mol%	T (°C)	t (h)	% Conv.	ee %
1	1.17	2.5	20	<0.1	>98	0
2	1.6	2.5	50	16	>98	5
3	1.6 ^a	5	50	16	>98	9
4	1.8 ^a	5	50	16	>98	9

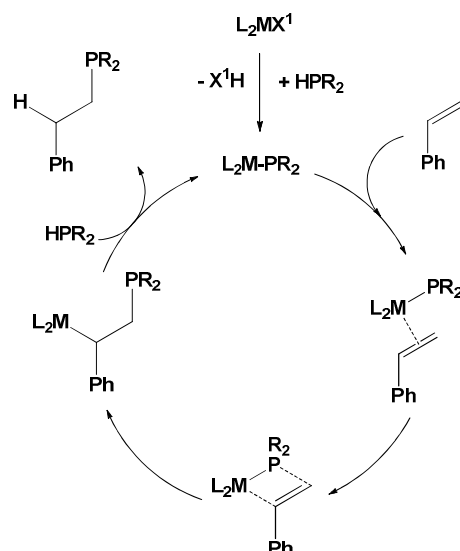
^a 1:1 mixture of heteroleptic and homoleptic analogue.

Entries 3 and 4 were both conducted with a 1:1 mixture of heteroleptic:homoleptic complex by addition of the relevant homoleptic compound e.g. **1.7** to the solution of the redistributed heteroleptic compound, e.g. **1.6**. As briefly mentioned the increase in homoleptic compound concentration can steer the redistribution equilibrium to form the heteroleptic compound and minimise the presence (<2%) and thus impact of $[\text{Ca}\{\text{N}(\text{SiMe}_3)_2\}_2(\text{THF})_2]$. As with hydroamination the authors also note inactivity of the homoleptic species towards hydrosilylation.

In results that closely mirror those achieved in asymmetric hydroamination, the enantioselectivities were low (5-9% ee). Again the low selectivities are attributed to the facile ligand redistribution of the catalysts. It also suggests that the true catalytic species although proposed as L_2MH (Scheme 18) may be CaH_2 if L_2MH undergoes ligand redistribution that heavily favours the formation of homoleptic $\text{Ca}(\text{L}_2)_2$ complex and CaH_2 . Evidence for this is provided by the authors' observation that addition of PhSiH_3 to heteroleptic **1.6** resulted in the exclusive formation of homoleptic **1.7** and CaH_2 and presumably $\text{PhSiH}_2\text{N}(\text{SiMe}_3)_2$.

1.2.3 Hydrophosphination

Hydrophosphination is the addition of P-H to an unsaturated C-C bond allowing the synthesis of a variety of phosphines that are often utilised as ligands in traditional transition metal chemistry. The catalytic cycle for hydrophosphination is presented in Scheme 21 and is reminiscent of both those presented for hydroamination (Scheme 9, Section 1.2.1) and hydrosilylation (Scheme 18, Section 1.2.2). Like intermolecular hydroamination and hydrosilylation, hydrophosphination is entropically disfavoured. A consequence of this is substrates suitable for intermolecular hydrophosphination (like those used in hydrosilylation) also need to be activated. Steric hindrance around the alkene moiety is known to affect substrates that can undergo intermolecular hydrophosphination, where sufficient steric impeachment around the substrate unsaturation can result in reduced or nil activity.¹⁰⁸ For comparison lanthanides are known to facilitate both inter- and intramolecular hydrophosphination.¹⁰⁹



Scheme 21 Proposed mechanism for the organocalcium mediated hydrophosphination of styrene. (L_2 = bidentate mono-anionic ligand; $M = Ca$; X^1 = anionic σ -bound species, for example $[N(SiMe_3)_2]^-$ or $[C(SiMe_3)_3]^-$).

Hill *et al.* published the first example of an organocalcium complex applied to intermolecular hydrophosphination in 2007 using the increasingly exploited BDI supported calcium complex **1.1**.¹⁰⁸ Hill and co-workers were able to successfully hydrophosphinate a small range of substrates (Table 8). Generally reaction conditions are more forcing for these examples of hydrophosphination than those of hydrosilylation or hydroamination. Of particular interest is the apparent trend for formation of the *syn* (*cis*) addition products which are said to be *anti*-Markovnikov as addition of the phosphine moiety occurs at the least sterically hindered/substituted carbon. In systems containing multiple instances of C=C bonds hydrophosphination occurs again at the least substituted C=C site leading to strict regioselectivity. Reactivity is also dictated by the steric demands of the alkene, more hindered substrates such as α -methylstyrene, 1,2-diphenylethylene, and *trans*-stilbene did not readily react under similar conditions to the substrates used in entries 1-4 Table 8.

The use of more activated alkenes hydrophosphination (i.e. 2-vinyl-pyridine cf. styrene), caused vinyl-polymerisation to become more favourable over hydrophosphination. This is not entirely unexpected since the polymerisation of 2-vinylpyridine has long been reported to be possible with the heavier AE metals.¹⁰ This result suggests that competition occurs between the rate of substrate insertion into the Ca-C σ -bond and that of the σ -bond metathesis step mediated by the phosphine substrate. This preference for polymerisation

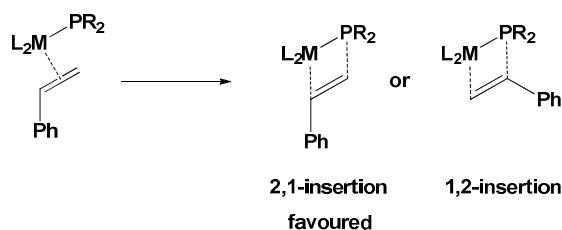
over hydrophosphination holds true regardless of addition of excessive amounts of the phosphine reagent in an attempt to promote hydrophosphination.

The authors allude that exclusive regioselectivity (2,1-addition) observed with styrene (entry 1) is again a result of a preferential geometry of the benzylcalcium intermediate $[L_2Ca\text{C}\underline{H}PhCH_2(PR_2)]$, which is formed by reaction of the calcium catalyst with a molecule of styrene. The insertion between the calcium and the α -carbon to the phenyl results in a more stable complex conformation. If addition had occurred at the least substituted carbon of the C=C forming $[L_2Ca\text{C}\underline{H}_2CHPh(PR_2)]$ the intermediate would be less stable and thus more reactive (Scheme 22). The 2,1-addition intermediate is more stable than the 1,2-addition intermediate due to the effect of the phenyl substituent on stabilising the developing anionic charge. Due to calcium's ionic bonding when the reaction proceeds via a 2,1-addition, the phenyl group is able to assist in stabilising the developing anionic charge on the α -carbon to the phenyl ring, adjacent to the calcium centre, lowering the activation energy required in the insertion step (Scheme 22).

Table 8 Hydrophosphination of alkenes with Ph_2PH and 10 mol% of **1.1** in C_6D_6 .

Entry	Substrate	Product(s)	T (°C)	t (h)	Conv. (%)
1			75	20	95
2			25	24	95
3			75	24	78
4			75	13	94 ^a

^a 20 mol % catalyst.



Scheme 22 Preferred 2,1-addition for styrene with calcium (L_2 = bidentate mono-anionic ligand; $\text{M} = \text{Ca}$; X^1 = anionic σ -bound species, for example $[\text{N}(\text{SiMe}_3)_2]^-$ or $[\text{C}(\text{SiMe}_3)_3]^-$).

In addition Hill and co-workers found that hydrophosphination was unsuccessful between diphenylphosphine (Ph_2PH) and diphenylethyne ($\text{Ph-C}\equiv\text{C-Ph}$) with 10 mol% $[\text{Ca}\{\text{N}(\text{SiMe}_3)_2\}(\text{THF})_2]$ in C_6D_6 , instead affording the insoluble $[\text{Ca}(\text{PPh}_2)_2(\text{THF})_4]$. This raises two points, the first being that a heteroleptic calcium complex (LCaX) is required in the hydrophosphination cycle, not a homoleptic one (L_2Ca) as seen by the isolation of **1.20** (fig. 13). Secondly $[\text{Ca}(\text{PPh}_2)_2(\text{THF})_4]$ is known to be catalytically active in the hydrophosphination of diphenylethyne and/or diphenylbutadiyne with diphenylphosphine.¹¹⁰ The authors reasoned that the suppression of catalytic activity was simply due to the complexes low solubility in C_6D_6 , whereas the original report by Wasterhausen *et al.* conducted reactions in THF.

The proposed reaction mechanism (Scheme 21) has been derived from the isolation of complex **1.20** (Fig. 13). **1.20** was proven catalytically active and the addition of 10 mol% to a solution of diphenylphosphine and styrene resulted in the successful hydrophosphination of the substrates. This evidence lends support to the formation of a calcium-phosphine complex able to undergo further reaction. Further evidence for this mechanism was provided by reaction of **1.20** with an excess of diphenylethyne ($\text{Ph-C}\equiv\text{C-Ph}$) and 1 equivalent of $\text{HN}(\text{SiMe}_3)_2$. It was observed that after 45 minutes at 75 °C in C_6D_6 a 1:1 mixture of (*E*)- $\text{PhC(H)-C(PPh}_2\text{)Ph}$ and the calcium bis(trimethylsilyl)amide complex **1.1** was formed.

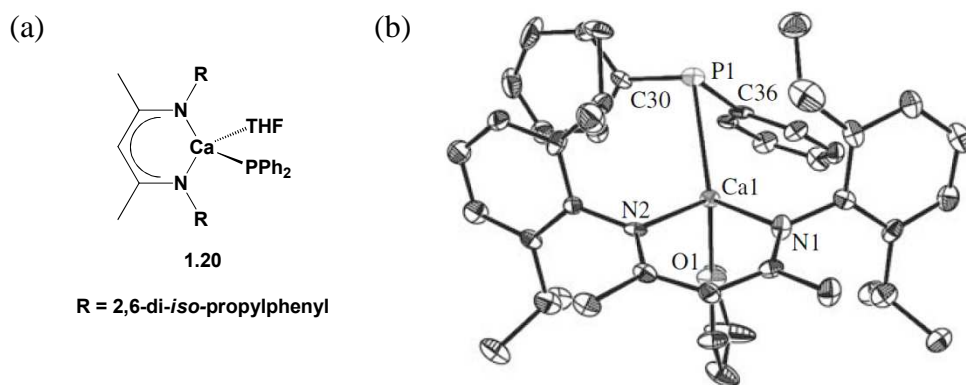


Fig. 13 (a) complex **1.20** and (b) ORTEP representation of **1.20** thermal ellipsoids at 20% probability with H atoms omitted for clarity.¹⁰⁸

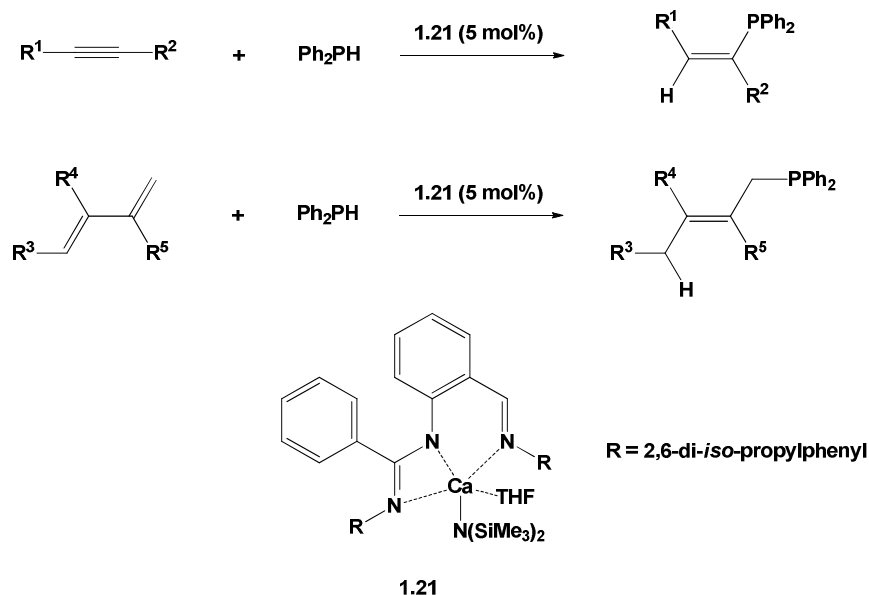
These two reactions indicate that initially the calcium catalyst L_2MX^1 reacts with PHR_2 to afford L_2MPR_2 with the concomitant formation of X^1H . The newly formed calcium-phosphine (e.g. **1.20**) undergoes further reactivity from the insertion of the alkene or alkyne substrate into the Ca-P σ -bond, before the phosphide complex is regenerated by further reaction with the phosphine, generating the phosphine product.

The latest contribution to calcium catalysed intermolecular hydrophosphination of alkenes and alkynes was reported by Hu and Cui.¹¹¹ The authors use a tridentate amidinate supported calcium amide, compound **1.21** (Scheme 23). **1.21** proves to be a robust complex showing no decomposition or ligand redistribution even at 160 °C which is indicative of the excellent stabilising properties of the tridentate amidinate ligand. Compound **1.21** is monomeric in the solid state, taking a 5-coordinate calcium centre and adopting a tetragonal pyramid geometry.

The catalytic ability of **1.21** was tested over a range of intermolecular hydrophosphination reactions involving 1,3-conjugated dienes, alkynes and sterically hindered alkenes. Like preceding hydrophosphination catalysts **1.21** is not active for unactivated C=C substrates, for example 1-hexene or 4-hexyne, instead showing moderate activity for activated substrates with yields of 72-100% obtained within 2-24 hours at temperatures between 25 and 75 °C.

Even so this activity is higher than the previous examples like **1.1** for instance. Of particular note is the ability of **1.21** to catalyse the hydrophosphination of α -methylstyrene and *cis*-stilbene, both substrates that complex **1.1** was unable to catalyse. In the tested reactions both sterically hindering and electron-donating groups on substrates resulted in

lower yields. Also noteworthy is the excellent regioselectivity induced by **1.21** in many of the products. As previously discussed all products formed are consistent with 2,1-insertions (Scheme 22). The predominance of *Z*-isomer products is dissimilar to that typically achieved with calcium BDI supported complex **1.1**.



Scheme 23 Hydrophosphination of alkenes and alkynes with catalyst **1.21**.

1.2.3.1 – Hydrophosphination of Carbodiimides

Hill *et al.* contributed further findings to the area of hydrophosphination in 2008 investigating the hydrophosphination of carbodiimides (Scheme 24).¹¹² They showed that synthesis of phosphaguanidies was possible in a similar manner to the synthesis of guanidine derivatives produced by hydroamination.⁸⁸ Their study incorporated all the heavier AE elements and the catalyst structure employed was again metal analogues of complex **1.1** with the other AE congeners. They report the reaction between diphenylphosphine and 1,3-di-*iso*-propylcarbodiimide catalysed by 1.5 mol% of **1.1**.



Scheme 24 Hydrophosphination of carbodiimides mediated by calcium.

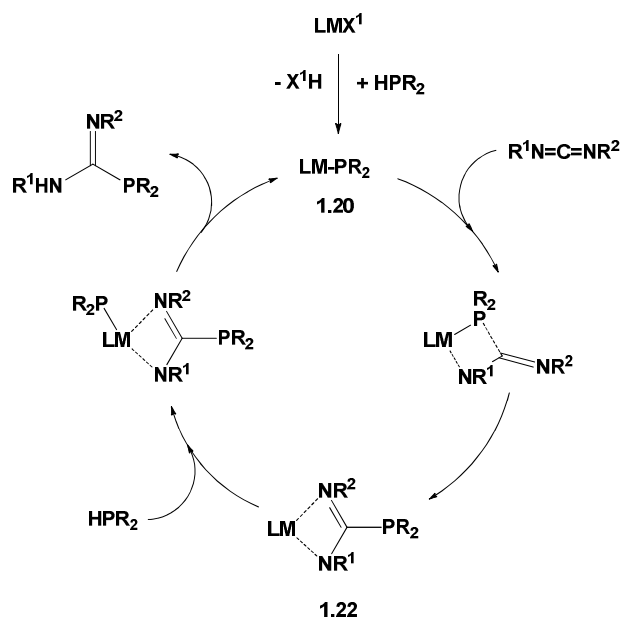
The reaction progressed under ambient temperature to give a yield of 99% after 6 hours, although it was 90% complete after 1 hour. This is remarkable considering the very mild reaction conditions (this reaction does not proceed without a catalyst).

Catalyst loadings are significantly lower than the typical 10-20 mol% used in many of the reactions discussed within this Chapter. This is also the same for the two other calcium amides probed, $[\text{Ca}\{\text{N}(\text{SiMe}_3)_2\}_2(\text{THF})_2]$ and THF-free analogue $[\text{Ca}\{\text{N}(\text{SiMe}_3)_2\}_2]$ which were used at 2 and 3 mol% in the same reaction respectively, achieving similar yields of >95% in a shorter duration (between 1-4 hours depending on the substrate). Whilst the substrates 1,3-di-*iso*-propylcarbodiimide and 1,3-dicyclopentylcarbodiimide were readily converted to their corresponding phosphaguanidine products, the more sterically demanding 1,3-di-*tert*-butylcarbodiimide and 1,3-dicyclohexylcarbodiimide analogues proved unreactive under these conditions. It is likely the steric bulk of these substrates inhibit the reaction by preventing coordination of the carbodiimide to the calcium centre.

Changing the phosphine from diphenylphosphine to dicyclohexylphosphine suppressed catalytic activity. The authors hypothesise that in this case the reduced acidity of the dicyclohexylphosphine compared to that of the diphenylphosphine could be a contributing factor meaning the catalyst activation step was left uninitiated. ^{31}P NMR studies were undertaken to probe this postulation. They found no resonances relating to the initial protonolysis step (formation of L_2MPR_2).

The homoleptic calcium amide complexes are more catalytically active than that of heteroleptic **1.1**. This is in contrast to that of the hydrophosphination of alkenes which depended upon a heteroleptic complex as the active species (**1.20**, Fig. 13 and Scheme 21). The catalytic cycle shown in Scheme 25 summarises the proposed reaction mechanism.

The initiation step is thought to be through the formation of the calcium-alkylphosphine (LM-PR_2 , e.g. **1.20**, Fig. 13), since reaction of **1.1** with just the carbodiimide yielded no insertion products even under prolonged conditions of 60 °C. Rapid insertion of the carbodiimide into the Ca-P σ -bond occurs allowing formation of the phosphaguanidinate (step 2, Scheme 25). Isolation and solid state characterisation by single crystal X-ray crystallography has been accomplished on the phosphaguanidinate (**1.22**, Fig. 14). Complex **1.22** was also determined to be monomeric in nature in a solution of C_6D_6 .



Scheme 25 Proposed mechanism for the organocalcium mediated hydrophosphination of carbodiimides. (L = β -diketimidato ligand **1.1**; M = Ca; X¹ = anionic σ -bound species, for example [N(SiMe₃)₂]).

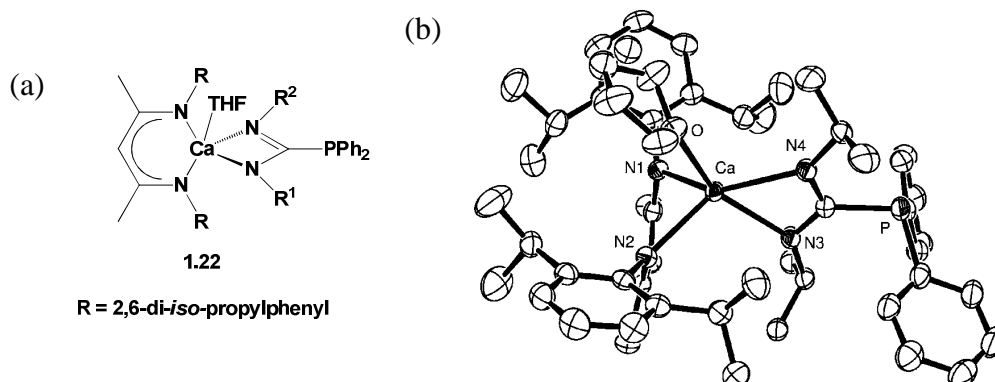


Fig. 14 (a) complex **1.22** and (b) ORTEP representation of **1.22** thermal ellipsoids at 50% probability with H atoms omitted for clarity.¹¹²

Interestingly no activity was observed when the isolated analogue of the proposed catalyst resting state, complex **1.22**, had diphenylphosphine added to it. Based upon behaviour of similar systems we might have expected to observe the protonolysis of the diphenylphosphine and the σ -bond metathesis step resulting in the formation of the phosphaguanidine and the reformation of [LM-PPh₂]. Instead no activity was observed until additional carbodiimide substrate was added to the mixture whereupon catalytic turnover leading to phosphaguanidine product was observed.

An equilibrium occurring between the calcium-phosphaguanidinate complex **1.22** and HPPh_2 , as well as **1.20** and the phosphaguanidine product formed at the end of the catalytic cycle, was suggested as a rationale for these observations. With these two equilibria present in solution, **1.20** is assumed to be present at low concentrations, however readily reacts with a molecule of carbodiimide substrate to form **1.22** allowing for catalyst turnover and product formation. It was suggested that like all heterofunctionalisations concerning calcium they proceed first by substrate insertion followed by σ -bond metathesis to yield the product. However in this case there was also a degree of reversibility with respect to both steps presented in this reaction mechanism.

1.2.4 Hydrogenation

The field of hydrogenation has thus far been monopolised by the use of d-block metals and so the discovery of an alternative should be regarded as somewhat of a breakthrough. C-H bond formation through the addition of hydrogen to an unsaturated bond has so far only been investigated using calcium compounds from the heavier AE metals. An extension of their hydrosilylation investigations utilising the chiral calcium complex **1.18** (Fig. 11), Harder and co-workers reported the first calcium mediated hydrogenation of a number of styrene derivatives in 2008.¹¹³

Successful hydrogenation of a range of substrates; 1,1-diphenylethene (DPE), 1,3-cyclohexadiene, and α -methylstyrene was effected using compounds **1.17** ($[\text{Ca}(\text{Me}_2\text{N}(\text{C}_6\text{H}_4)\text{CHSiMe}_3)_2(\text{THF})_2]$) and **1.18** ($[\text{CaH}(\text{BDI})(\text{THF})]_2$), and no reaction was observed with CaH_2 (Table 9). Reaction conditions were mild with temperatures ranging from ambient to 60 °C, under a 20 bar atmosphere of H_2 . In a similar fashion to the hydrosilylation reactions conducted using the same two catalysts it was noted that the reaction outcome was sensitive to solvent polarity. In THF or mixtures of THF / HMPA (entries 4-6) reactions proceeded at lower temperatures and with shorter reaction times than in benzene. Reactions in benzene were often accompanied with small quantities of precipitate, presumably insoluble dimeric material. The source of this dimeric material (in the case of DPE being the substrate, 1,1,3,3-tetraphenylbutane) has been suggested as the outcome of reaction between a molecule of DPE substrate and $(\text{Ph}_2\text{CCH}_3)^-$.

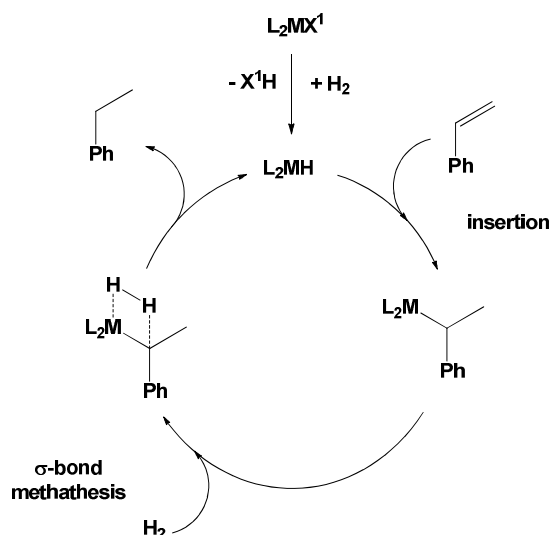
The anion $(\text{Ph}_2\text{CCH}_3)^-$ being a direct result of insertion of a molecule of DPE substrate into the catalyst (Scheme 26). For the hydrogenation of styrene (entries 2, 3, and 7) apolar solvents were required to prevent the formation of polystyrene; the use of THF or THF/HMPA mixtures resulted in the complete suppression of hydrogenation in favour of polymerisation.

Table 9 Hydrogenation of activated alkenes by calcium complexes **1.17** and **1.18**.

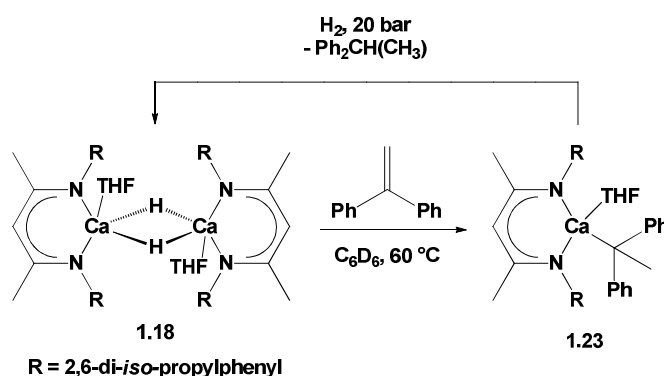
Entry	Substrate	Cat.	Cat. Mol%	Solvent	T (°C)	t (h)	Conv. (%)	Product
1	DPE	1.18	5	C_6H_6	60	17	49	Ph_2CHCH_3
2	Styrene	1.18	5	C_6H_6	20	15	97 ^a	PhCH_2CH_3
3	α -methylstyrene	1.18	5	C_6H_6	60	25	60	$\text{PhCH}(\text{CH}_3)_2$
4	DPE	1.17	2.5	C_6H_6	60	17	41	Ph_2CHCH_3
5	DPE	1.17	2.5	THF	20	3.5	92 ^b	Ph_2CHCH_3
6	DPE	1.17	2.5	THF/ HMPA ^d	20	1.5	96 ^c	Ph_2CHCH_3
7	Styrene	1.17	2.5	C_6H_6	20	15	85 ^e	PhCH_2CH_3
8	cyclohexadiene	1.17	2.5	C_6H_6	20	22	96 ^f	Cyclohexene

^a total conversion >99% with 3% dimeric material. ^b total conversion 94% with 2% dimeric material. ^c total conversion >99% with 4% dimeric material. ^d 7% mixture of HMPA. ^e total conversion >99% with 15 oligomeric material. ^f traces of dimeric material observed.

The catalytic cycle presented in Scheme 26 depicts the hydrogenation of styrene with H_2 , as a representative activated alkene. Support for this mechanism was obtained by the reaction between complex **1.18** with DPE (Scheme 27). The insertion of one equivalent of DPE into the organocalcium complex resulting in complex **1.23**, which was isolated and characterised via single crystal structure determination.¹¹³ In addition, under mild conditions (20 °C, 20 bar H_2) complex **1.18** was reformed alongside the hydrogenated product $\text{Ph}_2\text{CH}(\text{CH}_3)$. The subsequent hydrogenation step of **1.23** was significantly faster in polar solvents such as THF than in benzene (5 min. cf. 15 h).



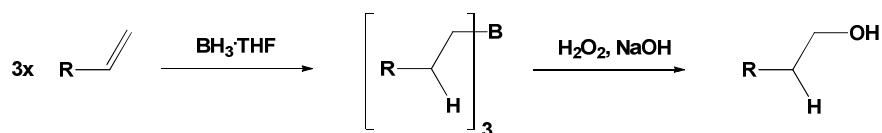
Scheme 26 Proposed mechanism for the organocalcium mediated hydrogenation of styrene. (L_2 = bidentate mono-anionic ligand; $M = Ca$; X^1 = anionic σ -bound species, for example $[N(SiMe_3)_2]^-$ or $[C(SiMe_3)_3]^-$).



Scheme 27 Stoichiometric addition of calcium hydride complex **1.18** to DPE and subsequent protonation of the reactive intermediate by H_2 .

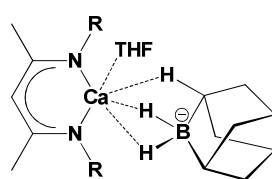
1.2.5 Hydroboration of Alkenes

Hydroboration is a synthetically useful reaction allowing for the preparation of boron-functionalised molecules that can subsequently undergo further reaction to create useful substrates like alcohols or amines (Scheme 28). Until recently, AE mediated hydroboration of alkenes had remained unreported, although it is a known reaction with lanthanides.⁷⁶⁻⁷⁸ Harder and Spielmann investigated the employment of **1.18** (Fig. 11) but later went on to expand their investigations using complexes **1.17** (Fig. 10) and **1.24** (Fig. 15).¹¹⁴



Scheme 28 Hydroboration of an alkene with subsequent conversion to an alcohol.

An activated alkene, a common substrate requirement for heterofunctionalisation reactions was once again necessary. 1,1-diphenylethylene (DPE) was again chosen as the model substrate due to its inert reactivity towards polymerisation. Uncatalysed reaction does not readily occur between DPE and catecholborane (1,3,2-benzodioxaborole, HBCat) at room temperature, instead requires heating to 100 °C. Under these conditions 96% substrate conversion to the boronic ester ($\text{Ph}_2\text{CHCH}_2\text{Bcat}$) is achieved in 20 hours. 2.5 mol% of **1.18** takes 72 hours to achieve the same level of conversion, whilst allowing the reaction to proceed under ambient conditions highlighting the influence of the metal. Catalyst **1.17** achieves 90% conversion in 20 hours at 50 °C. It should be noted that the aforementioned reactions took place without addition of solvent. When these reactions are conducted in solvent both reaction times increase three-fold and yields drop, in some cases up to 60%.

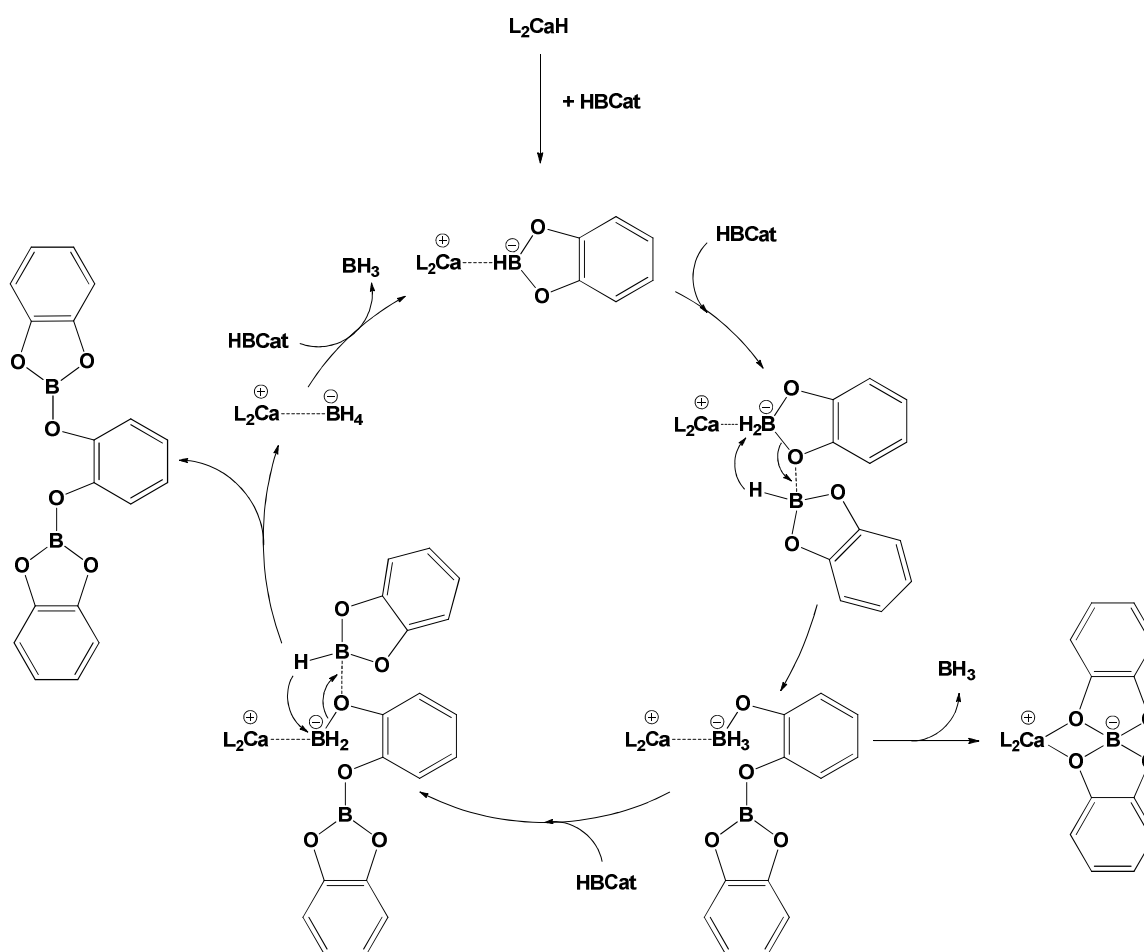


1.24

R = 2,6-di-*iso*-propylphenyl

Fig. 15 Calcium compound **1.24**.

When compounds **1.18**, **1.17** and **1.24** were applied to the hydroboration of DPE with HBCat they were shown to be catalytically active, however contrary to the expected boronic esters ($\text{Ph}_2\text{CHCH}_2\text{OBCat}$), the product was a borane: $(\text{Ph}_2\text{CHCH}_2)_3\text{B}$. From this result the authors suggest that these catalysts cannot be regarded as “true” catalyst, but go on to liken them to a “Trojan horse” type reaction. In this case the “catalysts” accelerate the decomposition of the HBCat to $\text{B}_2(\text{Cat})_3$ and BH_3 , with BH_3 being the true active species. The fact the reactive species is BH_3 prohibits any control over chemo-, regio- or enantioselectivity through catalyst design. The authors careful analysis of the reaction products allowed for the tentative proposal of the mechanism presented in Scheme 29.

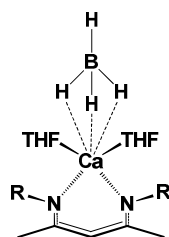


Scheme 29 Proposed mechanism for the calcium assisted hydroboration of HBCat.

One of the key intermediate species, L_2Ca-BH_4 has been prepared by reaction of **1.18** with $BH_3(SMe_2)$. The resulting product has been characterised in the solid state as monomeric BDI supported complex $[(CH(C(CH_3)N(C_6H_3^iPr)_2)Ca\{BH_4\}(THF)_2]$, bearing a coordinated BH_4 moiety and two THF molecules. It takes a tetragonal pyramid conformation with the BH_4 capping 3 hydrogens to be a κ^3 -anionic ligand (**1.25**, Fig. 16).

The authors also report that reaction of **1.18** with pinacolborane (4,4,5,5-tetramethyl-1,3,2-dioxaborolane, HBPIn) resulted in the formation of a trimeric species $[(CH(C(CH_3)N(C_6H_3^iPr)_2)Ca\{H_2BPIn\})_3]$. Trimeric calcium species are known,²⁹ moreover reaction of the trimer with DPE did not result in any reaction. This further exemplifies that hydroboration does not occur via reaction between the alkene and H_2BPIn^- anion.

In light of the true catalytic species being BH_3 and ligand design being currently inconsequential, use of calcium borohydride ($\text{Ca}(\text{BH}_4)_2$) provides a cost-effective and less moisture sensitive alternative to the aforesaid complexes. The use of $\text{Ca}(\text{BH}_4)_2$ has been shown to be an effective and a remarkably selective catalyst in the presence of ethylacetate to produce alcohols from terminal alkenes.¹¹⁵



1.25

R = 2,6-di-*iso*-propylphenyl**Fig. 16** Calcium hydroboration intermediate compound **1.25**.

In summary the use of organocalcium compounds over an impressive range of molecular reactions has arisen from the rapid expansion of studies concerning this area over recent years. Due to its attractive properties as a catalyst development of organocalcium compounds continues to swell alongside our knowledge of these systems. Whilst these developments have led to a higher degree of understanding, progress concerning asymmetric application of organocalcium compounds is severely underdeveloped in comparison. To develop high-performing, selective catalysts, a better insight into the chemical/structural features necessary to achieve this is urgently required. It is hoped that when added to the current asymmetric examples, the work contained within this Thesis will help reduce this void in the literature and provide a key starting point for the production of the next generation of asymmetric calcium catalysts.

1.3 References

1. D. Seyferth, *Organometallics*, **2009**, 28, 1598.
2. W. D. Buchanan, D. G. Allis and K. Ruhlandt-Senge, *Chem. Commun.*, **2010**, 46, 4449.
3. S. Harder, *Chem. Rev.*, **2010**, 110, 3852.
4. P. T. Anastas and J. C. Warner, *Green Chemistry: Theory and Practice*, Oxford University Press, New York, 1998.
5. R. Morris Bullock, *Catalysis Without Precious Metals*, Wiley-VCH, Weinheim, 2010.
6. J. I. van der Vlugt, *Eur. J. Inorg. Chem*, **2012**, 363.
7. S. Gilroy, P. C. Bethke and R. L. Jones, *J. Cell Sci.*, **1993**, 106, 453.
8. S. R. Taylor, *Geochimica et Cosmochimica Acta*, **1964**, 28, 1273.
9. S. Harder, F. Fiel and A. Weeber, *Organometallics*, **2001**, 20, 1044.
10. W. E. Lindsell, F. C. Roberston and I. Soutar, *Eur. Polym. J.*, **1983**, 19, 115.
11. F. Feil and S. Harder, *Eur. J. Inorg. Chem*, **2003**, 18, 3401.
12. D. F.-J. Piesik, K. Häbe and S. Harder, *Eur. J. Inorg. Chem*, **2007**, 5652.
13. Z. Zhong, P. J. Dijkstra, C. Birg, M. Westerhausen and J. Feijen, *Macromolecules*, **2003**, 34, 3863.
14. Z. Zhong, P. Schneiderbauer, P. J. Dijkstra and M. Westerhausen, *Polym. Bull*, **2003**, 51, 175.
15. P. Lecomte and R. Jérôme, *Ring Opening Polymerization*, John Wiley & Sons, Inc., 2004.
16. M. H. Chisholm, J. Gallucci and K. Phomphrai, *Chem. Commun.*, **2003**, 48.
17. D. J. Darensbourg, W. Choi, O. Karroonnirun and N. Bhuvanesh, *Macromolecules*, **2008**, 41, 3493.
18. D. J. Darensbourg, W. Choi and C. P. Richers, *Macromolecules*, **2007**, 40, 3521.
19. D. J. Darensbourg, W. Choi, P. Ganguly and C. P. Richers, *Macromolecules*, **2006**, 39, 4374.
20. H.-Y. Chen, H.-Y. Tang and C.-C. Lin, *Polymer*, **2007**, 48, 2257.
21. Y. Sarazin, R. H. Howard, D. L. Hughes, S. M. Humphrey and M. Bochmann, *Dalton Trans.*, **2006**, 340.
22. M. G. Cushion and P. Mountford, *Chem. Commun.*, **2011**, 47, 2276.

23. L. Clark, M. G. Cushion, H. E. Dyer, A. D. Schwarz, R. Duchateau and P. Mountford, *Chem. Commun.*, **2010**, 46, 273.
24. B. Liu, T. Roisnel, J.-P. Guégan, J.-F. Carpentier and Y. Sarazin, *Chem. Eur. J.*, **2012**, Advanced Article.
25. Y. Sarazin, D. Rosca, V. Poirier, T. Roisnel, A. Silverstru, L. LMaron and J.-F. Carpentier, *Organometallics*, **2010**, 29, 6569.
26. M. Helou, O. Miserque, J.-M. Brusson, J.-F. Carpentier and S. M. Guillaume, *Chem. Cat. Chem.*, **2010**, 2, 306.
27. N. Ajellal, J.-F. Carpentier, C. Guillaume, S. M. Guillaume, M. Helou, V. Poirier, Y. Sarazin and A. Trifonov, *Dalton Trans.*, **2010**, 39, 8363.
28. V. Poirier, T. Roisnel, J.-F. Carpentier and Y. Sarazin, *Dalton Trans.*, **2009**, 9820.
29. S.-M. Ho, C.-S. Hsiao, A. Datta, C.-H. Hung, L.-C. Chang, T.-Y. Lee and J.-H. Haung, *Inorg. Chem.*, **2009**, 48, 8004.
30. T. Suzuki, N. Yamagiwa, Y. Matsuo, S. Sakamoto, K. Yamaguchi, M. Shibasaki and R. Noyori, *Tetrahedron Lett.*, **2001**, 42, 4669.
31. Y. M. A. Yamada and S. Ikegami, *Tet. Lett.*, **2000**, 2165.
32. S. Saito and S. Kobayashi, *J. Am. Chem. Soc.*, **2006**, 128, 8704.
33. G. Kumaraswamy, N. Jena, M. N. V. Sastry and P. B. Markondaiah, *Adv. Syn. Catal.*, **2005**, 347, 867.
34. S. Kobayashi and Y. Yamashita, *Accounts of Chemical Research*, **2010**, 44, 58.
35. M. R. Crimmin, A. G. M. Barrett, M. S. Hill and P. A. Procopiou, *Org. Lett.*, **2007**, 9, 331.
36. G. Kumaraswamy, M. N. V. Sastry, N. Jena, K. R. Kuma and M. Vairamani, *Tetrahedron: Asymmetry*, **2003**, 14, 3797.
37. L. Orzechowski, G. Jansen and S. Harder, *J. Am. Chem. Soc.*, **2006**, 128, 14676.
38. L. Orzechowski, G. Jansen, M. Lutz and S. Harder, *Dalton Trans.*, **2009**, 2958.
39. M. J. Vanden Eynden, K. Kunchithapatham and J. P. Stambuli, *J. Org. Chem.*, **2010**, 75, 8542.
40. M. J. Vanden Eynden and J. P. Stambuli, *Org. Lett.*, **2008**, 10, 5289.
41. A. G. M. Barrett, M. R. Crimmin, M. S. Hill, P. B. Hitchcock, S. L. Lomas, P. A. Procopiou and K. Suntharalingam, *Chem. Commun.*, **2009**, 2299.
42. A. G. M. Barrett, M. R. Crimmin, M. S. Hill, P. B. Hitchcock, G. Kociok-Kohn and P. A. Procopiou, *Inorg. Chem.*, **2008**, 47, 7366.
43. F. Buch and S. Harder, *Organometallics*, **2007**, 26, 5132.

44. A. Torvisco, A. Y. O'Brien and K. Ruhlandt-Senge, *Coord. Chem. Rev.*, **2011**, 255, 1268.
45. J. S. Alexander and K. Ruhlandt-Senge, *Eur. J. Inorg. Chem*, **2002**, 2761.
46. J. S. Alexander and K. Ruhlandt-Senge, *Chem. Eur. J.*, **2004**, 10, 1274.
47. M. Westerhausen, *Coord. Chem. Rev.*, **1998**, 176, 157.
48. C. Eaborn, K. Izod and D. J. Smith, *J. Organomet. Chem.*, **1995**, 500, 89.
49. F. Buch and S. Harder, *Z. Naturforsch.*, **2008**, 63b, 169.
50. C. Ruspic and S. Harder, *Inorganic Chemistry*, **2007**, 46, 10426.
51. M. R. Crimmin, I. J. Casely and M. S. Hill, *J. Am. Chem. Soc.*, **2005**, 127, 2042.
52. D. C. Bradley, M. B. Hursthouse, A. A. Ibrahim, K. M. Abdul Malik, M. Motevalli, R. Moseler, H. Powell, J. D. Runnacles and A. C. Sullivan, *Polyhedron*, **1990**, 9, 2959.
53. A. Asadi, A. G. Avent, M. P. Coles, C. Eaborn, P. B. Hitchcock and D. J. Smith, *J. Organomet. Chem.*, **2004**, 689, 1238.
54. M. Harvey, T. P. Hanusa and V. G. Young Jr., *Angew. Chem. Int. Ed*, **1999**, 38, 217.
55. P. Jochmann, T. S. Dols, T. P. Spaniol, L. Perrin, L. Maron and J. Okuda, *Angew. Int. Ed. Engl*, **2009**, 48, 5715.
56. M. R. Crimmin, A. G. M. Barrett, M. S. Hill, D. J. MacDougall, M. F. Mahon and P. A. Procopiou, *Chem. Eur. J.*, **2008**, 14, 11292.
57. F. Feil and S. Harder, *Organometallics*, **2000**, 19, 5010.
58. C. Eaborn, S. A. Hawkes, P. B. Hitchcock and J. D. Smith, *Chem. Commun.*, **1997**, 1961.
59. T. P. Hanusa, *Coord. Chem. Rev.*, **2000**, 210, 329.
60. S. Harder, *Angew. Chem. Int. Ed*, **2004**, 43, 2714.
61. A. G. M. Barrett, M. R. Crimmin, M. S. Hill and P. A. Procopiou, *Proc. R. Soc. A*, **2010**, 466, 927.
62. S. Hong and T. J. Marks, *Acc. Chem. Res.*, **2004**, 37, 673.
63. I. Aillaud, J. Collin, J. Hannedouche and E. Schulz, *Dalton Trans.*, **2007**, 5105.
64. S. Hong, S. Tian, M. V. Metz and T. J. Marks, *J. Am. Chem. Soc.*, **2003**, 125, 14768.
65. N. Meyer, A. Zulys and P. W. Roesky, *Organometallics*, **2006**, 25, 4179.
66. J. Hannedouche, I. Aillaud, J. Collin, E. Schulz and A. Trifonov, *Chem. Commun.*, **2008**, 3552.

67. J. Y. Kim and L. Tom, *Org. Lett.*, **2005**, 7, 1737.
68. S. Bambirra, H. Tsurugi, D. van Leusen and B. Hessen, *Dalton Trans.*, **2005**, 1157.
69. M. A. Giardello, V. P. Conticello, L. Brard, M. R. Gagné and T. J. Marks, *J. Am. Chem. Soc.*, **1994**, 116, 10241.
70. M. R. Douglass, C. L. Stern and T. J. Marks, *J. Am. Chem. Soc.*, **2001**, 123, 10221.
71. A. M. Kawaoka, M. R. Douglass and T. J. Marks, *Organometallics*, **2003**, 22, 4630.
72. P.-F. Fu, L. Brard, L. Yanwu and T. J. Marks, *J. Am. Chem. Soc.*, **1995**, 117, 7157.
73. G. A. Molander, E. D. Dowdy and B. C. Noll, *Organometallics*, **1998**, 17, 3754.
74. G. Jeske, H. Lauke, H. Mauermann, H. Schumann and T. J. Marks, *J. Am. Chem. Soc.*, **1985**, 107, 8111.
75. G. A. Molander and J. Winterfeld, *J. Organomet. Chem.*, **1996**, 524, 275.
76. K. N. Harrison and T. J. Marks, *J. Am. Chem. Soc.*, **1992**, 114, 9220.
77. C. M. Crudden and D. Edwards, *Eur. J. Org. Chem.*, **2003**, 2003, 4695.
78. E. A. Bijpost, R. Duchateau and J. H. Teuben, *J. Mol. Cat. A Chem.*, **1995**, 121.
79. K. C. Hultsch, *Org. Biomol. Chem.*, **2005**, 3, 1819.
80. M. R. Crimmin, M. Arrowsmith, A. G. M. Barrett, I. J. Casey, M. S. Hill and P. A. Procopiou, *J. Am. Chem. Soc.*, **2009**, 131, 9670.
81. J. E. Baldwin, *J. Chem. Soc., Chem. Commun.*, **1976**, 734.
82. S. Datta, P. W. Roesky and S. Blechert, *Organometallics*, **2007**, 26, 4392.
83. T. K. Panda, C. G. Hrib, P. G. Jones, J. Jenter, P. W. Roesky and M. Tamm, *Eur. J. Inorg. Chem.*, **2008**, 4270.
84. J. Jenter, R. Köppe and P. W. Roesky, *Organometallics*, **2011**, 30, 1404.
85. S. R. Neal, A. Ellern and A. D. Sadow, *J. Organomet. Chem.*, **2011**, 696, 228.
86. A. G. M. Barrett, I. J. Casey, M. R. Crimmin, M. S. Hill, J. R. Lachs, M. F. Mahon and P. A. Procopiou, *Inorg. Chem.*, **2009**, 48, 4445.
87. M. Arrowsmith, M. S. Hill and G. Kociok-Kohn, *Organometallics*, **2009**, 28, 1730.
88. J. R. Lachs, A. G. M. Barrett, M. R. Crimmin, G. Kociok-Kohn, M. S. Hill, M. F. Mahon and P. A. Procopiou, *Eur. J. Inorg. Chem.*, **2008**, 4173.
89. A. G. M. Barrett, C. Brinkmann, M. R. Crimmin, M. S. Hill, P. Hunt and P. A. Procopiou, *J. Am. Chem. Soc.*, **2009**, 131, 12906.
90. C. Brinkmann, A. G. M. Barrett, M. S. Hill and P. A. Procopiou, *J. Am. Chem. Soc.*, **2012**, 134, 2193.

91. M. Arrowsmith, M. R. Crimmin, A. G. M. Barrett, M. S. Hill, G. Kociok-Kohn and P. A. Procopiou, *Organometallics*, **2011**, 30, 1493.
92. M. E. Jung and G. Piizii, *Chem. Rev.*, **2005**, 105, 1735.
93. J. Koller and R. G. Bergman, *Chem. Commun.*, **2010**, 46, 4577.
94. A. Mukherjee, S. Nembenna, S. T. K., S. Pillai Sarish, P. K. Ghorai, H. Ott, D. Stalke, S. K. Mandal and H. W. Roesky, *Angew. Chem. Int. Ed*, **2011**, 50, 3968.
95. T. E. Müller, K. C. Hultsch, M. Yus, F. Foubelo and M. Tada, *Chem. Rev.*, **2008**, 108, 3795.
96. H. Schumann, S. Schutte, H.-J. Kroth and D. Lentz, *Angew. Chem. Int. Ed*, **2004**, 43, 6208.
97. M. Wiecko, C. Eidamshaus, R. Köppe and P. W. Roesky, *Dalton Trans.*, **2008**, 4837.
98. Y. Li and T. J. Marks, *Organometallics*, **1996**, 15, 3770.
99. P. Horrillo-Martinez and K. C. Hultsch, *Tetrahedron Lett.*, **2009**, 50, 2054.
100. X. Zhang, T. J. Emge and K. C. Hultsch, *Angew. Chem. Int. Ed*, **2012**, 51, 394.
101. A. G. M. Barrett, T. C. Boorman, M. R. Crimmin, M. S. Hill, G. Kociok-Kohn and P. A. Procopiou, *Chem. Commun.*, **2008**, 5206.
102. A. G. M. Barrett, M. R. Crimmin, M. S. Hill, P. B. Hitchcock and P. A. Procopiou, *Dalton Trans.*, **2008**, 4474.
103. F. Feil and S. Harder, *Eur. J. Inorg. Chem*, **2005**, 4438.
104. A. G. M. Barrett, M. R. Crimmin, M. S. Hill, P. B. Hitchcock, S. L. Lomas, M. F. Mahon and P. A. Procopiou, *Dalton Trans.*, **2010**, 39, 7393.
105. F. Buch, J. Brettar and S. Harder, *Angew. Chem. Int. Ed*, **2006**, 45, 2741.
106. J. Spielmann and S. Harder, *Eur. J. Inorg. Chem*, **2008**, 1480.
107. B. Marciniak, *Hydrosilylation: a comprehensive review on recent advances*, 1 edn., Springer, 2009.
108. M. R. Crimmin, A. G. M. Barrett, M. S. Hill, P. B. Hitchcock and P. A. Procopiou, *Organometallics*, **2007**, 26, 2953.
109. K. Takaki, K. Komeyama and K. Takehira, *Tetrahedron*, **2003**, 59, 10381.
110. T. M. A. Al-Shboul, H. Görls and M. Westerhausen, *Inorg. Chem. Commun.*, **2008**, 11, 1419.
111. H. Hu and C. Cui, *Organometallics*, **2012**, 31, 1208.
112. M. R. Crimmin, A. G. M. Barrett, M. S. Hill, P. B. Hitchcock and P. A. Procopiou, *Organometallics*, **2008**, 27, 497.

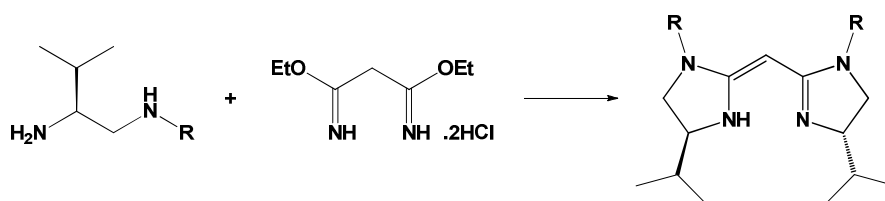
113. J. Spielmann, F. Buch and S. Harder, *Angew. Int. Ed.*, **2008**, 47, 9434.
114. S. Harder and J. Spielmann, *J. Organomet. Chem.*, **2012**, 698, 7.
115. S. Narasimhan, K. Ganeshwar Prasad and S. Madhavan, *Tet. Lett.*, **1995**, 36, 1141.

Chapter Two

Chiral Ethylene Diamine Synthesis

2.1 Introduction

Synthesis of the C_2 -symmetric bisimidazoline (R-BIM) ligands discussed in Chapter 4 can be realised from the condensation of two equivalents of a chiral ethylene diamine with one equivalent of diethylmalonimidate dihydrochloride (Scheme 1).^{1,2} To later probe R-BIMs as supporting ligands for calcium complexes, an efficient synthetic pathway for producing the aforementioned chiral ethylene diamines is required (referred to as diamine(s) henceforth).



Scheme 1 Preparation of bisimidazoline ligands.

Currently only a small number of commercially available diamines suitable for our purposes exist where a popular choice when synthesising chiral imidazoline compounds is (*R,R*)-1,2-diphenylethylenediamine **2.1** (Fig. 1).³⁻⁸ A principal aim of this research is to fully assess with a view to better understanding the effect of varying the N-R substituent of the diamine and R-BIM ligands. Consequently it is crucial to allow the introduction of as many different alkyl/aryl groups as possible in the synthetic pathway. Given the rich availability of affordable primary amines, a synthetic methodology was developed around introduction of the N-R substituent at an early stage. Several routes were considered for assembling the library of diamines required. All routes considered are multistep processes based upon functional group conversion of an amino acid's carboxylic acid moiety to generate a second amine group. The first method examined exploits the interchange of an amino acid's carboxylic acid moiety to an acid anhydride (Section 2.2.2).

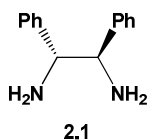


Fig. 1 Commercially available (*R,R*)-1,2-diphenylethylenediamine (**2.1**).

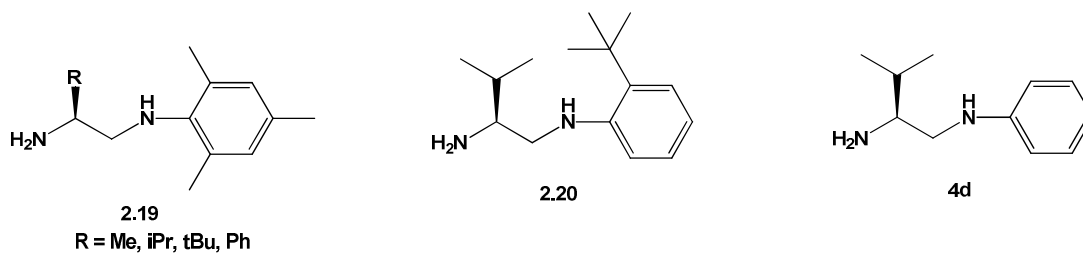
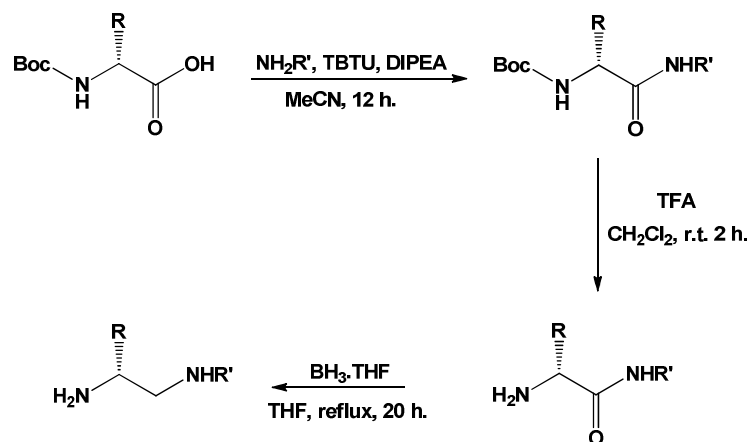


Fig. 2 Diamines synthesised via an acid anhydride methodology by Mauduit *et al.*.

Variation of this method has been used by Mauduit *et al.* to great success producing a range of diamines from their corresponding starting *tert*-butyloxycarbonyl (Boc) protected amino acid (Fig. 2).⁸ The second method involves an aziridine intermediate (Section 2.3),⁹ and the third a coupling reaction developed by Jacobsen *et al.*¹⁰ and implemented by Pfaltz *et al.* (Scheme 2).¹ The fourth method resulted from the research detailed within this Thesis and has since been published by our group (Section 2.4).¹¹ Our method makes use of converting an amino acid's carboxylic acid functionality to an acid chloride before undergoing subsequent reaction.

Routes one, three, and four all utilised an amino acid bearing a protecting group bound to the primary amine. Common examples of commercially available amino acids used in this field include L-valine **2.2**, D-phenylglycine **2.3** or L-phenylalanine **2.4** (Fig. 3). Of these routes each invokes reactivity at the carboxylic acid moiety, resulting in a more reactive intermediate. Further reaction of the newly formed intermediate with a primary amine then follows. The protecting group is then removed and the resulting amino-amide need only undergo reduction of the amide in order to obtain the diamine.



Scheme 2 Alternative diamine synthesis published by Pfaltz *et al.*.

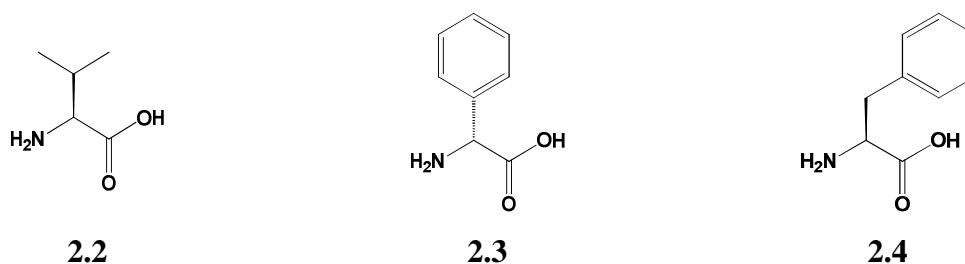


Fig. 3 Commercially available L-valine **2.2**, D-phenylglycine **2.3**, and L-phenylalanine **2.4**.

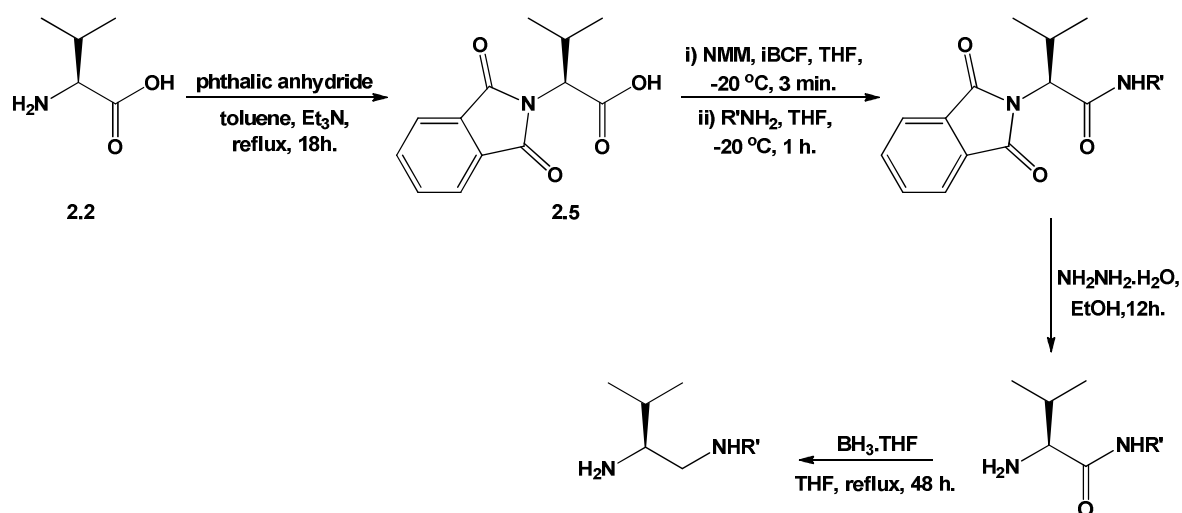
Whilst the route used by Pfaltz *et al.* in Scheme 2 may appear the most attractive due to its high yields, moderately wide substrate application, and short synthetic pathway, it is not without its drawbacks. The coupling reagent *O*-(benzotriazol-1-yl)-*N,N,N',N'*-tetramethyluronium tetrafluoroborate (TBTU) is moderately expensive and used in equimolar equivalence thus generating significant quantities of by-products. In accordance with the project aim to deliver inexpensive catalysts with minimal environmental impact, it was deemed necessary to seek an alternative method to deliver the target diamine. This is in part, the reasoning behind pursuing the various different methodologies discussed in this Chapter.

Ultimately neither the acid anhydride nor the aziridine routes delivered the target diamines. Instead the development of a new synthetic pathway was implemented. Proceeding via an acid chloride intermediate this new approach gave rise to a powerful and versatile synthetic strategy as further discussed in Section 2.4. The new pathway successfully led to the production of a host of new diamines at reduced cost compared to both Jacobsen's and Pfaltz's methods. The new methodology was also successful when scaled up. Instances of up to 14 g of pure diamine were recorded. When compared to literature reports that often deal with scales producing approximately 3 g of isolated diamine, the new methodology represents a considerable step forward.

The following sections discuss the methodologies explored en-route to establishment of the new procedure as well as addressing concerns of chiral centre racemisation during the new synthesis.

2.2 Route One – Acid Anhydride Intermediate

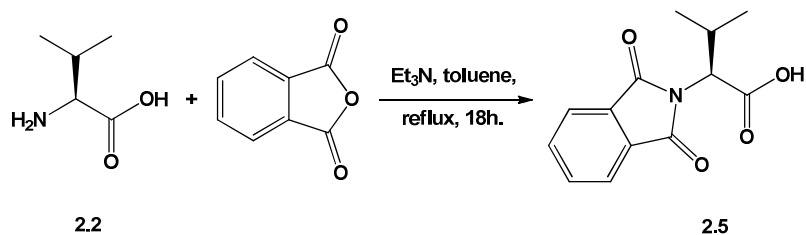
2.2.1 Amino Acid Protection



Scheme 3 Diamine synthesis via a mixed anhydride.

The four-step pathway to a diamine via an anhydride intermediate is provided in Scheme 3.^{3, 6, 12} Protection of the amine moiety of the amino acid commonly uses a Boc protecting group.¹ Choice of an appropriate protecting group is of great importance, especially when trying to evade chiral-centre racemisation. With this in mind, the phthalimide protecting group is an apt choice since the reaction conditions required for amine protection/deprotection are relatively mild. Use of the phthalimide protecting group also ensures no acidic protons are left bound to the nitrogen of the amine reducing its overall reactivity.¹³ Discussion relating to synthetic strategies for protection/deprotection using phthalimide are discussed herein and in Section 2.4.2 respectively. From this point forth all reference to the starting amino acid discussed should be taken as L-valine unless specified, since this amino acid was the starting material used in the majority of examples when developing the syntheses discussed within this Chapter.

Protection of the L-valine amine group using phthalic anhydride was undertaken as a one-pot-reaction on scales up to 100 g with respect to the starting amino acid (Scheme 4). Toluene proved to be a suitable solvent due to favourable reagent solubility in the medium and its high boiling point which allowed for the reaction to proceed within an acceptable duration. As the reaction progresses, water is generated as a by-product. Refluxing in toluene facilitates the extraction of water when coupled with Dean-Stark apparatus driving the reaction.



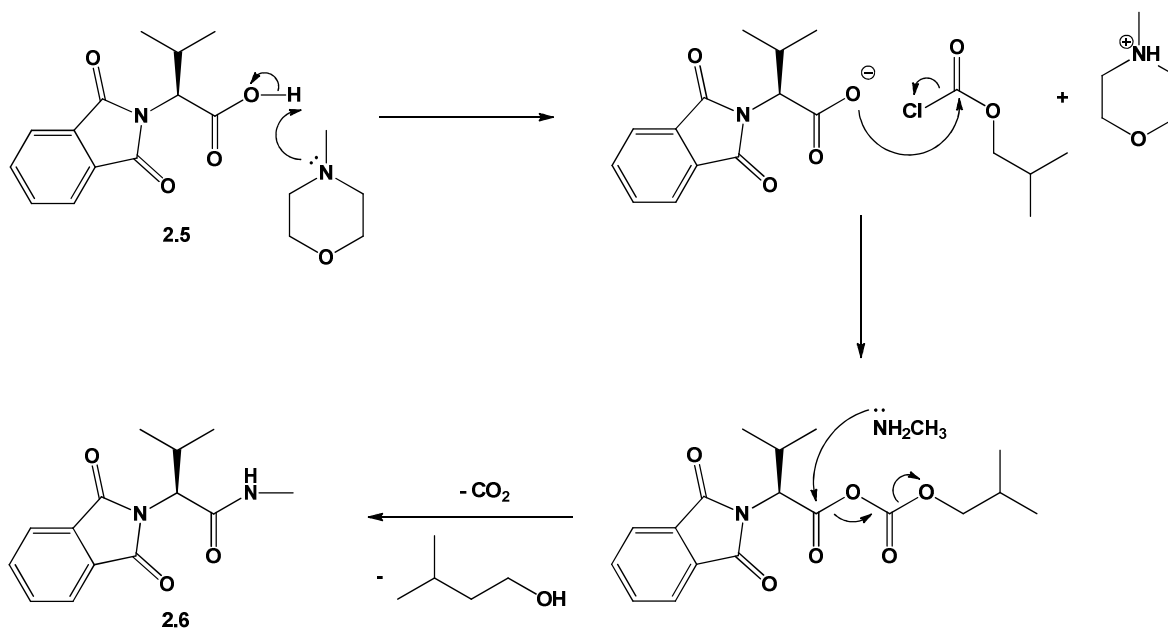
Scheme 4 Phthalic anhydride protection of L-valine.

In the case of L-valine, the one-pot reaction was heated at reflux for 18 hours. Ensuing acid work-up provided **2.5** in high yields. Phthalimide protection was also successfully completed starting from D-phenylglycine **2.3** or L-phenylalanine **2.4** on 100 g scales and reflects the success recorded in the literature.¹²

Amine protection was complete in two hours in the case of L-phenylalanine. Prolonged heating at reflux of D-phenylglycine resulted in the solution becoming increasingly coloured. This implies potential chemical changes occurring within the molecule, for example decomposition.¹⁴ The reason for an extended duration at reflux with L-valine (cf. L-phenylalanine or D-phenylglycine) was simply to increase yields. Small yield improvements were continually observed until a plateau at 12 hours without detriment to product **2.5**. Whilst **2.5** was not typically purified further before commencing the next step of the synthesis, care was needed to ensure the absence of triethylammonium salt, which was problematic in larger reaction scales.¹⁵

2.2.2 Amidation of N-phthaloyl valine via an Acid Anhydride Route

Amidation of the protected amino acid (step 2, Scheme 3), was initially attempted by the method described by Haufe *et al.*¹² This method has mild reaction conditions thereby reducing the risk of stereocentre racemisation whilst also being versatile, according to the work of Mauduit *et al.* (Fig. 2).⁸ In this method N-methylmorpholine (NMM) abstracts the hydroxyl proton of the carboxylic acid. The resulting carboxy anion attacks the *iso*-butylchloroformate (iBCF) reagent resulting in a mixed anhydride. The addition of a primary amine should effect the formation of an amide (e.g. **2.6**), carbon dioxide and *iso*-butanol, after nucleophilic attack at the α -carbonyl to the stereocentre (Scheme 5).



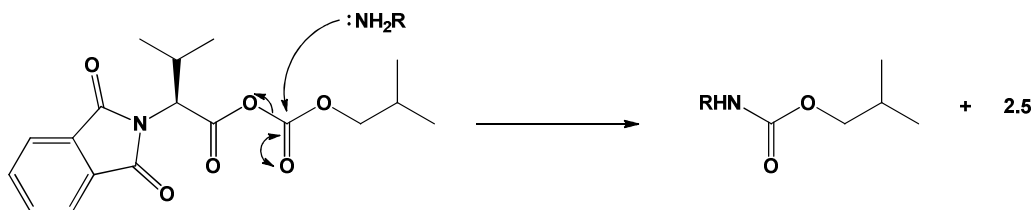
Scheme 5 Amidation by way of a mixed anhydride intermediate.

The viability of this reaction pathway was assessed using methylamine, due to its low steric demands (cf. *tert*-butyl amine) and having already been successfully employed in a similar reaction.¹²

Whilst successful with methylamine, significantly lower yields were obtained when performing the same reaction with alternative primary amines. In such instances, the formation of an *iso*-butyl-containing by-product was the major product. The *iso*-butyl structural feature was determined from characteristic resonances present in the ^1H NMR spectra: a doublet at 0.87 ppm integrating to 6 protons signifying the presence of the two methyl groups, and a one proton multiplet at 1.97 ppm, was assigned to the methine. The doublet at 3.94 ppm integrates to two protons and is indicative of the CH_2 group. These resonances compare favourably to those of the starting material iBCF, which are recorded at 0.98 ppm (doublet), 2.05 ppm (multiplet), and 4.11 ppm (doublet) respectively.

Why an amine substrate other than methylamine is unsuccessful could be due to the increased steric requirements of the new substrate. It can be envisioned the increase in steric demand from the new amine results in attack of the least hindered carbonyl of the mixed anhydride (Scheme 6), since the desired point of reaction is restricted by the *iso*-propyl stereo-directing group of the protected amino acid **2.5**.

Whether this limitation was apparent to the original authors remains to be seen as they report no amidation products other than those involving methylamine. As a side note, variation of reaction temperature and/or duration proved futile in all cases. In a response to these limitations an alternative method to obtain the target diamines was necessary, leading to the investigation of route two (Section 2.3).



Scheme 6 Reaction between the mixed anhydride intermediate and the primary amine resulting in the formation of the observed by-product.

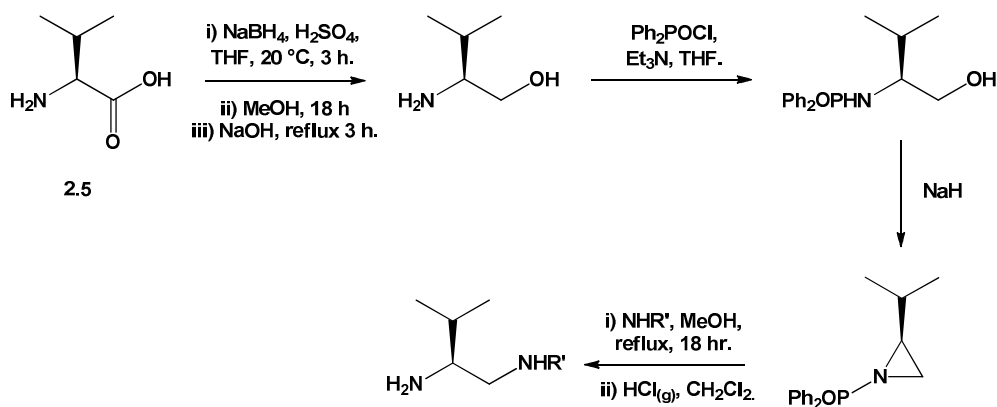
2.3 Route Two – Aziridine Intermediate

After the problematic pathway described in Section 2.2.1, a second method based upon aziridine formation and its successive ring-opening to afford the target diamines was pursued. The synthetic pathway investigated is presented in Scheme 7 and is a derivative of work published by Masamune *et al.*,¹⁶ Sweeny *et al.*,^{17, 18} and Russell *et al.*⁹

The first step describes the reduction of L-valine to its corresponding primary alcohol L-valinol and was performed on scales up to 100 g of L-valine (step 1, Scheme 7). The proceeding protection of the amine group of the aforementioned L-valinol was undertaken with diphenylphosphinyl chloride (Dpp) and preceded smoothly. Moderate yields between 40-50% of isolated aziridine were recorded and is on a par with literature precedence.^{17, 18}

Efforts to ring-open the aziridine using 4-fluoroaniline **2.7** or 4-methoxyaniline **2.8** were low yielding (<30%). Analysis of the crude reaction mixture indicated unreacted aziridine and amine starting materials, even under forcing conditions (7 days at vigorous reflux). It was therefore concluded that longer reaction times were unlikely to provide significant improvements in yield.

Much of the work concerning aziridines was carried out using the Dpp protecting group, however use of the tosyl group (Ts) has also been reported.¹⁹ We questioned whether altering the protecting group would have any impact on the ease of aziridine ring-opening in a bid to improve floundering yields. Whilst protection using Ts proved problem free the deprotection proved troublesome.²⁰ Exchanging the protection group led to greater input with respect to purification and no improvements in the yield were seen.



Scheme 7 Aziridine ring-opening to form a diamine.

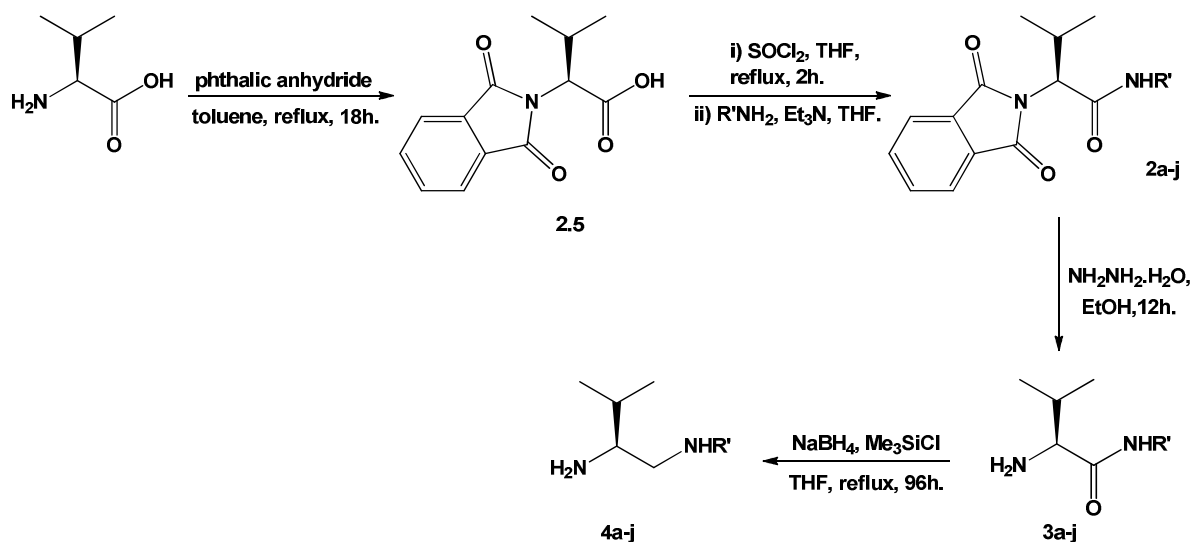
2.3.1 Catalysed Aziridine Ring-Opening

Previous attempts at ring-opening the aziridine with a primary amine under reflux conditions gave poor yields (<30%) making it prudent to investigate known catalysts for this reaction. A few examples arose from the literature, mainly the use of $\text{Sn}(\text{OTf})_2$, $\text{Cu}(\text{OTf})_2$, $\text{Yb}(\text{OTf})_3$, and $\text{La}(\text{OTf})_3$.^{21, 22} From these we trialed $\text{Cu}(\text{OTf})_2$, and $\text{Yb}(\text{OTf})_3$. As suggested in the literature 5 mol% of catalyst was added to the reaction (step 4, Scheme 7). No noticeable yield improvements were obtained with either metal-triflate even if reactions were heated at reflux for 2-3 days. This is in stark contrast to the success demonstrated in the literature which reports completion of ring-opening in yields of up to 80% when at reflux for only 18 hours.²² From observations using thin layer chromatography $\text{Yb}(\text{OTf})_3$ catalysed reactions at a faster rate than $\text{Cu}(\text{OTf})_2$, however this difference was negligible. Increased catalyst loadings of 20 mol% failed to improve upon previous yields and pursuit of the synthetic pathway was discontinued accordingly.

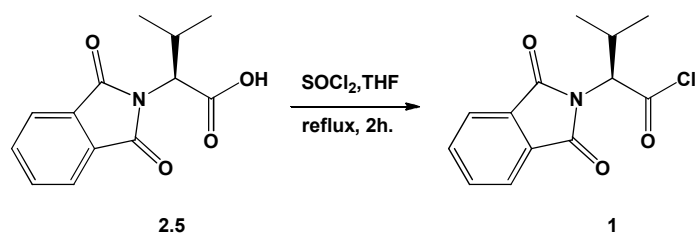
2.4 Route Three – Acid Chloride Intermediate

The limited success of routes one and two led to efforts being directed towards the new synthetic pathway shown in Scheme 8. The protection step using the phthalimide protecting group is as previously described in Section 2.2.1. The new route revolves around the amidation of an acid chloride intermediate with a series of primary amines and anilines. Thionyl chloride (SOCl_2) is a common reagent used to achieve the conversion of carboxylic acids to acid chlorides,²³⁻²⁷ and addition of an amine to an acid chloride is a well known reaction to produce amides.^{23, 24, 28,29}

Carboxylic acid conversion to the acid chloride was carried out on scales between 1.5-10 g of the N-phthaloyl valine **2.5**. ^1H NMR analysis of the reaction mixture indicated the reaction was complete after 2 hours (Scheme 9). The acid chloride was isolated as a pale yellow solid and characterised by ^1H NMR spectroscopy, and X-ray crystallography. ^1H NMR spectra showed the resonance of the proton at the chiral centre experienced a minor downfield shift from 4.63 ppm to 4.74 ppm upon conversion from the carboxylic acid to the acid chloride. The resonances related to the protons contained within the phenyl moiety of the phthalimide protecting group also experienced a shift downfield, though this change is significantly less pronounced ($\Delta\delta$ 0.03-0.04 ppm). All other proton resonances remained comparable to the protected L-valine **2.5**.



Scheme 8 General preparation of diamines (R = 4- $\text{C}_6\text{H}_4\text{F}$ (**a**), 4- $\text{C}_6\text{H}_4\text{OCH}_3$ (**b**), 4- $\text{C}_6\text{H}_4\text{CH}_3$ (**c**), C_6H_5 (**d**), 4- $\text{C}_6\text{H}_4\text{NO}_2$ (**e**), 3,5- $\text{C}_6\text{H}_3(\text{CH}_3)_2$ (**f**), $\text{CH}(\text{CH}_3)(\text{C}_6\text{H}_5)$ (**g**), $\text{CH}(\text{CH}_3)_2$ (**h**), $\text{C}(\text{CH}_3)_3$ (**i**), and 4- $\text{C}_6\text{H}_4\text{N}(\text{CH}_3)_2$ (**j**)).



Scheme 9 Carboxylic acid conversion to the corresponding acid chloride.

Conversion was most successful when carried out in THF using 1.05 equivalents of SOCl_2 with respect to **2.5**. Under these conditions reaction scale-up proceeded with ease allowing the reaction to be carried out on scales up to 120 g of the starting compound **2.5**. Once isolated, the acid chloride **1** was easily stable for up to three months when stored under an inert atmosphere.

Isolation of **1** from a mixture of chloroform:hexane as single crystals suitable for X-ray analysis led to its structural characterisation as shown in Fig. 4. Examination of the structure indicates the phthalimide group is identical to similarly reported literature compounds.¹² The phthalimide carbonyl bond length O(3)-C(13) of 1.214(10) Å shows a negligible elongation compared to O(2)-C(6) recorded as 1.187(9) Å. Both carbonyl bonds appear marginally shorter than typical C=O bond lengths in phthalimide moieties of 1.207 Å (range 1.146-1.388 Å) as reported in the Cambridge Structural Database. The acid chloride carbonyl O(1)-C(1) is measured as 1.170(9) Å, which is again approximately 0.03 Å shorter than the average C=O bond length of 1.202 Å (range 1.136-1.507 Å) in acid chloride systems. The length of C(1)-Cl(1) is measured as 1.812(10) Å. This bond length is marginally longer than average C-Cl acid chloride bonds (range 1.458-1.833 Å, mean = 1.755 Å). Of note is the observed hybridisation around N(1), which is calculated as being planar (360(2) ° with the range 358-362 °) (Table 1).

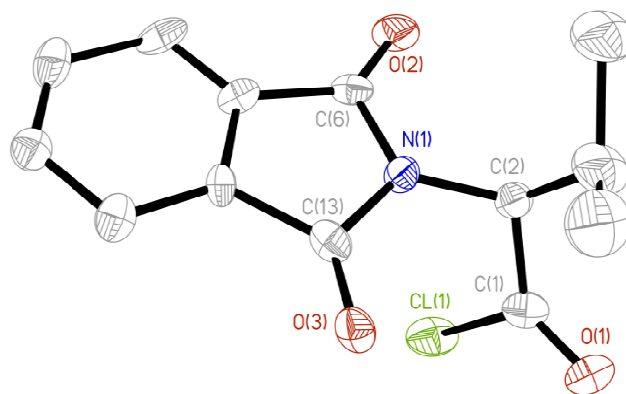


Fig. 4 Molecular structure of protected acid chloride compound **1**. Thermal ellipsoids drawn at 25% probability with hydrogen atoms are omitted for clarity.

Table 1 Selected bond angles of protected acid chloride compound **1**.

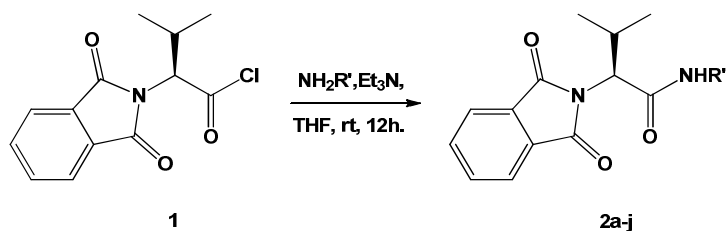
Atoms	Angle (°)	Atoms	Angle (°)
N(1)-C(6)-O(2)	123.4(8)	C(1)-C(2)-N(1)	111.9(7)
N(1)-C(13)-O(3)	125.1(8)	Cl(1)-C(1)-C(2)	112.1(7)
C(2)-N(1)-C(6)	122.9(6)	Cl(1)-C(1)-O(1)	118.7(8)
C(2)-N(1)-C(13)	123.6(6)	O(1)-C(1)-C(2)	129.2(9)
C(6)-N(1)-C(13)	113.1(7)		

2.4.1 Amidation via an Acid Chloride

The amidation procedure shown in Scheme 10 is the concluding part of step two in the overall synthesis as outlined in Scheme 8. Variation of the diamine N-R substituent is built in at this stage of the synthesis through the simple variation of the primary amine enlisted. The most efficient yields were obtained starting from 15 g of protected acid chloride **1**. The amidation proceeded by dissolving **1** in anhydrous THF with addition of the selected amine (**2.7-2.16**, Table 2) as a triethylamine mixture. In cases where the amine was a solid it was pre-dissolved in a mixture of THF/Et₃N, for example, *p*-methoxyaniline **2.8** and *p*-methylaniline **2.9**. Ten derivatives were prepared in order to assess the generality of the procedure. Both aliphatic and electron withdrawing/donating aromatic groups were employed to encompass a representative cross-section of steric and/or electronic properties of the N-R substituent.

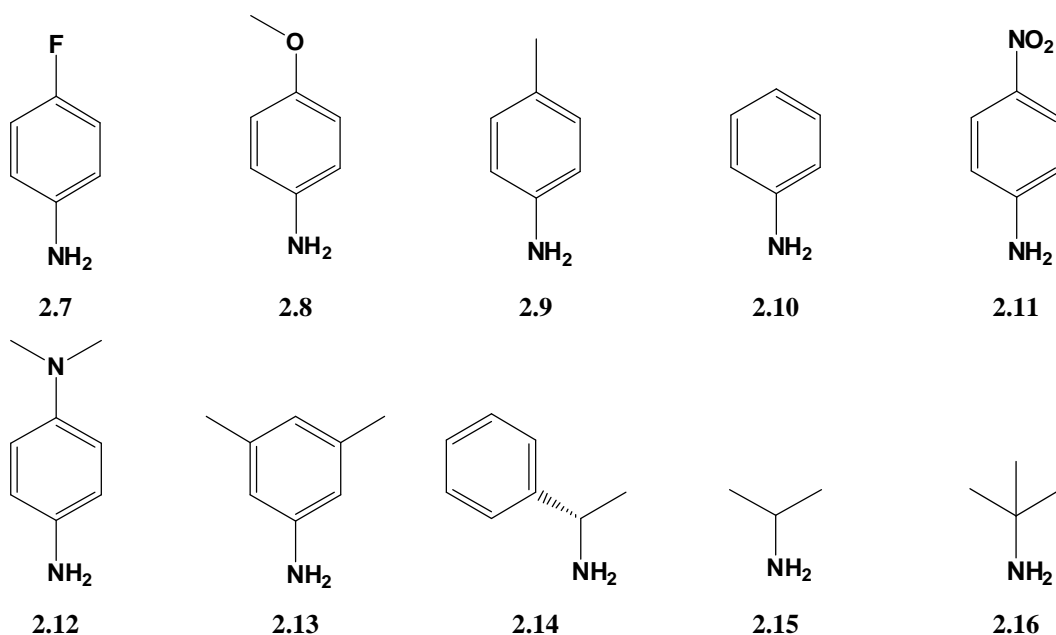
The chiral primary amine ((*S*)-(-)-1-phenylethylamine) **2.14** was decisive for determining if racemisation at the stereocentre was occurring. This is further detailed in Section 2.5.

The reaction was found to proceed immediately on addition of the primary amine, with a large quantity of precipitate generated (Et_3NCl). Addition of *N,N*-dimethylaminopyridine (DMAP) as a catalyst for the amidation reaction is reported in the literature.⁴ The addition of 10 mg of DMAP to our reactions also gave improved yields, but only with the 4- $\text{C}_6\text{H}_4\text{F}$, aniline, *iso*-propyl, and *tert*-butyl, derivatives **2a**, **2d**, **2h**, and **2i** respectively. Improvements were the most notable when forming protected amide **2d**, where yields were increased from 60% to 90%. Interestingly the addition of DMAP to the amidation involving 4- $\text{C}_6\text{H}_4\text{OCH}_3$ **2b** consistently resulted in a slight decrease in overall yield. This effect was not seen in other electron-withdrawing groups such as 4- $\text{N}(\text{CH}_3)_2$ **2j**. After isolating the amidated product **2a-j** the compound underwent deprotection without further purification.



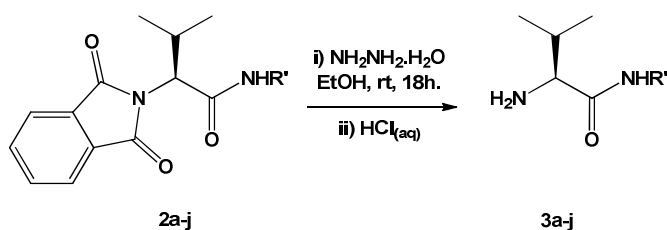
Scheme 10 Amidation of protected acid chloride **1** to its corresponding amide.

Table 2 Primary amines used to synthesise protected amides **2a-j**.



2.4.2 Removal of Phthalamide Protecting Group

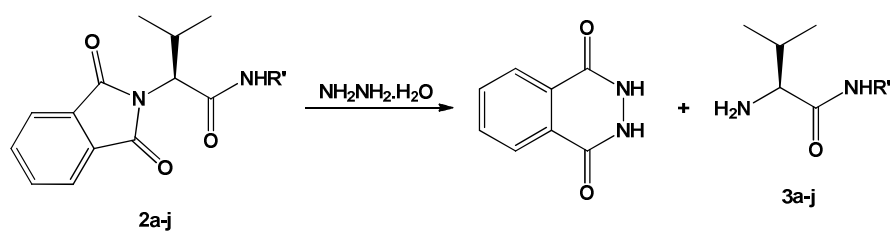
To attain the desired amino-amide deprotection of the phthalamide group must occur (step 3, Scheme 8). The chosen method is a modification of that presented by Sen and Roach (Scheme 11),³⁰ which is itself a derivative of the synthesis proposed by Ing and Manske in 1926.³¹ The deprotecting reagent hydrazine is relatively mild and afforded the amino-amides in good yield at ambient temperature (**3a-j**, Scheme 11). This method proved comparable to alternative methods, e.g. NaBH₄ under alcoholic conditions, followed by the addition of acetic acid which is then heated at 80 °C giving the deprotected amino-amide with no reported loss in optical activity.¹³ However, hydrazine remained the preferred reagent in this report owing to the milder reaction conditions.



Scheme 11 Phthalimide removal with hydrazine (R = 4-C₆H₄F (**a**), 4-C₆H₄OCH₃ (**b**), 4-C₆H₄CH₃ (**c**), C₆H₅ (**d**), 4-C₆H₄NO₂ (**e**), 3,5-C₆H₃(CH₃)₂ (**f**), CH(CH₃)(C₆H₅) (**g**), CH(CH₃)₂ (**h**), C(CH₃)₃ (**i**), and 4-C₆H₄N(CH₃)₂ (**j**)).

Upon addition of hydrazine formation of a precipitate was observed within 60 minutes. The reaction was allowed to continue for a further 18 hours before acid workup. The insertion of hydrazine into the phthalimide moiety of the protected amides **2a-j** releases the desired amino-amide **3a-j** (Scheme 12) and results in the formation of phthalylhydrazide **2.17**. This is able to undergo acid catalysed hydrolysis, forming phthalic acid **2.19**, which is the white precipitate observed during deprotection.^{31, 32}

After removal of the phthalic acid by filtration, the amino-amides **3a-j** were regularly obtained as their corresponding HCL salts in yields of $\geq 90\%$ when starting with up to 30 g of **2a-j**. The HCl salts of **3a-j** were characteristically cream coloured in appearance with the exception of **3e** which was intensely yellow. After work-up the purity of **3a-j** was such that further purification was not necessary before proceeding with the reduction stage (Section 2.4.3).



Scheme 12 Hydrazinolysis of the protected amino-amide **2a-j**.

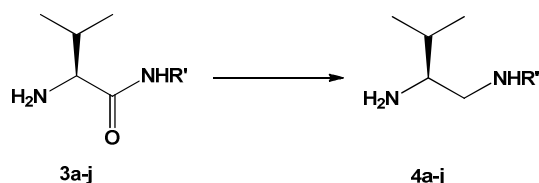
It is worthy to highlight that during work-up, the product amino-amides **3a-j** were obtained as the hydrochloride salts. Neutralisation and thus, purification of the amino-amides was found to be strongly affected by pH. If the pH was too acidic or too basic the amino-amide remained in the aqueous phase. This gave rise to low yields of low purity product after extraction with dichloromethane. The precise pH range was found to be amino-amide specific, but generally a value between pH 7-8 allowed for adequate extraction of the amino-amide into dichloromethane. Amino-amide 4-C₆H₄OCH₃ **3b** was one such example that strictly remained in the aqueous phase and could not be extracted into organic solvents even when adhering to strict control of the pH. In this case the organic phase only contained a trace amount of the amino-amide. Accordingly, the aqueous fraction was evaporated under reduced pressure and the remaining solid then dissolved in THF and filtered to remove NaCl (the by-product of neutralising the HCl amino-amide salts with NaOH_(aq)). The amino-amide was dried *in vacuo* and was of sufficient purity to proceed to the reduction stage without further workup.

¹H NMR spectroscopy was a powerful tool in determining the successful deprotection of **2a-j** to **3a-j**. The ¹H NMR spectra of **3a-j** all have a clear absence of resonances pertaining to aromatic bound protons of the phthalimide protecting group. The doublet resonance characteristic of the proton bound to the carbon at the stereocentre displays a dramatic shift upfield upon conversion from **2a-j** to **3a-j** (with the exception of C₆H₅ bearing **3d**). The difference in chemical shift experienced is typically in the region of $\Delta\delta$ -0.80 ppm (**2a-j** = 4.57-4.19 ppm, mean = 4.45 ppm; **3a-j** = 5.27-2.20 ppm, mean = 3.64 ppm). Compound **3d** is the only example to display an upfield chemical shift for this resonance (H₂NCH₂CH(CH₃)₂), although the chemical shift difference is in line with normal trends *ca.* $\Delta\delta$ +0.80 ppm. Such a significant change in the frequency of this resonance indicates that the proton at the stereocentre it is now subject to a different chemical environment when compared to its protected state *viz.* the chiral-centre proton now has an NH₂ group adjacent opposed to the more electron-withdrawing phthalimide moiety.

It is also apparent that the multiplet characteristic of the *iso*-propyl methine experiences a change in chemical environment upon undergoing deprotection, which is to be expected. Though less pronounced than that of the proton situated at the stereocentre the change in chemical shift in ^1H NMR spectra is typically upfield; $\Delta\delta$ -0.57 ppm (**2a-j** = 2.93-2.70 ppm, mean = 2.87 ppm; **3a-j** = 2.44-2.09 ppm, mean = 2.30 ppm). All remaining resonances in the ^1H NMR spectra remained static between conversion from protected **2** to deprotected amide **3**.

2.4.3 Amide Reduction

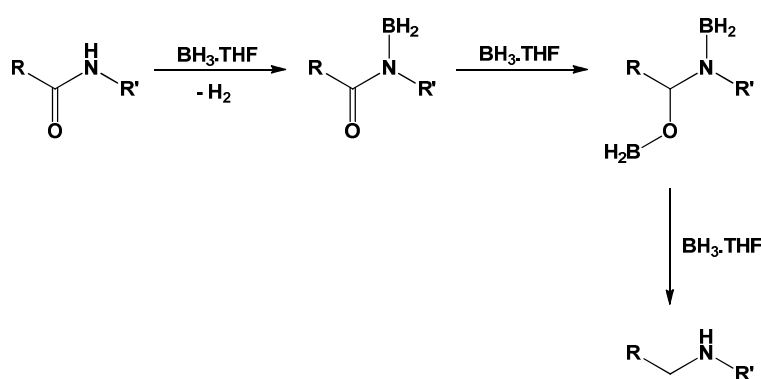
Reduction of **3a-j**'s amide moiety to its corresponding amine is the final synthetic step to realise the target diamines **4a-j** (Scheme 13). LiAlH_4 was found to be unsuitable, with only starting material being recovered from the reaction mixture. The lack of reaction with LiAlH_4 was surprising and is very tentatively owed to the formation of unreactive aluminium complexes by way of the basic LiAlH_4 reacting with the acidic proton of the secondary amide.³³ The highly reactive nature of LiAlH_4 also prompts concern over potential racemisation of the chiral-centre of the secondary amide being reduced, since a literature example is known where this has been the case.³⁴



Scheme 13 Amino-amide **3a-j** reduction to their corresponding diamine **4a-j**.

Borane ($\text{BH}_3 \cdot \text{THF}$) was found to be a suitable reducing reagent.³⁵ Studies by Brown and Heim show the rate of reduction is fastest with tertiary amides and slowest with primary amides. In the case of the secondary amides Brown and Heim noted that the nature of the N-R substituent did have an effect on the rate of reduction. Aliphatic substituents tended to react at a faster rate than those bearing aromatic substituents. Substituents in the *ortho* position of the aromatic substituent were found to exhibit a greatly retarded rate of reaction, whereas substituents at the *para* position had little effect upon the rate. These observations indicate this procedure should be applicable to the wide range of amides produced thus far.

Brown and Heim explain that when reducing secondary amides to their corresponding amines the quantity of borane added needs to provide six “active hydrides” for successful reduction, where an “active hydride” is equivalent to one B-H bond.³⁵ One hydride to react with the hydrogen on the nitrogen of the secondary amine, a further two reactive hydrides to provide the hydrogens required for the formation of the new CH₂ group and another three hydrides (one equivalent of BH₃) which forms an adduct with the newly reduced molecule (Scheme 14). Compounds **3a-j** also bear a primary amine moiety which is able to coordinate with a molecule of borane. This necessitates the need for an additional equivalent of the reagent during reaction.

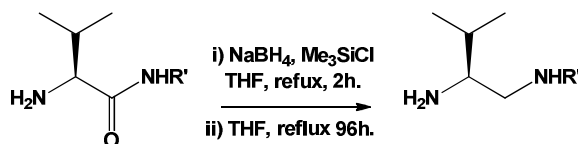


Scheme 14 Amide to amine reduction using BH₃.THF.

Literature reductions of tertiary and secondary amides were essentially complete after one hour at reflux starting from 2 g of substrate, whilst our reactions were heated to reflux for 48 hours since we observed heating at reflux for longer durations led to notably increased yields. This was especially true with increasing scale (2 g to ≥ 8 g). Specifically it was found that yields of **4a-j** could be improved with vigorous reflux for 96 hours. Under these conditions yields were often $\geq 85\%$. With *iso*-propyl and *tert*-butyl diamines (**4h** and **4i**) consistent yields of up to 94% were exhibited. Durations of reflux greater than 96 hours did not promote yields. Yield improvements were also afforded when using four equivalents of borane instead of three.

Larger scale reactions (>3-4 g amino amide **3a-j**) resulted in the handling of large quantities of 1 M borane solution, giving rise to less control over heat transfer. Consequently more concentrated borane sources were sought; the most successful being the *in situ* preparation of borane from sodium borohydride and chlorotrimethylsilane as described by Whiting *et al.* (Scheme 15).³⁶ This was established as superior to using 10 M BH₃(SMe₂).

Whiting *et al.* describe the reduction of a tertiary amide to its corresponding amine by creating a suspension of NaBH₄ in THF and adding SiMe₃Cl to the mixture, which was then heated at reflux for two hours before adding the amino amide substrate. Interestingly after amino amide addition the reaction was allowed to proceed for 64 hours suggesting that extended reaction times may not be uncommon in these types of reactions.



Scheme 15 Amide to amine reduction using borane *in-situ*.

Using the generation of BH₃.THF *in-situ* we were able to successfully synthesise diamines **4a-j**. This could be performed on scales up to 20 g and still give high yields of product that required minimal purification after workup. It is anticipated that further increases in reduction scale would be entirely feasible. Interestingly just as Brown and Heim observed, our studies also showed no significant yield variations between varying *para* substituents of the aromatic N-R substituents of the secondary amide. This supports the theory that under these reaction conditions electronic variation through altering the electron donating/withdrawing properties of the *para* substituent has little effect on the overall yield.

Purification of diamines **4a-j** was achieved using column chromatography over silica. Diamines **4a-j** were characterised by ¹H NMR, ¹³C NMR, and IR spectroscopies and mass spectrometry. Studies alluded that the only major by-product from the reduction reaction was unreacted amino-amide (**3a-j**), which could be recovered during diamine purification and re-reduced. Identification of diamines **4a-j** was elementary from the starting amino-amides **3a-j**. High-resolution mass spectra of the purified diamines **4a-j** were in excellent agreement of theoretical weights and contained no fragments attributed to the starting amino-amide.

¹H NMR spectra of **4a-j** show notable difference in recorded resonance patterns compared to pre-reduction compounds **3a-j**. The most notable difference is the inclusion of two new resonances with accompanying fine structure caused by the new diastereotopic CH₂ environment in the diamine molecule. In aromatic N-R substituents the resonances for the CH₂ moiety are typically at 3.26 and 2.80 ppm. In non-aromatic substituents **4g-i** the

analogous resonances are seen at 2.60 and 2.44-2.20 ppm. In both cases the fine structure of the resonances are either an apparent quartet or triplet integrating to one proton per resonance.

In keeping with previous trends the proton bound to the carbon at the chiral centre records a resonance with a multiplet fine structure that shifts further upfield upon conversion from the amino-amide to diamine. In aromatic substituents the change in chemical shift is upfield; $\Delta\delta$ -1.19 ppm (**3a-f**, **3j** = 5.27-3.48 ppm, mean = 3.97 ppm; **4a-f**, **4j** = 3.03-2.72 ppm, mean = 2.78 ppm). In the non-aromatic substituents the change in chemical shift is also upfield although within a narrower range and less pronounced; $\Delta\delta$ -0.72 ppm (**3a-f**, **3j** = 3.22-3.12 ppm, mean = 3.18 ppm; **4a-f**, **4j** = 2.47-2.44 ppm, mean = 2.45 ppm).

As noted in the conversion of **2a-j** to **3a-j**, the methine of the *iso*-propyl experiences a change in resonance chemical shift. The same is true when amino-amides **3a-j** are reduced to diamines **4a-j**. Again the resonance assigned to the methine hydrogen experiences a further shift upfield. For diamines bearing aromatic N-R substituents the change in chemical shift is upfield; $\Delta\delta$ -0.64 ppm (**3a-f**, **3j** = 2.44-2.09 ppm, mean = 2.32 ppm; **4b-f**, **4j** = 1.70-1.66 ppm, mean = 1.68 ppm). In the non-aromatic N-R substituents the change in chemical shift is also upfield and in keeping with trends, is within a narrower range and less pronounced; $\Delta\delta$ -0.73 ppm (**3a-f**, **3j** = 3.22-3.12 ppm, mean = 3.18 ppm; **4a-f**, **4j** = 2.47-2.44 ppm, mean = 2.45 ppm). What arises from analysis of the changes in the stereocentre proton and methine proton is that upon progression from protected amide **2a-j** to amino-amide **3a-j** and eventually diamine **4a-j**, is that these characteristic resonances shift progressively upfield with only one exception, the C₆H₅ bearing compound **3d**.

For the first time the resonances of the CH₃ groups of the *iso*-propyl moiety displayed a notable change in recorded resonance between conversion from the amino-amide to diamine. Whilst there has been very marginal chemical shift differences of the two indicative doublets resonance *ca.* 1.1 and 0.90 ppm of **2a-j** and **3a-j**, the CH₃ groups in all compounds except **4d** (N-R = C₆H₅) and **4g** (N-R = CH(CH₃)(C₆H₅)) display an apparent triplet fine structure at approximately 0.98 ppm distinguishing it noticeably from its amino-amide analogue. Shift changes pertaining to both aromatic and non-aromatic N-R substituents could not be generalised and were often compound specific.

$^{13}\text{C}\{\text{H}\}$ spectra showed that once formed diamines **4a-j** exhibit a resonance between 49-48 ppm from the methylene carbon ($\underline{\text{C}}\text{H}_2$) environment (determined from 2D ^1H - ^{13}C correlation HSQC experiments). This observation lends support to the formation of the diamine along with an absence of a carbonyl resonance, which should not be present in the final diamine (the lack of carbonyl resonance is reaffirmed by the IR spectra that show no absorption between the typical range for an amide $\text{C}=\text{O}$ of $1640\text{-}1695\text{ cm}^{-1}$). Expected aromatic and non-aromatic resonances relating to the individual N-R substituents were observed where expected, depending upon the nature of the substituent.

2.5 Racemisation of the Chiral Centre

Announced in the mid-1950's as a miracle cure for morning sickness in expectant mothers, thalidomide (**2.17**) has since become iconic with the devastating teratogenic effects seen in the offspring of the mothers who were prescribed the drug.^{37, 38} Unknown at the time the therapeutic enantiomer racemised *in-vivo* forming the teratogenic-inducing enantiomer as well.³⁹ And it was during reduction of a carbonyl group in the α -position to the chiral centre that the 2-aminopyrroline ligand **2.18** also underwent racemisation.⁴⁰ Due to the compelling structural parallels between **2.17** and **2.18** when compared to compounds **1**, **2a-j**, and **3a-j** it would be prudent to explore their potential of racemisation as well.

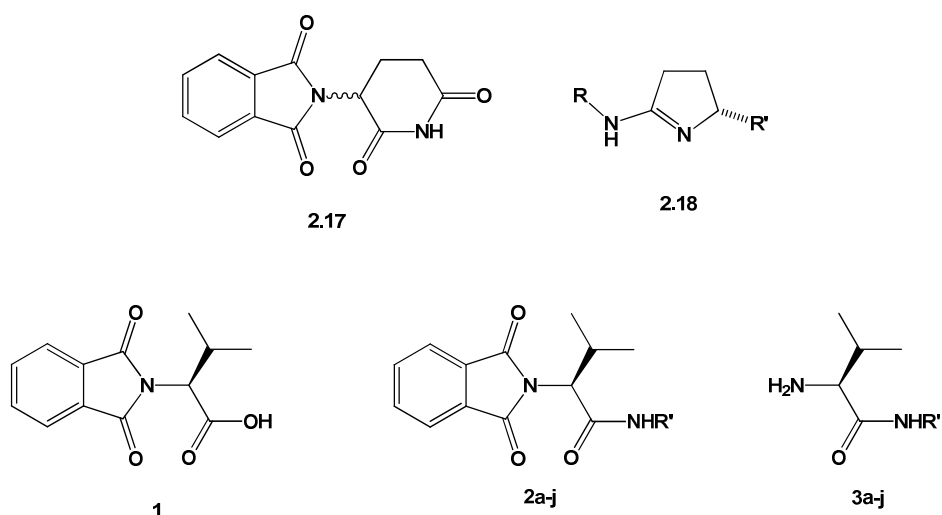
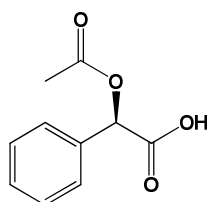


Fig. 5 Thalidomide (**2.17**), 2-aminopyrroline (**2.18**), Protected L-valine (**1**), amidation (**2a-j**), and deprotection (**3a-j**) compounds share structural similarities.

With regards to **1**, **2a-j**, and **3a-j**, the most significant feature is the potential for tautomerism to occur in the molecule resulting in racemisation of the chiral-centre. Since tautomerism can be base catalysed (by abstraction of a proton at the α -position to the carbonyl) the acidity of the proton bound to the chiral centre could be of significant importance. As this proton is within close proximity to an electronegative nitrogen atom its acidity is likely to be increased, opening it up to attack from a base/nucleophile. Of lesser importance, the carbon atom at the centre of chirality is also adjacent to the nitrogen atom, potentially increasing the chance of nucleophilic attack.

In order to assess the enantiopurity of the diamines, studies were undertaken to look for signs of racemisation. This was pursued in two different manners, the first exploiting the use of *R*-(-)- α -acetylmandelic acid (**2.21**, Fig. 6), which is known to form intimate ion-pairs that are used to determine enantiomeric excess.⁴¹ This is the same tactic used in Chapters 3 and 4 to allow the determination of enantiomeric excess of the pyrrolidine products from hydroamination. To accomplish this two solutions of pure diamine **4a** (N-R = 4-C₆H₄F) and **4i** (N-R = C(CH₃)₃) were made in chloroform-d₁ and 1.5 equivalents of chiral acid **2.21** added. Both samples were then studied by NMR spectroscopy to observe if classical “doubling” of the resonance signals occurred due to the formation of diastereomeric ion-pairs between **2.21** and the diamine.⁴² NMR spectra showed no such doubling effect suggesting that the diamine was enantiopure.

**2.21****Fig. 6** *R*-(-)- α -acetylmandelic acid.

To confirm these findings a second methodology was chosen that involved the inclusion of a second (enantiopure) stereocentre into a diamine at the amidation stage. The advantage of this experiment was the ability to analyse the molecule after each subsequent step of the synthesis until the final diamine had been rendered. If racemisation was taking place during the synthesis by utilising this approach it should be trivial to identify by virtue of diastereomer formation (distinguishable by NMR spectroscopy) at which step racemisation was occurring, thus allowing the issue to be suitably addressed.

The typical diamine synthesis was undertaken using chiral amine $\text{NH}_2\text{CH}(\text{CH}_3)(\text{C}_6\text{H}_5)$ **2.14** (Table 2) in place of previous examples. After each stage of the synthesis ^1H NMR spectra indicated the presence of only a single diastereomer. Example spectra recorded from ^1H NMR studies on the final diamine **4g** are presented in Fig. 7 and an enlargement for clarity between 3.90-0.60 ppm in Fig. 8.

The outcome from both experiments allowed for confident progression towards using the diamine library synthesised for the synthesis of the C_2 -symmetric bisimidazoline analogues which are later discussed in Chapter 4. The enantiopure diamines **4a-j** were also tested for their suitability as supporting ligands in calcium complexes and the resulting complexes' stereoselectivity in hydroamination. This is covered in detail in Chapter 3.

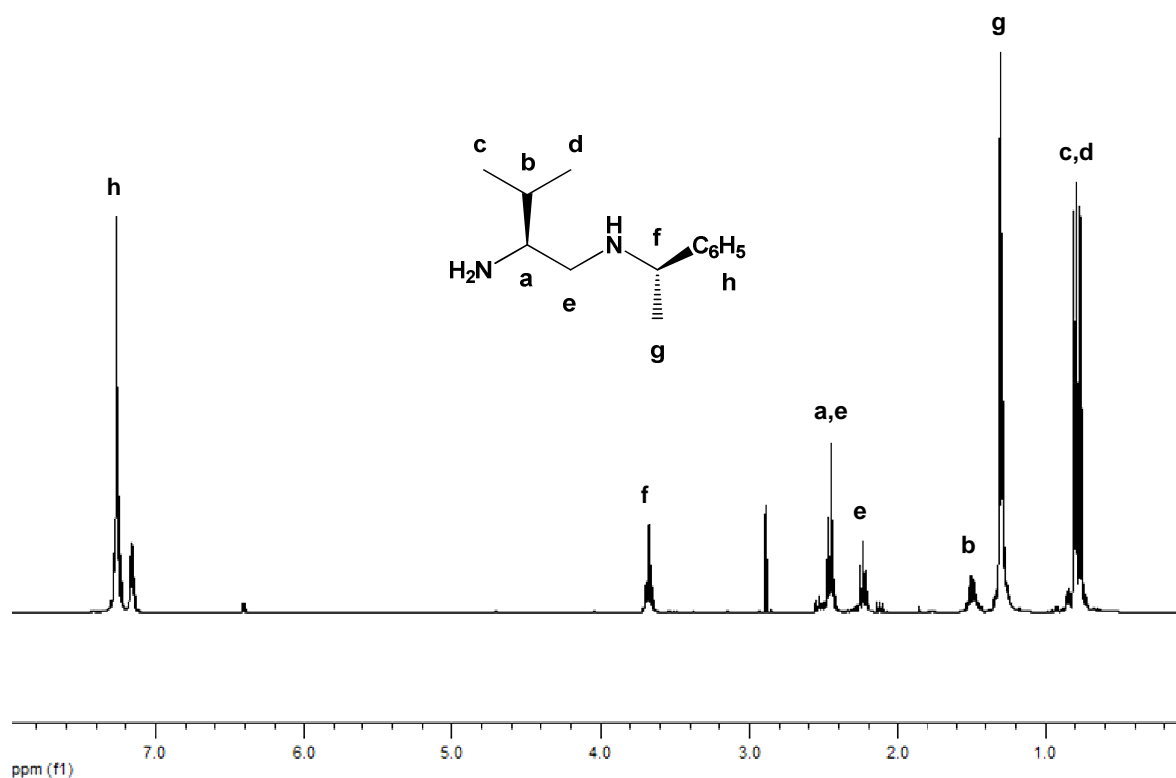


Fig. 7 ^1H NMR spectra of diamine **4g** for evidence of diastereoisomers.

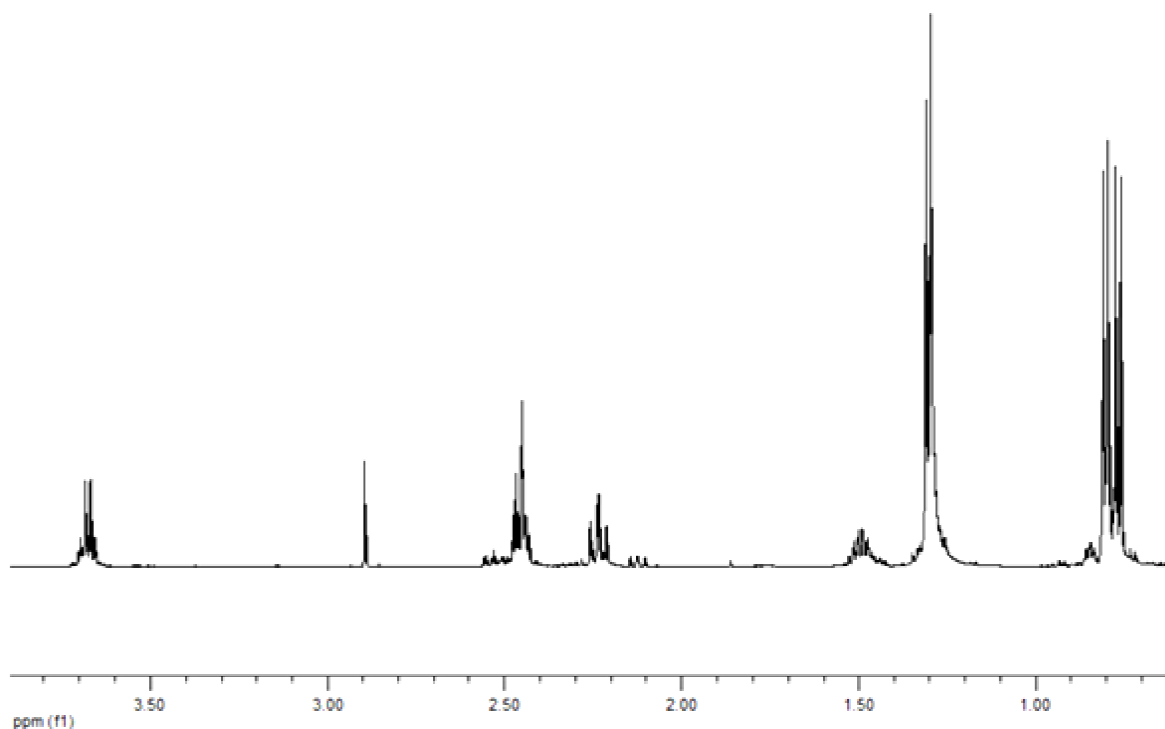


Fig. 8 ^1H NMR spectra enlargement between 3.90-0.6 ppm of diamine **4g**.

Since the chiral supporting ligands are used in asymmetric catalysis, if racemisation of the ligands had occurred then the ability of the ligand to transfer select chiral information to the catalytically active site in catalysis would have been severely compromised. This can be visually explained using the bisimidazoline supported calcium complexes from Chapter 4 with the aid of reaction quadrants (Figs. 9 and 10). By dividing the space surrounding the complex into quadrants it becomes easier to see how the C_2 -symmetry element of the bisimidazoline ligand helps to reduce the number of varying substrate approaches.

In Fig. 9, if the substrate approaches from either quadrant B or C then the environment around it is identical. However, when looking at substrate approach to bind with the metal centre in quadrants A and D it is apparent the quadrants are related by symmetry. Quadrants A and D are mirror images of one another so substrate approach should be identical in each. The presence of this symmetry element limits the number of substrate vector approaches and potential transition states where chiral information is transferred from the complex to the substrate. The outcome of fewer transition state conformations should lead to higher enantioselectivity.

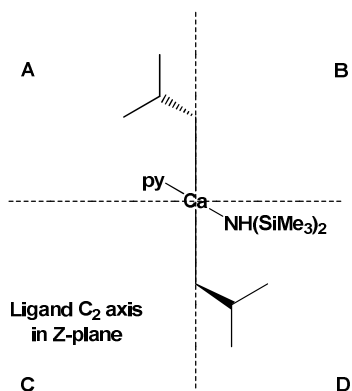


Fig. 9

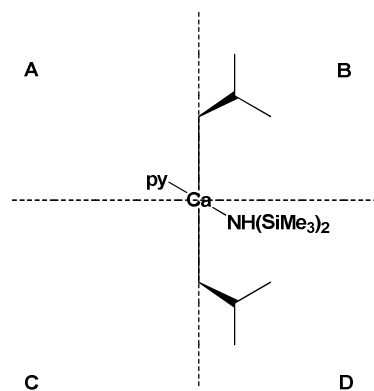


Fig. 10

Figs. 9 & 10 Reaction quadrants for a C_2 symmetric and non- C_2 symmetric bisimidazoline-calcium complex.

If quadrants A and D were not symmetry-related (Fig. 10), then it can be envisioned that the substrate could approach to bind with the metal centre from many additional vectors. This happens because there is a change in the stereochemistry of the *iso*-propyl moiety. It acts as a “steric shield” around a certain proportion of the metal centre face. When the stereochemistry changes (between Figs. 9 and 10) it results in one face of the metal centre being significantly more open to binding with the substrate. As substrate approach is less defined, new substrate approach vectors can be taken leading to more potential transition states and less stereoselectivity from the complex on the substrate. This will ultimately lower recorded enantiomeric excess.

When this principle is applied to the diamine based ligands used in Chapters Three and Four on calcium, if the complexes contain ligands of both *R* and/or *S*-configuration then opposing, competing stereochemical information will be imparted onto the reacting substrates leading to a mixture of *R* and *S* products. As a result, this will compromise recorded enantiomeric excesses.

2.6 References

1. B. Ramalingam, M. Neuburger and A. Pfaltz, *Synthesis*, **2006**, 4, 572.
2. J. S. Wixey and B. D. Ward, *Dalton Trans.*, **2011**, 40, 7693.
3. M. Achmatowicz, A. Szumna, T. Zielinski and J. Jurczak, *Tetrahedron*, **2005**, 61, 9031.
4. G. Anikumar, S. Bhor, M. K. Tse, M. Klawonn, B. Bitterlich and M. Beller, *Tetrahedron: Asymmetry*, **2005**, 16, 3536.
5. S. Bhor, G. Anilkumar, M. K. Tse, M. Klawonn, C. Dobler, B. Bitterlich, A. Grotevendt and M. Beller, *Org. Lett.*, **2005**, 7, 3393.
6. J. Brown, S. C. K. Su and J. A. Shafer, *J. Am. Chem. Soc.*, **1966**, 88, 4468.
7. H. Liu and D.-M. Du, *Adv. Synth. Catal.*, **2009**, 351, 489.
8. D. Rix, S. Labat, L. Toupet, C. Crévisy and M. Mauduit, *Eur. J. Inorg. Chem.*, **2009**, 1989.
9. A. J. Davenport, D. L. Davies, J. Fawcett and D. R. Russell, *J. Organomet. Chem.*, **2006**, 691, 3445.
10. J. Su, T. P. Vachal and E. N. Jacobsen, *Adv. Synth. Catal.*, **2001**, 343, 197.
11. J. S. Wixey and B. D. Ward, *Chem. Commun.*, **2011**, 47, 5449.
12. D. M. Shendage, R. Fuhlich and G. Haufe, *Org. Lett.*, **2004**, 6, 3675.
13. J. O. Osby, M. G. Martin and B. Ganem, *Tetrahedron Lett.*, **1984**, 25, 2093.
14. S. Ma, C. A. Busacca, K. R. Frandrick, T. Bartholomeyzik, N. Haddad, S. Shen, H. Lee, A. Saha, N. Yee, C. Senanayake and N. Grinberg, *Org. Lett.*, **2010**, 12, 2782.
15. H. E. Gottlieb, V. Kotlyar and A. Nudelman, *J. Org. Chem.*, **1997**, 62, 7512.
16. A. Abiko and S. Masamune, *Tetrahedron Lett.*, **1992**, 33, 5517.
17. A. A. Cantrill, H. M. I. Osborn and J. B. Sweeny, *Tetrahedron*, **1998**, 54, 2181.
18. H. M. I. Osborn, A. A. Cantrill and J. B. Sweeny, *Tetrahedron Lett.*, **1994**, 35, 3159.
19. W. Howson, H. M. I. Osborn and J. Sweeney, *J. Chem. Soc. Perkin Trans*, **1995**, 1, 2439.
20. M. C. Elliott, N. N. E. El Sayed and J. S. Paine, *Org. Biomol. Chem.*, **2008**, 6, 2611.
21. M. Meguro, N. Asao and Y. Yamamoto, *Tetrahedron Lett.*, **1994**, 35, 7395.
22. G. Sekar and V. K. Singh, *J. Org. Chem.*, **1999**, 64, 2537.

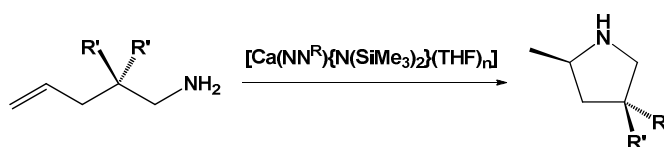
23. M. B. Smith and J. March, *Advanced Organic Chemistry*, 6th edn., Wiley, London, 2007.
24. J. Clayden, N. Greeves, S. Warren and P. Wothers, *Organic Chemistry*, OUP, Oxford, 2001.
25. C. F. H. Allen, J. R. Byers Jr and W. J. Humphlett, *Org. Synth.*, **1963**, 4, 739.
26. M. W. Rutenberg, *Org. Synth.*, **1963**, 4, 620.
27. N. A. Boland, I. J. Casey, S. J. Hynes, J. W. Matthews and M. P. Smyth, *J. Org. Chem.*, **2002**, 67, 3919.
28. J. Zabicky, *The Chemistry of Amides*, Wiley-Interscience, London, 1970.
29. M. Jedrzejczak, R. E. Motie and D. P. N. Satchell, *J. Chem. Soc. Perkin Trans 2*, **1993**, 599.
30. S. E. Sen and S. L. Roach, *Synthesis*, **1995**, 756.
31. H. R. Ing and R. H. F. Manske, *J. Chem. Soc.*, **1926**, 2348.
32. J. Bishop Tingle and S. J. Bates, *J. Am. Chem. Soc.*, **1910**, 32, 1319.
33. V. M. Micovic and L. Mihailovic, *J. Org. Chem.*, **1954**, 18, 1190.
34. A. C. Donohue and R. J. W., *Aust. J. Chem.*, **1995**, 48, 1741.
35. H. C. Brown and P. Heim, *J. Org. Chem.*, **1973**, 38, 912.
36. S. W. Coghlan, R. L. Giles, J. A. K. Howard, L. G. F. Patrick, M. R. Probert, G. E. Smith and A. Whiting, *J. Organomet. Chem.*, **2005**, 690, 4784.
37. T. D. Stephens, C. J. W. Bundle and B. J. Fillmore, *Biochem. Pharmacol.*, **2000**, 59, 1489.
38. M. Melchert and A. List, *Int. J. Biochem. Cell Biol.*, **2007**, 39, 1489.
39. B. Konche and G. Blaschke, *J. Chromatogr. A*, **1994**, 666, 235.
40. B. D. Ward, H. Risler, K. Weitershaus, S. Bellemin-Laponnaz, H. Wadepohl and L. H. Gade, *Inorg. Chem.*, **2006**, 45, 7777.
41. G. Zi, F. Zhang, L. Xiang, Y. Chen, W. Fang and H. Song, *Dalton Trans.*, **2010**, 39, 4048.
42. G. H. P. Roos and A. Donovan, R., *Science and Technology*, **2000**, 5, 11.

Chapter Three

Calcium Complexes Supported by Diamine Ligands

3.1 Introduction

Whilst Hill *et al.* had shown calcium's potential for catalytic intramolecular hydroamination in 2005 (Scheme 1),¹ it wasn't until 2008 when Buch and Harder published the first example of a chiral bisoxazoline (BOX) supported calcium complex $[\text{Ca}(\text{BOX})\{\text{N}(\text{SiMe}_3)_2\}(\text{THF})_2]$ (Fig. 1, **1.6**) demonstrating stereoselectivity, even if markedly low (*ca.* 4-6% ee).² As discussed previously in Chapter 1, Section 1.2.1.2, the low enantiomeric excess obtained was deemed to be a direct result of ligand redistribution within the system. The formation of inactive homoleptic $[\text{Ca}(\text{BOX})_2]$, as well as active, but non-stereoselective $[\text{Ca}\{\text{N}(\text{SiMe}_3)_2\}_2(\text{THF})_2]$ will not only affect catalytic rates but also result in racemic products being formed.



Scheme 1 Asymmetric hydroamination catalysis ($\text{R}' = \text{Me}$ **A** and Ph **B**).

Targeted development towards improved chiral calcium systems was not reported until 2010. Sadow *et al.* employed the chiral tris(oxazolonyl)borato calcium complex **1.9** (Fig. 1) in asymmetric hydroamination where enantioselectivities of up to 18% were noted.³ The magnesium analogue of **1.9** out-performed its calcium counterpart when applied to the same hydroamination reactions yielding enantiomeric excesses of up to 36%. This is not an isolated case of magnesium attaining higher stereoselectivity than calcium when applied to asymmetric hydroamination. Preceding improvements with calcium reported by Sadow *et al.*, magnesium was already recorded as achieving greater enantiomeric excesses of 14% (*cf.* Buch and Harder's 4-6% ee). As of 2012 Hultsch *et al.* utilised the magnesium complex **1.11** (Fig. 2) in a wide variety of intramolecular hydroamination reactions where stereoselectivities were very favourable for a wide range of substrates recorded between 51-93% ee.⁴

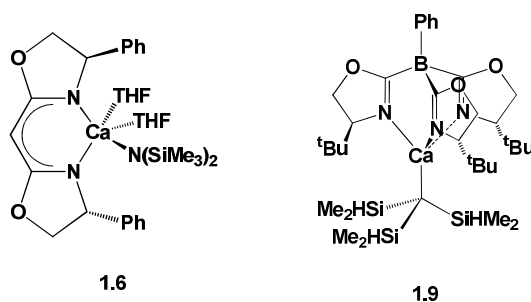


Fig. 1 Literature examples of chiral calcium complexes **1.6** and **1.9**.

This trend highlights that the progress of calcium compounds for asymmetric hydroamination is underdeveloped when compared to magnesium. As Group 2 is descended complexes show a greater propensity to undergo ligand redistribution, which is why magnesium complexes are typically more defined than calcium, and why there are currently no strontium or barium compounds reported in asymmetric hydroamination.

The low enantiomeric excesses reported with calcium in asymmetric hydroamination is in-part related to the scarcity of calcium-specific publications in this field, affirming the research areas current infant state. It is in this light the contributions contained within this Thesis and the parts of this work that have been published, provide valuable insight for the field.^{5, 6} The employment of chiral ethylene diamine (NN^{R}) supported calcium complexes as discussed within became the third published example of such a system applied to the asymmetric hydroamination of simple aminoalkenes. It is hoped that building upon these discussed developments the feat of synthesising a high-performing catalyst for asymmetric hydroamination is realised in the not too distant future.

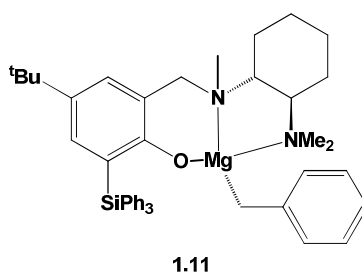
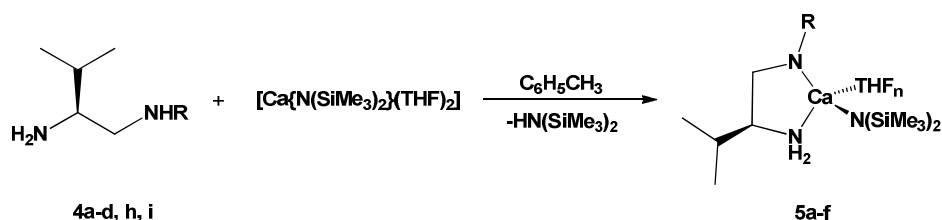


Fig. 2 Phenoxyamine magnesium complex (**1.11**) achieved 93% ee in asymmetric intramolecular hydroamination.

3.2 Preparation of Calcium Complexes Supported by Diamine Ligands

Preparation of the diamine calcium complexes was achieved by reaction of the protio-ligand (**4a-d, h, i**) with $[\text{Ca}\{\text{N}(\text{SiMe}_3)_2\}_2(\text{THF})_2]$ in benzene- d_6 or toluene (Scheme 2). The compounds were isolated as yellow/orange precipitates that were only soluble in THF, being insoluble in hydrocarbon solvents and unstable in chlorinated solvents.



Scheme 2 Preparation of the NN^{R} calcium complexes (R = 4- $\text{C}_6\text{H}_4\text{F}$ (**5a**), 4- $\text{C}_6\text{H}_4\text{OCH}_3$ (**5b**), 4- $\text{C}_6\text{H}_4\text{CH}_3$ (**5c**), 4- C_6H_5 (**5d**), ^iPr (**5e**), and ^tBu (**5f**)).

The method of synthesising complexes **5a-f** is often exploited due to the facile preparation of the AE metal amide $[\text{Ca}\{\text{N}(\text{SiMe}_3)_2\}_2(\text{THF})_2]$, their solubility in a range of solvents, and the production of the volatile by-product $\text{HN}(\text{SiMe}_3)_2$.^{7, 8} Whilst the diamine and calcium amide are both soluble in a range of solvents the resulting complexes exhibit very limited solubility, which is also reflected in the literature.^{2, 3, 5, 6, 8, 9} Solubility issues coupled with the highly reactive nature of calcium complexes often impedes their isolation and detailed characterisation. This phenomenon is also observed with the bisimidazoline (R-BIM) calcium complexes of Chapter 4. It can be imagined that when the complexes are dissolved in donor solvents such as THF, that lability increases due to binding competition between ligand and donor solvent.

Solubility of complexes **5a-f** in hydrocarbon solvents is further hindered by the inclusion of KI traces, a by-product of $[\text{Ca}\{\text{N}(\text{SiMe}_3)_2\}_2(\text{THF})_2]$ synthesis. Inclusions of KI can be avoided through extraction of $[\text{Ca}\{\text{N}(\text{SiMe}_3)_2\}_2(\text{THF})_2]$ into hexane upon work up.

In a bid to improve the solubility of the diamine calcium complexes in hydrocarbon solvents, exchange of the coordinating amide $[\text{N}(\text{SiMe}_3)_2]^-$ was replaced with benzyl $[\text{CH}_2(\text{C}_6\text{H}_5)]^-$ and *tert*-butyl benzyl $[\text{CH}_2(4\text{-C}_6\text{H}_4^t\text{Bu})]^-$ ligands.¹⁰ Both alternatives were prepared according to literature procedures before being reacted with a chosen diamine in the same manner as depicted in Scheme 2. With respect to solubility both the aromatic calcium complexes were less soluble in commonly used solvents systems than the original

$[\text{Ca}(\text{NN}^{\text{R}})\{\text{N}(\text{SiMe}_3)_2\}(\text{THF})_n]$. Whilst the *tert*-butyl benzyl bearing complex displayed greater solubility than its benzyl analogue the improvement was unsubstantial when compared to the original calcium amide.

3.3 Spectroscopic Characterisation

Detailed characterisation was heavily restricted for the $[\text{Ca}(\text{NN}^{\text{R}})\{\text{N}(\text{SiMe}_3)_2\}(\text{THF})_n]$ complexes **5a-f** due to their aforesaid solubility limitations and labile nature in ethereal solvents. Working in ethereal solutions with calcium compounds also carries the potential for ether cleavage. Ether cleavage is most typically observed in dibenzyl AE metal compounds $[\text{Ca}\{\text{CH}_2(\text{C}_6\text{H}_5)\}_2]$, where the benzyl ligand reacts readily with a proton in the α -position to the oxygen of the ether to form toluene. Whilst predominantly observed in benzyl containing AE compounds, the “Big R” supported $[\text{Ca}\{\text{CH}(\text{TMS})_3\}_2]$ is also known to react with ethers.¹¹ In contrast use of the hexamethyldisilazane anion $[\text{N}(\text{SiMe}_3)_2]^-$ demonstrates no such evidence of ether cleavage. NMR studies of the diamine calcium systems in THF- d_8 testify to this with the absence of resonances pertaining to ring-opened THF in NMR spectra.

In order to determine the extent of base coordination in THF- d_8 during analysis it was necessary to exchange the coordinating THF with pyridine (py). To prepare the pyridine complex analogues of **5a-f**, HNN^{R} (**4a-d, h, i**) was added to $[\text{Ca}\{\text{N}(\text{SiMe}_3)_2\}_2(\text{py})_2]$ in benzene.⁷ The reaction proceeded for 18 hours under ambient temperature followed by solvent and volatile by-product removal under reduced pressure to 4.0×10^{-2} mbar. The vacuum was monitored to ensure consistency between samples since it is known that prolonged exposure to reduced pressure can remove coordinated pyridine.⁶ The $[\text{Ca}(\text{NN}^{\text{R}})\{\text{N}(\text{SiMe}_3)_2\}(\text{py})_n]$ products **6a-f** were typically yellow/orange and obtained in good yields ($\geq 60\%$).

Like the THF adducts **5a-f**, the pyridine analogues **6a-f** were found to be only sparingly soluble in hydrocarbon solvents and underwent decomposition in chlorinated solvents. Whilst the majority of calcium complexes published to date have been analysed in benzene- d_6 , the need for analysis in THF- d_8 or mixtures thereof, is not unusual with calcium complexes and again reflects their insoluble nature.¹²⁻¹⁴

The NMR spectra of complexes **6a-f** in THF- d_8 were broad at ambient temperature. The fluxional process presumably arising from the lability of the NN^R ligands and the pyridine exchanging with THF, could not be completely “frozen out” using low temperature NMR analyses, within our instrumental capability (500 MHz, -90 °C).

Nevertheless 1H NMR spectra of each complex showed three distinct signals (although devoid of discernible fine structure) for the ethyl backbone of the diamine ligand. Signals were typically recorded between 3.00-2.80 ppm and 2.63-2.45 ppm for the CH_2 proton nuclei and for the proton at the chiral centre, between 2.60-2.57 ppm with the exception of complex **6c** which records a downfield shift of 2.72 ppm. The proton nuclei corresponding to the methine and the two methyl groups of the *iso*-propyl moiety display characteristic resonances. The methine proton gives a signal between 1.66-1.55 ppm, the exception being **6e** where the presence of two *iso*-propyl groups within the molecule records a broader range of 1.67-1.47 ppm. In complexes **6b**, **e**, and **f**, the methyl protons are typically recorded as two separate resonances with integration indicating three protons per environment. Complexes **6a**, **c**, and **d** however exhibit an apparent singlet for the two groups suggesting the methyl groups are in near-identical chemical environments for these examples. Generally signals for the methyl groups are recorded between 1.07-0.76 ppm. Differences in solvent between the data recorded for the protio-diamine and the diamine of the calcium complex nullifies direct comparison.

Parallel observations of distinctive resonances for the coordinated ligands are noted with respect to the $^{13}C\{^1H\}$ NMR spectra of complexes **6a-f**. The carbon nucleus at the chiral centre deviates very little between each complex, typically observed at 60.4-57.5 ppm with the adjacent CH_2 carbon nucleus recorded between 60.4-47.2 ppm. Resonance signals pertaining to the *iso*-propyl moiety are observed between 36.7-33.0 ppm for the methine and two signals are recorded for the two methyl groups between 20.5-19.7 and 18.6-17.9 ppm respectively.

The indication of a single $[N(SiMe_3)_2]^-$ moiety was evident from the relative integration of the signal at *ca.* 0 ppm in the 1H NMR spectra. Nonetheless, traces of two additional bis(trimethylsilyl)amide species of comparable chemical shift appear evident in all complexes. One such source can be speculated as being residual $HN(SiMe_3)_2$. Although a volatile by-product of the complexation reaction it has proven persistent when trying to remove it in its entirety, even through recrystallisation or extensive durations *in vacuo*.

The same phenomenon was observed during the synthesis of the R-BIM calcium complexes (Chapter 4, Section 4.3.2). The identity of the second bis(trimethylsilyl) species has remained undetermined. It is known that the presence of an excess of an acidic ligand can result in nitrogen-silicon bond cleavage to form ammoniate complexes of the form $[L_2M(NH_4)(H_2N(SiMe_3))]$.¹⁵ However reaction between liberated $HN(SiMe_3)_2$ and the protio-diamine/R-BIM ligand to give $H_2N(SiMe_3)$ and Me_3SiL and any subsequent protonolysis products is unlikely. This is due to the basic nature of the ligands and therefore an alternative side reaction is in operation or liberated $HN(SiMe_3)_2$ could be acting as a donor ligand and in exchange with THF and/or pyridine.

The presence of the fluorine nucleus in complex **6a** allows for exploitation of this NMR handle. ^{19}F NMR spectroscopy reveals a broad single resonance at -141.57 ppm, denoting a single environment, lending evidence to the structure not being a mixture of products.

The relative intensity of the coordinated pyridine in complexes **6a-f** was also intriguing. When the alkyl-substituted diamines **6e** and **f** were investigated, the number of pyridine ligands was less reproducible, ranging from 0.3–0.6 equivalents. This suggests that the pyridine is only weakly bound to the calcium. Attempts to prepare the base-free complex $[Ca(NN^R)\{N(SiMe_3)_2\}]$ by subjecting the complex to extended periods under vacuum were unsuccessful in all cases. In contrast approximately one molar equivalent of coordinated pyridine was observed in complexes **6a-d**, which decreased only marginally after extended periods *in vacuo*. It is currently unclear as to the observed differences in pyridine coordination between alkyl and aryl systems although it can be hesitantly suggested that the difference may lie in the variation of steric constraints imposed by the different N-substituents of the diamines.

Given the different degrees that pyridine coordinates to the calcium and the extremity of the NN^R ligand lability, the possibility of complexes **6a-f** existing as dimers or oligomers cannot be discounted even with the success of the bulky $[N(SiMe_3)_2]^-$ ligand in preventing such an occurrence in other systems.¹⁶ In all likelihood the actual structure of complexes **6a-f** could be an exchanging mixture of monomeric and oligomeric species. Such an occurrence is not unexpected given the inclination of similar Grignard reagents to undergo facile redistribution processes.¹⁷

Synthesis of three homoleptic complexes $[\text{Ca}(\text{NN}^{\text{R}})_2]$ (R = 4-C₆H₅F **7a**, Ph **7b**, and ^tBu **7c**) was achieved through combination of two equivalents of protio-ligand NN^R (**4a**, **d**, and **i**) with one equivalent of $[\text{Ca}\{\text{N}(\text{SiMe}_3)_2\}_2(\text{py})_2]$ in toluene. The reaction was allowed to proceed for 18 hours at ambient temperature before the resulting complex was isolated as yellow/orange precipitates and dried *in vacuo*. As with the heteroleptic complexes **5a-f** and **6a-f**, the homoleptic complexes **7a-c** were only soluble in THF.

Synthesis of the homoleptic complexes results in the liberation of two equivalents of HN(SiMe₃)₂ and pyridine. In an attempt to remove these by-products compounds **7a-c** were dried *in vacuo* for an extended period of time. After such time only trace amounts of pyridine were observed in corresponding NMR spectra. The near quantitative removal of pyridine in the homoleptic complexes **7a-c** is in stark contrast to that of heteroleptic complexes **6a-f** where removal of pyridine is never total. As previously noted with the heteroleptic complexes, small quantities of bis(trimethyl)silyl amide species remained present. The remaining presence of bis(trimethyl)silylamide species is characteristic in both homoleptic and heteroleptic NN^R calcium complexes and is mirrored in the observations of the R-BIM calcium complexes discussed in Chapter 4 Section 4.3.2. Pursuit of further purification to remove all traces of the bis(trimethyl)silyl amide again proved unsuccessful.

Comparison of spectroscopic data between the heteroleptic (**6a**, **d**, and **f**) and homoleptic analogues **7a-c** reveals that both species have rather different spectroscopic signatures. This evidence supports speculation that the heteroleptic species **6a-f** show little to no formation of homoleptic species in solution. Whilst differences in chemical shift are trivial with respect to the *iso*-propyl stereodirecting group, resonances attributed to the ethylene backbone exhibit chemical shift variations of greater note. The differences are pronounced in both ¹H (up to Δδ 0.2 ppm downfield cf. heteroleptic complex) and ¹³C{¹H} spectra (up to Δδ 5 ppm upfield cf. heteroleptic complex) with the exception of the alkyl complexes. Comparison of the ¹³C NMR data of the *tert*-butyl complex **7c** when compared to its heteroleptic derivative **6f**, displays significantly less pronounced chemical shift divergence (Δδ 0.2 ppm upfield cf. heteroleptic complex) than the aromatic complexes.

Dissimilarities in chemical shift are also observed in resonance signatures of the specific N-R substituents. Comparison of the ¹H and ¹³C{¹H} NMR spectra of the phenyl substituent(s) of **6d** and **7b** is the most distinctive of all examples. Variation between resonances of the N-R substituent in the heteroleptic and corresponding homoleptic

complex varies to the same degree as resonances for the ethylene backbone ($\Delta\delta$ 0.2 ppm in the ^1H NMR spectra and $\Delta\delta$ 5 ppm in the $^{13}\text{C}\{^1\text{H}\}$ NMR spectra). As previously observed the resonances of the N-R substituent of the alkyl complexes **6f** and **7c** show a chemical shift divergence to a lesser degree than in the aromatic examples.

The ^{19}F NMR spectrum of $[\text{Ca}(\text{NN}^{\text{ArF}})_2]$ **7a** records a signal at -130.64 ppm (293 K) compared to -141.62 ppm of the heteroleptic analogue $[\text{Ca}(\text{NN}^{\text{ArF}})\{\text{N}(\text{SiMe}_3)_2\}(\text{py})]$ **6a** at (293 K). At a reduced temperature of 263 K **6a** shows minimal temperature dependence of the chemical shift (-141.62 ppm), whereas at the same temperature the spectra of the homoleptic analogue **7a** now gives two separate resonances at -141.09 ppm and -130.64 ppm. This denotes a distinct difference in fluorine environments between the heteroleptic and homoleptic compounds. The absence of fluorine resonances attributed to the homoleptic complex in the spectra of the heteroleptic complex further supports the presence of the heteroleptic species only.

The analysis of IR data obtained from the diamine ligands and subsequent heteroleptic and homoleptic complexes is less revealing with respect to structural data not already deduced from NMR spectroscopic techniques. We were unable to ascribe which amine moiety is favoured for deprotonation when coordinated to calcium as absorption for primary and secondary amines N-H stretches overlap and are characteristically broad. C-N absorptions of both primary and secondary amines also occupy the same band of absorbance: 1350-1200 cm^{-1} for aromatics and 1250-1000 cm^{-1} for aliphatic amines. However one absorption at 1260 ($\pm 2 \text{ cm}^{-1}$) is common to all heteroleptic and homoleptic complexes and signifies a C-N stretch of the amine but is not indicative of whether it arises from a primary or secondary amine. Addition of the pyridine complicates the region since it also produces an absorption signal resulting from its amine moiety.

Other absorptions of note are those relating to the aromatic C-F bond of diamine NN^{ArF} **4a**, heteroleptic complex **6a** and homoleptic analogue **7a**. Absorption between 1250-1100 cm^{-1} is identifiable even with aromatic C-H in-plane bending observed between 1250-950 cm^{-1} . The stronger absorbance of the C-F stretch is seen at 1216 cm^{-1} in **4a**, 1219 cm^{-1} in **6a** and 1218 cm^{-1} in **7a**. Absorbencies relating to other structural features such as phenyl derivatives, alkyl moieties of the ligand backbone, and the *iso*-propyl group were observed within their typical regions.

3.4 DFT

In order to gain an insight into the structure of the proposed mononuclear species **5a-f** (Scheme 2) and determine which of the amine moieties is preferentially deprotonated the structures of $[\text{Ca}(\text{NN}^{\text{R}})\{\text{N}(\text{SiMe}_3)_2\}(\text{py})]$ ($\text{R} = 4\text{-C}_6\text{H}_4\text{F}$ **7a_{calc}**, Ph **7b_{calc}**, and ^tBu **7c_{calc}**) were calculated using density functional methods by Dr. Benjamin Ward. The computed structures of heteroleptic complexes **7a_{calc}-c_{calc}** are displayed in Fig. 3. It was calculated that the structures of **7a_{calc}-c_{calc}** with the diamine deprotonated at the secondary amine were approximately 13 kcal mol^{-1} ($\sim 54 \text{ kJ mol}^{-1}$) more stable than when the diamine ligand was deprotonated at the primary amine (Fig. 4, conformation a vs. b)

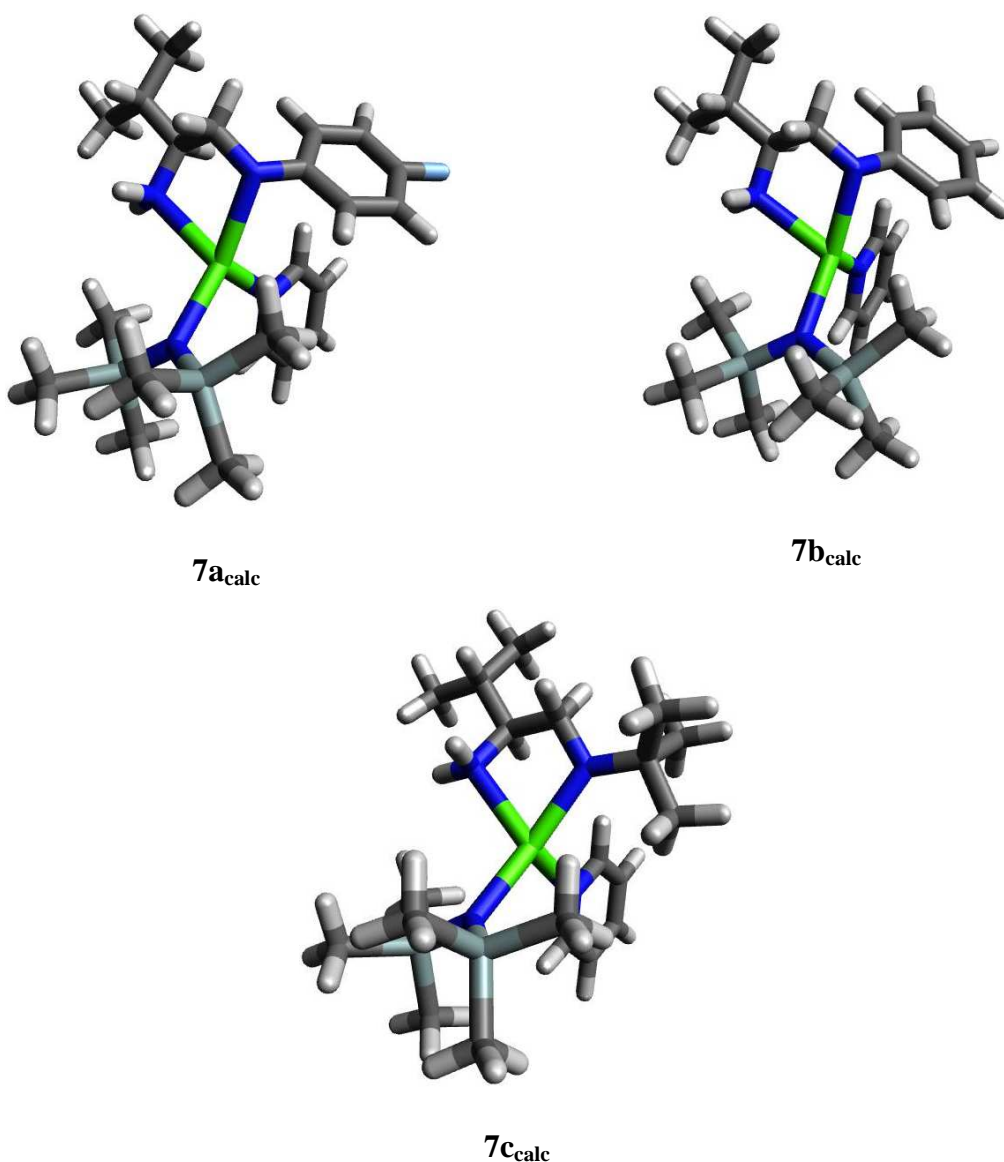


Fig. 3 Calculated structures of $[\text{Ca}(\text{NN}^{\text{R}})\{\text{N}(\text{SiMe}_3)_2\}(\text{py})]$ complexes **7a_{calc}-c_{calc}**.



Fig. 4 Preferred deprotonation of the diamine at the secondary amine (a), and less favoured deprotonation at the primary amine moiety (b).

The structure of compounds $[\text{Ca}(\text{NN}^{\text{Ar-F}})\{\text{N}(\text{SiMe}_3)_2\}(\text{py})]$ **7a_{calc}** and $[\text{Ca}(\text{NN}^{\text{Ph}})\{\text{N}(\text{SiMe}_3)_2\}(\text{py})]$ **7b_{calc}** are isostructural and indicate a significant deviation of the amido nitrogen from the expected trigonal planar geometry. The sum of the angles subtended around the nitrogen of the N-R moiety being 339.5° for **7a_{calc}** and 336.4° for **7b_{calc}**. This is in contrast to the sum of angles around the nitrogen of the N-R in $[\text{Ca}(\text{NN}^{\text{tBu}})\{\text{N}(\text{SiMe}_3)_2\}(\text{py})]$ **7c_{calc}** which total 358.1° , indicating a trigonal planar geometry. The consequence of the non-planar conformation in **7a_{calc}** and **7b_{calc}** is that the phenyl ring is orientated to provide a chiral environment at the calcium centre. This may explain the effective stereocontrol in hydroamination catalysis, particularly in the case of **7b_{calc}**.

Amides (NR_2) are known to be anionic, 2 or 4 electron donors since they are able to form σ -bonds but can also donate the p-orbital lone pair into an empty d-orbital of a metal. This creates additional π -bonding interactions between the ligand and the metal and results in the amide taking a trigonal planar geometry to accommodate the orbital overlap. In the case of calcium we do not expect there to be any significant π -bonding between the diamine and calcium centre due to the 3d-orbitals being significantly high in energy to be rendered inaccessible. Therefore there is less electronic preference for the nitrogen to adopt a trigonal planar geometry.

3.5 Intramolecular Hydroamination Catalysis

As detailed in Chapter 1 Section 1.2.1 and illustrated in Scheme 1, hydroamination be it inter- or intramolecular is defined as the formal addition of an N-H bond across an unsaturated bond. Hydroamination presents itself as a very attractive means to prepare a wide range of nitrogen containing compounds via a 100% atom-efficient route. Coupled with the successful mediation of this reaction with organocalcium complexes and reports that stereoselectivity can be achieved, albeit low levels, makes this reaction an ideal candidate to which we are able to measure and compare the performance of our newly developed calcium catalysts.

All intramolecular hydroamination catalysis experiments were conducted using the novel complexes $[\text{Ca}(\text{NN}^{\text{R}})\{\text{N}(\text{SiMe}_3)_2\}(\text{THF})_n]$ **5a-j**. These were generated *in-situ* from the respective ligand and $[\text{Ca}\{\text{N}(\text{SiMe}_3)_2\}_2(\text{THF})_2]$ before being reacted with catalytic substrates **A** and **B** (Scheme 1). Progress of the hydroamination reaction with each catalyst was monitored by ^1H NMR spectroscopy at regular intervals appropriate to the reaction duration. During each reaction the introduction of resonances corresponding to the cyclised pyrrolidine emerge and increase in intensity as a function of time, whilst resonances relating to the starting 2,2-dialkylpent-4-en-1-amine (referred to as aminoalkene henceforth) substrate lessen in intensity with product conversion. An example ^1H NMR spectra stack plot from the complete catalytic conversion of substrate **B** by complex $[\text{Ca}(\text{NN}^{\text{tBu}})\{\text{N}(\text{SiMe}_3)_2\}(\text{THF})_n]$ **5f** is presented in Fig. 5 overleaf.

With each spectrum the product conversion is calculated from comparison of the integration of notable resonances corresponding to the aminoalkene precursor and resulting pyrrolidine product.¹ Typically in the starting aminoalkene the two multiplets at 5.40 ppm and 4.95 ppm (ratio 1:2 calculated via integration) are chosen. These two resonances pertain to the $-\text{CH}=\text{CH}_2$ double bond present in the aminoalkene. These signals are compared to the emerging doublet *ca.* 1.00 ppm, which is attributed to the *exo*-methyl group coupling with the hydrogen nucleus in the newly formed pyrrolidine. The aminoalkene only forms the cyclised pyrrolidine during intramolecular hydroamination, and no isomerisation or other by-products were observed.¹⁸

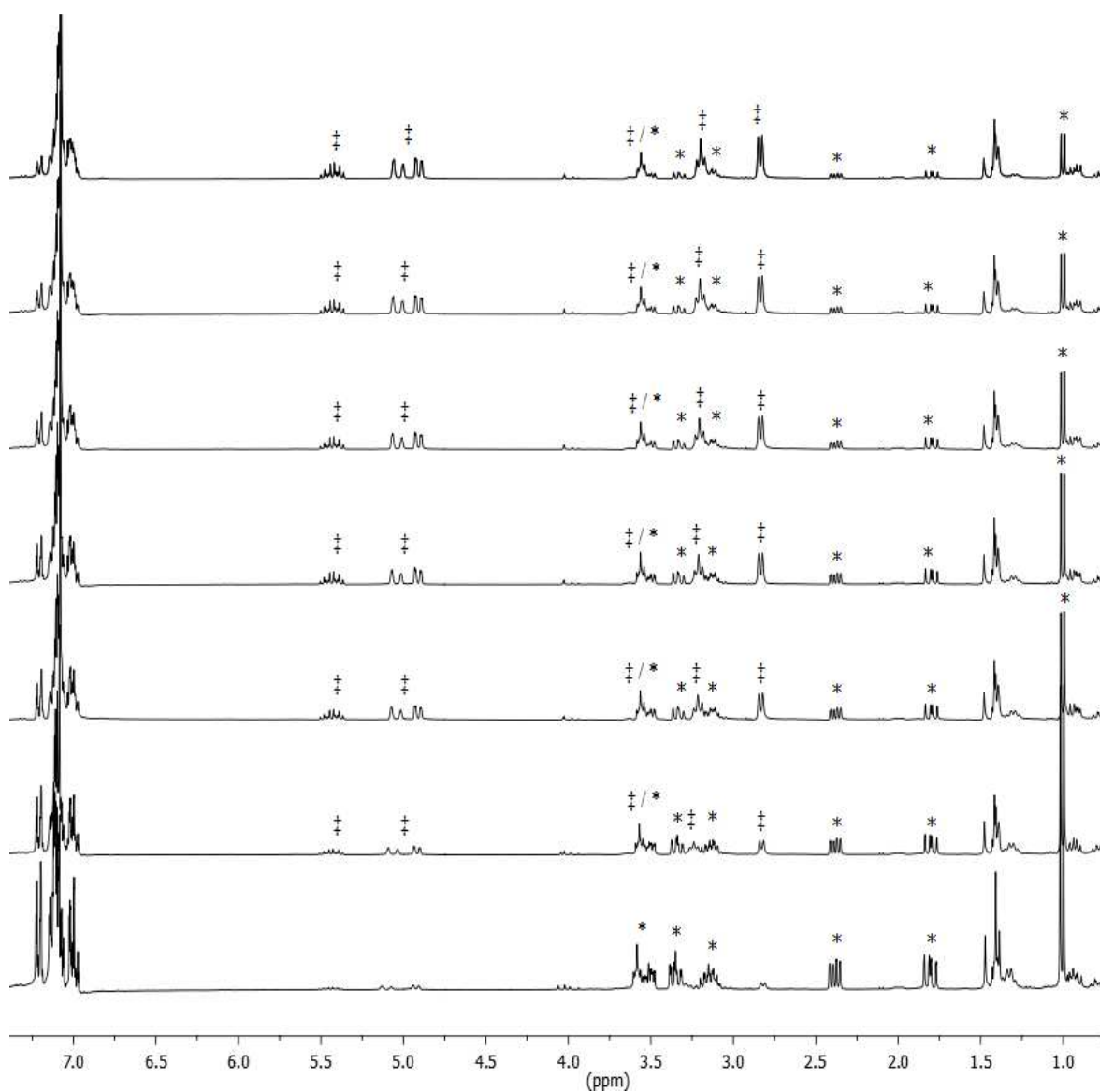


Fig. 5 ^1H NMR stack plot of spectra from the cyclisation of substrate **B** (‡) to its corresponding pyrrolidine product (*) with $[\text{Ca}(\text{NN}^{\text{tBu}})\{\text{N}(\text{SiMe}_3)_2\}(\text{THF})_n]$ **5f** in C_6D_6 at 293 K. Spectra proceed from top ($t = 0$ h) to bottom ($t = 6$ h).

From product conversion data conversion curves can be constructed. One such example is shown in Fig. 6. All additional conversion curves for this Chapter are supplied in Appendix A. The method employed for initial rate determination involved the collection of ^1H NMR spectra at staggered intervals during catalytic reactions. The time intervals between spectra collection were reaction dependent, ranging from every 10 minutes to every 30 minutes or more in slower reactions, until no further conversion was observed. The conversion curves were curve fitted to an exponential decay function $y = Ae^{-bx}$. The initial rate was given by the slope at the origin ($x=0$) and was determined by differentiation of the equation: $dy/dx = -A/b$ for $x = 0$. The resulting initial rate figures are listed in Table 1.

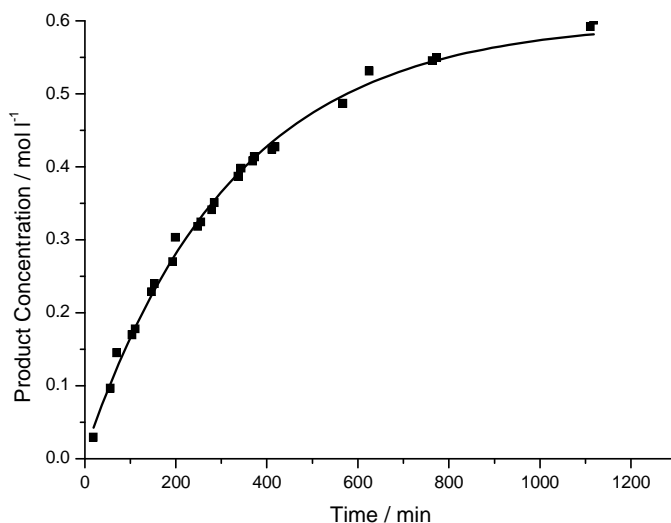


Fig. 6 Example conversion curve for the catalytic hydroamination of substrate **B** using 10 mol% $[\text{Ca}(\text{NN}^{\text{Ph}})\{\text{N}(\text{SiMe}_3)_2\}(\text{THF})]$ **5d** in C_6D_6 at 293 K.

Enantioselectivities were determined using ^1H NMR spectroscopy, with the aid of adding an excess of chiral derivatising agent *R*-(-)- α -acetylmandelic acid **2.21** (Fig. 7)^{19, 20} to the pyrrolidine containing reaction mixture. This occasions a characteristic “doubling” of each resonance in the ^1H NMR spectra, as typified by the presence of stereoisomers as discussed in Chapter 2, Section 2.5.²¹

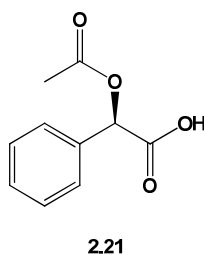


Fig. 7 *R*-(-)- α -acetylmandelic acid **2.21** used for ee determination.

Once *R*-(-)- α -acetylmandelic acid **2.21** was added to the pyrrolidine mixture the doublet resonance caused by the exo-methyl moiety of the pyrrolidine product (*ca.* 1.00 ppm) appeared as two doublets corresponding to the two diastereomeric ion-pairs. Enantiomeric excess is determined from comparison of the integration of each pair of resonances using line-fitting software as part of the Mestre-C or iNMR software packages. Fig. 8 displays two examples of an expanded section of a ^1H NMR spectra displaying the now doubled-doublet of the methyl signal of the pyrrolidine. In Spectrum (a), the combined integration

of peaks 0 and 1 is equal to the sum of 2 and 3, denoting the sample is racemic. This is to be expected since the catalyst used in this example was the non-stereoselective $[\text{Ca}\{\text{N}(\text{SiMe}_3)_2\}_2(\text{THF})_2]$ compound. Fig. 8, Spectrum (b), depicts the corresponding region of the ^1H NMR spectra where the characteristic doubled-doublet methyl resonance of the pyrrolidine product is observed for enantiomeric excess determination. In the case of Spectrum (b), the sum of integration from peaks 0 and 1 is not equal to the sum of 2 and 3, and differences in integration signify an enantiomeric excess of 26%. This value was achieved with catalyst **5d** ($[\text{Ca}(\text{NN}^{\text{Ph}})\{\text{N}(\text{SiMe}_3)_2\}(\text{THF})]$) when applied to the hydroamination of substrate **B**.

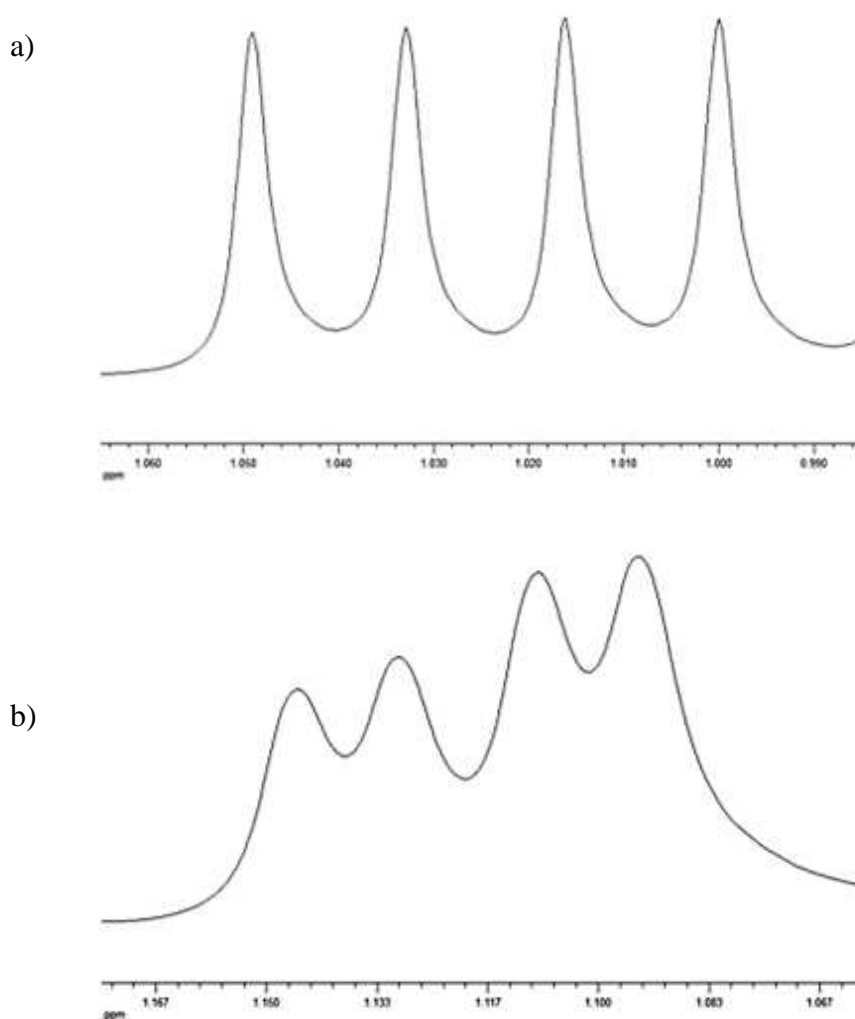


Fig. 8 (a) ^1H NMR spectra from racemic catalytic reaction of $[\text{Ca}\{\text{N}(\text{SiMe}_3)_2\}(\text{THF})_2]$ with substrate **A** with *R*-(-)- α -acetylmandelic acid, (b) ^1H NMR spectra from catalytic reaction between **5d**, $[\text{Ca}(\text{NN}^{\text{Ph}})\{\text{N}(\text{SiMe}_3)_2\}(\text{THF})]$ and substrate **B** with the addition of *R*-(-)- α -acetylmandelic acid **2.21**. Enantiomeric excess calculated at 26%.

3.5.1 Catalytic Performance and Enantioselectivity

The performance and enantioselectivities of the tested catalyst systems are presented in Table 1. All examples proceeded at significantly slower rates than that of $[\text{Ca}\{\text{N}(\text{SiMe}_3)_2\}_2(\text{THF})_2]$, which is to be expected when adding a sterically demanding spectator ligand. For reference use of $[\text{Ca}\{\text{N}(\text{SiMe}_3)_2\}_2(\text{THF})_2]$ as the catalyst sees substrate **A** (Scheme 1) converted to 99% pyrrolidine in 23-29 hours under ambient conditions (entry 1), whilst substrate **B** rapidly achieves >99% conversion with the reaction reaching completion before collection of ^1H NMR data can be accomplished (*ca.* 7 minutes, entry 11).

Interestingly when complex **5a** is employed as a catalyst no catalytic activity is observed (entries 2, 3, and 12). At ambient temperatures this is also the case with compounds **5b** and **5d**, with substrate **A** only (entries 4 and 7 respectively). At elevated temperatures (50 °C) **5b** and **5d** do display catalytic activity. Thus compound **5a** remains unique in the fact that it shows no catalytic activity even at elevated temperatures (up to 80°C) for prolonged durations. All homoleptic complexes (**7a-c**) tested as catalysts also displayed no catalytic activity. Since NMR data suggests that preparation of the heteroleptic complex **6a** appears devoid of its homoleptic analogue, redistribution of the complex would not appear to be the cause of this examples inaction with the THF analogue **5a**.

Most noteworthy is the phenyl N-R substituent catalyst **5d** with substrate **B**, in which the chiral pyrrolidine is formed in a 26% ee (entry 9). This degree of enantioselectivity represents a remarkable increase from the 5-10% obtained with the calcium BOX complexes² and is higher than with the most recent calcium complexes reported by Sadow *et al.*³ Catalyst **5b** displays a marginally lower ee of 21% (entry 14), but interestingly is also only active with substrate **B** at ambient temperature. Both these examples do display activity with substrate **A** at 50 °C even if conversions of 35% and 40% respectively are markedly low (entries 5 and 8). Even then poor yields at elevated temperatures are accompanied with a racemic mix of pyrrolidine product.

An explanation to why catalysts **5b** and **5d** show significantly higher selectivity than others currently remains unclear. The observation of the complexes that record induced selectivity (entries 6, 9, and 14-16) favour the *geminal*-phenyl aminoalkene (substrate **B**), suggests that π - π stacking/interactions between substrate and the supporting ligand's aromatic N-R substituent might be important during the catalytic cycle. The lack of such a ligand-

substrate interaction between the catalyst and substrate **A** may also explain why the aromatic N-R substituted ligands display predominantly poor selectivities with this substrate. From the DFT calculations of complexes **7a_{calc}** and **7b_{calc}** discussed in Section 3.4, the deviation from linearity of the amine and typical trigonal-planar orientation, causing favourable chiral orientation of the phenyl ring might be an important factor of the success of both complexes **5b** and **5d**.

Table 1 Asymmetric hydroamination of amino-olefins using 10 mol% catalyst in C₆D₆.

Entry	Catalyst	N-R	Substrate	Temp (K)	Initial Rate/ mol dm ⁻³ s ⁻¹	Conv.% ^a	ee% ^b
1	[Ca] ^e	-	A	293	5.0(2)×10 ⁻⁵	>99	0
2	5a	4-C ₆ H ₄ F	A	293	-	-	-
3	5a	4-C ₆ H ₄ F	A	353 ^d	-	-	-
4	5b	4-C ₆ H ₄ OCH ₃	A	293	-	-	-
5	5b	4-C ₆ H ₄ OCH ₃	A	323	2.4(1)×10 ⁻⁷	40	0
6	5c	4-C ₆ H ₄ CH ₃	A	293	1.1(1)×10 ⁻⁶	82	8
7	5d	C ₆ H ₅	A	293	-	-	-
8	5d	C ₆ H ₅	A	323	5.2(2)×10 ⁻⁶	35	0
9	5e	ⁱ Pr	A	293	2.3(1)×10 ⁻⁶	>99	12
10	5f	^t Bu	A	293	5.9(8)×10 ⁻⁷	90	0
11	[Ca] ^e	-	B	293	^c	>99	0
12	5a	4-C ₆ H ₄ F	B	293	-	-	-
13	5a	4-C ₆ H ₄ F	B	353 ^d	-	-	-
14	5b	4-C ₆ H ₄ OCH ₃	B	293	5.6(3)×10 ⁻⁵	96	21
15	5c	4-C ₆ H ₄ CH ₃	B	293	4.3(2)×10 ⁻⁶	93	8
16	5d	C ₆ H ₅	B	293	3.0(1)×10 ⁻⁵	80	26
17	5e	ⁱ Pr	B	293	4.9(2)×10 ⁻⁵	>99	5
18	5f	^t Bu	B	293	1.1(1)×10 ⁻⁴	>99	6

^a Determined from ¹H NMR spectra upon no further observable conversion. ^b Determined by ¹H NMR spectroscopy using *R*-(-)- α -acetylmandelic acid.¹⁹ ^c Reaction complete <7 min, rate unrecorded. ^d Attempt at 323 K recorded no activity, yield or selectivity. ^e Complex [Ca] = [Ca{N(SiMe₃)₂}₂(THF)₂].

Excluding the racemic examples (entries 1-5, 7-9, and 10-13), enantiomeric excess ranged from 5-26%. Whilst catalysts **5b** and **5d** yielded the highest enantioselectivities (entries 14 and 16) with substrate **B**, catalyst **5e** remains the only example to show preference for substrate **A** (entry 9). Catalyst **5e**'s alkyl (*tert*-butyl) N-R substituent, opposed to the aromatic examples discussed may prompt consideration that aromatic N-R substituents are better suited for substrate **B**, and diamines bearing alkyl substituents for substrate **A**, however this appears unfounded. Supporting evidence is seen with catalyst **5f**. Whilst bearing an *iso*-propyl N-R substituent observation shows a preference for substrate **B** (entry 10 cf. 18), 4-C₆H₄CH₃ substituent bearing complex **5c** also contravenes this postulation by showing the same selectivities for both substrates (8% ee, entries 6 and 15).

Whilst acquisition of applaudable enantioselectivities is highly desirable, attention must be exercised as to the rate and yield of product attainment. All active catalysts at ambient temperature displayed good product yield of $\geq 80\%$ and reduced yields were only seen in cases where elevated reaction temperatures were used (entries 5 and 8). At raised temperatures complex stability over long reaction times becomes questionable. Examples are known where poor reactivity was attributed to complex decomposition at elevated reaction temperatures over long reaction periods.²²

Of the two examples that attained the highest enantiomeric excesses (entries 14 and 16), both display comparable initial rates of $5.6(3)\times 10^{-5}$ and $3.0(1)\times 10^{-5}$ mol dm⁻³ s⁻¹ respectively (Substrate **B** range = $4.3(2)\times 10^{-6}$ – $1.1(1)\times 10^{-4}$ mol dm⁻³ s⁻¹; average = 4.99×10^{-5} mol dm⁻³ s⁻¹). Both rates are on a par to other entries contained in Table 1; however entry 14 with catalyst **5b** shows an increase in yield (96%) opposed to entry 16 with catalyst **5d** (80%). In practical terms diamine reaction times (till recorded conversion) tended to proceed over a period of 72 hours.

Comparison of the catalytic performance of the calcium diamine complexes **5a-f** to existing calcium examples and the closely related lanthanides in hydroamination can be conducted by looking at several key areas: catalyst loading, reaction conditions and time, yield, and enantioselectivities. Several recent reviews cover a wide range of aminoalkene substrates explored with lanthanide complexes, and the reader is directed to these for further reading.^{18, 23-25}

The use of 10 mol% of catalyst in our studies was chosen deliberately, owing to it being a common quantity for catalyst loading in hydroamination reactions carried out using calcium compounds.¹⁻³ Examples where catalyst loadings of 2-5 mol% have been successfully employed with calcium are also known.^{22, 26} In a few cases higher quantities are acknowledged, however loadings above 15-20 mol% are not known and examples using 20 mol% tend only to be employed in cases where unacceptable yields were obtained with lower quantities. It should also be mentioned that the highest catalyst loadings are confined to substrates of longer chain length than either substrate **A** or **B**, presumably to increase rates of forming larger ring sizes. With regards to its lighter congener magnesium, a similar range of catalyst loadings have been employed i.e. 2-10 mol%.²⁷ In lanthanide mediated hydroamination, generally lower catalyst loadings are routinely employed, ranging from 1-5 mol%.^{18, 23, 25}

When comparing the reaction times of the diamine systems **5a-f**, this is the first study to investigate initial rates, as many reports only quote observed reaction time in relation to hours/days. Irrespective of this, it is clear compounds **5a-f** perform at a significantly slower rate when put side by side to other known calcium examples.^{1-3, 22, 26, 28-31} The majority of literature calcium catalysts deliver rapid conversions, especially with aminoalkene substrates **A** and **B**. Final yields are regularly achieved in two hours or significantly less e.g. 20-30 minutes. Comparison of catalysts **5a-f** with the lanthanides results in a similar trend where reactivity of the diamines is significantly diminished upon comparison. The greater abundance of lanthanide literature naturally leads to a wider range of reported reaction times where examples showing comparable rates to the diamines in hydroamination exist, i.e. several days to reach final yield.³² On average the lanthanides experience similarly high reactivity as some of the calcium and other AE metal catalysts do, converting substrates within several hours, not days. With regards to substrate **A** the lanthanides typically cyclise this substrate in 12 hours and substrate **B** (already observed as the more easily cyclised substrate) in 2 hours or less.

The ability to execute hydroamination reactions under ambient temperatures is very appealing and is a common trait shared between the AE metals and lanthanides alike. The use of increased reaction temperatures, for example 60-80 °C is less regular in both though should not be considered infrequent. Raised reaction temperatures are necessary for substrates that form 6-membered (or larger) heterocyclic compounds or bear more sterically demanding substituents than substrates **A** and **B**. In any case, increases in

reaction temperature lead to faster reaction times and improvements in yield, albeit to the detriment of enantiomeric excess in the case of the lanthanides. Upon first inspection it would appear that the case of catalyst **5a** (entries 3, 4, 12, and 13, Table 1) showing complete inactivity even at temperatures of 80 °C, is not an isolated example.^{22, 26} Even so, the literature examples reported stunted reactivity when using substrates bearing either mono- or dimethyl substitution at the terminal alkene, or upon substrates aiming to form 7-membered rings. Both features are identified as factors that impede reactivity due to sterics, though neither of these factors are present in the simpler substrates **A** and **B** and so the lack of activity recorded by **5a** with these substrates should be regarded as abnormal until other examples emerge from the literature.

The employment of lanthanides in hydroamination has been very successful, and rightly so when observing very consistent product yields of $\geq 95\%$. The AE metals also demonstrate many examples of near quantitative conversion over a range of substrates.²⁸ Yet, it would appear the range of conversion is more disperse than that observed in the lanthanides. In calcium and AE metals, the typical conversion range could be extended to 85-99%. In light of this the yields experienced by the diamine catalysts **5a-f** are very agreeable with the majority of examples. The only exceptions are the noticeably poor yields of entries 5 and 8 of Table 1.

As revealed, the enantiomeric excess of 26% achieved by diamine supported catalyst **5d** (entry 16, Table 1) represents the leading figure in this field at the time of writing. Currently literature examples of calcium mediated asymmetric hydroamination remain sparse with two previous reports. One from Buch and Harder² (4-10% ee) and another from Sadow *et al.*³ (18% ee), which are discussed in greater detail in Chapter 1, Section 1.2.1.2. The improvement in obtained enantiomeric excess by calcium compound **5d** represents a sizeable increase over the literature, however when compared to magnesium it is still significantly behind.

Magnesium mediated hydroamination frequently achieves higher enantiomeric excesses in comparison to calcium aided hydroamination. Sadow *et al.* provided an excellent comparative investigation by probing the magnesium analogue of the calcium system which achieved 18% ee. When compared side by side in identical reactions the magnesium catalyst achieved enantiomeric excesses of 27-36%. More recently even these moderate enantiomeric excesses have been dwarfed by the report from Hultsch *et al.* demonstrating

enantiomeric excesses of up to 93% in hydroamination reactions.⁴ Examples of lanthanide catalysts in asymmetric hydroamination is significantly more developed and generally outperforms the aforementioned calcium examples, including our own in asymmetric hydroamination. There is a significant range of recorded enantiomeric excesses when utilising lanthanides, from racemic up to 87% ee, though commonly averaging between 45-60% ee.^{18, 20, 23, 24}

In conclusion, chiral 1,2-diamines as supporting ligands for calcium complexes have been shown as moderately efficient stereodirecting scaffolds. Whilst there is clearly room for improvement the significant increase in obtained enantiomeric excesses compared to previously cited literature examples remains promising. Whilst further investigation of complex structure is warranted, expanding the understanding of the mechanism behind hydroamination may prove fruitful and help shed further insight into the notion of important ligand/substrate interactions being an influential factor on stereoselectivity.

3.6 References

1. M. R. Crimmin, I. J. Casely and M. S. Hill, *J. Am. Chem. Soc.*, **2005**, 127, 2042.
2. F. Buch and S. Harder, *Z. Naturforsch.*, **2008**, 63b, 169.
3. S. R. Neal, A. Ellern and A. D. Sadow, *J. Organomet. Chem.*, **2011**, 696, 228.
4. X. Zhang, T. J. Emge and K. C. Hultsch, *Angew. Chem. Int. Ed*, **2012**, 51, 394.
5. J. S. Wixey and B. D. Ward, *Dalton Trans.*, **2011**, 40, 7693.
6. J. S. Wixey and B. D. Ward, *Chem. Commun.*, **2011**, 47, 5449.
7. D. C. Bradley, M. B. Hursthouse, A. A. Ibrahim, K. M. Abdul Malik, M. Motevalli, R. Moseler, H. Powell, J. D. Runnacles and A. C. Sullivan, *Polyhedron*, **1990**, 9, 2959.
8. J. S. Alexander and K. Ruhlandt-Senge, *Eur. J. Inorg. Chem*, **2002**, 2761.
9. S. Harder, *Chem. Rev.*, **2010**, 110, 3852.
10. S. Harder, S. Muller and E. Hubner, *Organometallics*, **2004**, 23, 178.
11. C. Eaborn, S. A. Hawkes, P. B. Hitchcock and J. D. Smith, *Chem. Commun.*, **1997**, 1961.
12. L. Orzechowski, G. Jansen, M. Lutz and S. Harder, *Dalton Trans.*, **2009**, 2958.
13. F. Feil and S. Harder, *Organometallics*, **2000**, 19, 5010.
14. P. Jochmann, T. S. Dols, T. P. Spaniol, L. Perrin, L. Maron and J. Okuda, *Angew. Int. Ed. Engl*, **2009**, 48, 5715.
15. S. Chadwick, U. Englich and K. Ruhlandt-Senge, *Angew. Chem. Int. Ed*, **1998**, 37, 3007.
16. W. D. Buchanan, D. G. Allis and K. Ruhlandt-Senge, *Chem. Commun.*, **2010**, 46, 4449.
17. D. Seyferth, *Organometallics*, **2009**, 28, 1598.
18. T. E. Müller, K. C. Hultsch, M. Yus, F. Foubelo and M. Tada, *Chem. Rev.*, **2008**, 108, 3795.
19. G. Zi, F. Zhang, L. Xiang, Y. Chen, W. Fang and H. Song, *Dalton Trans.*, **2010**, 39, 4048.
20. J. Y. Kim and L. Tom, *Org. Lett.*, **2005**, 7, 1737.
21. G. H. P. Roos and A. Donovan, R., *Science and Technology*, **2000**, 5, 11.
22. M. R. Crimmin, M. Arrowsmith, A. G. M. Barrett, I. J. Casey, M. S. Hill and P. A. Procopiou, *J. Am. Chem. Soc.*, **2009**, 131, 9670.

23. D. V. Vitanova, F. Hampel and K. C. Hultsch, *J. Organomet. Chem.*, **2011**, 696, 321.
24. K. C. Hultsch, D. V. Gribkov and F. Hampel, *J. Organomet. Chem.*, **2005**, 690, 4441.
25. S. Hong and T. J. Marks, *Acc. Chem. Res.*, **2004**, 37, 673.
26. M. Arrowsmith, M. S. Hill and G. Kociok-Kohn, *Organometallics*, **2009**, 28, 1730.
27. P. Horrillo-Martinez and K. C. Hultsch, *Tetrahedron Lett.*, **2009**, 50, 2054.
28. A. G. M. Barrett, M. R. Crimmin, M. S. Hill and P. A. Procopiou, *Proc. R. Soc. A*, **2010**, 466, 927.
29. S. Datta, P. W. Roesky and S. Blechert, *Organometallics*, **2007**, 26, 4392.
30. J. Jenter, R. Köppe and P. W. Roesky, *Organometallics*, **2011**, 30, 1404.
31. M. Arrowsmith, M. R. Crimmin, A. G. M. Barrett, M. S. Hill, G. Kociok-Kohn and P. A. Procopiou, *Organometallics*, **2011**, 30, 1493.
32. N. Meyer, A. Zulys and P. W. Roesky, *Organometallics*, **2006**, 25, 4179.

Chapter Four

Chiral Bisimidazoline Supported Calcium Complexes

4.1 Introduction

In 2008 Buch and Harder's bisoxazoline (BOX) supported calcium complex **1.6** was the first reported example of asymmetric hydroamination mediated by an AE metal (Fig. 1).¹ Although a positive step forward with organocalcium chemistry the recorded enantiomeric excesses were notably poor (5-10% ee). Our aim was to build upon this result, principally through judicious ligand selection/modification where we elected to employ bisimidazolines as the starting scaffold. As can be seen, both the oxazoline (**a**) and imidazoline (**b**) ligand frameworks are structurally similar (Fig. 2).

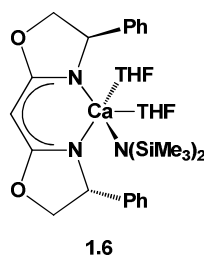


Fig. 1 [Ca(BOX){N(SiMe₃)₂}(THF)₂] complex (**1.6**).

Since their first implementation in asymmetric catalysis in 1986,² oxazolines have emerged as highly successful supporting ligands for a wide range of catalysis reactions. A sub-class of the oxazoline is the bisoxazoline which has become popular since its establishment in the early 1990's by the likes of Evans³ and Corey.⁴ Pronounced success led to their classification as a privileged ligand and so it seems sensible and fitting that the first ligand deployed on calcium for asymmetric hydroamination was a BOX. Comprehensive reviews have been written about the implementation of BOXs in asymmetric catalysis and provide greater breadth of the area.⁵⁻⁷

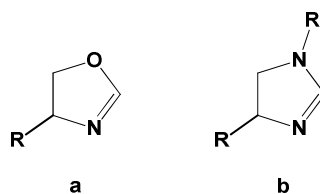


Fig. 2 Oxazoline (a) and 2-imidazoline (b) motifs.

The BOX complex **1.6** used by Buch and Harder is one of the simpler oxazoline derivatives sporting two oxazoline rings bridged by a single carbon linker. Many poly(oxazoline) variations exist, for example bis(oxazoliny)phenyl (PheBOX) **4.1** and bis(oxazoliny)phenyl)amines (BOPA) **4.2** (Fig. 3).

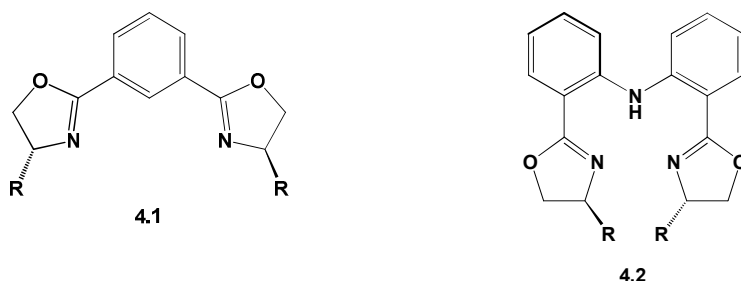
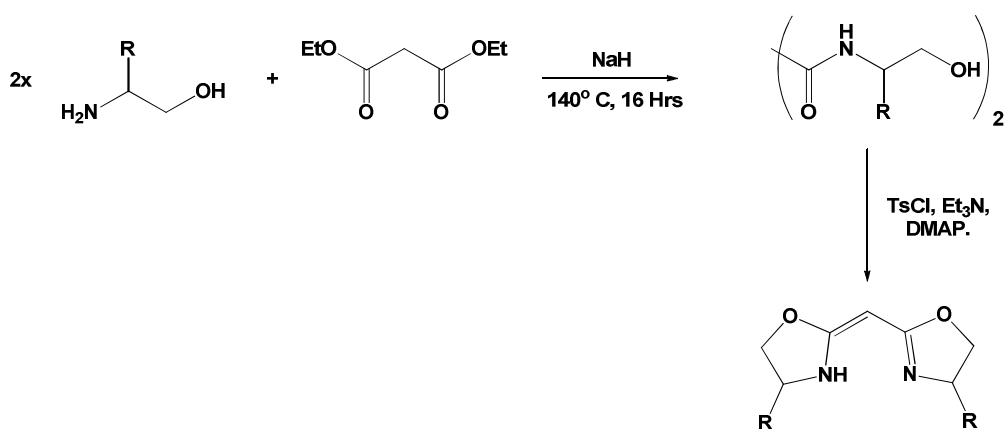


Fig. 3 PheBOX (**4.1**) and BOPA (**4.2**).

The presence of a C_2 -symmetry axis (or higher, e.g. C_3) in many of the polyoxazoline ligands is a feature that can aid success in asymmetric catalysis. It has the potential to enhance enantioselectivity by reducing the number of diastereomeric transition states by invoking symmetry to render transition states equivalent (Chapter 1, Section 2.5).

Coordination between the BOX and selected metal takes place through the donor nitrogen atom present in each oxazoline ring. Binding at this point places the stereodirecting groups within close proximity of the metal centre allowing for effective transfer of chiral information onto the catalytic substrate at the reaction centre. The trivial synthesis of BOXs from chiral amino alcohols permits a degree of structural variety, allowing the ligand to be fine tuned to suit its application. The stereodirecting groups can be varied and the bridge can be diverse in complexity (Scheme 1).^{8,9}



Scheme 1 Preparation of BOXs.

Whilst oxazolines are structurally similar to imidazolines, imidazolines offer the advantage of the additional N-R moiety allowing for alteration of electronic, in addition to steric, properties of the ligand which cannot be achieved in BOXs. This advantage has been discussed in the literature on several occasions, however reports into systematic alterations of this group and subsequent effects upon the reactivity of their metal complexes has so far remained elusive.¹⁰⁻¹²

Although the first example of a 2-imidazoline ((b), Fig. 2) was published in 1888, there is only a small number of reports exploiting its bisimidazoline sub-class in asymmetric catalysis.¹² One of the first examples of a bisimidazoline employed in asymmetric catalysis was reported by Casey *et al.* who used a variety of the ligands coupled with PdCl₂. These complexes were applied to asymmetric alkylation reactions in which favourable yields of >90% and enantiomeric excesses of >70% were observed. Bisimidazoline complex **4.3** (Fig. 4) was directly compared with its BOX supported analogue **4.4**. Complex **4.3** was found to out-perform BOX complex **4.4** with respect to both yield and stereoselectivity.¹³ Here the authors attributed the increased basic nature of the bisimidazoline compared to its corresponding BOX to have induced a shorter Pd-N bond length (though no structural verification of this was undertaken). They postulated that a shorter Pd-N bond length would result in drawing the stereodirecting groups closer to the metal centre and thus impart a stronger influence upon incoming substrates. It should also be highlighted that they suspected the increased backbone rigidity was also a contributing factor to improved enantiomeric excess.

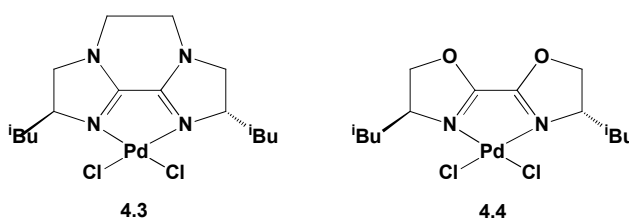
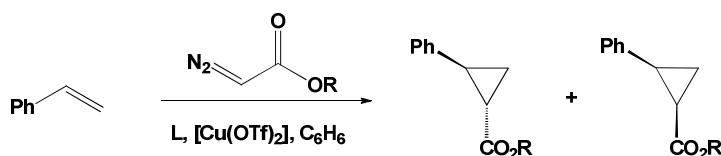


Fig. 4 Bisimidazoline complex **4.3** and BOX complex **4.4** reported in Pd mediated allylic alkylation.

Another example from 2007 illustrates Beller *et al.* deploying a N,N,N'-pyridinebis(imidazoline) ligand on a ruthenium complex which was later applied to asymmetric transfer hydrogenation of a prochiral ketone.^{14, 15} Results showed that the complexes bearing R-BIMs consistently out-performed similar BOXs supported complexes on both yield and ee. The same group also explored asymmetric epoxidation using a Pybox

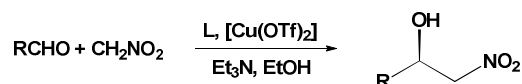
bisimidazoline, where they recognised the potential advantages of fine-tuning the N-R substituent.¹⁶ However, this only resulted in moderate enantiomeric excesses (43-71% ee), which were substrate dependant. Sadly no BOXs were directly tested for comparison.

Around the same time Arai *et al.*¹⁷ and Pfaltz *et al.*¹⁸ were developing bisimidazoline supported copper triflate complexes for asymmetric cyclopropanation of styrene (Scheme 2), which provided both groups with good yields and high enantiomeric excesses of up to 86%.



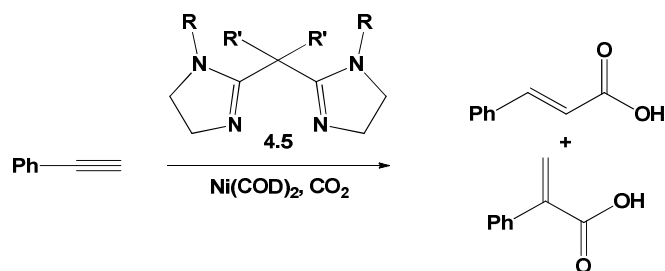
Scheme 2 Cyclopropanation of styrene.

2007 also saw You *et al.* report the use of bisimidazoline supported copper complexes used for asymmetric nitroaldol (Henry) reactions (Scheme 3). The bisimidazoline complexes they developed showed excellent enantioselectivities (93-98% ee) with both aromatic and aliphatic substrates. The authors remarked that BOXs based around *tert*-butyl stereodirecting groups were comparatively successful at this reaction. Yet the downside is the initial synthetic costs of starting from the *tert*-butyl amino acid derivative, which was less cost effective than the bisimidazolines You *et al.* synthesised.



Scheme 3 Asymmetric nitroaldol (Henry) reaction.

The use of bisimidazolines as supporting ligands was also demonstrated by Iwasawa *et al.* through nickel catalysed coupling of CO₂ with alkynes (Scheme 4).¹⁹ Of note is the bisoxazolines used (**4.5**) during this study do not contain the typically included stereocentre (cf. **4.3**), which is often included by design from synthesis using a chiral amino acid as detailed in Section 4.2. This reaction was concerned with regioselectivity rather than stereoselectivity of the final products and in this respect the ligand proved very successful. They also demonstrated that the regioselective preference could be tailored through variation of the N-R substituent and bridge structure.



Scheme 4 Nickel catalyzed coupling of CO₂ with alkynes.

A select few examples of bisimidazolines employed as organocatalysts are known. Tsogoeve and Göbel *et al.* published the novel diprotonated bisimidazoline **4.6** (Fig. 5)²⁰ that clearly demonstrates the incorporation of commercially available diamine **2.1**, previously mentioned in Chapter 2. The organocatalyst **4.6** was tested in chiral Brønsted-acid asymmetric Diels-Alder reactions where a significant acceleration of the reaction was noted though recorded enantioselectivities were low to moderate. In 2008 Göbel *et al.* published an update to their work with newly designed diprotonated ligands that again accelerated reaction times producing good yields, but experienced no improvement upon aforementioned enantioselectivities. It was noted that counter ion choice was of significant importance.²¹ Overall the enantioselectivities of the bisoxazolines investigated by Göbel *et al.* compare poorly to the 70% enantiomeric excess recorded with oxazoline derivatives, however reactivity was increased by approximately 50 fold.

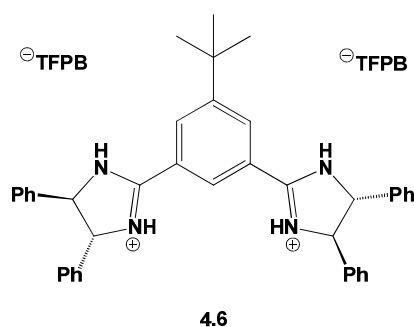


Fig. 5 Novel diprotonated R-BIM from Göbel *et al.*

TFPB = tetrakis(3,5-bistrifluoromethylphenyl)borate.

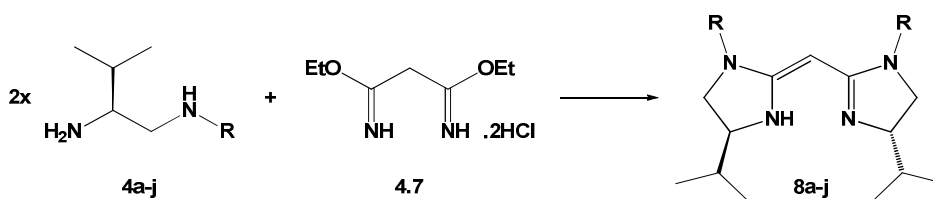
It becomes clear the majority of the literature concerning the application of systems bearing bisimidazoline ligands, whether supporting ligands on d-block metals or catalysts in their own right has predominantly developed in the last ten years. It is therefore understandable that bisimidazoline ligands have not been exploited with AE metals until now.

Our studies of bisimidazoline supported calcium complexes serve to probe several areas of interest simultaneously: will the additional N-R substituents improve the catalytic performance of the complex compared to Buch and Harder's BOX counterpart **1.6**? Will systematic variation of the electronic and associated steric properties of the N-R substituent result in improved ligand performance or aid ligand redistribution suppression?

Since the area of bisimidazolines remains significantly underdeveloped compared to BOXs any studies involving bisimidazolines will increase the knowledge of these ligands leading to their potential application to a wider field other than AE metals.

4.2 Ligand Synthesis and Characterisation

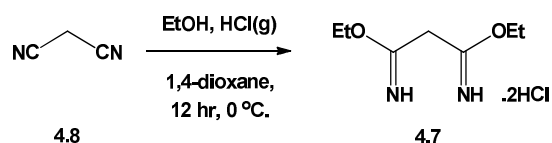
Although many adaptations of the bisimidazoline scaffold exist the targeted bisimidazoline systems of this study consist of two imidazoline rings bridged by a single CH₂ link (**8a-j**, Scheme 5). In essence we aim to prepare the imidazoline analogues of the BOX type synthesised in Scheme 1. This type of bisimidazoline scaffold will be abbreviated as "R-BIM" henceforth. Strategies to prepare R-BIMs are similar in nature to those used for obtaining the related BOX analogues. Our chosen methodology to synthesise the target R-BIMs is derived from work published by Pfaltz *et al.* involving the condensation of two equivalents of diamine with an imino ether (Scheme 5). Not only is this a proven method but it also makes use of our previously developed synthetic pathway for producing chiral diamines (Chapter 2, Section 2.4).¹⁸



Scheme 5 Preparation of bisimidazoline ligands (R = 4-C₆H₄F (**4a/8a**), 4-C₆H₄OCH₃ (**4b/8b**), 4-C₆H₄CH₃ (**4c/8c**), C₆H₅ (**4d/8d**), 4-C₆H₄NO₂ (**4e/8e**), 3,5-C₆H₃(CH₃)₂ (**4f/8f**), CH(CH₃)(C₆H₅) (**4g/8g**), ⁱPr (**4h/8h**), ^tBu (**4i/8i**), 4-C₆H₄N(CH₃)₂ (**4j/8j**).

4.2.1 Ligand Bridge Component

As described in Scheme 5, reaction of a selected diamines **4a-j** with diethyl malonimidate dihydrochloride **4.7** aims to successfully synthesis the target R-BIMs **8a-j**.¹⁸ The two equivalents of diamine are provided from the diamine synthesis as detailed in Chapter 2, Section 2.4 and acquisition of the imino ether **4.7** can be accomplished using the synthesis described by Göbel *et al.* in Scheme 6.²² Göbel *et al.* achieved the synthesis of the imino ether starting from malononitrile **4.8** in anhydrous 1,4-dioxane, to which ethanol is added at 0 °C over a period of 12 hours. During this time HCl gas is sparged through the system resulting in the product **4.7** precipitating from the reaction medium as a white solid that can be isolated in yields of >90%. Although stored under an inert atmosphere (since hydrolysis is known with these types of molecules)^{23, 24} **4.7** displayed a shelf-life of approximately 1.5 months, showing signs of decolouration thereafter (white to an increasing yellow hue). After such times where colouration was apparent reaction yields of R-BIM synthesis were reduced. Storage of **4.7** away from light sources improved the longevity.

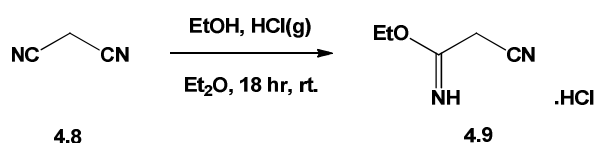


Scheme 6 Preparation of diethyl malonimidate dihydrochloride (**4.7**).

The idea of converting a nitrile group to an imidate has been known since 1825 and is often referred to as the Pinner reaction.²⁴ Many variations of this reaction have taken place over the years but the use of either methanol or ethanol remains the most popular choice. The necessary methanol or ethanol can either been added as a reagent using an ethereal solvent as the reaction medium,²⁵ or having the methanol/ethanol fulfilling the role of both reagent and solvent.²⁶ Whilst the present method above is acid catalysed the reaction can also be base catalysed. This is typically with sodium metal in ethanol to form the neutral imino ether.²⁷

With regards to conducting the Pinner reaction in an ethereal solvent, 1,4-dioxane is common and consequently it is unsurprising the use of THF has also been reported.²⁵ It could be assumed that diethyl ether would likely allow the preparation of **4.7**, however much to our surprise rather than isolating imino ether **4.7** the monoimidate **4.9** is isolated instead (Scheme 7).²⁸ In this circumstance, extended reaction times and excess addition of

ethanol fail to yield **4.7** when diethyl ether was the solvent medium. The ability to synthesise the mono-imidate **4.9** paves the way for some potentially exciting new ligand synthesis developments, which are discussed in Chapter 5.



Scheme 7 Preparation of a mono-substituted imidate **4.9**.

Over the course of our studies several improvements to the procedure described in Scheme 6 were found. The reaction proceeded without issue at ambient temperature instead of 0 °C, and ethanol did not have to be added over an elongated period of time but could be added stoichiometrically at the start of the reaction. Our studies show the solution need only be sparged with HCl(g) for 2-3 hours, contrasting the reported 18 hours. Greatest yield improvements were noted when the HCl(g) was dry. This was achieved by liberating HCl gas from oven dried ammonium chloride using concentrated sulphuric acid. ¹H and ¹³C NMR studies were conducted on the purified product **4.7** and were complimentary with literature values.²² IR spectroscopy proved to be a powerful technique in assessing purity since the absorbance pertaining to the nitrile bond is very characteristic (*ca.* 2265 cm⁻¹) in **4.9** compared to that of the imide bond in both **4.7** and **4.9** (*ca.* 1650-1665 cm⁻¹).

Pflatz's method allowed successful preparation of R-BIMs **8a-j** (Scheme 5) on a starting scale of 1-2 g of diamine substrate. Yields of isolated R-BIM were moderate in all cases (~35%). Further improvements were not seen through extension of reaction times nor conducting the coupling reactions in higher boiling point solvents, for example chloroform, 1,2-dichloroethane, or chlorobenzene.²⁹ Regardless of which solvent was used, isolated yields of the air and moisture stable R-BIMs did not exceed 40%.

Reactions were typically clean and pure R-BIM was obtained by basic workup followed by column chromatography over silica. Purification was straightforward since it only required the separation of the R-BIM from unreacted diamine starting material. Using column chromatography over a silica gel matrix was sufficient in all but two cases. The Ar^{NO2}-BIM **8e** was recovered through crystallisation from hot toluene, which was subsequently stored at -18 °C overnight before filtering the solid (orange) and drying *in vacuo*. The iPr-BIM **8h** was obtained by precipitation from a mixture of warm hexane/dichloromethane.

During purification of the R-BIMs ^1H NMR data contained resonances that were easily identifiable as either R-BIM or residual diamine. The difference in chemical shifts was most pronounced and distinguishable for the proton attached at the chiral centre and the diastereotopic protons of the adjacent methylene (CH_2) group. For example Ar^{F} -BIM **8a** displays ^1H NMR resonances at 3.75 (NCH_2), 3.64 (NCH_2CH) and 3.39 (NCH_2) ppm, compared to diamine **4a** which has resonances at 3.38 (NCH_2), 3.27 (NCH_2CH) and 3.03 (NCH_2) ppm respectively. The ^{13}C NMR spectra of the newly formed R-BIMs also show a new resonance typically recorded between 165-160 ppm which is attributed to the carbon environment of the newly formed imide ($\text{C}=\text{N}$). This recorded resonance is also consistent with observations made when forming BOXs.^{30, 31}

The significant shift of recorded resonances in the ^1H NMR spectra is also mirrored in the ^{13}C NMR spectra for the carbon at the chiral centre and the carbon of the adjacent methylene group. A downfield shift is observed for all resonances. For example in Ar^{F} -BIM **8a** resonances at 65.2 (NCH_2CH) and 55.8 (NCH_2) ppm, compared to diamine **4a** resonances of 57.6 (NCH_2CH) and 44.2 (NCH_2) ppm respectively. These relative changes in chemical shift are observed for all R-BIM derivatives compared to their starting diamine analogue with only small variations which are N-R substituent dependent.

The IR spectrum of the isolated R-BIMs indicates the formation of the imine $\text{C}=\text{N}$ by the strong absorption recorded in the region between 1569-1623 cm^{-1} . This absorbance is distinctly absent from the diamines. There are also small changes in absorbance in the region 3300-3700 cm^{-1} of the R-BIMs compared to their diamine analogues, which is assumed to be a result of the change of the primary and secondary amine of the diamine into the imidazoline of the R-BIM.

Whilst R-BIMs **8a-j** are unsubstituted at the bridge carbon, substitution at this point is possible. For example, simple derivations would be mono- or dimethyl substitution (**4.10** and **4.11**, Fig. 6).^{32, 33}

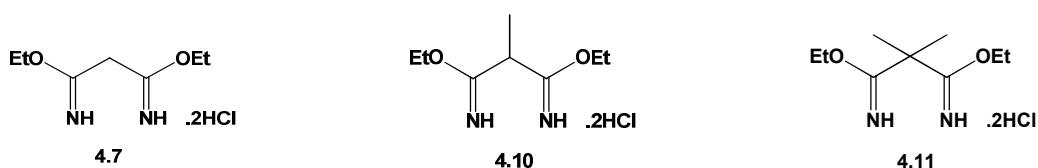


Fig. 6 Diimidate bridge variations **4.7**, **4.10**, and **4.11**.

Upon complexation with calcium the R-BIM is deprotonated becoming an anionic ligand, along with the elimination of $\text{HN}(\text{SiMe}_3)_2$. The remaining hydrogen at the bridge is sterically unimposing, potentially increasing the chances of attack at this position and the ensuing ligand decomposition. The mono-methyl substitution present in compound **4.10** would still allow complexation of an anionic ligand with calcium, but the more sterically demanding methyl could help prevent undesired side reactions. Conversely use of the dimethyl substituted bridge **4.11** is likely to result in rather different chemical behaviour of the complex since there is no longer a proton to abstract from the R-BIM tautomer. The ligand would remain neutral and the calcium atom would retain two bound $\text{N}(\text{SiMe}_3)_2$ groups, i.e. $[\text{Ca}(\text{R-BIM})\{\text{N}(\text{SiMe}_3)_2\}_2(\text{THF})_n]$, resulting in significantly different behaviour compared to its mono-amide counterpart $[\text{Ca}(\text{R-BIM})\{\text{N}(\text{SiMe}_3)_2\}(\text{THF})]$.

4.2.2 Structural Tautomers and Evidence of Diastereoisomerism

From ^1H NMR studies on the R-BIM ligands it is believed that the uncomplexed R-BIM ligands exist in either tautomeric form (**a** or **c**, Fig. 7). This is unsurprising since an analogous form is seen in the structurally related BOXs.^{34, 35} In tautomers **a** and **c** the bridge carbon is sp^2 hybridised and the nitrogen moieties contain a long pair in a p-orbital. This conformation results in conjugation over a planar 6π -system between the two imidazoline rings. The additional stability this conformation brings likely renders them preferable to **b**. ^1H NMR data also supports this by showing only one proton (calculated from integration) bound to the bridge carbon. The resonance from this proton arises between 3.70-3.58 ppm, however it is not observed in most cases. This suggests very broad signals as the molecule exchanges between tautomeric forms **a-c** (Fig. 7). Low temperature ^1H NMR studies were undertaken in an endeavour to see if the exchange could be “frozen out” to support this theory, however at temperatures of $-60\text{ }^\circ\text{C}$ in CDCl_3 , the exchange could not be sufficiently slowed to recorded this.

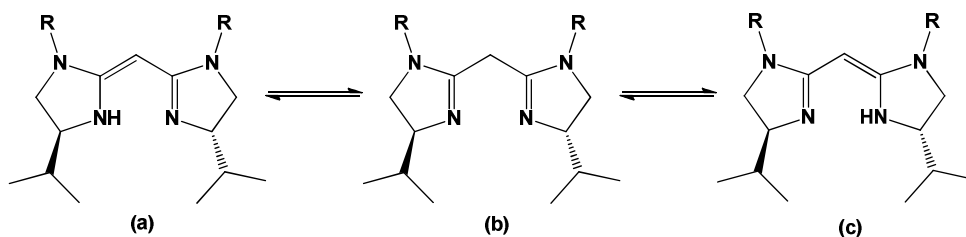
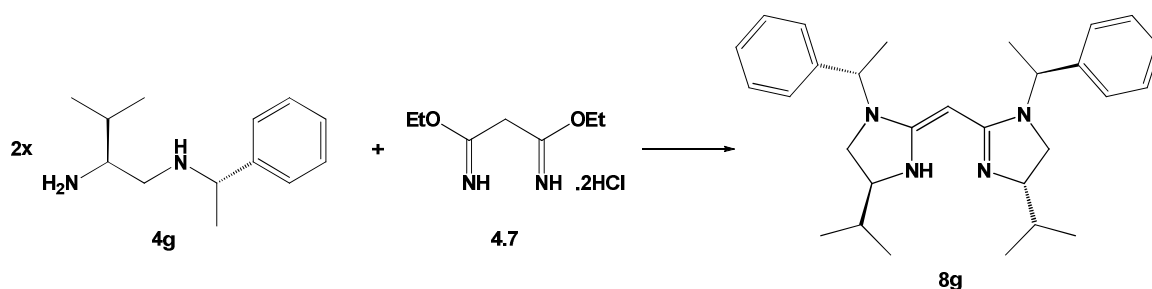


Fig. 7 R-BIM suggested tautomeric forms.

When investigating possible racemisation occurrence during the development of the diamine synthesis in Chapter 2, Section 2.5, a diamine with two stereocentres was prepared (**4g**). Investigating possible racemisation/epimerisation we utilised the typical R-BIM synthesis seen in Scheme 5 and incorporated bis-chiral diamine **4g** into the synthesis with the aim of recovering a single diastereoisomer of the N-R = PhMeH-BIM product **8g** (Scheme 8). The resulting product was a white solid with a recorded yield of 34% which is comparable with the isolated yields of R-BIMs **8a-j**. As with previous ^1H NMR studies on the bis-chiral diamine **4g**, studies on PhMeH-BIM **8g** showed no evidence of diastereoisomers in the form of resonance duplication at close chemical shifts.³⁶ Whilst 4 chiral centres exist in PhMeH-BIM **8g** diastereoisomerism can occur in the presence of one or more chiral centres. In the case of R-BIMs **8a-j** (exclusive of **8g**) this could result in *S,S*, *R,R*, or *S,R*, *R,S* conformations

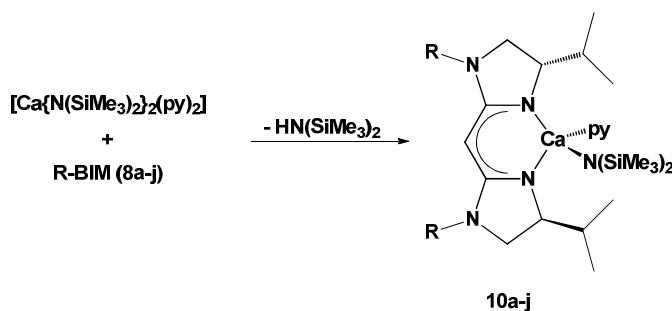


Scheme 8 Preparation of R-BIM **8g**.

4.3 Chiral Calcium Complexes Supported by Bisimidazolines

4.3.1 Complex Synthesis

Preparation of the R-BIM calcium complexes **9a-j** was achieved by reaction of the protio-ligand **8a-j** with $[\text{Ca}\{\text{N}(\text{SiMe}_3)_2\}_2(\text{THF})_2]$ in benzene- d_6 . For larger scales toluene or nondeuterated benzene was used. For pyridine analogues **10a-j** $[\text{Ca}\{\text{N}(\text{SiMe}_3)_2\}_2(\text{py})_2]$ was used (Scheme 9). In all cases yellow/orange precipitates were obtained that were only soluble in THF- d_8 , being insoluble in hydrocarbon solvents and unstable in chlorinated solvents. This is in stark contrast compared to calcium BOX complexes that were soluble and characterised in benzene- d_6 .¹ Despite this, the low solubility experienced with calcium complexes **9a-j** and **10a-j** is in keeping with the solubility issues experienced with the diamine supported calcium complexes as previously detailed in Chapter 3.^{1, 29, 37-39}



Scheme 9 Preparation of $[\text{Ca}(\text{R-BIM})\{\text{N}(\text{SiMe}_3)_2\}(\text{py})_2]$ complexes **10a-j**

(R = 4- $\text{C}_6\text{H}_4\text{F}$ (**10a**), 4- $\text{C}_6\text{H}_4\text{OCH}_3$ (**10b**), 4- $\text{C}_6\text{H}_4\text{CH}_3$ (**10c**), C_6H_5 (**10d**), 4- $\text{C}_6\text{H}_4\text{NO}_2$ (**10e**), 3,5- $\text{C}_6\text{H}_3(\text{CH}_3)_2$ (**10f**), $\text{CH}(\text{CH}_3)(\text{C}_6\text{H}_5)$ (**10g**), ^iPr (**10h**), ^tBu (**10i**), 4- $\text{C}_6\text{H}_4\text{N}(\text{CH}_3)_2$ (**10j**).

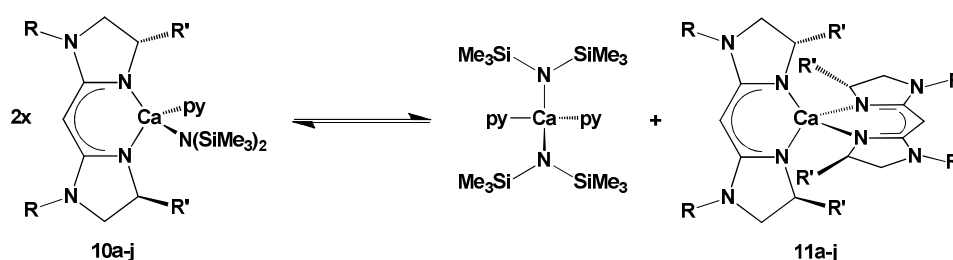
All hydroamination catalysis experiments were conducted using complexes $[\text{Ca}(\text{R-BIM})\{\text{N}(\text{SiMe}_3)_2\}(\text{THF})]$ **9a-j**, however, for complete characterisation it was necessary to exchange the coordinating THF with pyridine in order to determine the extent of base coordination in THF- d_8 . To prepare the pyridine analogues protio-R-BIM ligand was added to $[\text{Ca}\{\text{N}(\text{SiMe}_3)_2\}_2(\text{py})_2]$ in benzene. The reaction proceeded for 18 hours at ambient temperature followed by solvent and volatile by-product removal under reduced pressure to 4.0×10^{-2} mbar. This was done to ensure a level of consistency between each sample and since prolonged exposure to vacuum conditions can remove coordinated pyridine.⁴⁰ The remaining product, typically orange, was then dissolved in THF- d_8 for further analysis.

Synthesis of homoleptic $[\text{Ca}(\text{R-BIM})_2]$ complexes **11a-j** was achieved by reaction of two equivalents of protio-ligand (**8a-j**) with one equivalent of $[\text{Ca}\{\text{N}(\text{SiMe}_3)_2\}_2(\text{py})_2]$ in either benzene or toluene. The reaction was allowed to proceed for 18 hours at ambient temperature before the resulting complex was dried *in vacuo* and subsequently dissolved in THF- d_8 for analysis. Under these conditions $\geq 90\%$ conversion was noted but with mild heating at 40 °C overnight $\geq 97\%$ conversion was achieved on all examples. Extended heating did not see higher conversions nor display evidence of decomposition, suggesting a moderate level of complex stability. This observed stability is on par with that generally observed with comparable calcium complexes that are stable for at 60 °C reasonable durations.^{41, 42}

The formation of homoleptic complexes **11a-j** results in two equivalents of liberated $\text{HN}(\text{SiMe}_3)_2$ and pyridine respectively. In order to remove these by-products complexes **11a-j** were dried *in vacuo*. As a result only trace amounts of pyridine were observed in NMR spectra with small quantities of $\text{HN}(\text{SiMe}_3)_2$. The persistent presence of $\text{HN}(\text{SiMe}_3)_2$ even after recrystallisation attempts is characteristic in both homoleptic and heteroleptic R-BIM calcium complexes, and mirrors observation of the diamine calcium complexes discussed in Chapter 3. The homoleptic complex solubility was noticeably greater than the heteroleptic analogues, especially in hydrocarbon solvents.

4.3.2 Complex Characterisation

NMR spectra of the heteroleptic species **10a-j** in THF-d_8 , were well-defined at ambient temperature (in stark contrast to the diamine complexes $[\text{Ca}(\text{NN}^{\text{R}})\{\text{N}(\text{SiMe}_3)_2\}(\text{py})_n]$ **6a-f** of Chapter 3) but showed a distinct mixture of the heteroleptic species **10a-j** and the corresponding homoleptic complex **11a-j**. This redistribution is illustrated in Scheme 10 and has been previously discussed in Chapter 1, Section 1.1.1.



Scheme 10 Redistribution of $[\text{Ca}(\text{R-BIM})\{\text{N}(\text{SiMe}_3)_2\}(\text{py})]$ to $[\text{Ca}\{\text{N}(\text{SiMe}_3)_2\}_2(\text{py})_2]$ and $[\text{Ca}(\text{R-BIM})_2]$ (R = 4- $\text{C}_6\text{H}_4\text{F}$ (**10a/11a**), 4- $\text{C}_6\text{H}_4\text{OCH}_3$ (**10b/11b**), 4- $\text{C}_6\text{H}_4\text{CH}_3$ (**10c/11c**), C_6H_5 (**10d/11d**), 4- $\text{C}_6\text{H}_4\text{NO}_2$ (**10e/11e**), 3,5- $\text{C}_6\text{H}_3(\text{CH}_3)_2$ (**10f/11f**), $\text{CH}(\text{CH}_3)(\text{C}_6\text{H}_5)$ (**10g/11g**), ^iPr (**10h/11h**), ^tBu (**10i/11i**), 4- $\text{C}_6\text{H}_4\text{N}(\text{CH}_3)_2$ (**10j/11j**).

Superimposed ^1H or ^{13}C NMR spectra of a chosen heteroleptic complex $[\text{Ca}(\text{R-BIM})\{\text{N}(\text{SiMe}_3)_2\}(\text{py})]$ with its homoleptic analogue $[\text{Ca}(\text{R-BIM})_2]$ showed feature resonances were distinctly shifted upon comparison. This was most noticeable with the *iso*-propyl groups of the stereodirecting groups within a complex. An example stack plot of the ^1H NMR spectra from complex $[\text{Ca}(\text{Ar}^{\text{OMe}}\text{-BIM})\{\text{N}(\text{SiMe}_3)_2\}(\text{py})]$ **10b** and its homoleptic analogue $[\text{Ca}(\text{Ar}^{\text{OMe}}\text{-BIM})_2]$ **11b** are shown in Fig. 8.

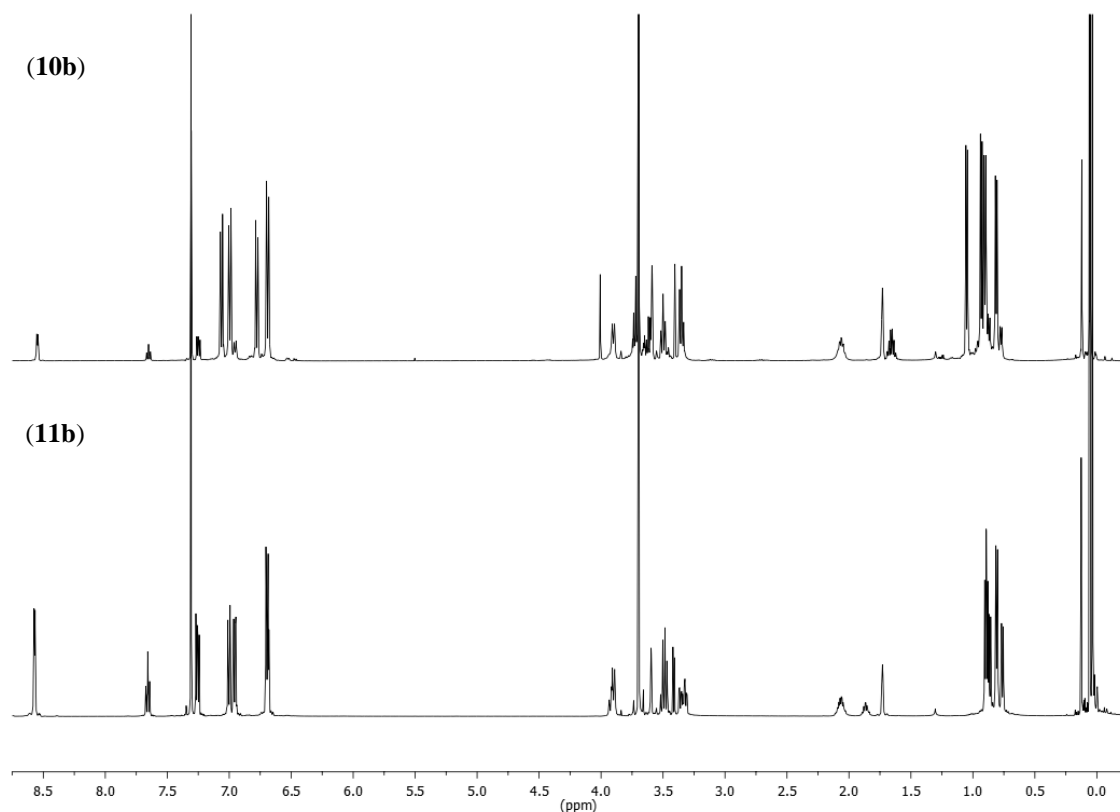


Fig. 8 Stacked ¹H NMR spectra of [Ca(Ar^{OMe}-BIM){N(SiMe₃)₂}(py)] **10b** (top trace) and [Ca(Ar^{OMe}-BIM)₂] **11b** (bottom trace) in THF-d₈ at 293 K.

Resonance analysis of the *iso*-propyl groups of the heteroleptic complex **10b** gives signals at 2.06 and 1.86 ppm for the methine of the *iso*-propyl moieties and 0.88, 0.85, 0.80, and 0.75 ppm for the *iso*-propyl methyl groups. This compares to the resonances of homoleptic complex **11b** at 2.05 and 1.65 for the methine, and at 1.04, 0.92, 0.89, and 0.80 ppm for the methyl groups respectively. The resonances in the region of 4.5-2.5 ppm are regularly assigned to the protons bound to the carbon of the chiral centre and the adjacent methylene (CH₂) group. This region in the ¹H NMR spectra can display complicated resonance patterns resulting from the overlap of the multiplet signal of the proton at the chiral centre and the apparent triplet/doublet of doublets fine structure of the adjacent CH₂ diastereotopic protons.

There are however exceptions. The NMR data indicates that the bound R-BIM ligands of the homoleptic complexes [Ca(^{*i*}Pr-BIM)₂] **11h** and [Ca(Ar^{NMe2}-BIM)₂] **11j** exist in one uniform chemical environment. For example **11h** shows a singlet resonance at 3.71 ppm caused by the protons at each ligands bridge head and integration confirms two protons in

that environment. This is clearly different to the bridge proton resonance at 3.31 ppm that integrates to one proton in the heteroleptic analogue $[\text{Ca}(\text{}^i\text{Pr-BIM})\{\text{N}(\text{SiMe}_3)_2\}(\text{py})]$ **10h**.

The uniform ligand environment of these examples is also reflected in the IR spectra of the heteroleptic and related homoleptic complexes (**10h/11h** and **10j/11j**). When comparing IR spectra of aforementioned hetero- and homoleptic complexes all recorded absorbance frequencies vary less than 10 cm^{-1} between the absorbance in the heteroleptic species and then its homoleptic analogue. This difference is far greater in all other comparisons of hetero- and homoleptic calcium complexes.

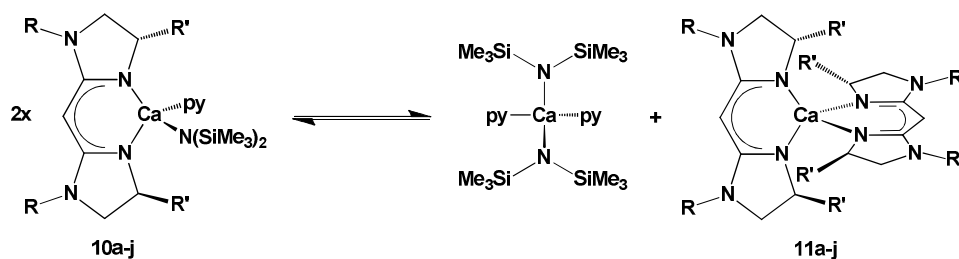
Examining the resonances attributed to coordinated pyridine in the ^1H NMR spectra of $[\text{Ca}(\text{R-BIM})\{\text{N}(\text{SiMe}_3)_2\}(\text{py})]$ **10a-j** showed that one equivalent of pyridine was bound, and that there is no or little deviation upon variation of the N-R substituent. This contrasts Bush and Harders' BOX complex **1.6**, which had two equivalents of base coordinated, although this was THF as opposed to pyridine. The inclusion of one equivalent of bound pyridine is also observed with the diamine calcium complexes $[\text{Ca}(\text{NN}^{\text{R}})\{\text{N}(\text{SiMe}_3)_2\}(\text{py})]$ **6a-d**. The exceptions were the *iso*-propyl and *tert*-butyl diamine complexes **6e** and **6f**, which are the only examples to show sub-stoichiometric quantities (0.3-0.6) of pyridine coordinated (Chapter 3, Section 3.3).

NMR spectroscopic analysis of the heteroleptic complexes **10a-j** demonstrated three distinctive trimethylsilane environments (^1H NMR $\delta = 0.04, 0.03, \text{ and } 0.02$ ppm. ^{13}C NMR $\delta = 6.0, 2.7, \text{ and } 1.4$ ppm). Whilst $\text{HN}(\text{SiMe}_3)_2$ is expected to be a volatile by-product even after repeated recrystallisation attempts and extensive drying *in vacuo* all traces were unable to be removed. We suppose the cause of this is due to similar reasons these environments were observed with the heteroleptic diamine complexes **6a-f**. One resonance from bound $[\text{N}(\text{SiMe}_3)_2]^-$ in the heteroleptic complex, and one from residual free $\text{HN}(\text{SiMe}_3)_2$, of which some may re-coordinated to the calcium centre and the final resonance from the trimethylsilane environments present in the redistribution product $[\text{Ca}\{\text{N}(\text{SiMe}_3)_2\}_2(\text{py})_2]$.

The R-BIM complexes also display no evidence of ether-cleavage whilst in THF-d_8 , this was also the case for the diamine complexes of Chapter 3 but has been observed in the literature.³⁷

4.4 Complex Redistribution

Ligand redistribution equilibria as shown in Scheme 10 were expected due to the nature of AE metal complexes (Chapter 1 Section 1.1.1) and Buch and Harder also report such behaviour with calcium BOX complexes.¹ In the case of Buch and Harders' $[\text{Ca}(\text{BOX})\{\text{N}(\text{SiMe}_3)_2\}(\text{THF})_2]$ complex **1.6** (Fig. 1) they observed that the redistribution ratio of heteroleptic:homoleptic was 80:20 respectively.



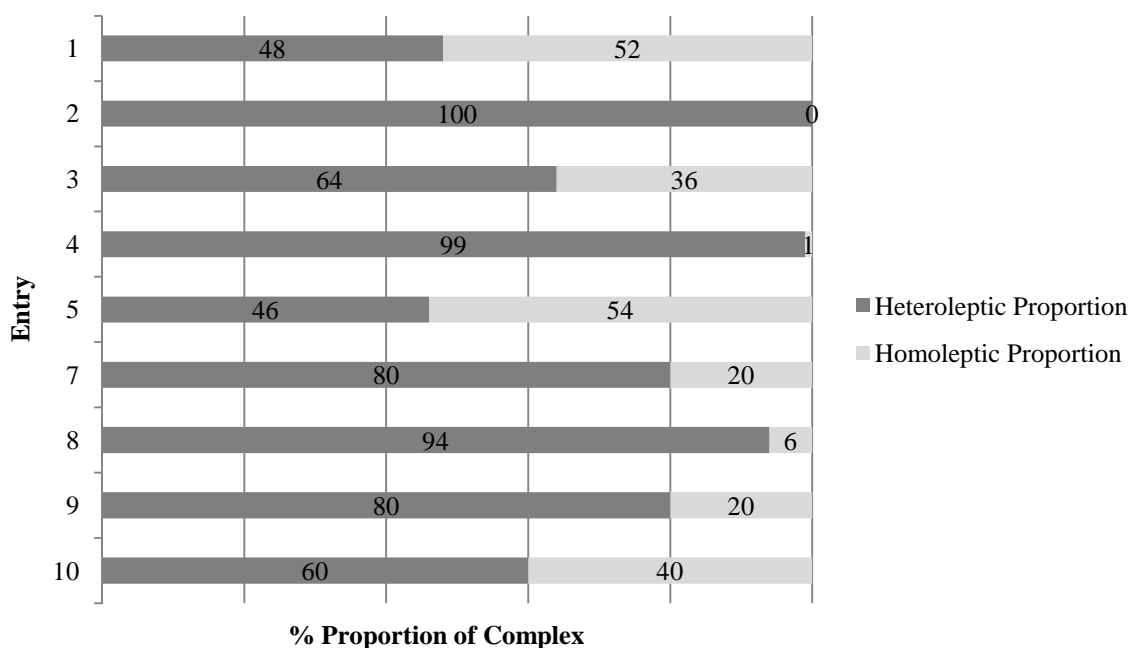
Scheme 10 Redistribution of $[\text{Ca}(\text{R-BIM})\{\text{N}(\text{SiMe}_3)_2\}(\text{py})]$ to $[\text{Ca}\{\text{N}(\text{SiMe}_3)_2\}_2(\text{py})_2]$ and $[\text{Ca}(\text{R-BIM})_2]$ (R = 4- $\text{C}_6\text{H}_4\text{F}$ (**10a/11a**), 4- $\text{C}_6\text{H}_4\text{OCH}_3$ (**10b/11b**), 4- $\text{C}_6\text{H}_4\text{CH}_3$ (**10c/11c**), C_6H_5 (**10d/11d**), 4- $\text{C}_6\text{H}_4\text{NO}_2$ (**10e/11e**), 3,5- $\text{C}_6\text{H}_3(\text{CH}_3)_2$ (**10f/11f**), $\text{CH}(\text{CH}_3)(\text{C}_6\text{H}_5)$ (**10g/11g**), ^iPr (**10h/11h**), ^tBu (**10i/11i**), 4- $\text{C}_6\text{H}_4\text{N}(\text{CH}_3)_2$ (**10j/11j**)).

Variation of the R-BIM N-R substituent showed a significant effect on the favoured equilibrium position at ambient temperature as tabulated in Table 1 and graphically represented in Fig. 9. Some complexes existed as an equal distribution between heteroleptic complex **10** and homoleptic complex **11** for example **10a/11a** (entry 1), and **10f/11f** (entry 6). All other examples have an equilibrium position that favours heteroleptic formation. This varies from 60-100% with respect to proportion of heteroleptic species present in solution (THF- d_8). Both *iso*-propyl **10h** and *tert*-butyl **10i** bearing complexes showed a strong preference towards the formation of the heteroleptic species at 94:6 and 80:20 **10:11** respectively (entries 8 and 9).

Table 1 Redistribution of $[\text{Ca}(\text{R-BIM})\{\text{N}(\text{SiMe}_3)_2\}(\text{py})]$ **10** to $[\text{Ca}(\text{R-BIM})_2]$ **11** and $[\text{Ca}\{\text{N}(\text{SiMe}_3)_2\}_2(\text{py})_2]$ in THF- d_8 at 298 K.

Entry	Complex	N-R	10:11 ^a	K^b	ΔG kJ mol ⁻¹
1	10a	4-C ₆ H ₄ F	48:52	1.17	-0.39
2	10b	4-C ₆ H ₄ OCH ₃	100:0	0	-
3	10c	4-C ₆ H ₄ CH ₃	64:36	0.32	2.8
4	10d	C ₆ H ₅	99:1	0.01	11.2
5	10e	4-C ₆ H ₄ NO ₂	- ^c	-	-
6	10f	3,5-C ₆ H ₃ (CH ₃) ₂	46:54	1.18	-0.39
7	10g	CH(CH ₃)(C ₆ H ₅)	80:20	0.26	3.3
8	10h	ⁱ Pr	94:6	0.06	6.7
9	10i	^t Bu	80:20	0.06	6.7
10	10j	4-C ₆ H ₄ N(CH ₃) ₂	60:40	0.67	0.99

^a Determined by integration of ¹H NMR spectra. ^b Equilibrium constant determined at 298 K. ^c Complex insoluble.

**Fig. 9** Redistribution of $[\text{Ca}(\text{R-BIM})\{\text{N}(\text{SiMe}_3)_2\}(\text{py})]$ **10** to $[\text{Ca}(\text{R-BIM})_2]$ **11** and $[\text{Ca}\{\text{N}(\text{SiMe}_3)_2\}_2(\text{py})_2]$ in THF- d_8 at 298 K. Entry numbers correspond to Table 1.

When analysing steric and electronic variations of the R-BIM ligands and corresponding effect upon equilibrium position, it is relevant to recall that the redistribution equilibrium can be steered towards the desired heteroleptic complex by the presence of a higher concentration of the homoleptic species in relation to heteroleptic. Le Chatelier's principle denotes that upon addition of a higher quantity of homoleptic species the equilibrium will shift to oppose this change. The result of this will be to shift the equilibrium point to form more of the heteroleptic species. Buch and Harder investigated this principle in relation to the calcium BOX complexes. They detected that after addition of 1 extra equivalent of homoleptic BOX complex they were able to shift the equilibria towards heteroleptic complex formation. This resulted in a reduction in the quantity of active calcium salt $[\text{Ca}\{\text{N}(\text{SiMe}_3)_2\}_2(\text{THF})_2]$ present to approximately 2-3% when compared to solutions without additional homoleptic complex. Although able to coerce the equilibrium position in such a manner, catalytic performance of these mixtures showed no significant improvement on the enantiomeric excess obtained in hydroamination.¹ Due to the structural similarities of the BOXs and R-BIMs it is likely we would observe the same outcome following this approach, which is why structural variation of the ligand was explored instead.

Before discussion the electron-donating or withdrawing nature of a R-BIM's aromatic N-R substituent it is pertinent to categorise them according to their Hammett values (σ_x), which are listed in Table 2.⁴³

Table 2 Hammett σ_x values for R-BIM aromatic N-R substituents.

Entry	R-BIM	N-R	σ_x^a	
1	8e	4-C ₆ H ₄ NO ₂	0.78	↑ Electron-withdrawing
2	8a	4-C ₆ H ₄ F	0.06	
3	8d	C ₆ H ₅	0.00	
4	8f	3,5-C ₆ H ₃ (CH ₃) ₂	-0.07 ^b	↓ Electron-donating
5	8c	4-C ₆ H ₄ CH ₃	-0.17	
6	8b	4-C ₆ H ₄ OCH ₃	-0.27	
7	8j	4-C ₆ H ₄ N(CH ₃) ₂	-0.83	

^a All values are σ_p with the exception of Entry 4, which is σ_m .

^b σ_m value is for the meta mono-substituted CH₃ derivative.

Aromatic electron-donating substituent examples include Ar^{OMe}-BIM complex **10b** and Ar^{NMe₂}-BIM complex **10j**, which show ratios of 100:0 and 60:40 respectively for **10:11**. The remaining electron-donating substituents of complexes **10c** (Ar^{Me}-BIM), **10f** (Ar^{3,5Me}-BIM), and electron-neutral Ph-BIM (**10d**) demonstrate a similarly wide range of equilibrium positions from 46:54 to 99:1 with no discernible pattern.

Tentatively it appears that less sterically demanding substituents side with equilibrium positions favouring heteroleptic formation as seen in entries 4, 8, and 9. This is supported by the increased proportion of heteroleptic complex present in solution when comparing Ar^{Me}-BIM **10c** to Ar^{3,5Me}-BIM **10f**. These two examples show a dramatic shift in preference for heteroleptic formation from 46:54 to 64:36 (entries 3 and 6) within a typical error range of 2%.

Whilst a further shift towards heteroleptic formation in the equilibrium occurs when moving from Ar^{Me}-BIM **10c**, to the marginally smaller analogue Ph-BIM **10d**. We observe a change in equilibrium position from 64:36 to 99:1 in favour of the heteroleptic species (entry 3 vs. 4, Table 1). On these simple observations alone the same trend can be applied to the alkyl N-R substituents ⁱPr-BIM and ^tBu-BIM: entries 8 and 9. It is important to be aware that whilst this evidence appears to support the notion that smaller N-R substituents on the R-BIM could lead to more favourable heteroleptic formation, the difference in steric demands between two substituents is often negligible. For example the Ar^{Me}-BIM is not too dissimilar in its steric demands when compared to Ph-BIM. The added methyl group of the Ar^{Me}-BIM is also orientated at a direction and distance appreciably far away from the metal centre so as not to impart a stereodirecting role. It is more likely that a complex interplay of steric and electronic factors dictate the equilibrium positions observed and have yet to be understood fully.

Indeed when examining the relative electron-withdrawing and donating N-R substituents' effect on the redistribution equilibrium, the observation that less sterically hindering substituents tend to result in an equilibrium preference for heteroleptic complex formation is less clear-cut. This is supported by comparison of the equilibrium data for Ar^{Me}-BIM complex **10c**, 64:36 and Ar^{OMe}-BIM **10b**, 100:0 (**10:11**). They are arguably similar in structure yet different equilibrium positions advocate that the electron-donating nature of the 4-C₆H₄OCH₃ substituent in complex **10b** could be influencing the equilibrium position.

It could be envisioned that donating electron density through the ligand towards the metal centre creates a stronger binding ligand better able to resist the rate at which the redistribution equilibrium is achieved. The equilibrium position for **10h** is 60:40 (**10h:11h**) yet the amino group is electron-donating like the methoxy group of **10b**. Thus we would also expect to observe a slower rate at which the ligand redistribution equilibrium is reached however this is not the case as all equilibrium positions were established within similar times.

¹H NMR investigations established that all complexes had reached their respective equilibrium position within 10 minutes of complexation occurring. This evidence supports observations of fast reaction rates when protio-ligands **8a-j** are reacted with the calcium starting material [Ca{N(SiMe₃)₂}(THF)₂] or [Ca{N(SiMe₃)₂}(py)₂] and is in agreement with the facile nature of the BOX complexes synthesis. Whilst the R-BIMs, diamine and BOX ligands all displayed rapid complexation, some literature examples have required more forcing conditions, and heating for an extended duration to ensure complexation.⁴¹

Since the electron-withdrawing Ar^{NO₂}-BIM **10i** was insoluble we were unable to determine an equilibrium position, leaving the single electron-withdrawing Ar^F-BIM complex **10a**. This was one of only two examples displaying a partiality for homoleptic complex formation in solution. Initial comparison of this result to others suggests **10a**'s steric demands could be compared with that of Ar^{Me}-BIM **10c**, which displays a much higher affinity for heteroleptic formation. Probing correlations related to **10a**'s electron-withdrawing nature shows a slightly higher preference for heteroleptic formation over a marginally electron-donating derivative, for example Ar^{3,5Me}-BIM **10f** (48:52 compared with 46:54 (**10:11**) respectively). Electron-withdrawing N-R substituents would lead to a weaker donating ability of the coordinating nitrogen atoms of the R-BIM ligand. This in turn would lead to a weaker coordinating ligand and a complex that would be more susceptible to redistribution reaching redistribution equilibrium faster than stronger bound ligands.

At this juncture it becomes appropriate to ask whether the obtained enantioselectivities with a catalyst is dependent upon the redistribution equilibrium position (**10:11**) or the rate at which that equilibrium position is achieved. If electron-donating groups aid resistance to complex redistribution, then we hope to observe higher enantiomeric excesses and slower catalytic rates. The slower catalytic rates would suggest a lower quantity of

[Ca{N(SiMe₃)₂}(THF)₂] present, which is well known to catalyse the hydroamination of aminoalkenes rapidly.^{29, 44} For electron-withdrawing groups lower stereoselectivity would be expected alongside increased reaction rates for the opposite reasons. However slow reaction rates (cf. [Ca{N(SiMe₃)₂}(THF)₂]) would still be anticipated since we are employing a bulky spectator ligand. Redistribution by-product [Ca(R-BIM)₂] is catalytically inactive and in keeping with observations homoleptic diamine complexes (Ca(NN^R) (7a-c) Chapter 3) and the observations of Buch and Harder.¹

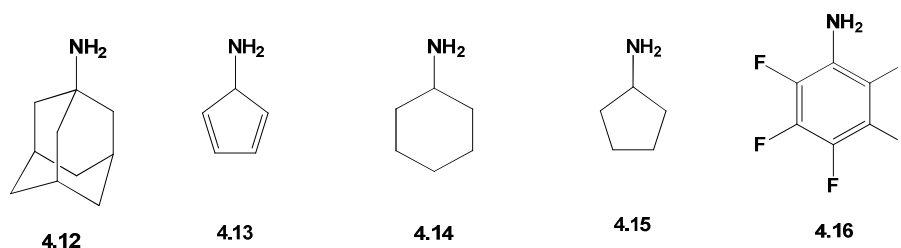


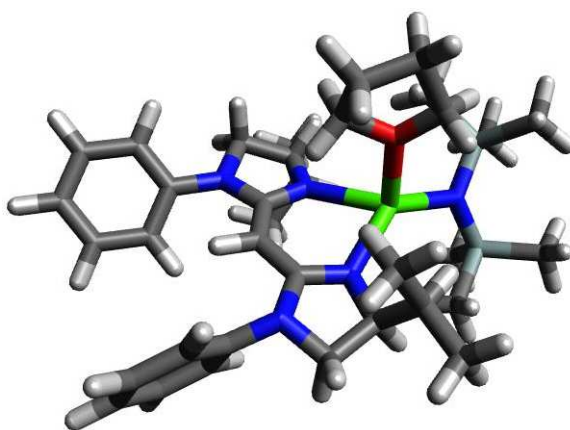
Fig. 10 Alternative N-R substituents to consider for R-BIM library (4.12-4.16).

It is apparent that whilst trends may imply certain structural/electronic features help dictate redistribution trends, a larger ligand library would require testing to see if these initial observations hold true. Comparison of less sterically demanding N-R alkyl derivatives, such as methyl and ethyl compared to *tert*-butyl and *iso*-propyl. Conversely increasing the steric demand, of N-R with groups such as adamantylamine 4.12 (Fig. 10). When studying steric effects of more relatively electron-neutral examples ($\sigma_x \sim 0$, Table 2), alterations in appended ring size might also help test aforementioned observations. For example, substituting aniline in the R-BIM synthesis with the five-membered ring cyclopenta-2,4-diene-1-amine 4.13, to see if the smaller ring had a preference for an equilibrium position towards heteroleptic formation. Cyclic nonaromatic derivatives would also be interesting to consider for comparison with the more extensively studied aromatic analogues, for example the use of cyclohexanamine 4.14 or cyclopentanamine 4.15. Due to the insoluble nature of the heteroleptic and homoleptic Ar^{NO₂}-BIM bearing complexes 10e and 11e, a suitable alternative to compare to Ar^F-BIM complexes 10a/11a would be pentafluoroaniline 4.16, due to its electron-withdrawing nature.

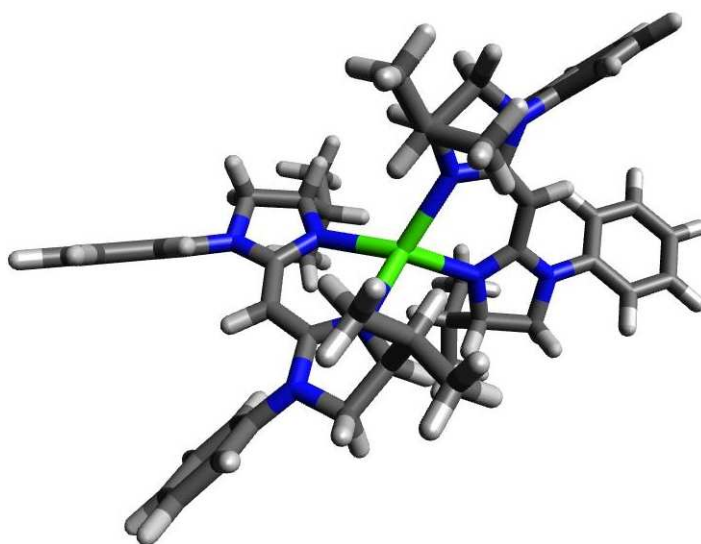
ΔG_{293} values were calculated from the equilibrium coefficients, which were found to be small and almost negligible.

4.5 DFT

In order to gain insight into the proposed mononuclear species $[\text{Ca}(\text{R-BIM})\{\text{N}(\text{SiMe}_3)_2\}(\text{THF})]$ and $[\text{Ca}(\text{R-BIM})_2]$ ($\text{R} = 4\text{-C}_6\text{H}_4\text{F}$, Ph , and ${}^t\text{Bu}$), their structures were calculated using density functional methods. Only example structures of the heteroleptic complex $[\text{Ca}(\text{Ph-BIM})\{\text{N}(\text{SiMe}_3)_2\}(\text{THF})]$ **12a** and homoleptic complex $[\text{Ca}(\text{Ph-BIM})_2]$ **12b** are presented in Fig. 11 since all variations were found to be isostructural.



12a



12b

Fig. 11 Calculated structure of heteroleptic $[\text{Ca}(\text{Ar}^{\text{Ph}}\text{-BIM})\{\text{N}(\text{SiMe}_3)_2\}(\text{THF})]$ **12a** and homoleptic $[\text{Ca}(\text{Ph-BIM})_2]$ **12b**.

From calculated structural data undertaken by Dr. Benjamin Ward, variation of the R-BIM N-R substitution (R = 4-C₆H₄F, 4-C₆H₄OCH₃, 4-C₆H₄CH₃, Ph, and ^tBu) results in no marked electronic influence on the charge of the nitrogen donor atoms, nor the calcium centre. The Mulliken charge of the R-BIM nitrogen donors demonstrates negligible deviation ranging between -1.282 to -1.283 e. The Mulliken charge of the calcium centre records a similarly negligible variation, with examples ranging over 1.095 to 1.099 e. There is also minimal variation of Ca-N_{BIM} bond length upon R-BIM N-R variation (range = 2.391-2.426 Å) suggesting that the steric demands of the N-R substituent are of more concern with respect to catalytic reactivity than electronics would appear to be.

Table 3 Experimental and calculated redistribution of [Ca(R-BIM){N(SiMe₃)₂}(THF)] to [Ca(R-BIM)₂] (R = 4-C₆H₄F **10a/11a**, Ph **10d/11d**, and ^tBu **10i/11i**) and [Ca{N(SiMe₃)₂}(THF)₂] at 298 K.

Entry	Complex	N-R	Experimental ΔG kJ mol ⁻¹	Calculated ΔG kJ mol ⁻¹
1	10a/11a	4-C ₆ H ₄ F	-0.4	6.9
2	10d/11d	C ₆ H ₅	11.2	6.3
3	10i/11i	^t Bu	6.7	16.7

Calculated ΔG of exchange between [Ca(R-BIM){N(SiMe₃)₂}(THF)] **10** to [Ca(R-BIM)₂] **11** (R = 4-C₆H₄F, Ph, and ^tBu) and [Ca{N(SiMe₃)₂}(THF)₂] at 298K were also calculated. These were compared against the experimentally determined values listed in Table 1, Section 4.4. A comparison of the calculated and experimentally determined values is tabulated in Table 3. The calculated values ΔG are within typical error margins of 2-3 kcal (8-12 kJ) commonly accepted for DFT calculations. When compared to the experimentally determined values, the calculated values are of a similar magnitude to the experimentally determined values.

4.6 Catalytic Performance

Table 4 Asymmetric hydroamination of amino-alkenes using 10 mol% [Ca(R-BIM){N(SiMe₃)₂}(THF)] in C₆D₆ at 293 K.

Entry	Complex	N-R	Substrate ^e	Initial Rate/ mol dm ⁻³ s ⁻¹	Conv.% ^a	Time ^f	ee% ^b
1	[Ca] ^c	-	A	5.0(2)×10 ⁻⁵	>99	23h	0
2	9a	4-C ₆ H ₄ F	A	6.8(3)×10 ⁻⁸	3	3.5d	9
3	9b	4-C ₆ H ₄ OCH ₃	A	7.2(3)×10 ⁻⁷	32	24d	0
4	9c	4-C ₆ H ₄ CH ₃	A	5.1(5)×10 ⁻⁷	8	7d	0
5	9d	C ₆ H ₅	A	9.5(4)×10 ⁻⁸	4	6.5d	0
6	9e	4-C ₆ H ₄ NO ₂	A	Insoluble	-	-	-
7	9f	3,5-C ₆ H ₃ (CH ₃) ₂	A	8.5(4)×10 ⁻⁷	64	17d	10
8	9g	CH(CH ₃)(C ₆ H ₅)	A	-	-	-	-
9	9h	ⁱ Pr	A	-	-	-	-
10	9i	^t Bu	A	7.3(4)×10 ⁻⁷	18	7d	12
11	9j	4-C ₆ H ₄ N(CH ₃) ₂	A	-	-	-	-
12	[Ca] ^c	-	B	- ^d	>99	<7m	0
13	9a	4-C ₆ H ₄ F	B	1.8(1)×10 ⁻⁵	>99	39h	9
14	9b	4-C ₆ H ₄ OCH ₃	B	9.7(4)×10 ⁻⁵	>99	5.5h	6
15	9c	4-C ₆ H ₄ CH ₃	B	1.0(1)×10 ⁻⁴	95	7h	5
16	9d	C ₆ H ₅	B	1.1(1)×10 ⁻⁵	60	39h	0
17	9e	4-C ₆ H ₄ NO ₂	B	Insoluble	-	-	-
18	9f	3,5-C ₆ H ₃ (CH ₃) ₂	B	3.1(1)×10 ⁻⁴	>99	7h	0
19	9g	CH(CH ₃)(C ₆ H ₅)	B	-	-	-	-
20	9h	ⁱ Pr	B	-	-	-	-
21	9i	^t Bu	B	6.4(3)×10 ⁻⁵	>99	6.5h	12
22	9j	4-C ₆ H ₄ N(CH ₃) ₂	B	-	-	-	-

^a Determined from ¹H NMR spectra. ^b Determined by ¹H NMR spectroscopy using (R)-(-)-*O*-acetylmandelic acid.⁴⁵ ^c [Ca] = [Ca{N(SiMe₃)₂(THF)₂}. ^d Reaction complete <7 minutes, rate undetermined. ^e Substrate **A** = 1-amino-2,2-dimethyl-4-pentene and substrate **B** = 1-amino-2,2-diphenyl-4-pentene (Scheme 11). ^f Time until conversion ceased, determined from ¹H NMR spectra.

The application of complexes $[\text{Ca}(\text{R-BIM})\{\text{N}(\text{SiMe}_3)_2\}(\text{THF})]$ **9a-j** to hydroamination catalysis produced mixed results (Table 4), with conversion ranging from 0-32% with a handful of examples exhibiting 60% or higher (>90%). From data obtained there appears to be little “middle-ground” with conversion tending to side with more extreme differences. When looking at this data related to the substrate used, these trends can be deciphered with more ease.

4.6.1 Enantiomeric Excess Determination

The enantiomeric excesses of hydroamination pyrrolidine product (Table 4) were determined using the same ^1H NMR procedure as discussed in Chapter 3, Section 3.5. An excess of chiral derivatising agent *R*-(-)- α -acetylmandelic acid **2.21** (Fig. 12)^{45, 46} was added to the pyrrolidine product containing reaction mixture and determination of enantiomeric excess was deduced from integration of characteristic resonances using line-fitting software as part of the Mestre-C or iNMR software packages.

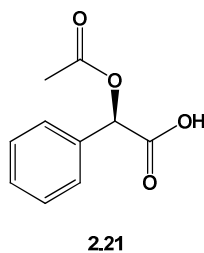
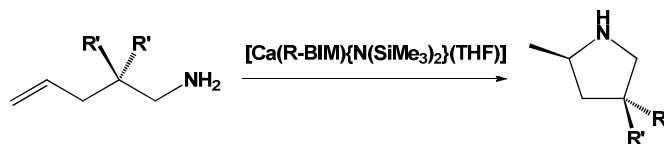


Fig. 12 *R*-(-)- α -acetylmandelic acid **2.21** used for ee determination.

4.6.2 Kinetics of Catalysis

Calculation of rate data from product conversion curves is presented in Table 4 and was pursued to allow quantitative comparison of catalytic activity between the various R-BIM supported calcium complexes employed in hydroamination (Scheme 11). When reacted with $[\text{Ca}\{\text{N}(\text{SiMe}_3)_2\}_2(\text{THF})_2]$ substrates **A** and **B** display largely different reactivity rates even without the presence of a bulky supporting ligand. Substrate **A** exhibits 99% conversion between 23-29 hours (dependent on ambient temperature fluctuations) and substrate **B** consistently achieves >99% conversion rapidly, completing the reaction before collection of ^1H NMR data can be accomplished (*ca.* 7 minutes with equipment at Cardiff

University). Unsurprisingly catalytic reactions of $[\text{Ca}(\text{R-BIM})\{\text{N}(\text{SiMe}_3)_2\}(\text{THF})]$ with substrate **A** were significantly slower than with substrate **B**. This is also in agreement with observations recorded with the calcium diamine complexes $[\text{Ca}(\text{NN}^{\text{R}})\{\text{N}(\text{SiMe}_3)_2\}(\text{THF})]$ discussed in Chapter 3.



Scheme 11 Asymmetric hydroamination catalysis ($\text{R}' = \text{Me}$ **A**, Ph **B**, H **C**).

The method employed for initial rate determination involved the collection of ^1H NMR spectra at staggered intervals during catalytic reactions (an example conversion curve recorded and used to determine initial rate is provided in Fig. 13). The time intervals between spectra collection were reaction dependant ranging from every 3 minutes to 30 minutes or more for slower reactions. This was undertaken until no further conversion was calculated by ^1H NMR. The conversion curves were curve fitted to an exponential decay function $y = Ae^{-bx}$. The initial rate, given by the slope at the origin ($x=0$), was determined by differentiation of the equation: $dy/dx = -A/b$. All accompanying conversion curves for reactions discussed in this chapter are supplied in Appendix B.

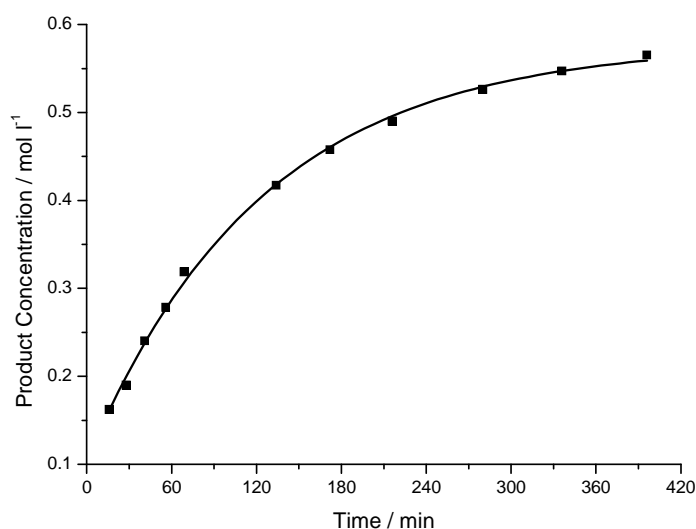


Fig. 13 Conversion for the catalytic hydroamination of substrate **B** using 10 mol% $[\text{Ca}(\text{^tBu-BIM})\{\text{N}(\text{SiMe}_3)_2\}(\text{THF})]$ **9i** in C_6D_6 at 293 K.

All catalysis results listed in Table 4 were conducted using 10 mol% catalyst to allow for comparison of results with literature results, as 10 mol% is a common loading.^{1, 42, 44, 47, 48} Curious about effects of catalyst quantity upon hydroamination, catalytic reactions using 5, 10, and 20 mol% of **9a**, **c**, and **i**, were monitored (Table 5), with representative conversion curves are provided in Fig. 14.

Table 5 Asymmetric hydroamination of amino-olefin substrate **B** using 5, 10, or 20 mol% [Ca(R-BIM){N(SiMe₃)₂}(THF)] in C₆D₆ at 293 K.

Entry	Complex	mol% catalyst	Initial Rate/ mol dm ⁻³ s ⁻¹
1	9a	5	-
2	9a	10	1.8(1)×10 ⁻⁵
3	9a	20	4.0(3)×10 ⁻⁵
4	9c	5	2.5(1)×10 ⁻⁶
5	9c	10	1.0(1)×10 ⁻⁴
6	9c	20	2.2(4)×10 ⁻⁴
7	9i	5	-
8	9i	10	6.4(3)×10 ⁻⁶
9	9i	20	1.1(1)×10 ⁻⁴

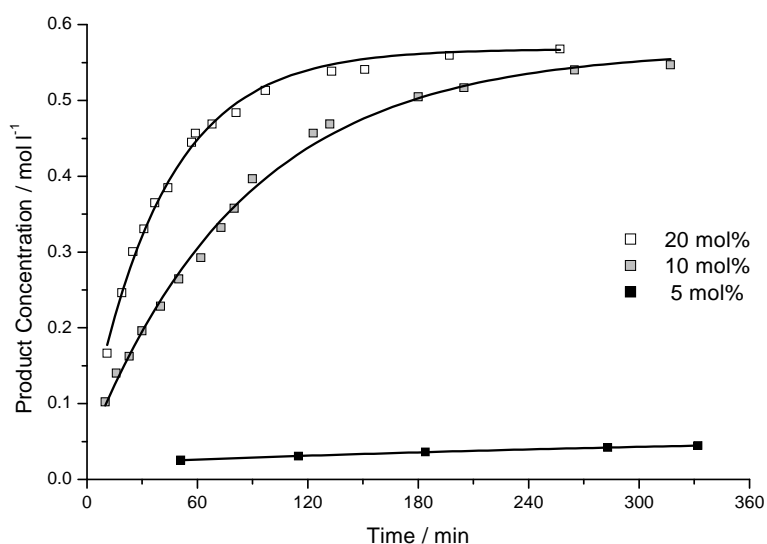


Fig. 14 Conversion for the catalytic hydroamination of substrate **B** using 5, 10, and 20 mol% of [Ca(Ar^{Me}-BIM){N(SiMe₃)₂}(THF)] **9c** in C₆D₆ at 293 K.

The trend of doubling catalyst concentration leading to approximate doubling of the initial rate is consistent with a first order reaction with respect to catalyst and is in agreement with those findings published by Marks.³¹ Marks investigated hydroamination using bisoxazoline complexes of lanthanides (**4.17**, Fig. 15).

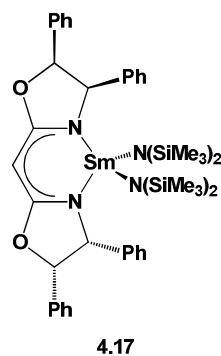


Fig. 15 Bis(oxazolinato)lanthanide complex [Sm(BIM){N(SiMe₃)₂]₂ **4.17**.

4.6.3. Catalyst Performance Analysis

Complexes **9e**, **g**, **h**, and **j**, show no catalytic activity with either substrate (entries 6/17, 8/19, 9/20, and 11/22 Table 4). It would appear that when employing [Ca(R-BIM){N(SiMe₃)₂}(THF)] type complexes to catalytic conversion of substrate **B**, if they do not catalyse its cyclisation, then it would not cyclise substrate **A** under ambient conditions either.

Pondering if these complexes evoked a higher energy barrier to catalysis, the catalytic performance of complexes **9g**, **h**, and **j** with substrates **A** and **B** was investigated at 50 °C and 80 °C. Unlike the calcium diamine catalysts evaluated at elevated temperatures (Chapter 3 Section 3.5.1), the R-BIM complexes that had no catalytic activity at ambient temperature displayed no activity at temperatures up to 80 °C for prolonged durations (up to 14 days). Complex [Ca(Ar^{NMe2}-BIM){N(SiMe₃)₂}(THF)] **9j** displayed increasing amounts of precipitate during monitoring at 80 °C. It is assumed this was from decomposition of the complex and was only observed in this particular complex. Rationalisation of these findings proves difficult due to ever-present contradictions. The three examples themselves have no obviously common structural parallels with respect to various steric and/or electronic attributes.

When examining them individually complex $[\text{Ca}(\text{}^i\text{PrR-BIM})\{\text{N}(\text{SiMe}_3)_2\}(\text{THF})]$ **9h** could be imagined to show similar catalytic performance to that of **9i**, the *tert*-butyl analogue due to their comparable chemical structures. Comparison of their catalytic performance data is conflicting, with **9h** showing no catalytic activity whereas complex **9i** arguably demonstrates the best combination of selectivity and rate figures of all complexes over both substrates (entries 10 and 21).

Complex redistribution equilibria that favour the heteroleptic complex are common traits of the non-active complexes **9g** and **9j**. However this characteristic cannot be so simply attributed to their poor activity since complexes **9b-d**, **9f** and **9i** do not support this (entries 3-5, 7, 10, 14-16, 18, and 21). When looking at steric and/or electronic properties of an R-BIM there is currently no clear correlation as to why these three complexes exhibit no catalytic activity. These trends also have no correlation to applicable diamine supported calcium catalysts since the iso-butyl bearing $[\text{Ca}(\text{NN}^i\text{Pr})\{\text{N}(\text{SiMe}_3)_2\}(\text{THF})]$ **5e** is catalytically active in intramolecular hydroamination. Diamine based catalysts where N-R is PhMeH or Ar^{NMe2} were not synthesised and so cannot be compared to their R-BIM equivalents.

Of the remaining complexes that recorded catalytic activity several interesting patterns emerge. The complex that catalysed both substrates fastest was **9f** (entries 7 and 18) followed by complex **9c** (entries 4 and 15). From this point the order of quickest initial rate changes depending on substrate. For substrate **A** fastest to slowest proceeds: Ar^{3,5Me}-BIM (**9f**) > Ar^{Me}-BIM (**9c**) > Ar^{OMe}-BIM (**9b**) > ^tBu-BIM (**9i**) > Ar^F-BIM (**9a**) > Ph-BIM (**9d**), and for substrate **B**: Ar^{3,5Me}-BIM (**9f**) > Ar^{Me}-BIM (**9c**) > ^tBu-BIM (**9i**) > Ar^{OMe}-BIM (**9b**) > Ph-BIM (**9d**) > Ar^F-BIM (**9a**).

It would appear the redistribution equilibria position could be in part responsible, since Ar^{3,5Me}-BIM **9f** has the lowest proportion of heteroleptic complex in solution at 298 K (46:54, entry 6, Table 1). Data then signifies that the reactivity generally decreases independent of substrate, as the redistribution equilibrium shifts to a greater proportion of heteroleptic complex (Table 6). Whilst this generally holds true complex $[\text{Ca}(\text{Ar}^{\text{F}}\text{-BIM})\{\text{N}(\text{SiMe}_3)_2\}(\text{THF})]$ **9a** is the exception with a redistribution equilibrium favouring formation of the homoleptic species, yet demonstrating a poor initial rate with both substrates in respect to the other R-BIM complexes analysed.

Explanation for this anomaly might arise from the electron-withdrawing nature of the N-R substituent. In the case of complex **9a** electronics opposed to redistribution equilibrium position may bear an over-riding influence on catalytic performance.

Table 6 Apparent initial rate dependence on ligand redistribution ratios **10:11**.

Rank	Substrate A	N-R	10:11	Substrate B	10:11	N-R
(Fastest)	9f	3,5-C ₆ H ₃ (CH ₃) ₂	46:54	9f	46:54	3,5-C ₆ H ₃ (CH ₃) ₂
2 nd	9c	4-C ₆ H ₄ CH ₃	64:36	9c	64:36	4-C ₆ H ₄ CH ₃
3 rd	9i	^t Bu	80:20	9b	100:0	4-C ₆ H ₄ OCH ₃
4 th	9b	4-C ₆ H ₄ OCH ₃	100:0	9i	80:20	^t Bu
5 th	9d	C ₆ H ₅	99:1	9a	48:52	4-C ₆ H ₄ F
(Slowest)	9a	4-C ₆ H ₄ F	48:52	9d	99:1	C ₆ H ₅

Treatment of product conversion and ee data by ranking the performance of the catalysts (Tables 7 and 8) shows no correlations between ligand redistribution equilibrium or trends relating to steric and/or electronic demands.

Table 7 Hydroamination product conversion dependence on ligand redistribution ratios **10:11**.

Rank	Substrate A	Conv. %	10:11	Substrate B	Conv. %	10:11
1 st	9f	64	46:54	9f, 9a, 9b, 9i	99	various
2 nd	9b	32	100:0	9c	95	64:36
3 rd	9i	18	80:20	9d	60	99:1
4 th	9c	8	64:36	-	-	-
5 th	9d	4	99:1	-	-	-
6 th	9a	3	48:52	-	-	-

Table 8 Hydroamination enantioselectivity dependence on redistribution ratios **10:11**.

Rank	Substrate A	ee %	10:11	Substrate B	ee %	10:11
1 st	9i	12	80:20	9i	12	80:20
2 nd	9f	10	46:54	9a	9	48:52
3 rd	9a	9	48:52	9b	6	100:0
4 th	9c, 9b, 9d	0	various	9c	5	64:36
5 th	-	-	-	9d, 9f	0	various

It is apparent that inconsistencies to the predicted behaviour have emerged. Complexes that redistribute to favour formation of active, yet non-stereospecific, $[\text{Ca}\{\text{N}(\text{SiMe}_3)_2\}_2(\text{THF})_2]$ and inactive $[\text{Ca}(\text{R-BIM})_2]$ do display faster initial rates as a result of increased concentration of $[\text{Ca}\{\text{N}(\text{SiMe}_3)_2\}_2(\text{THF})_2]$. On the other hand this does not always result in high substrate conversion. The data also fails to reflect anticipated results with respect to enantioselectivity. It is expected that solutions containing higher proportions of $[\text{Ca}\{\text{N}(\text{SiMe}_3)_2\}_2(\text{THF})_2]$ should show lower enantiomeric excess when compared to those with lower quantities of the non-stereoselective calcium complex.

Comparison of the R-BIM ee data with the diamine complexes of Chapter 3 goes to highlight another unexpected trend when evaluating complexes **9a**, **9f**, and **9i**. All other catalytically active complexes, R-BIM or diamine, have shown an inclination for faster initial rates, higher conversion and better ee with substrate **B** (discounting examples of non-selective results). Complexes **9a** and **9i** appear not to show substrate preference giving the same ee for both substrate **A** and **B**. Complex **9f** being the only example to show preference for substrate **A** over **B**.

Justification of the results from complexes **9a** and **9i** can be rationalised through consideration of the limits of accuracy of the data when working with conversions as low as 3% (complex **9a**). At such low conversions error is likely to be compounded compared to higher conversions. Whilst every effort was made to minimise error, the result of 9% ee could vary up to $\pm 3\%$. It could be a similar cause for the same substrate enantiomeric excesses of complex **9i** or purely coincidental. Reasoning for why complex $[\text{Ca}(\text{Ar}^{3,5\text{Me}}\text{-BIM})\{\text{N}(\text{SiMe}_3)_2\}(\text{THF})]$ **9f** invokes a preference for substrate **A** over the normal trend for substrate **B** remains unclear but could possibly be due to steric demands during a catalysis transition step. Since complex **9f** is the only example to be substituted at

the *meta* positions of the aromatic N-R substituent. It would be interesting to scrutinize other *meta* substituted examples to see if they demonstrated similar substrate preference behaviour.

In context of the BOX calcium complexes tested by Buch and Harder both types of calcium complex (R-BIM or BOX) show redistribution equilibria that are not typically 50:50 (heteroleptic:homoleptic), both catalyse hydroamination at a slower rate than $[\text{Ca}\{\text{N}(\text{SiMe}_3)_2\}_2(\text{THF})_2]$, and both complexes generally favour substrate **B** over substrate **A**. Whilst Buch and Harder experienced enantiomeric excesses between 4-6% with the phenyl BOX calcium complex (**1.6**, Fig. 1), enantiomeric excesses with the R-BIM calcium complexes showed improved enantiomeric excesses up to 12%.

When evaluating the success of the aforementioned $[\text{Ca}(\text{R-BIM})\{\text{N}(\text{SiMe}_3)_2\}(\text{THF})]$ complexes they have shown improvements on some of the early literature examples with respect to selectivity, however lag behind others, i.e. enantioselectivities of 18% from a trisoxazoline complex reported by Sadow and co-workers,³⁹ and the 26% ee induced by phenyl diamine complex **6d** of Chapter 3.⁴⁰ It is interesting that whilst the highest enantiomeric excess was achieved with a diamine bearing a phenyl N-R substituent, in the case of the R-BIM complexes the most favourable N-R substituent for overall catalytic performance (rate/selectivity) is *tert*-butyl. Like many of the discussed results this highlights that there appears to be no crossover between N-R substituents of the diamine and its R-BIM calcium complex counterpart, i.e. $[\text{Ca}(\text{NN}^{\text{Ph}})\{\text{N}(\text{SiMe}_3)_2\}(\text{py})_n]$ and $[\text{Ca}(\text{Ph-BIM})\{\text{N}(\text{Si}(\text{Me}_3)_2\}(\text{THF})]$ both displaying the highest enantiomeric excesses.

From this discussion we can determine that R-BIMs are currently, unlikely to be the optimum ligand for inducing greatly improved selectivity, i.e. >26% ee. However whilst research involving organocalcium complexes applied to hydroamination catalysis is still in its infancy, they provide valuable models for investigations concerning ligand alteration and subsequent effects upon catalytic performance. The modular nature of these ligands still has room for exploitation; the extension of synthesised and tested examples of varying N-R substituents, alternative bridge motifs and stereodirecting group alterations are all conceivable and may still yield more desirable enantiomeric excesses.

In review, the employment of R-BIMs with variation of the N-R substituent has successfully improved the enantiomeric excesses obtained in intramolecular hydroamination of substrates **A** and **B** when compared to the initial attempts by Buch and Hard with calcium BOX complexes. Whilst variation of the N-R substituent can affect the ligand redistribution position it appears to have little effect upon the rate at which this equilibrium is achieved. The employment of one particular N-R substituent has not resulted in significant improvement upon catalytic performance when compared to the library tested.

Whilst the data collected doesn't allow for discrete behaviour patterns to be deciphered, it dismisses the assumption that complexes exhibiting a ligand redistribution equilibrium favouring formation of the heteroleptic species give better catalytic performance. In addition, it would seem that additional factors dictate the conversion and ee of a reaction. Certainly NMR evidence suggests that what was thought to be discrete, liberated HNSiMe_3 isn't necessarily the case since there is a possibility it may act as a donor ligand in solution. This finding points towards the possibility of previously unforeseen interactions taking place with the calcium centre which are likely to impact on overall catalytic performance.

Although these studies direct us to believe that the redistribution equilibrium position is of lesser importance than first postulated at the beginning of this Thesis. It does raise the question of whether the rate of which ligand redistribution is established plays a more significant role with respect to catalytic performance. Further investigation to probe this postulation is likely to take the form of employing supporting ligands that are more kinetically inert than either the diamines or R-BIMs. For example, ligand scaffolds that only undergo rearrangement upon forcing conditions such as significant heating.

4.7 References

1. F. Buch and S. Harder, *Z. Naturforsch.*, **2008**, 63b, 169.
2. G. C. Hargaden and P. J. Guiry, *Chem. Rev.*, **2009**, 109, 2505.
3. D. A. Evans, K. A. Woerpel, M. M. Hinman and M. M. Faul, *J. Am. Chem. Soc.*, **1991**, 113, 726.
4. E. J. Corey, N. Imai and H.-Y. Zhang, *J. Am. Chem. Soc.*, **1991**, 113, 728.
5. H. Nishiyama, *Chem. Soc. Rev.*, **2007**, 36, 1133.
6. S. Dagorne, S. Bellemin-Laponnaz and A. Maisse-Francois, *Eur. J. Inorg. Chem.*, **2007**, 913.
7. D. Rechavi and M. Lemaire, *Chem. Rev.*, **2002**, 102, 3467.
8. C. Foltz, M. Enders, S. Bellemin-Laponnaz, H. Wadepohl and L. H. Gade, *Chem. Eur. J.*, **2007**, 13, 5994.
9. A. Abiko and S. Masamune, *Tetrahedron Lett.*, **1992**, 33, 5517.
10. T. Arai, N. Yokoyama and A. Yanagisawa, *Chem. Eur. J.*, **2008**, 14.
11. S. Bhor, G. Anilkumar, M. K. Tse, M. Klawonn, C. Dobler, B. Bitterlich, A. Grotevendt and M. Beller, *Org. Lett.*, **2005**, 7, 3393.
12. H. Liu and D.-M. Du, *Adv. Synth. Catal.*, **2009**, 351, 489.
13. N. A. Boland, I. J. Casey, S. J. Hynes, J. W. Matthews, H. Müller-Bunz and P. Wilkes, *Org. Biomol. Chem.*, **2004**, 2, 1995.
14. S. Enthaler, B. Hagemann, S. Bhor, G. Anikumar, M. K. Tse, B. Bitterlich, K. Junge, G. Erre and M. Beller, *Adv. Synth. Catal.*, **2007**, 349, 853.
15. S. Enthaler, B. Hagemann, S. Bhor, G. Anikumar, M. K. Tse, B. Bitterlich, K. Junge, G. Erre and M. Beller, *Chem. Eur. J.*, **2011**, 17, 14375.
16. G. Anikumar, S. Bhor, M. K. Tse, M. Klawonn, B. Bitterlich and M. Beller, *Tetrahedron: Asymmetry*, **2005**, 16, 3536.
17. T. Arai, T. Mizukami, N. Yokoyama, D. Nakazato and A. Yanagisawa, *Synlett*, **2005**, 17, 2670.
18. B. Ramalingam, M. Neuburger and A. Pfaltz, *Synthesis*, **2006**, 4, 572.
19. M. Aoki, M. Kaneko, S. Izumi, K. Ukai and N. Iwasawa, *Chem. Commun.*, **2004**, 2568.
20. S. B. Tsogoeva, G. Dürner, M. Bolte and M. W. Göbel, *Eur. J. Org. Chem.*, **2003**, 1661.
21. D. Akalay, G. Dürner, J. W. Bats and M. W. Göbel, *J. Org. Chem.*, **2008**, 72, 5618.

22. D. Akalay, G. Durner, J. W. Bats, M. Bolte and M. W. Gobel, *J. Org. Chem.*, **2007**, 72, 5618.
23. M. B. Smith and J. March, *Advanced Organic Chemistry*, 6th edn., Wiley, London, 2007.
24. R. Roger and D. G. Neilson, *Chem. Rev.*, **1961**, 61, 179.
25. Y. Bok-Lee, M. G. Yang, Y. Y. Lee and J. K. Lee, *Tetrahedron Lett.*, **1990**, 31, 1170.
26. A. N. Mandal, S. R. Raychaudhuri and A. Chatterjee, *Synthesis*, **1983**, 727.
27. F. C. Schaefer and G. A. Peters, *J. Org. Chem.*, **1961**, 26, 412.
28. *United States Pat.*, 2003.
29. J. S. Wixey and B. D. Ward, *Dalton Trans.*, **2011**, 40, 7693.
30. V. K. Aggarwal, L. Bell, M. P. Coogan and P. Jubault, *J. Chem. Soc. Perkin Trans. I*, **1998**, 2037.
31. S. Hong, S. Tian, M. V. Metz and T. J. Marks, *J. Am. Chem. Soc.*, **2003**, 125, 14768.
32. *Repub. Korea Pat.*, 1997.
33. E. Diez-Barra, A. de la Hoz, A. Moreno and P. Sanchez-Verdu, *J. Chem. Soc. Perkin Trans*, **1991**, 1, 2589.
34. J. M. Atkins, S. A. Moteki, S. G. DiMagno and J. M. Takacs, *Org. Lett.*, **2006**, 8, 2759.
35. V. Čaplar, Z. Raza, M. Roje, V. Tomišić, G. Horvat, J. Požar, I. Piantanida and M. Žinić, *Tetrahedron*, **2005**, 60, 8079.
36. G. H. P. Roos and A. Donovan, R., *Science and Technology*, **2000**, 5, 11.
37. J. S. Alexander and K. Ruhlandt-Senge, *Eur. J. Inorg. Chem*, **2002**, 2761.
38. S. Harder, *Chem. Rev.*, **2010**, 110, 3852.
39. S. R. Neal, A. Ellern and A. D. Sadow, *J. Organomet. Chem.*, **2011**, 696, 228.
40. J. S. Wixey and B. D. Ward, *Chem. Commun.*, **2011**, 47, 5449.
41. M. R. Crimmin, A. G. M. Barrett, M. S. Hill, D. J. MacDougall, M. F. Mahon and P. A. Procopiou, *Dalton Trans.*, **2009**, 9715.
42. S. Datta, P. W. Roesky and S. Blechert, *Organometallics*, **2007**, 26, 4392.
43. C. Hansch, A. Leo and R. W. Taft, *Chem. Rev.*, **1991**, 91, 165.
44. M. R. Crimmin, I. J. Casely and M. S. Hill, *J. Am. Chem. Soc.*, **2005**, 127, 2042.
45. G. Zi, F. Zhang, L. Xiang, Y. Chen, W. Fang and H. Song, *Dalton Trans.*, **2010**, 39, 4048.

46. J. Y. Kim and L. Tom, *Org. Lett.*, **2005**, 7, 1737.
47. M. R. Crimmin, M. Arrowsmith, A. G. M. Barrett, I. J. Casey, M. S. Hill and P. A. Procopiou, *J. Am. Chem. Soc.*, **2009**, 131, 9670.
48. M. Arrowsmith, M. S. Hill and G. Kociok-Kohn, *Organometallics*, **2009**, 28, 1730.

Chapter Five

A Potential New Class of Ligand - Imoxazolines

5.1 Introduction

There is a constant quest for innovative ligand development or variation of existing platforms for their evaluation as supporting ligands in functional metal complexes. In this Thesis two types of ligand, bisoxazoline (BOX, (a), Fig. 1) and bisimidazoline (R-BIM, (c), Fig. 1) ligands have been referred to and compared upon a multitude of occasions.

During the course of synthesising the R-BIMs presented in Chapter 4, Section 4.2, we noted that a small modification to the R-BIM synthesis could lead to the potential development of a new ligand class. The new ligand class deemed “imoxazoline” (IMOX) would essentially be a BOX/R-BIM structural hybrid bearing one oxazoline and imidazoline ring within its structure ((b), Fig. 1).

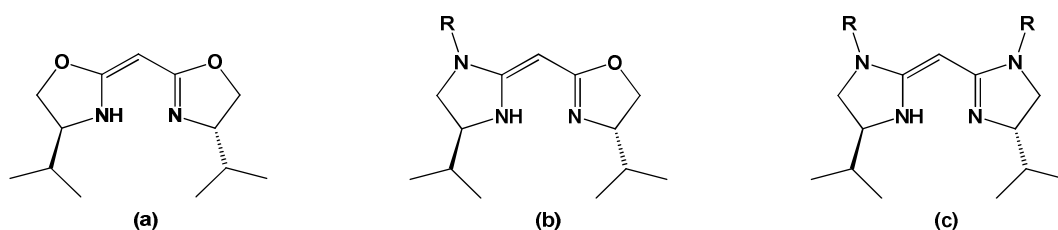


Fig. 1 BOX (a), IMOX (b), and R-BIM (c).

Although possessing C_1 symmetry the IMOX ligand structure contains a *pseudo* C_2 -axis of symmetry trisecting the methylene bridge, giving a coordination environment similar in nature to the BOX and BIM parent ligands. Like both BOX and R-BIMs the stereodirecting groups of the IMOX (*iso*-propyl as depicted in Fig. 1) are still within close proximity of the metal binding centre and able to provide steric shielding and impart chiral information upon substrates that would either be bound to, or approaching the metal centre.

The modular construction of an IMOX could present a significant advantage over traditional BOX and R-BIMs with respect to variation of the stereodirecting groups. The two stereodirecting groups being identical is currently a pre-requisite for BOX and R-BIM ligands, however through judicious selection of the components required to assemble an IMOX (a diamine and an amino alcohol), it is theoretically possible to have two different stereodirecting groups. For example one *iso*-propyl moiety bound to the oxazoline ring and a *tert*-butyl group bound to the imidazoline of the IMOX.

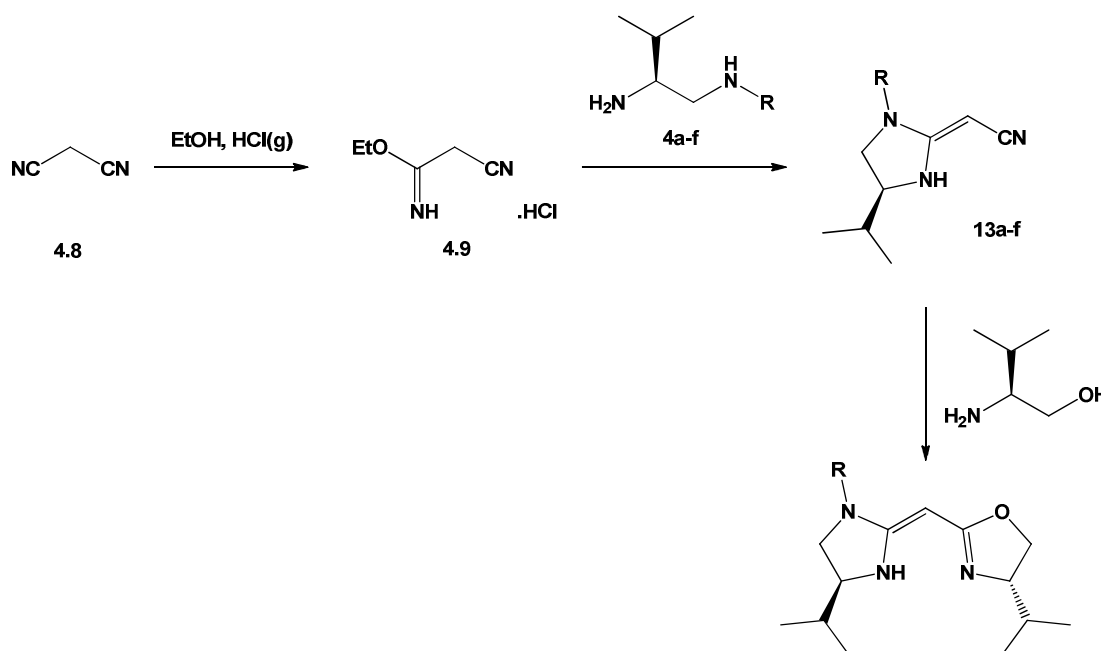
If synthetically successful with IMOXs, implementation of inequivalent stereodirecting groups could theoretically also be transferred to BOX and R-BIM ligands through the sequential construction of oxazoline or imidazoline rings. This flexibility over stereodirecting group selection would provide access to a previously unexplored area, where the fine tuning the ligand by mixing stereodirecting groups is rendered a real possibility.

The retention of the imidazoline N-R moiety within the IMOX would still allow for the rich variation of electronic and/or steric properties of the ligand akin to those discussed with R-BIMs, whilst likely to display properties between those of the BOX and BIM ligands. Again the flexibility of the IMOX platform at this point has the potential for ligand fine-tuning towards desirable features, resulting from the inclusion of a particular N-R substituent.

At this moment the effects on ligand performance when varying stereodirecting groups and the many potential variations of the N-R substituent remains to be seen, but provides an exciting academic prospect to explore. As IMOX ligands are unreported in the literature their application as a ligand to a much wider field of chemistry other than calcium assisted hydroamination would also be of potential significance. This would be most significant for asymmetric catalysis where BOX and R-BIM ligands have already demonstrated a wealth of success. This would also go hand-in-hand with being able to draw parallels between the performance of IMOXs with BOX and R-BIM ligands.

5.2 Ligand Precursor Synthesis and Characterisation

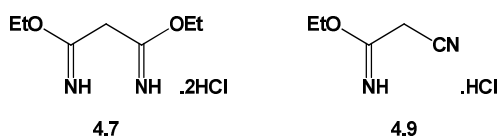
Achievement of the desired IMOX ligands is dependent upon the formation of the ethyl 2-cyanoacetimidate hydrochloride compound **4.9**. Reaction of **4.9** with one equivalent of diamine (**4a-f**) allows for the formation of the required imidazoline ring. Upon ring-closing the mono-imidazoline species (R-MIM **13a-f**) is produced. Fashioning the oxazoline unit is proposed by reaction of the R-MIM with an amino alcohol, for example L-valinol as shown in Scheme 1 overleaf.



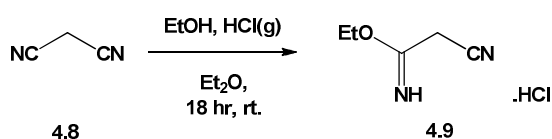
Scheme 1 Proposed synthetic route to IMOXS.

5.2.1 Ethyl 2-Cyanoacetimidate Hydrochloride Synthesis

Whilst designing the synthetic pathway to the desired R-BIMs discussed in Chapter 4, Section 4.2.1, it was noted that subtle modification of the reaction conditions described by Göbel *et al.* (Scheme 2) used to synthesise the imidate **4.7** would instead yield the mono-imidate **4.9**.^{1,2}

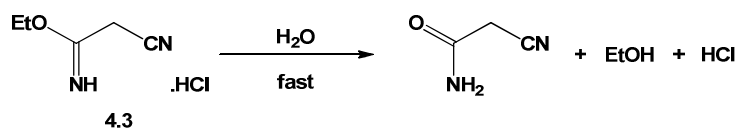
Fig. 2 Diimidate **4.7** and mono-substituted imidate **4.9**.

Starting with malononitrile (**4.8**) in anhydrous diethyl ether, ethanol was then added at room temperature. HCl gas was sparged through the system for 4 hours where **4.9** precipitates from the solution upon formation. After filtration and drying *in vacuo* a white solid in near quantitative yield is obtained.

Scheme 2 Preparation of a mono-substituted imidate **4.9**.

The production of the mono-imidate **4.9** is surprising considering the diimidate analogue **4.7** is formed in either 1,4-dioxane or THF, both ethereal solvents.³ It was postulated that under the above conditions the insoluble nature of the mono-imidate salt **4.9** in diethyl ether results in the cessation of the reaction prohibiting the second nitrile group conversion to an imidate; whereas the monoimidate is partially soluble in 1,4-dioxane/THF, thus facilitating conversion into the diimidate **4.7**.

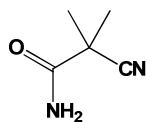
The resulting mono-imidate salt **4.9** was stored under an inert atmosphere in an opaque container to reduce exposure to light sources. These actions were necessary to prolong the shelf life of the material, which was observed to discolour at a faster rate than **4.7**. The longevity of **4.9** was typically 3 weeks compared to the 6 weeks of diimidate **4.7**. Once compound discolouration was evident for either, decreased yields were typical with their use in subsequent reactions. Containment within an inert atmosphere is required to prevent imidate hydrolysis (Scheme 3). Hydrolysis of such imidate compounds to the corresponding amide is known in the literature.⁴⁻⁷ Hydrolysis is catalysed in the presence of water and the formation of the amide is generally fast and goes to completion. This is especially true in the case of low number aliphatic chains such as **4.7** and **4.9**, which tend to be more hydroscopic than longer chain examples.⁴



Scheme 3 Hydrolysis of an imidate to the resulting amide.

Distinguishing between the mono-imidate **4.9** and diimidate **4.7** proves straightforward when comparing spectroscopic data. IR spectroscopy shows a very prominent band at 2265 cm^{-1} which arises from the $\text{C}\equiv\text{N}$ present in **4.9**. As expected this band is absent in the IR spectrum of **4.7**. There are also small variations in absorbance frequency of the $\text{C}=\text{N}$ for **4.9** at 1651 cm^{-1} compared to **4.7** at 1662 cm^{-1} . Comparison of ^1H NMR spectra brings to light a moderate change in chemical shift arising from the different environments around the two protons bound to the bridge carbon. In **4.9** the resonance corresponding to these two protons (adjacent to the nitrile group) is observed at 4.01 ppm compared to 4.21 ppm for the same protons in **4.7**.

^{13}C NMR of both compounds show significant differences. The inclusion of the $\text{C}\equiv\text{N}$ frequency of **4.9** at 115.1 ppm is noticeably absent in the spectra of **4.7**. Both compounds show a large difference in resonances attributed to the carbon atom at the bridge, recorded at 24.5 ppm (**4.9**) and 41.2 ppm (**4.7**). Less significant chemical shifts are observed for the $\text{C}=\text{N}$ carbons, being detected at 164.3 ppm (**4.9**) and 166.5 ppm (**4.7**).



15

Fig. 3 decomposition product **15**.

Whilst the solid state structure of **4.9** could not be confirmed directly, crystals suitable for X-ray diffraction were grown by David Collis of the hydrolysis product **15** (Fig. 3). Compound **15** is the related dimethyl substituted derivative of **4.9**. The molecular structure of **15** presented in Fig. 4 was solved by Dr. Benjamin Ward. Until this point all imidate salt examples presented in this Thesis have been unsubstituted at the bridge carbon. **15** is a derivative of an alternative dimethyl substituted bridge that was being explored at the time within the group, utilising the same synthetic procedure as discussed at the beginning of this Section.⁸ The molecular structure of **15** concisely shows substitution has only occurred at one nitrile group and that the resulting imidate group has undergone hydrolysis (Scheme 3).

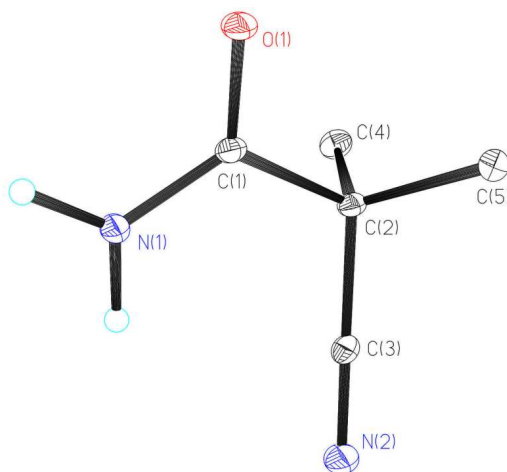
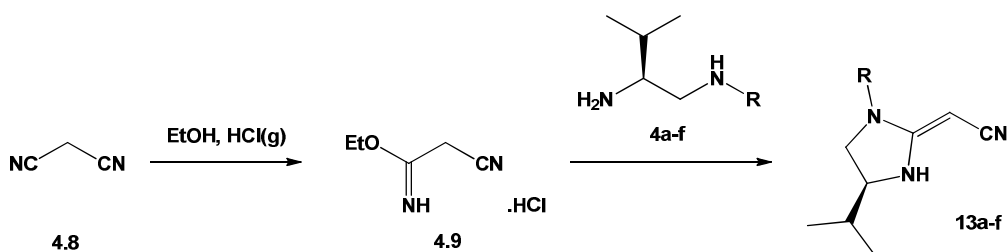


Fig. 4 Molecular structure of mono substituted imide hydrolysis product **15**. Ellipsoids are drawn at 25% probability. H atoms are omitted for clarity with the exception of those bound to N(1).

The crystallographic data from **15** shows only one notable deviation from expected bond lengths. This comes from the bond length between N(1)-C(1). N-C bond lengths are commonly 1.47 Å, though in the case of **15** this bond length is measured as 1.332(2) Å. Explanation for this shorter bond length, more consistent with sp^2 hybridised atoms (N=C 1.29 Å) is due to usual amide resonance present within the molecule. The delocalisation of electron density present within this functional group results in an increase of sp^2 character opposed to sp^3 resulting in a shorter, stronger bond.

5.2.2 Mono-imidazoline IMOX Precursors

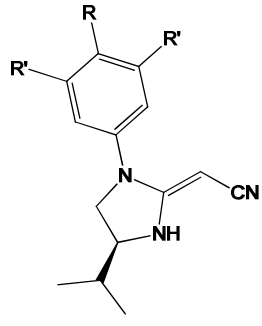
The mono-imidate **4.9** was reacted with 1 equivalent of diamine **4a-f** under typical conditions as described in step 2 of Scheme 4, resulting in the formation of mono-imidazolines (R-MIMs) **13a-f**. Yields for this reaction were fair, ranging between 30-40%, which is mirrored in the R-BIM formation proceeding via an analogous synthetic pathway.



Scheme 4 Synthesis of R-MIMs **13a-f**.

Analysis of the crude products from reaction between **4.9** and diamines **4a-f** indicated the presence of the desired R-MIM (**13a-f**, Table 1) with the only by-product being unreacted diamine. Of the spectroscopic methods, IR and ^{13}C NMR spectra gave the most insight for structural deduction. Using IR spectroscopy noticeable changes in absorbance frequencies were prominent between starting material **4.9** and the products **13a-f**. The absorbance assigned to the $\text{C}\equiv\text{N}$ shifts significantly from 2265 cm^{-1} in **4.9** to between $2172\text{-}2194\text{ cm}^{-1}$ in **13a-f**. Bands related to the $\text{C}=\text{N}$ showed less pronounced changes though common occurred at lower absorbance frequencies by $30\text{-}40\text{ cm}^{-1}$.

Table 1 R-MIMs **13a-f** synthesised with various N-R substituents.

	Entry	Compound	R	R'
	1	13a	F	H
	2	13b	OCH ₃	H
	3	13c	CH ₃	H
	4	13d	H	H
	5	13e	NO ₂	H
	6	13f	H	CH ₃

¹³C NMR spectra showed several significant chemical shift variations between **13a-f**, and their starting diamine analogues and **4.9**. The chemical shift of $\underline{\text{C}}\equiv\text{N}$ in **4.9** was observed at 115.1 ppm, however in **13a-f** it is recorded between 123-126 ppm. This shift signifies a loss of electron density around this nucleus, most likely due to the newly introduced resonance within **13**. Frequency changes between the $\underline{\text{C}}=\text{N}$ in **4.9** and **13a-f** were not as pronounced tending to be 1-2 ppm downfield with respect to **4.9**. Nevertheless recorded signals for the carbon atom at the bridge were noticeably different. In **4.9** the resonance for the bridge carbon was recorded at 24.5 ppm, whereas in **13a-f** the same carbon nuclei had a resonance between 36-37 ppm, suggesting a large change in chemical environment around this point.

The ¹H NMR spectra of **13a-f** are very similar to their related R-BIM analogues. The resonances assigned in **13a-f** to the proton at the chiral centre and two hydrogen nuclei of the CH₂ moiety were shifted upfield by as much as 1 ppm, when compared to the relevant diamine starting material. Changes in resonances for the aromatic proton nuclei were less significant and those assigned to the *iso*-propyl moiety less again. For the mono-imidazoline **13a** ¹⁹F NMR studies recorded a resonance of -114.81 ppm compared to the starting diamine **4a**, which records a signal at -128.11 ppm for the same fluorine nuclei of the 4-C₆H₄F N-R substituent. These data support the formation of **13a**, which was further supported by X-ray analysis of its solid state structure as depicted in Fig. 5 (*vide infra*).

Purification of **13a-f** proved straightforward through recrystallisation from an equal mixture of warm dichloromethane/hexane allowed to cool to -16 °C. From this technique X-ray quality single crystals were obtained and the molecular structures of R-MIMs **13a-c** and **13f** are highlighted in Fig. 5. All crystallographic data for these R-MIMs are contained within Appendices D-G.

5.2.2.1 R-MIM Molecular Structures

Resulting from analysis of the molecular structures of compounds **13a-c** and **13f** (Fig. 5) it is apparent that each example supports the resonance form previously shown in Scheme 4. This agrees with the favoured conformation seen in BOXs and also provides strong supporting evidence that the same resonance conformation is likely prevalent in R-BIM structures.

Comparison of the molecular structures of **13a-c** and **13f** reveals them to be isostructural. However the asymmetric unit of both Ar^{OMe}-MIM **13b** and Ar^{Me}-MIM **13c** contain 4 independent molecules whereas Ar^F-MIM **13a** and Ar^{3,5Me}-MIM **13f** only contain 2. Selected bond lengths and angles of all compounds are tabulated in Tables 2 and 3 for comparison, with accompanying values from other independent molecules included in parentheses.

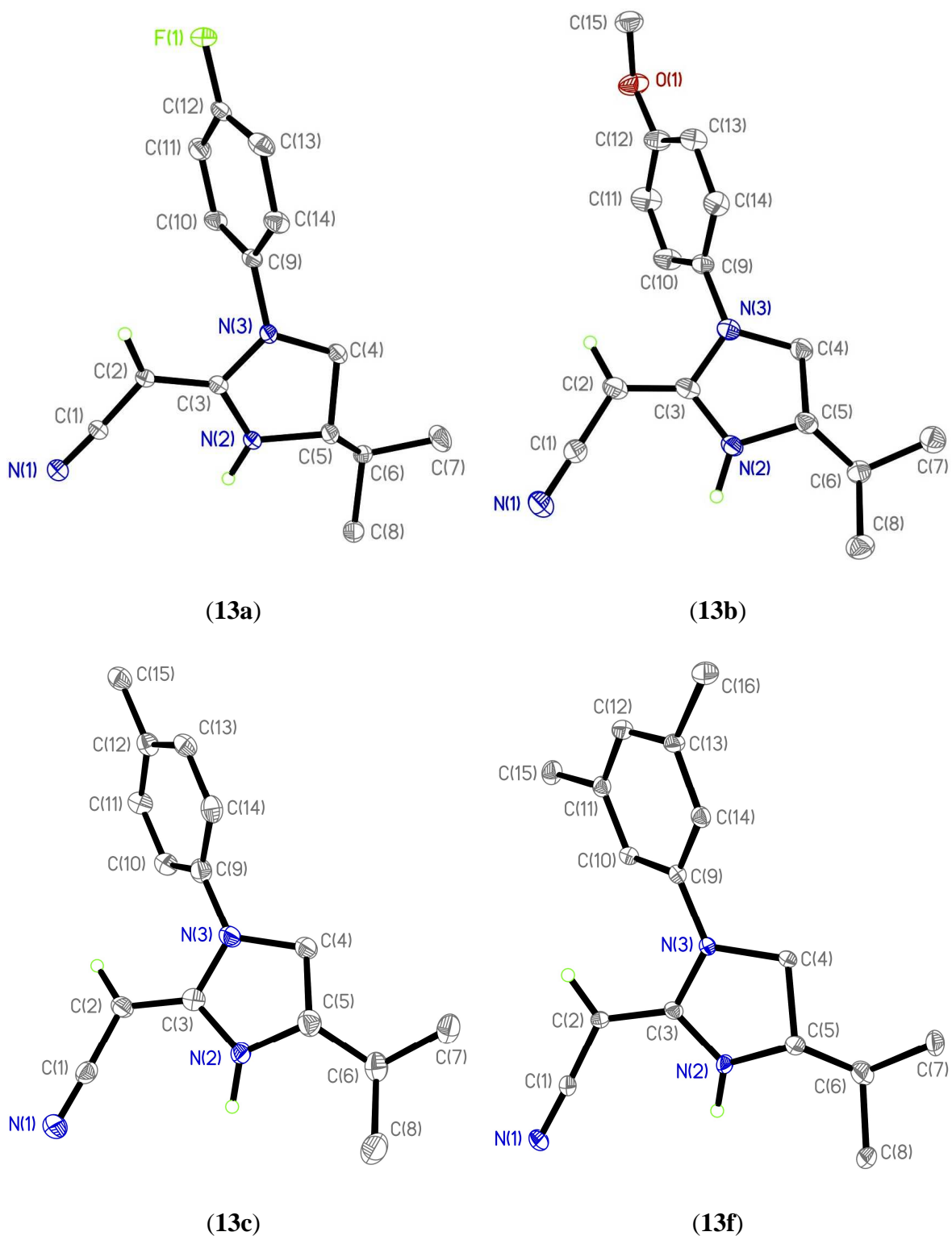


Fig. 5 Molecular structures of R-MIMS **13a-c** and **13f**. Ellipsoids are drawn at 25% probability. H atoms are omitted for clarity with the exception of C(2) and N(2).

Table 2 Selected bond lengths of R-MIMs **13a-c** and **13f**. All lengths are quoted in Å.

Compound	N-R	C(1)-N(1)	N(2)-C(3)	C(3)-N(3)	N(3)-C(9)
13a	4-C ₆ H ₄ F	1.155(6)	1.353(6)	1.374(6)	1.435(6)
		[1.153(6)]*	[1.357(6)]	[1.366(6)]	[1.415(6)]
13b	4-C ₆ H ₄ OCH ₃	1.159(7)	1.365(7)	1.373(6)	1.420(6)
		[1.143(7)]	[1.351(7)]	[1.370(6)]	[1.440(7)]
		[1.146(7)]	[1.361(7)]	[1.371(6)]	[1.433(7)]
		[1.162(7)]	[1.340(7)]	[1.373(7)]	[1.416(7)]
13c	4-C ₆ H ₄ CH ₃	1.140(8)	1.368(7)	1.363(8)	1.425(8)
		[1.165(8)]	[1.349(7)]	[1.375(8)]	[1.411(7)]
		[1.155(8)]	[1.352(7)]	[1.372(7)]	[1.408(7)]
		[1.158(8)]	[1.359(7)]	[1.353(8)]	[1.439(7)]
13f	3,5-C ₆ H ₃ (CH ₃) ₂	1.158(6)	1.359(5)	1.360(6)	1.411(6)
		[1.150(6)]	[1.350(5)]	[1.380(6)]	[1.426(6)]

* Figures in parentheses are from other independent molecules in the asymmetric unit.

Of all C≡N lengths, Ar^{OMe}-MIM **13b** was measured at 1.140(8) Å, marginally shorter than the average of 1.154 Å (range = 1.140(8)-1.165(8) Å), which is not significantly different to typical C≡N lengths of 1.141 Å (range = 1.110-1.668 Å). All compound bond angles between N(1)-C(1)-C(2) were between 177.3(5)-179.3(6) ° indicating a slight deviation from true linearity.

Evaluation of the bond lengths and angles within the imidazoline ring were uniform (within error) between each compound. The bond angle N(2)-C(3)-N(3) was the most acute within the imidazoline ring, showing a minor distortion from typical tetrahedral angles of 109.4 °, instead being measured as 108.5 °. This is within the average range of between 107.6(5)-109.6(5) °. In literature related compounds the typical bond angle for N(2)-C(3)-N(3) is 107.80 ° (range = 96.23-115.12 °). The C-N bond lengths of each imidazoline from compounds **13a-c** and **13f** record and average length of 1.361 Å (range = 1.340(7)-1.380(6) Å), which shows no significant deviation from related bond lengths that average 1.377 Å (range = 1.225-1.567 Å).

Table 3 Selected bond angles of R-MIMs **13a-c** and **13f**. All angles are quoted in °.

Compound	N-R	N(1)-C(1)-C(2)	C(3)-N(2)-C(5)	C(3)-N(3)-C(4)
13a	4-C ₆ H ₄ F	177.3(5)	111.1(3)	110.1(4)
		[177.6(5)]*	[112.3(4)]	[111.3(4)]
13b	4-C ₆ H ₄ OCH ₃	179.2(7)	111.0(4)	110.0(4)
		[178.8(6)]	[112.3(5)]	[109.6(5)]
		[179.3(6)]	[111.0(5)]	[109.4(5)]
		[178.8(6)]	[110.8(5)]	[110.9(5)]
13c	4-C ₆ H ₄ CH ₃	177.8(6)	109.9(5)	110.5(5)
		[179.8(7)]	[112.3(5)]	[109.6(5)]
		[177.6(6)]	[111.0(5)]	[109.4(5)]
		[178.9(6)]	[110.8(5)]	[110.9(5)]
13f	3,5-C ₆ H ₃ (CH ₃) ₂	177.6(5)	112.5(4)	110.8(4)
		[176.2(5)]	[110.6(4)]	[109.5(4)]

* Figures in parentheses are from other independent molecules in the asymmetric unit.

The bond lengths of both C(1)-C(2) and C(2)-C(3) were identical in all compounds within error. The average length for C(1)-C(2) being 1.401 Å (range 1.381(9)-1.416(6) Å) and 1.373 Å (range = 1.341(8)-1.387(7) Å) for C(2)-C(3). Both bond lengths are shorter than typical C-C bond lengths contained in similar moieties which average at 1.50 Å (range = 1.400-1.606 Å). The shorter bond lengths of C(1)-C(2) and C(2)-C(3) are more comparable to C=C bonds in simple alkenes. These have an average length of 1.339 Å (range = 1.315-1.391 Å) reflecting sp^2 hybridisation between the atoms. This evidence supports the delocalisation of electron density over this area of the molecule. The average bond angle between C(1)-C(2)-C(3) is 121.3 ° (range = 119.3(6)-124.2(4) °) with Ar^{3,5Me2}-MIM **13f** displaying the largest angle of 124.2 °. This angle is typically larger than comparable compounds in the CSD, which demonstrate an average angle of 113.9 ° over a range of 108.7-127.3 °.

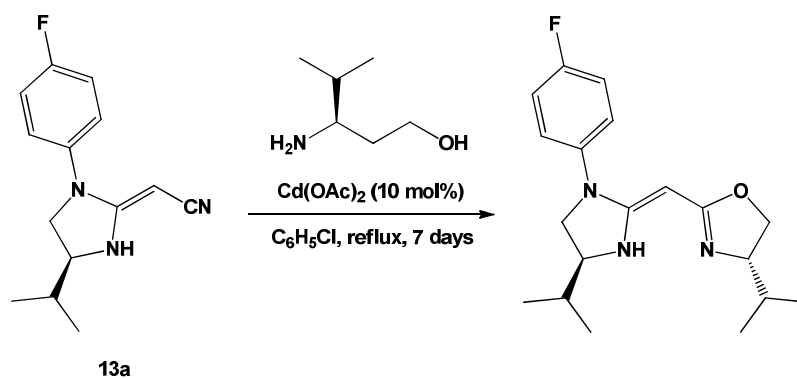
All other bond angles contained within the R-MIM structures **13a-c** and **13f**, notably the phenyl and isopropyl moieties have unexceptional bond lengths and angles.

5.3 Attempted IMOX Ligand Synthesis

Successful isolation of pure monocyclised imidazoline intermediates (R-MIMs) **13a-f** allowed progression to the final step of the proposed IMOX synthesis. The final step requires the activation of the remaining nitrile moiety and subsequent ring closure with a suitable amino-alcohol to form the oxazoline unit (step 3, Scheme 1).

Preliminary investigations showed that to activate the nitrile group of the R-MIM to react with L-valinol would require the presence of a Lewis acid catalyst. From the literature it is known that both $\text{Cd}(\text{OAc})_2$,⁹ ZnCl_2 ¹⁰ and Zn-clusters¹¹ can be used in the successful formation of oxazolines between nitriles and amino-alcohols. The Lewis acidic metals activate the nitrile group towards nucleophilic attack from the amine of the amino-alcohol. These reactions were typically undertaken in refluxing chlorobenzene for ≥ 12 hours under inert conditions.

Addition of 10 mol% $\text{Cd}(\text{OAc})_2$ to the reaction mixture of Ar^{F} -MIM **13a** and L-valinol as described by the literature was explored (Scheme 5). Experimental progress was monitored after several days; upon there being no evidence of reaction progress (concluded via NMR techniques of reaction interval aliquots) the reaction was allowed to proceed for 7 days. Concluding such time analysis of the crude reaction mixture was undertaken. ^1H NMR spectra of the crude mixture showed complex overlap of resonances, signifying the presence of many reaction products. This was confirmed by TLC, which indicated the existence of at least 5 species. Nominal resolution mass spectrometry gave indications of starting materials and unidentifiable fragments with no signals corresponding to the target IMOX, or fragments thereof.



Scheme 5 Proposed $\text{Cd}(\text{OAc})_2$ catalysed oxazoline formation to generate an IMOX ligand.

Upon separation of the reaction mixture large quantities of starting materials **13a** and L-valinol were isolated, along with small quantities (<100 mg) of an unidentified species. The unknown compound was obtained by Kate Smith and Mass spectrometry and IR analysis of the unidentified compound was undertaken. These techniques revealed that instead of isolating the desired IMOX, a compound with $m/z = 221.14$ and no absorbance in the $C\equiv N$ region at 2176 cm^{-1} had been isolated. These results indicated that an analogue of **13a** was probable due to a comparable m/z and lack of the distinctive absorbance of the $C\equiv N$. NMR studies were undertaken in an effort to reveal the identity of the unknown compound. All data obtained alluded to the likely formation of compound **16** (Fig. 6).

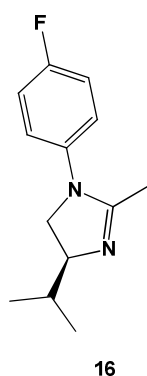


Fig. 6 $Cd(OAc)_2$ aided IMOX synthesis by-product **16**.

Whilst the NMR spectra of **16** and **13a** share a high proportion of common resonances, additions of a singlet signal integrating to 3 hydrogen nuclei arises at 2.25 ppm in the 1H NMR spectra of **16**. 2D NMR alludes to its correspondence to an additional signal in the ^{13}C NMR at 12.9 ppm, thereby confirming the presence of the methyl group in place of the nitrile group of **13a**. ^{19}F NMR also supports the proposal of an analogue of **13a**, as the resonance of the fluorine nuclei in the 4- C_6H_4F N-R substituent experiences a shift from -114.81 ppm in **13a** upfield to -109.9 ppm in **16**. Whilst this could be considered a small shift, it still signifies a variance in structure between both compounds.

If the IMOX had been successfully synthesised then sizable differences would be observed in various analytical data, for example mass spectra of the molecular ion. Any addition of the new oxazoline frequencies in the NMR spectra would be stark in the 1H NMR spectrum, where three additional resonances are typically recorded between 3.4-4.5 ppm (solvent dependent) and give a similar fine structure to the CH_2 and CH of an imidazoline ring. All evidence at this time supports the formation of **16**.

The employment of ZnCl_2 and a tetranuclear zinc cluster published by Ohshima *et al.* (Fig. 7)¹¹ was subsequently investigated. In both cases even forcing conditions for several weeks failed to yield the target IMOX. All spectroscopic data confirms that only starting materials were returned upon work-up/purification.

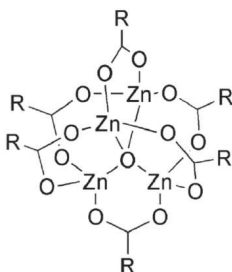


Fig. 7 Tetranuclear zinc cluster as prepared by Ohshima *et al.* ($\text{R} = \text{CF}_3$).

In a move away from previous attempts to activate the nitrile group of **13a-f** (in an effort to improve its reactivity with the L-valinol), interfunctional group conversion of the nitrile to an imidate in a similar manner to preparing compound **4.7** (Fig. 2) was attempted. The Ar^{F} -MIM **13a** was subjected to the same reaction conditions as used in the synthesis of **4.7**, where the hydrolysis product **14** (Fig. 8) was the only product obtained. Hydrolysis product **14** was obtained in near quantitative yields suggesting hydrolysis was total. The formation of **14** is likely due to water entering the system during the reaction, possibly during the generation of the $\text{HCl}_{(\text{g})}$ though currently the source remains unconfirmed.

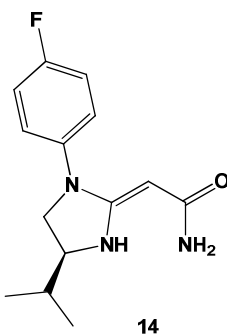
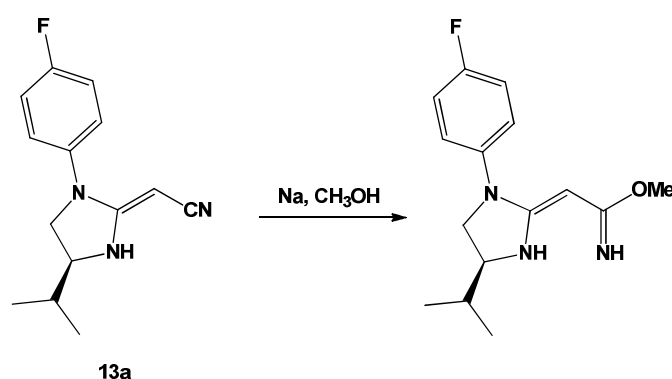


Fig. 8 Hydrolysis product **14**.

Careful analysis of the data was needed to confirm the structure of **14** when mass spectrometry recorded almost exclusively 264.1512 m/z . Strong evidence from the ^{13}C NMR and IR support the introduced carbonyl group with a resonance at 165.4 ppm and corresponding absorbance at 1668 cm^{-1} . The typical $\text{C}\equiv\text{N}$ absorbance at 2176 cm^{-1} is absent and replaced by the presence of an amide group in the IR spectra. This explains why the resonance of the carbonyl is noticeably upfield compared to typical $\text{C}=\text{O}$ frequencies (*ca.* 180 ppm). The additional electron density around the $\text{C}=\text{O}$ from the amide resonance forms and mono-imidazoline ligand provides supplementary shielding, inducing a lower recorded chemical shift.



Scheme 6 Proposed base catalysed procedure for imidate intermediate formation.

In conclusion it should be made clear that at the time of writing a total synthetic pathway towards the target IMOXS remained incomplete, as previously discussed synthetic pathways were unsuccessful in completing the final step of IMOXS ligand formation (Scheme 1). For future endeavours exploitation of the base catalysed method¹² to form the imidate may prove more fortuitous than the acid catalysed methods discussed in this Chapter (Scheme 6). If the base catalysed method were to be successful it is hoped that the imidate intermediate could then undergo cyclisation with an amino-alcohol to form the desired oxazoline unit creating the new IMOXS ligand.

5.4 References

1. *United States Pat.*, 2003.
2. D. Akalay, G. Durner, J. W. Bats, M. Bolte and M. W. Gobel, *J. Org. Chem.*, **2007**, 72, 5618.
3. Y. Bok-Lee, M. G. Yang, Y. Y. Lee and J. K. Lee, *Tetrahedron Lett.*, **1990**, 31, 1170.
4. R. Roger and D. G. Neilson, *Chem. Rev.*, **1961**, 61, 179.
5. M. B. Smith and J. March, *Advanced Organic Chemistry*, 6th edn., Wiley, London, 2007.
6. P. Deslongchamp and R. J. Taillefer, *Can. J. Chem.*, **1975**, 53, 3029.
7. G. L. Schmirer, *J. Am. Chem. Soc.*, **1968**, 90, 3478.
8. D. Collis, J. S. Wixey and B. D. Ward, *Unpublished Results*.
9. V. K. Aggarwal, L. Bell, M. P. Coogan and P. Jubault, *J. Chem. Soc. Perkin Trans. I*, **1998**, 2037.
10. S.-G. Kim, H. R. Seong, J. Kim and K. H. Ahn, *Tetrahedron Lett.*, **2004**, 45, 6835.
11. T. Ohshima, T. Iwasaki and K. Mashima, *Chem. Commun.*, **2006**, 2711.
12. F. C. Schaefer and G. A. Peters, *J. Org. Chem.*, **1961**, 26, 412.

Chapter Six

Experimental and Characterisation Data

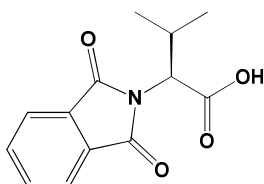
6.1 General Methods and Instrumentation

All manipulations of air and moisture sensitive species were performed under an atmosphere of argon or dinitrogen using standard Schlenk or glove box techniques. Solvents were dried by passing through an alumina drying column incorporated into a MBraun SPS800 solvent purification system, except in the case of tetrahydrofuran (THF), which was dried over potassium and distilled under argon. All solvents were degassed and stored under argon in Teflon valve ampoules. Chloroform-d was passed through a column of basic alumina before being stored over 4 Å molecular sieves prior to use. Dichloromethane-d₂ was dried over CaH₂, and benzene-d₆, toluene-d₈ and THF-d₈ were dried over potassium under an argon atmosphere before being vacuum transferred, freeze pump thaw degassed and stored in a glove box. All other reagents were purchased from commercial suppliers and used as received unless otherwise stated.

Air sensitive samples for NMR spectroscopy were prepared in a glovebox under a dinitrogen atmosphere using 5 mm Nolan NMR tubes equipped with J. Young Teflon valves. All other samples were prepared in Wilmad 5 mm NMR tubes. NMR spectra were recorded on Bruker Avance DPX 250, 400, 500, or Jeol Eclipse 300 spectrometers. NMR spectra are quoted in ppm and were referenced internally relative to the residual protio-solvent (¹H) or solvent (¹³C) resonances, or externally to CCl₄ (¹³C) or CFCl₃ (¹⁹F); all coupling constants are quoted in Hertz. In all cases, NMR assignments were confirmed by the use of two-dimensional ¹H-¹H or ¹H-¹³C correlation experiments (COSY, HSQC and HMBC). Mass spectra were recorded on a Waters LCT Premier XE or Waters GCT Premier mass spectrometer by the Mass Spectrometry Service at the School of Chemistry, Cardiff University or by the EPSRC National Mass Spectrometry Service Centre, Swansea. Infrared spectra were prepared as liquid films on NaCl plates, or as KBr pellets and were recorded on a Jasco 660-Plus FT/IR spectrometer. Infrared data are quoted in wavenumbers (cm⁻¹).

6.2 Experimental and Characterisation Data for Chapter Two

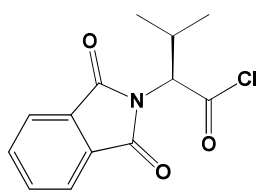
6.2.1 Preparation of N-phthaloyl valine [2.5]



To a solution of L-valine (100 g 854 mmol) in toluene (1.5 l), phthalic anhydride (139.07 g, 939 mmol) and triethylamine (119.2 ml 854 mmol) were added. The mixture was heated to reflux for 18 hours before being allowed to cool to room temperature. The product was washed using HCl (2 M, 2 × 500 ml) and further washed with a brine solution (2 × 250 ml). The aqueous fractions were combined and further washed with toluene (250 ml) before being reduced in volume under reduced pressure to realise a white crystalline solid (75% yield).

^1H NMR data (CDCl_3 , 400.1 MHz, 293 K): $\delta_{\text{H}} = 7.87$ (2 H, m, PhtH), 7.74 (2 H, m, PhtH), 4.63 (1 H, d, $^3J_{\text{HH}} = 8.4$ Hz, PhtCH), 2.75 (1 H, m, CH(CH $_3$) $_2$), 1.16 (3 H, d, $^3J_{\text{HH}} = 6.7$ Hz, CH(CH $_3$) $_2$), 0.91 (3 H, d, $^3J_{\text{HH}} = 6.7$ Hz, CH(CH $_3$) $_2$) ppm. All data corresponds to that reported by Haufe *et al.*¹

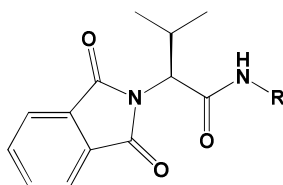
6.2.2 Preparation of N-phthaloylvalinoylchloride [1]



To a solution of N-phthaloylvaline **2.5** (85 g, 344 mmol) in dry THF (500 ml), SOCl_2 (23.35 ml, 361.2 mmol) was added drop wise under a flow of argon. The solution was heated to reflux for 4 hours before allowing to cool to room temperature, and drying the solid *in vacuo*, yielding a pale yellow solid. The reaction gave near quantitative yields and the N-phthaloylvalinoylchloride was used without further purification.

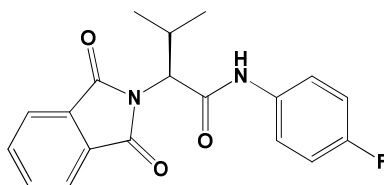
^1H NMR data (CDCl_3 , 400.1 MHz, 293 K) $\delta_{\text{H}} = 7.90$ (2 H, m, PhtH), 7.80 (2 H, m, PhtH), 4.74 (1 H, d, $^3J_{\text{HH}} = 8.4$ Hz, PhtCH), 2.74 (1 H, m, CH(CH_3)₂), 1.15 (3 H, d, $^3J_{\text{HH}} = 6.7$ Hz, (CH₃)₂CH), 0.91 (3 H, d, $^3J_{\text{HH}} = 6.7$ Hz, (CH₃)₂CH) ppm.

6.2.3 Preparation of N-phthaloyl protected amino amides [2a-j]



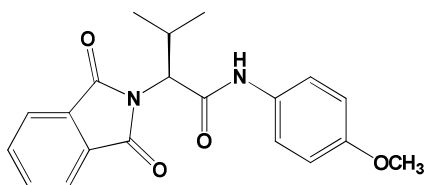
Protected valinoylchloride (**1**) (15 g, 56.4 mmol) was dissolved in dry THF (300 ml) and a solution of the desired amine (55.3 mmol) and triethylamine (8.67 ml, 62.1 mmol) added sequentially to the solution of protected valinoylchloride under a flow of argon. *N,N*-dimethylaminopyridine (DMAP) can be added in catalytic amounts at this stage to give higher yields. The solution was allowed to stir at room temperature for 18 hours before being reduced in volume under reduced pressure. The product was dissolved in NaOH (10% solution, 75 ml) and extracted into dichloromethane (3×100 ml) before being dried over Na_2SO_4 . After drying the solid *in vacuo*, the protected amide was obtained in a 50-90% yield compound depending.

6.2.3.1 [2a]



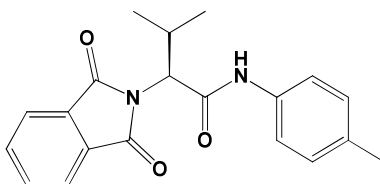
^1H NMR data (CDCl_3 , 400.1 MHz, 293 K): $\delta_{\text{H}} = 7.90$ (2 H, m, PhtH), 7.78 (2 H, m, PhtH), 7.53 (2 H, dd, $^3J_{\text{HH}} = 9.1$ Hz, ArH), 7.00 (2 H, app. t, $^3J_{\text{HH}} = 8.6$ Hz, ArH), 4.52 (1 H, d, $^3J_{\text{HH}} = 11.6$ Hz, PhtCH), 2.90 (1 H, m, CH(CH_3)₂), 1.16 (3 H, d, $^3J_{\text{HH}} = 6.6$ Hz, CH(CH_3)₂), 0.89 (3 H, d, $^3J_{\text{HH}} = 6.6$ Hz, CH(CH_3)₂) ppm.

6.2.3.2 [2b]



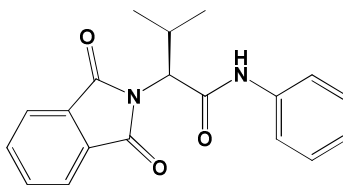
^1H NMR data (CDCl_3 , 250.1 MHz, 293 K): $\delta_{\text{H}} = 7.87$ (2 H, m, PhtH), 7.76 (2 H, m, PhtH), 7.46 (2 H, d, $^3J_{\text{HH}} = 9.0$ Hz, ArH), 6.83 (2 H, d, $^3J_{\text{HH}} = 9.0$ Hz, ArH), 4.50 (1 H, d, $^3J_{\text{HH}} = 11.6$ Hz, PhtCH), 3.76 (3 H, s, 4- $\text{C}_6\text{H}_5\text{OCH}_3$), 2.91 (1 H, m, CH(CH $_3$) $_2$), 1.16 (3 H, d, $^3J_{\text{HH}} = 6.5$ Hz, CH(CH $_3$) $_2$), 0.89 (3 H, d, $^3J_{\text{HH}} = 6.5$ Hz, CH(CH $_3$) $_2$) ppm.

6.2.3.3 [2c]



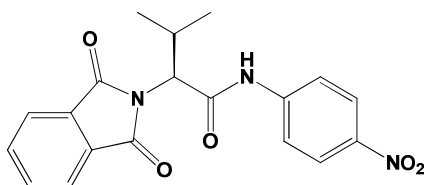
^1H NMR data (CDCl_3 , 400.1 MHz, 293 K): $\delta_{\text{H}} = 7.89$ (2 H, m, PhtH), 7.77 (2 H, m, PhtH), 7.44 (2 H, d, $^3J_{\text{HH}} = 8.3$ Hz, ArH), 7.10 (2 H, d, $^3J_{\text{HH}} = 8.3$ Hz, ArH), 4.51 (1 H, d, $^3J_{\text{HH}} = 11.6$ Hz, PhtCH), 2.91 (1 H, m, CH(CH $_3$) $_2$), 2.29 (3 H, s, 4- $\text{C}_6\text{H}_4\text{CH}_3$), 1.16 (3 H, d, $^3J_{\text{HH}} = 6.5$ Hz, CH(CH $_3$) $_2$), 0.89 (3 H, d, $^3J_{\text{HH}} = 6.5$ Hz, CH(CH $_3$) $_2$) ppm.

6.2.3.4 [2d]



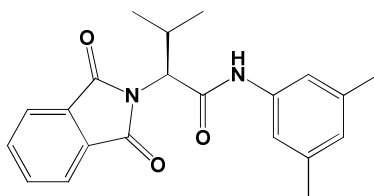
^1H NMR data (CDCl_3 , 400.1 MHz, 293 K): $\delta_{\text{H}} = 7.89$ (2 H, m, PhtH), 7.73 (2 H, m, PhtH), 7.56 (2 H, d, $^3J_{\text{HH}} = 8.5$ Hz, ArH), 7.30 (2 H, app. t, $^3J_{\text{HH}} = 7.5$ Hz, ArH), 7.09 (1 H, app. t, $^3J_{\text{HH}} = 7.5$ Hz, ArH), 4.52 (1 H, d, $^3J_{\text{HH}} = 11.6$ Hz, PhtCH), 2.93 (1 H, m, CH(CH $_3$) $_2$), 1.17 (3 H, d, $^3J_{\text{HH}} = 6.5$ Hz, CH(CH $_3$) $_2$), 0.90 (3 H, d, $^3J_{\text{HH}} = 6.5$ Hz, CH(CH $_3$) $_2$) ppm.

6.2.3.5 [2e]



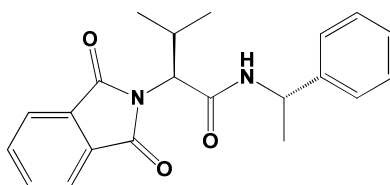
^1H NMR data (CDCl_3 , 400.1 MHz, 293 K): $\delta_{\text{H}} = 8.20$ (2 H, m, PhtH), 7.92 (2 H, m, PhtH), 7.75 (2 H, d, $^3J_{\text{HH}} = 9.1$ Hz, ArH), 4.57 (1 H, d, $^3J_{\text{HH}} = 11.6$ Hz, PhtCH), 2.89 (1 H, m, CH(CH $_3$) $_2$), 1.16 (3 H, d, $^3J_{\text{HH}} = 6.5$ Hz, CH(CH $_3$) $_2$), 0.91 (3 H, d, $^3J_{\text{HH}} = 6.5$ Hz, CH(CH $_3$) $_2$) ppm.

6.2.3.6 [2f]



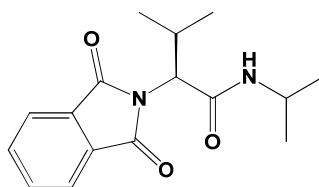
^1H NMR data (CDCl_3 , 250.1 MHz, 293 K): $\delta_{\text{H}} = 7.86$ (2 H, m, PhtH), 7.76 (2 H, m, PhtH), 7.20 (2 H, s, *o*-C $_6$ H $_3$ (CH $_3$) $_2$), 6.73 (1 H, *p*-C $_6$ H $_3$ (CH $_3$) $_2$), 4.51 (1 H, d, $^3J_{\text{HH}} = 11.5$ Hz, PhtCH), 2.93 (1 H, m, CH(CH $_3$) $_2$), 2.28 (6 H, s, 3,5-C $_6$ H $_3$ (CH $_3$) $_2$), 1.16 (3 H, d, $^3J_{\text{HH}} = 6.5$ Hz, CH(CH $_3$) $_2$), 0.89 (3 H, d, $^3J_{\text{HH}} = 6.5$ Hz, CH(CH $_3$) $_2$) ppm.

6.2.3.7 [2g]



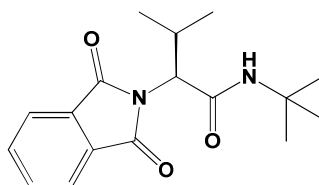
^1H NMR data (CDCl_3 , 250.1 MHz, 293 K): $\delta_{\text{H}} = 7.88\text{--}7.82$ (2 H, m, PhtH), 7.72–7.70 (2 H, m, PhtH), 7.40–7.32 (2 H, m, ArH), 7.30–7.24 (3 H, m, ArH), 5.10 (1 H, app. quin., $^3J_{\text{HH}} = 7.2$ Hz, HNCH(CH_3)(C_6H_5), 4.41 (1 H, d, $^3J_{\text{HH}} = 11.3$ Hz, PhtCH), 2.87 (1 H, m, CH(CH_3) $_2$), 1.50 (3 H, d, $^3J_{\text{HH}} = 6.9$ Hz, HNCH(CH $_3$)(C_6H_5), 1.17 (3 H, d, $^3J_{\text{HH}} = 6.6$ Hz, CH(CH $_3$) $_2$), 0.86 (3 H, d, $^3J_{\text{HH}} = 6.6$ Hz, CH(CH $_3$) $_2$) ppm.

6.2.3.8 [2h]



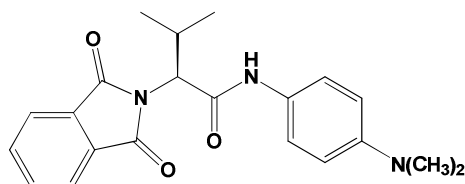
^1H NMR data (CDCl_3 , 400.1 MHz, 293 K): $\delta_{\text{H}} = 7.80$ (2 H, m, PhtH), 7.69 (2 H, m, PhtH), 4.29 (1 H, d, $^3J_{\text{HH}} = 11.4$ Hz, PhtCH), 3.97 (1 H, app. sept., $^3J_{\text{HH}} = 6.7$ Hz, CH(CH_3) $_2$), 2.73 (1 H, m, CH(CH_3) $_2$), 1.17 (3 H, d, $^3J_{\text{HH}} = 6.6$ Hz, CH(CH $_3$) $_2$), 1.09 (3 H, d, $^3J_{\text{HH}} = 6.7$ Hz, CH(CH $_3$) $_2$), 1.02 (3 H, d, $^3J_{\text{HH}} = 6.7$ Hz, CH(CH $_3$) $_2$), 0.77 (3 H, d, $^3J_{\text{HH}} = 6.6$ Hz, CH(CH $_3$) $_2$) ppm.

6.2.3.9 [2i]



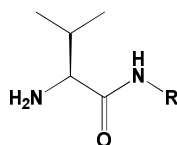
^1H NMR data (CDCl_3 , 400.1 MHz, 293 K): $\delta_{\text{H}} = 7.81$ (2 H, m, PhtH), 7.69 (2 H, m, PhtH), 4.19 (1 H, d, $^3J_{\text{HH}} = 11.4$ Hz, PhtCH), 2.70 (1 H, m, $\text{CH}(\text{CH}_3)_2$), 1.27 (9 H, s, $\text{C}(\text{CH}_3)_3$), 1.03 (3 H, d, $^3J_{\text{HH}} = 6.6$ Hz, $\text{CH}(\text{CH}_3)_2$), 0.76 (3 H, d, $^3J_{\text{HH}} = 6.6$ Hz, $\text{CH}(\text{CH}_3)_2$) ppm.

6.2.3.10 [2j]



^1H NMR data (CDCl_3 , 400.1 MHz, 293 K): $\delta_{\text{H}} = 7.87$ (2 H, m, PhtH), 7.75 (2 H, m, PhtH), 7.41 (2 H, d, $^3J_{\text{HH}} = 9.0$ Hz, ArH), 6.67 (2 H, d, $^3J_{\text{HH}} = 9.0$ Hz, ArH), 4.49 (1 H, d, $^3J_{\text{HH}} = 11.5$ Hz, PhtCH), 2.93 (1 H, m, $\text{CH}(\text{CH}_3)_2$), 2.89 (6 H, s, $p\text{-C}_6\text{H}_4\text{N}(\text{CH}_3)_2$), 1.16 (3 H, d, $^3J_{\text{HH}} = 6.6$ Hz, $\text{CH}(\text{CH}_3)_2$), 0.89 (3 H, d, $^3J_{\text{HH}} = 6.6$ Hz, $\text{CH}(\text{CH}_3)_2$) ppm.

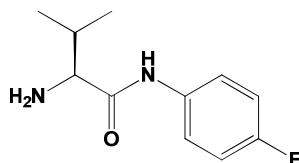
6.2.4 Preparation of deprotected N-phthaloyl protected amino amides [3a-j]



The protected N-phthaloyl amino amide **2a-j** (36.6 mmol) was dissolved in ethanol (250 ml) and to it, hydrazine monohydrate (9.60 ml, 51.2mmol) was added. The reaction was allowed to stir at room temperature for 18 hours before concentrated HCl (37%, 50 ml) was added and the solution allowed to stir vigorously for 1 hour. After such time the solution was reduced in volume under reduced pressure and dissolved in distilled water (50 ml). The solution was then made to a neutral pH using NaOH (10%) and washed with dichloromethane (3×50 ml). Deprotected amides soluble in dichloromethane were dried

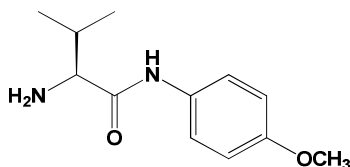
over Na_2SO_4 and the solid dried *in vacuo*. Water soluble deprotected amides were reduced in volume and re-dissolved in THF, filtered to remove insoluble impurities and again dried under reduced pressure. The products were typically obtained as white or light orange solids in 60-94% yield.

6.2.4.1 [3a]



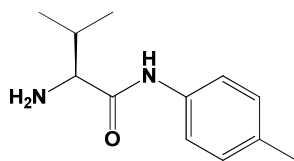
^1H NMR data (D_2O , 400.1 MHz, 293 K): $\delta_{\text{H}} = 6.97$ (2 H, m, ArH), 6.87 (2 H, m, ArH), 3.81 (1 H, d, $^3J_{\text{HH}} = 2.2$ Hz, H_2NCH), 2.09 (1 H, m, $\text{CH}(\text{CH}_3)_2$), 1.09 (3 H, d, $^3J_{\text{HH}} = 6.9$ Hz, $\text{CH}(\text{CH}_3)_2$) ppm.

6.2.4.2 [3b]



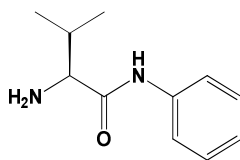
^1H NMR data (CDCl_3 , 400.1 MHz, 293 K): $\delta_{\text{H}} = 7.50$ (2 H, d, $^3J_{\text{HH}} = 8.8$ Hz, ArH), 6.86 (2 H, d, $^3J_{\text{HH}} = 8.8$ Hz, ArH), 3.78 (3 H, s, $4\text{-C}_6\text{H}_5\text{OCH}_3$), 3.38 (1 H, d, $^3J_{\text{HH}} = 3.4$ Hz, H_2NCH), 2.44 (1 H, m, $\text{CH}(\text{CH}_3)_2$), 1.04 (3 H, d, $^3J_{\text{HH}} = 6.9$ Hz, $\text{CH}(\text{CH}_3)_2$), 0.87 (3 H, d, $^3J_{\text{HH}} = 6.9$ Hz, $\text{CH}(\text{CH}_3)_2$) ppm.

6.2.4.3 [3c]



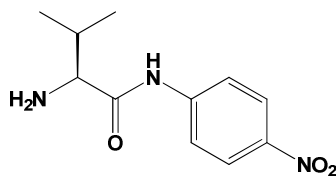
^1H NMR data (D_2O , 400.1 MHz, 293 K): $\delta_{\text{H}} = 7.37$ (2 H, d, $^3J_{\text{HH}} = 8.0$ Hz, ArH), 7.29 (2 H, d, $^3J_{\text{HH}} = 8.0$ Hz, ArH), 3.97 (1 H, d, $^3J_{\text{HH}} = 6.2$ Hz, H_2NCH), 2.35 (1 H, m, $\text{CH}(\text{CH}_3)_2$), 2.34 (3 H, s, 4- $\text{C}_6\text{H}_4\text{CH}_3$), 1.12 (6 H, d, $^3J_{\text{HH}} = 6.9$ Hz, $\text{CH}(\text{CH}_3)_2$) ppm.

6.2.4.4 [3d]



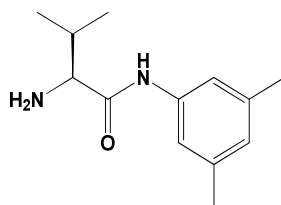
^1H NMR data (CDCl_3 , 400.1 MHz, 293 K): $\delta_{\text{H}} = 7.59$ (2 H, app. d, $^3J_{\text{HH}} = 8.6$ Hz, ArH), 7.30 (2 H, app. t, $^3J_{\text{HH}} = 7.5$ Hz, ArH), 7.08 (1 H, app. t, $^3J_{\text{HH}} = 7.5$ Hz, ArH), 5.27 (1 H, app. s, H_2NCH), 2.40 (1 H, m, $\text{CH}(\text{CH}_3)_2$), 1.02 (3 H, d, $^3J_{\text{HH}} = 6.9$ Hz, $\text{CH}(\text{CH}_3)_2$), 0.86 (3 H, d, $^3J_{\text{HH}} = 6.9$ Hz, $\text{CH}(\text{CH}_3)_2$) ppm.

6.2.4.5 [3e]



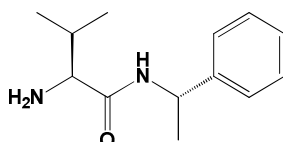
^1H NMR data (D_2O , 400.1 MHz, 293 K): $\delta_{\text{H}} = 8.21$ (2 H, d, $^3J_{\text{HH}} = 9.1$ Hz, ArH), 7.70 (2 H, d, $^3J_{\text{HH}} = 9.1$ Hz, ArH), 4.05 (1 H, d, $^3J_{\text{HH}} = 5.7$ Hz, H_2NCH), 2.34 (1 H, m, $\text{CH}(\text{CH}_3)_2$), 1.12 (3 H, d, $^3J_{\text{HH}} = 6.9$ Hz, $\text{CH}(\text{CH}_3)_2$), 1.09 (3 H, d, $^3J_{\text{HH}} = 6.9$ Hz, $\text{CH}(\text{CH}_3)_2$) ppm.

6.2.4.6 [3f]



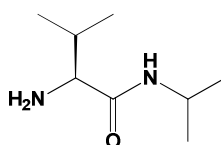
^1H NMR data (D_2O , 400.1 MHz, 293 K): $\delta_{\text{H}} = 7.05$ (2 H, s, $o\text{-C}_6\text{H}_3(\text{CH}_3)_2$), 6.93 (1 H, $p\text{-C}_6\text{H}_3(\text{CH}_3)_2$), 3.87 (1 H, d, $^3J_{\text{HH}} = 6.2$ Hz, H_2NCH), 2.28 (1 H, m, $\text{CH}(\text{CH}_3)_2$), 2.25 (6 H, s, $\text{C}_6\text{H}_3(\text{CH}_3)_2$), 1.05 (6 H, d, $^3J_{\text{HH}} = 6.9$ Hz, $\text{CH}(\text{CH}_3)_2$) ppm.

6.2.4.7 [3g]



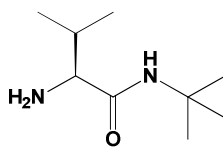
^1H NMR data (CDCl_3 , 400.1 MHz, 293 K): $\delta_{\text{H}} = 7.37\text{-}7.34$ (4 H, m, ArH), 7.30-7.26 (1 H, m, ArH), 5.16 (1 H, m, $\text{HNCH}(\text{CH}_3)(\text{C}_6\text{H}_5)$), 3.22 (1 H, d, $^3J_{\text{HH}} = 3.8$ Hz, H_2NCH), 2.32 (1 H, m, $\text{CH}(\text{CH}_3)_2$), 1.51 (3 H, d, $^3J_{\text{HH}} = 6.9$ Hz, $\text{HNCH}(\text{CH}_3)(\text{C}_6\text{H}_5)$), 1.00 (3 H, d, $^3J_{\text{HH}} = 6.9$ Hz, $\text{CH}(\text{CH}_3)_2$), 0.88 (3 H, d, $^3J_{\text{HH}} = 6.9$ Hz, $\text{CH}(\text{CH}_3)_2$) ppm.

6.2.4.8 [3h]



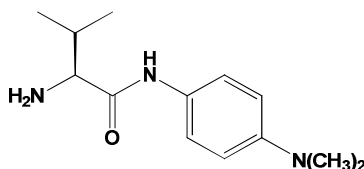
^1H NMR data (CDCl_3 , 400.1 MHz, 293 K): $\delta_{\text{H}} = 4.00$ (1 H, app. sept., $^3J_{\text{HH}} = 6.6$ Hz, $\text{CH}(\text{CH}_3)_2$), 3.12 (1 H, d, $^3J_{\text{HH}} = 4.8$ Hz, H_2NCH), 2.21 (1 H, m, $\text{CH}(\text{CH}_3)_2$), 1.09 (6 H, 2x dd, $^3J_{\text{HH}} = 7.0$ Hz, $\text{CH}(\text{CH}_3)_2$), 0.91 (3 H, d, $^3J_{\text{HH}} = 6.9$ Hz, $\text{CH}(\text{CH}_3)_2$), 0.75 (3 H, d, $^3J_{\text{HH}} = 6.9$ Hz, $\text{CH}(\text{CH}_3)_2$) ppm.

6.2.4.9 [3i]

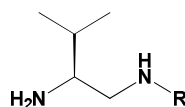


^1H NMR data (CDCl_3 , 400.1 MHz, 293 K): $\delta_{\text{H}} = 3.03$ (1 H, d, $^3J_{\text{HH}} = 3.9$ Hz, $\text{CH}(\text{CH}_3)_2$), 2.20 (1 H, m, $\text{CH}(\text{CH}_3)_2$), 1.28 (9 H, s, $\text{C}(\text{CH}_3)_3$), 0.90 (3 H, d, $^3J_{\text{HH}} = 6.9$ Hz, $\text{CH}(\text{CH}_3)_2$), 0.75 (3 H, d, $^3J_{\text{HH}} = 6.9$ Hz, $\text{CH}(\text{CH}_3)_2$) ppm.

6.2.4.10 [3j]



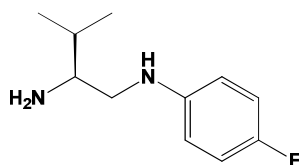
^1H NMR data (CDCl_3 , 400.1 MHz, 293 K): $\delta_{\text{H}} = 7.44$ (2 H, d, $^3J_{\text{HH}} = 8.9$ Hz, ArH), 6.67 (2 H, d, $^3J_{\text{HH}} = 8.9$ Hz, ArH), 3.48 (1 H, d, $^3J_{\text{HH}} = 3.6$ Hz, H_2NCH), 2.87 (6 H, s, $p\text{-C}_6\text{H}_4\text{N}(\text{CH}_3)_2$), 2.36 (1 H, m, $\text{CH}(\text{CH}_3)_2$), 1.00 (3 H, d, $^3J_{\text{HH}} = 6.9$ Hz, $\text{CH}(\text{CH}_3)_2$), 0.87 (3 H, d, $^3J_{\text{HH}} = 6.9$ Hz, $\text{CH}(\text{CH}_3)_2$) ppm.

6.2.5 Preparation of Diamines NN^{R} [4a-j]

To a suspension of NaBH_4 (5.58 g, 147.5 mmol) in THF (250 ml), SiMe_3Cl (23.57 ml, 184.3 mmol) was added and heated to reflux under an inert atmosphere for 2 hours. The reaction was allowed to cool to room temperature and then further cooled to -78 °C before addition of the amino amide **3a-j** (36.7 mmol, *ca.* 7 g), which was pre-dissolved in dry THF. The mixture was then heated to reflux under inert conditions for 4 days. After such time the solution was allowed to cool to room temperature and further cooled to 0 °C. Methanol (10 ml) and water (10 ml) were sequentially added to destroy any excess borane. After the effervescence subsided, the solution was reduced in volume under reduced

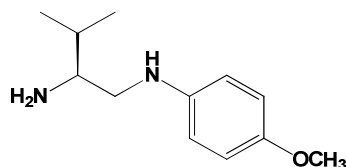
pressure, dissolved in NaOH (10%, 50 ml) and the product extracted with dichloromethane (3×50 ml). The organic layers were combined and dried over Na_2SO_4 before removing the solvent under reduced pressure. The crude diamine was purified using column chromatography over silica gel, typically using ethyl acetate and methanol (5-10% v/v). Once purified the diamines were obtained as orange to dark orange/red oils with typical yields of $>70\%$.² NMR analysis after adding *O*-acetylmandelic acid **2.21** indicated the presence of only a single enantiomer.

6.2.5.1 [4a]



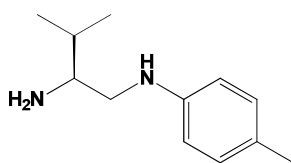
^1H NMR data (CDCl_3 , 500.1 MHz, 293 K): $\delta_{\text{H}} = 6.82$ (2 H, app. t, $^3J_{\text{HH}} = 8.8$ Hz, *m*- $\text{C}_6\text{H}_4\text{F}$), 6.57 (2 H, dd, $^3J_{\text{HH}} = 8.8$ Hz, $^3J_{\text{HF}} = 4.3$ Hz, *o*- $\text{C}_6\text{H}_4\text{F}$), 3.38 (1 H, dd, $^3J_{\text{HH}} = 3.4$ Hz, $^2J_{\text{HH}} = 14.0$ Hz, NCH_2), 3.27 (1 H, dd, $^3J_{\text{HH}} = 3.4$ Hz, $^2J_{\text{HH}} = 14.0$ Hz, NCH_2), 3.03 (1 H, m, H_2NCH), 2.04 (1 H, m, $(\text{CH}_3)_2\text{CH}$), 1.05 (6 H, app. t, $^3J_{\text{HH}} = 6.5$ Hz, $\text{CH}(\text{CH}_3)_2$), ppm. ^{19}F NMR data (CDCl_3 , 282.8 MHz, 293 K): $\delta_{\text{F}} = -128.11$ (s, *p*- $\text{C}_6\text{H}_4\text{F}$) ppm. $^{13}\text{C}\{^1\text{H}\}$ NMR data (CDCl_3 , 125.7 MHz, 293 K): $\delta_{\text{C}} = 156.1$ (d, $^1J_{\text{CF}} = 235.9$ Hz, *p*- $\text{C}_6\text{H}_4\text{F}$), 143.5 (d, $^4J_{\text{CF}} = 1.7$ Hz, *ipso*- $\text{C}_6\text{H}_4\text{F}$), 115.8 (d, $^2J_{\text{CF}} = 22.3$ Hz, *m*- $\text{C}_6\text{H}_4\text{F}$), 113.9 (d, $^3J_{\text{CF}} = 7.3$ Hz, *o*- $\text{C}_6\text{H}_4\text{F}$), 57.6 (H_2NCH), 44.2 (CH_2), 29.2 ($(\text{CH}_3)_2\text{CH}$), 18.8 (CH_3 isopropyl), 18.8 (CH_3 isopropyl) ppm. IR data (NaCl disc, cm^{-1}): 3345 (s), 3252 (m), 2965 (br. s), 2556 (w), 2458 (w), 1652 (w), 1609 (w), 1575 (m), 1529 (s), 1507 (s), 1470 (s), 1381 (w), 1321 (m), 1261 (s), 1216 (s), 1156 (w), 1135 (w), 1104 (s), 1086 (w), 1014 (w), 916 (w), 872 (w), 821 (s), 799 (m), 754 (w), 706 (w), 692 (w). Accurate mass ES-MS for $[\text{HNN}^{\text{ArF}}+\text{H}]^+$: $m/z = 196.1372$ (calc. for $\text{C}_{11}\text{H}_{17}\text{N}_2\text{F}$: 196.1376).

6.2.5.2 [4b]



^1H NMR data (CDCl_3 , 500.1 MHz, 293 K): $\delta_{\text{H}} = 6.77$ (2 H, d, $^3J_{\text{HH}} = 8.9$ Hz, *o*- $\text{C}_6\text{H}_4\text{OCH}_3$), 6.60 (2 H, d, $^3J_{\text{HH}} = 8.9$ Hz, *m*- $\text{C}_6\text{H}_4\text{OCH}_3$), 3.70 (3 H, s, $\text{C}_6\text{H}_4\text{OCH}_3$), 3.18 (1 H, dd, $^3J_{\text{HH}} = 3.4$ Hz, $^2J_{\text{HH}} = 11.6$ Hz, NCH_2), 2.78 (1 H, dd, $^3J_{\text{HH}} = 3.4$ Hz, $^2J_{\text{HH}} = 11.6$ Hz, NCH_2), 2.71 (1 H, m, H_2NCH), 1.66 (1 H, m, $(\text{CH}_3)_2\text{CH}$), 0.95 (6 H, dd, $^3J_{\text{HH}} = 9.8$ Hz, $^3J_{\text{HH}} = 6.8$ Hz, $\text{CH}(\text{CH}_3)_2$), ppm. $^{13}\text{C}\{^1\text{H}\}$ NMR data (CDCl_3 , 125.7 MHz, 293 K): $\delta_{\text{C}} = 152.0$ (*p*- $\text{C}_6\text{H}_4\text{OCH}_3$), 143.0 (*ipso*- $\text{C}_6\text{H}_4\text{OCH}_3$), 114.8 (*o*- $\text{C}_6\text{H}_4\text{OCH}_3$), 114.2 (*m*- $\text{C}_6\text{H}_4\text{OCH}_3$), 55.7 (OCH_3), 56.1 (H_2NCH), 49.2 (CH_2), 32.4 ($(\text{CH}_3)_2\text{CH}$), 19.3 (CH_3 isopropyl), 17.7 (CH_3 isopropyl) ppm. IR data (NaCl disc, cm^{-1}): 3364 (br. m), 3028 (w), 2956 (s), 2904 (s), 2871 (s), 2830 (s), 2066 (w), 1844 (w), 1618 (m), 1588 (m), 1518 (br. s), 1465 (s), 1442 (m), 1408 (w), 1386 (w), 1367 (w), 1295 (br. w), 1234 (br. s), 1179 (m), 1109 (w), 1076 (w), 1038 (s), 1003 (w), 910 (w), 820 (s), 747 (w), 722 (w), 424 (s), 404 (s). Accurate mass ES-MS for $[\text{HNN}^{\text{ArOMe}} + \text{H}]^+$: $m/z = 209.1652$ (calc. for $\text{C}_{12}\text{H}_{21}\text{N}_2\text{O}$: 209.1654).

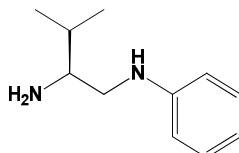
6.2.5.3 [4c]



^1H NMR data (CDCl_3 , 500.1 MHz, 293 K): $\delta_{\text{H}} = 7.00$ (2 H, d, $^3J_{\text{HH}} = 8.2$ Hz, *o*- $\text{C}_6\text{H}_4\text{CH}_3$), 6.58 (2 H, d, $^3J_{\text{HH}} = 8.2$ Hz, *m*- $\text{C}_6\text{H}_4\text{CH}_3$), 3.23 (1 H, dd, $^3J_{\text{HH}} = 3.4$ Hz, $^2J_{\text{HH}} = 12.0$ Hz, NCH_2), 2.84 (1 H, dd, $^3J_{\text{HH}} = 3.4$ Hz, $^2J_{\text{HH}} = 12.0$ Hz, NCH_2), 2.75 (1 H, m, H_2NCH), 2.25 (3 H, s, $\text{C}_6\text{H}_4\text{CH}_3$), 1.69 (1 H, m, $(\text{CH}_3)_2\text{CH}$), 0.97 (6 H, dd, $^3J_{\text{HH}} = 9.4$ Hz, $^3J_{\text{HH}} = 6.8$ Hz, $\text{CH}(\text{CH}_3)_2$), ppm. $^{13}\text{C}\{^1\text{H}\}$ NMR data (CDCl_3 , 125.7 MHz, 293 K): $\delta_{\text{C}} = 146.3$ (*ipso*- $\text{C}_6\text{H}_4\text{CH}_3$), 129.6 (*o*- $\text{C}_6\text{H}_4\text{CH}_3$), 126.4 (*p*- $\text{C}_6\text{H}_4\text{CH}_3$), 113.1 (*m*- $\text{C}_6\text{H}_4\text{CH}_3$), 56.1 (H_2NCH), 48.2 (CH_2), 32.3 ($(\text{CH}_3)_2\text{CH}$), 20.3 ($\text{C}_6\text{H}_4\text{CH}_3$), 19.2 (CH_3 isopropyl), 17.8 (CH_3 isopropyl) ppm. IR data (NaCl disc, cm^{-1}): 3365 (br. m), 3029 (w), 2956 (s), 2905 (s),

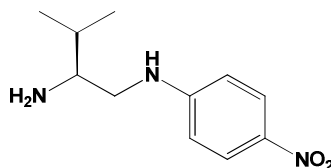
2871 (s), 2831 (s), 2065 (w), 1844 (w), 1733 (w), 1618 (m), 1588 (m), 1511 (s), 1464 (s), 1408 (m), 1386 (m), 1376 (m), 1296 (m), 1234 (s), 1179 (m), 1109 (w), 1076 (w), 1038 (s), 911 (w), 820 (s), 731 (w), 436 (br. s). Accurate mass ES-MS for $[\text{HNN}^{\text{ArMe}}+\text{H}]^+$: $m/z = 193.1697$ (calc. for $\text{C}_{12}\text{H}_{21}\text{N}_2$: 193.1705).

6.2.5.4 [4d]



^1H NMR data (CDCl_3 , 500.1 MHz, 293 K): $\delta_{\text{H}} = 7.18$ (2 H, app. t, $^3J_{\text{HH}} = 7.4$ Hz, $m\text{-C}_6\text{H}_5$), 6.70 (1 H, app. t, $^3J_{\text{HH}} = 7.4$ Hz, $p\text{-C}_6\text{H}_5$), 6.65 (2 H, d, $^3J_{\text{HH}} = 7.7$ Hz, $o\text{-C}_6\text{H}_5$), 3.25 (1 H, dd, $^3J_{\text{HH}} = 3.2$ Hz, $^2J_{\text{HH}} = 11.9$ Hz, NCH_2), 2.85 (1 H, app. t, $^2J_{\text{HH}} = 11.9$ Hz, NCH_2), 2.76 (1 H, m, H_2NCH), 1.69 (1 H, m, $(\text{CH}_3)_2\text{CH}$), 0.98 (3 H, d, $^3J_{\text{HH}} = 9.6$ Hz, $\text{CH}(\text{CH}_3)_2$), 0.96 (6 H, d, $^3J_{\text{HH}} = 9.6$ Hz, $\text{CH}(\text{CH}_3)_2$) ppm. $^{13}\text{C}\{^1\text{H}\}$ NMR data (CDCl_3 , 125.7 MHz, 293 K): $\delta_{\text{C}} = 148.6$ (*ipso*- C_6H_5), 129.1 ($m\text{-C}_6\text{H}_5$), 117.2 ($p\text{-C}_6\text{H}_5$), 112.9 ($o\text{-C}_6\text{H}_5$), 56.0 (H_2NCH), 47.9 (CH_2), 32.4 ($(\text{CH}_3)_2\text{CH}$), 19.2 (CH_3 isopropyl), 17.8 (CH_3 isopropyl) ppm. IR data (NaCl disc, cm^{-1}): 3370 (br. m), 3050 (m), 3021 (m), 2958 (s), 2871 (s), 2602 (w), 1918 (w), 1734 (m), 1675 (m), 1603 (s), 1506 (s), 1466 (m), 1442 (w), 1431 (w), 1387 (w), 1368 (w), 1321 (m), 1251 (m), 1179 (m), 1153 (w), 1068 (w), 1046 (w), 1028 (w), 991 (w), 868 (m), 749 (s), 692 (s), 408 (br. s). Accurate mass ES-MS for $[\text{HNN}^{\text{Ar}}+\text{H}]^+$: $m/z = 178.1465$ (calc. for $\text{C}_{11}\text{H}_{18}\text{N}_2$: 178.1470). All data corresponds to that reported in-part by Mauduit *et al.* and Russell *et al.*^{3,4}

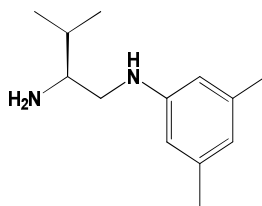
6.2.5.5 [4e]



^1H NMR data (CDCl_3 , 500.1 MHz, 293 K): $\delta_{\text{H}} = 8.04$ (2 H, d, $^3J_{\text{HH}} = 9.2$ Hz, $m\text{-C}_6\text{H}_4\text{NO}_2$), 6.50 (2 H, d, $^3J_{\text{HH}} = 9.2$ Hz, $o\text{-C}_6\text{H}_4\text{NO}_2$), 3.28 (1 H, app. ddd, $^2J_{\text{HH}} = 12.1$ Hz, $^3J_{\text{HH}} =$

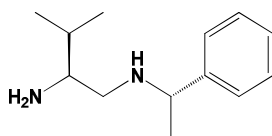
9.5 Hz, $^3J_{\text{HH}} = 3.8$ Hz, H_2NCH), 2.88 (1 H, app. ddd, $^2J_{\text{HH}} = 12.1$ Hz, $^3J_{\text{HH}} = 6.4$ Hz, $^3J_{\text{HH}} = 3.8$ Hz, H_2NCH), 2.72 (1 H, m, H_2NCH), 1.66 (1 H, m, $\text{CH}(\text{CH}_3)_2$), 0.96 (6 H, dd, $^3J_{\text{HH}} = 6.8$ Hz, $^3J_{\text{HH}} = 6.8$ Hz, $\text{CH}(\text{CH}_3)_2$) ppm. $^{13}\text{C}\{^1\text{H}\}$ NMR data (CDCl_3 , 125.7 MHz, 293 K): $\delta_{\text{C}} = 153.6$ (*p*- $\text{C}_6\text{H}_4\text{NO}_2$), 137.6 (*ipso*- $\text{C}_6\text{H}_4\text{NO}_2$), 126.0 (*m*- $\text{C}_6\text{H}_4\text{NO}_2$), 111.0 (*o*- $\text{C}_6\text{H}_4\text{NO}_2$), 55.9 (H_2NCH), 46.6 (CH_2), 32.7 ($(\text{CH}_3)_2\text{CH}$), 19.1 (CH_3 isopropyl), 17.7 (CH_3 isopropyl) ppm. IR data (NaCl disc, cm^{-1}): 3368 (s), 3300 (s), 3230 (s), 3179 (s), 3125 (m), 3041 (m), 2955 (s), 2925 (m), 2905 (m), 2868 (m), 2403 (br. w), 2221 (w), 1920 (w), 1769 (m), 1601 (s), 1562 (m), 1504 (m), 1468 (s), 1376 (m), 1367 (m), 1306 (br. s), 1182 (s), 1159 (m), 1131 (w), 1113 (s), 1035 (w), 1012 (m), 997 (m), 964 (w), 928 (w), 887 (m), 827 (s), 796 (w), 784 (w), 754 (s), 695 (m), 655 (m), 629 (w), 599 (w), 577 (w), 534 (m), 489 (s), 423 (m). Accurate mass ES-MS for $[\text{HNN}^{\text{ArNO}_2} + \text{H}]^+$: $m/z = 224.1389$ (calc. for $\text{C}_{11}\text{H}_{18}\text{N}_3\text{O}_2$: 224.1399).

6.2.5.6 [4f]



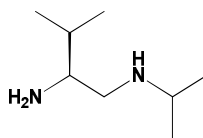
^1H NMR data (CDCl_3 , 400.1 MHz, 293 K): $\delta_{\text{H}} = 6.40$ (1 H, *p*- $\text{C}_6\text{H}_3(\text{CH}_3)_2$), 6.31 (2 H, s, *o*- $\text{C}_6\text{H}_3(\text{CH}_3)_2$), 3.25 (1 H, dd, $^2J_{\text{HH}} = 12.0$, $^3J_{\text{HH}} = 3.6$ Hz, NCH_2), 2.85 (1 H, dd, $^2J_{\text{HH}} = 12.0$, $^3J_{\text{HH}} = 9.2$ Hz, NCH_2), 2.76 (1 H, m, H_2NCH), 2.28 (6 H, s, $\text{C}_6\text{H}_3(\text{CH}_3)_2$), 1.70 (1 H, m, $\text{CH}(\text{CH}_3)_2$), 1.01 (3 H, d, $^3J_{\text{HH}} = 6.8$ Hz, $\text{CH}(\text{CH}_3)_2$), 0.99 (3 H, d, $^3J_{\text{HH}} = 6.8$ Hz, $\text{CH}(\text{CH}_3)_2$) ppm. $^{13}\text{C}\{^1\text{H}\}$ NMR data (CDCl_3 , 125.7 MHz, 293 K): $\delta_{\text{C}} = 148.7$ (*ipso*- $\text{C}_6\text{H}_3(\text{CH}_3)_2$), 138.6 (*m*- $\text{C}_6\text{H}_3(\text{CH}_3)_2$), 119.1 (*p*- $\text{C}_6\text{H}_3(\text{CH}_3)_2$), 110.8 (*o*- $\text{C}_6\text{H}_3(\text{CH}_3)_2$), 56.0 (H_2NCH), 48.0 (CH_2), 32.3 ($(\text{CH}_3)_2\text{CH}$), 21.3 ($\text{C}_6\text{H}_3(\text{CH}_3)_2$), 19.2 (CH_3 isopropyl), 17.6 (CH_3 isopropyl) ppm. IR data (NaCl disc, cm^{-1}): 3375 (br. m), 3020 (m), 2958 (br. s), 2729 (w), 1736 (m), 1602 (s), 1507 (s), 1468 (s), 1367 (m), 1338 (m), 1303 (w), 1243 (w), 1190 (s), 1097 (w), 1034 (w), 990 (w), 952 (w), 852 (m), 820 (s), 691 (s), 436 (br. s). Accurate mass ES-MS for $[\text{HNN}^{\text{Ar}3,5\text{Me}} + \text{H}]^+$: $m/z = 207.1862$ (calc. for $\text{C}_{13}\text{H}_{23}\text{N}_2$: 207.1861).

6.2.5.7 [4g]



^1H NMR data (CDCl_3 , 500.1 MHz, 293 K): $\delta_{\text{H}} = 7.28\text{--}7.22$ (4 H, m, ArH), 7.15 (1 H, m, ArH), 3.67 (1 H, q, $^3J_{\text{HH}} = 6.5$ Hz, $\text{HNCH}(\underline{\text{C}}\text{H}_3)(\text{C}_6\text{H}_5)$), 2.47 (1 H, t, $^3J_{\text{HH}} = 3.7$ Hz, NCH_2), 2.45–2.42 (1 H, m, H_2NCH), 2.25 (1 H, dd, $^3J_{\text{HH}} = 12.6$ Hz, $^4J_{\text{HH}} = 2.5$ Hz, NCH_2), 1.49 (1 H, m, $\underline{\text{C}}\text{H}(\text{CH}_3)_2$), (3 H, d, $^3J_{\text{HH}} = 6.6$ Hz, $\text{HNCH}(\underline{\text{C}}\text{H}_3)(\text{C}_6\text{H}_5)$), 0.80 (3 H, d, $^3J_{\text{HH}} = 6.8$ Hz, $\text{CH}(\underline{\text{C}}\text{H}_3)_2$), 0.76 (3 H, d, $^3J_{\text{HH}} = 6.8$ Hz, $\text{CH}(\underline{\text{C}}\text{H}_3)_2$) ppm. $^{13}\text{C}\{^1\text{H}\}$ NMR data (CDCl_3 , 125.7 MHz, 293 K): $\delta_{\text{C}} = 127.9$ ($m\text{-C}_6\text{H}_5$), 126.3 ($o\text{-C}_6\text{H}_5$), 126.2 ($p\text{-C}_6\text{H}_5$), 58.5 ($\text{HNCH}(\underline{\text{C}}\text{H}_3)(\text{C}_6\text{H}_5)$), 56.6 (H_2NCH), 52.0 (NCH_2), 31.8 ($\underline{\text{C}}\text{H}(\text{CH}_3)_2$), 24.1 ($\text{HNCH}(\underline{\text{C}}\text{H}_3)(\text{C}_6\text{H}_5)$), 19.1 ($\underline{\text{C}}\text{H}_3$ isopropyl), 17.1 ($\underline{\text{C}}\text{H}_3$ isopropyl) ppm. IR data (KBr disc, cm^{-1}): 3393 (m), 3313 (m), 3077 (w), 3058 (w), 3027 (m), 2961 (br. m), 2689 (br. m), 2588 (br. m), 2203 (br. m) 1958 (w), 1885 (w), 1821 (w), 1726 (w), 1633 (m), 1603 (m), 1556 (s), 1469 (m), 1449 (m), 1365 (br. m), 1301 (m), 1265 (w), 1231 (w), 1211 (w), 1157 (m), 1131 (m), 1063 (w), 1040 (w), 1029 (w), 943 (w), 916 (w), 815 (m), 765 (s), 738 (m), 701 (s), 577 (m) 543 (m), 520 (w), 466 (w), 423 (w). Accurate mass ES-MS for $[\text{HNN}^{\text{ArMeH}} + \text{H}]^+$: $m/z = 207.1859$ (calc. for $\text{C}_{12}\text{H}_{23}\text{N}_2$: 207.1861).

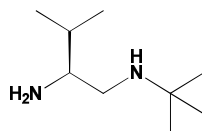
6.2.5.8 [4h]



^1H NMR data (CDCl_3 , 500.1 MHz, 293 K): $\delta_{\text{H}} = 2.67$ (1 H, m, $\text{HN}(\underline{\text{C}}\text{H}(\text{CH}_3)_2)$), 2.60 (1 H, dd, $^3J_{\text{HH}} = 3.2$ Hz, $^2J_{\text{HH}} = 11.3$ Hz, NCH_2), 2.46 (1 H, m, H_2NCH), 2.21 (1 H, app. t, $^2J_{\text{HH}} = 11.3$ Hz, NCH_2), 1.49 (1 H, m, $\underline{\text{C}}\text{H}(\text{CH}_3)_2$), 0.97 (6 H, d, $^3J_{\text{HH}} = 6.2$ Hz, $\text{CH}(\underline{\text{C}}\text{H}_3)_2$), 0.81 (6 H, d, $^3J_{\text{HH}} = 9.0$ Hz, $\text{CH}(\underline{\text{C}}\text{H}_3)_2$) ppm. $^{13}\text{C}\{^1\text{H}\}$ NMR data (CDCl_3 , 125.7 MHz, 293 K): $\delta_{\text{C}} = 56.1$ (H_2NCH), 50.5 ($\underline{\text{C}}\text{H}_2$), 49.0 ($\text{NHCH}(\underline{\text{C}}\text{H}_3)_2$), 32.3 ($\underline{\text{C}}\text{H}(\text{CH}_3)_2$), 22.3 ($\text{NHCH}(\underline{\text{C}}\text{H}_3)_2$), 22.1 ($\text{NHCH}(\underline{\text{C}}\text{H}_3)_2$), 19.1 ($\underline{\text{C}}\text{H}_3$ isopropyl), 17.7 ($\underline{\text{C}}\text{H}_3$ isopropyl) ppm. IR data (NaCl disc, cm^{-1}): 3668 (w), 3350 (m), 2962 (s), 2873 (m), 2251 (br. w), 1587 (m), 1497 (w), 1468 (m), 1414 (w), 1383 (m), 1368 (m), 1338 (w), 1321 (w), 1261 (m), 1168 (w),

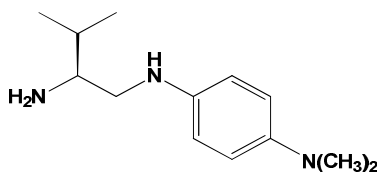
1071 (br. m), 1013 (m), 909 (s), 868 (w), 811 (br. m), 731 (s), 646 (m). Accurate mass ES-MS for $[\text{HNN}^{\text{iPr}}+\text{H}]^+$: $m/z = 145.1700$ (calc. for $\text{C}_8\text{H}_{21}\text{N}_2$: 145.1705).

6.2.5.9 [4i]



^1H NMR data (CDCl_3 , 500.1 MHz, 293 K) $\delta_{\text{H}} = 2.62$ (1 H, dd, $^3J_{\text{HH}} = 3.4$ Hz, $^2J_{\text{HH}} = 10.9$ Hz, NCH_2), 2.47 (1 H, m, H_2NCH), 2.26 (1 H, dd, $^3J_{\text{HH}} = 3.4$ Hz, $^2J_{\text{HH}} = 10.9$ Hz, NCH_2), 1.57 (1 H, m, $(\text{CH}_3)_2\text{CH}$) 1.07 (9 H, s, $\text{C}(\text{CH}_3)_3$), 0.89 (6 H, app. t, $^3J_{\text{HH}} = 6.9$ Hz, $\text{CH}(\text{CH}_3)_2$) ppm. $^{13}\text{C}\{^1\text{H}\}$ NMR data (CDCl_3 , 125.7 MHz, 293 K) $\delta_{\text{C}} = 57.1$ (H_2NCH), 50.2 ($\text{C}(\text{CH}_3)_3$), 46.3 (CH_2), 32.4 ($(\text{CH}_3)_2\text{CH}$), 28.9 ($(\text{CH}_3)_3\text{CH}$), 19.3 (CH_3 isopropyl), 17.7 (CH_3 isopropyl) ppm. IR data (NaCl disc, cm^{-1}): 3366 (br. m), 3297 (br. m), 2961 (s), 2929 (s), 2871 (s), 2283 (w), 1658 (m), 1579 (m), 1519 (w), 1467 (m), 1388 (m), 1363 (m), 1317 (w), 1230 (m), 1169 (w), 1091 (w), 1024 (w), 878 (w), 805 (w), 716 (w). Accurate mass ES-MS for $[\text{HNN}^{\text{tBu}}+\text{H}]^+$: $m/z = 158.1782$ (calc. for $\text{C}_9\text{H}_{22}\text{N}_2$: 158.1783).

6.2.5.10 [4j]

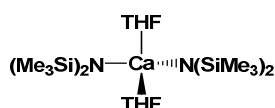


^1H NMR data (CDCl_3 , 500.1 MHz, 293 K): $\delta_{\text{H}} = 6.74$ (2 H, d, $^3J_{\text{HH}} = 8.8$ Hz, $o\text{-C}_6\text{H}_4\text{N}(\text{CH}_3)_2$), 6.62 (2 H, d, $^3J_{\text{HH}} = 8.8$ Hz, $m\text{-C}_6\text{H}_4\text{N}(\text{CH}_3)_2$), 3.19 (1 H, dd, $^3J_{\text{HH}} = 3.2$ Hz, $^2J_{\text{HH}} = 11.8$ Hz, NCH_2), 2.81 (6 H, br. s, $\text{N}(\text{CH}_3)_2$), 2.78 (1 H, dd, $^3J_{\text{HH}} = 2.4$ Hz, $^2J_{\text{HH}} = 12.7$ Hz, NCH_2), 2.72 (1 H, m, H_2NCH), 1.66 (1 H, m, $(\text{CH}_3)_2\text{CH}$), 0.95 (6 H, dd, $^3J_{\text{HH}} = 9.9$ Hz, $^3J_{\text{HH}} = 6.8$ Hz, $\text{CH}(\text{CH}_3)_2$) ppm. $^{13}\text{C}\{^1\text{H}\}$ NMR data (CDCl_3 , 125.7 MHz, 293 K) $\delta_{\text{C}} = 144.0$ ($p\text{-C}_6\text{H}_4\text{N}(\text{CH}_3)_2$), 141.1 ($ipso\text{-C}_6\text{H}_4\text{N}(\text{CH}_3)_2$), 115.9 ($o\text{-C}_6\text{H}_4\text{N}(\text{CH}_3)_2$), 114.5 ($m\text{-C}_6\text{H}_4\text{N}(\text{CH}_3)_2$), 56.1 (H_2NCH), 49.2 (CH_2), 42.2 ($\text{C}_6\text{H}_4\text{N}(\text{CH}_3)_2$), 32.3 ($(\text{CH}_3)_2\text{CH}$), 19.2 (CH_3 isopropyl), 17.7 (CH_3 isopropyl) ppm. IR data (NaCl disc, cm^{-1}): 3355 (br. s), 3029 (m), 2956 (br. s), 2871 (s), 2834 (s), 2790 (s), 2241 (w), 2044 (w), 1839 (br. w), 1618 (m), 1588

(m), 1519 (s), 1472 (s), 1417 (w), 1404 (w), 1386 (m), 1367 (m), 1320 (s), 1255 (s), 1211 (m), 1160 (w), 1140 (m), 1084 (w), 1036 (m), 944 (s), 873 (w), 815 (s), 733 (w), 438 (br. s). Accurate mass ES-MS for $[\text{HNN}^{\text{ArNMe}_2} + \text{H}]^+$: $m/z = 222.1967$ (calc. for $\text{C}_{13}\text{H}_{24}\text{N}_3$: 222.1970).

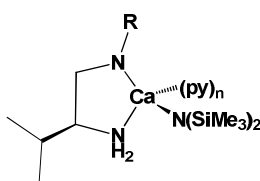
6.3 Experimental and Characterisation Data for Chapter Three

6.3.1 Preparation of $[\text{Ca}\{\text{N}(\text{SiMe}_3)_2\}_2(\text{THF})_2]$

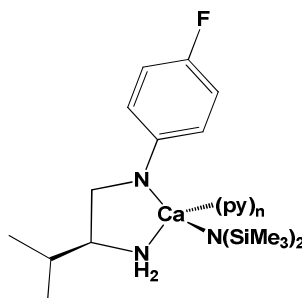


CaI_2 (1.47g, 5 mmol) was added to $\text{K}\{\text{N}(\text{SiMe}_3)_2\}$ (1.99g, 10 mmol) before being dissolved in dry THF and allowed to stir for 18 hours under an inert atmosphere. The solution was filtered away from the resulting salt precipitate and the solvent removed under reduced pressure to yield the white solid $[\text{Ca}\{\text{N}(\text{SiMe}_3)_2\}_2(\text{THF})_2]$. Further purification was achieved by extracting the product into hexane before drying the solid *in vacuo* over night to approximately 2×10^{-2} mbar.^{5,6} Data were consistent with that previously reported.^{7,8}

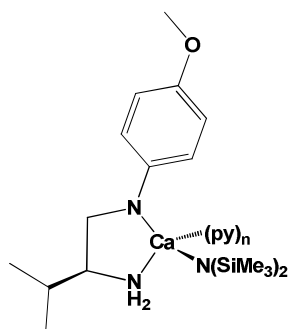
6.3.2 Preparation of $[\text{Ca}(\text{NN}^{\text{R}})\{\text{N}(\text{SiMe}_3)_2\}(\text{py})_n]$ [6a-f]



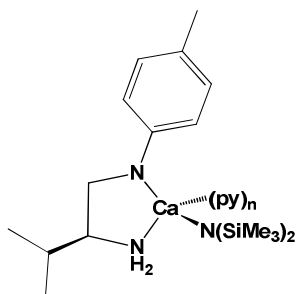
$[\text{Ca}\{\text{N}(\text{SiMe}_3)_2\}_2(\text{py})_2]$ was prepared from the corresponding analogue $[\text{Ca}\{\text{N}(\text{SiMe}_3)_2\}_2(\text{THF})_2]$ (*vide supra*) via literature procedures.⁷ The selected diamine **4a-j** (300 mg, 1.5 mmol) in toluene (20 ml) was added to 1 equivalent of $[\text{Ca}\{\text{N}(\text{SiMe}_3)_2\}_2(\text{py})_2]$ (793 mg, 1.5 mmol). The solution was agitated briefly and allowed to react for 18 hours at ambient temperature. The resulting complex was typically realised as an orange/red powder when dried *in vacuo* to approximately 4×10^{-2} mbar. The absolute configuration at the calcium of the diastereomeric complexes could not be determined owing to the highly labile nature observed in the collected spectroscopic data.

6.3.2.1 [Ca(NN^{ArF}){N(SiMe₃)₂}(py)] [6a]

¹H NMR data (THF-d₈, 300.5 MHz, 293 K): $\delta_{\text{H}} = 8.57$ (2 H, m, *o*-C₅H₅N), 7.67 (1 H, app. tt, ³J_{HH} = 7.7 Hz, ⁴J_{HH} = 1.5 Hz, *p*-C₅H₅N), 7.26 (2 H, m, *m*-C₅H₅N), 6.53 (2 H, app. t, ³J_{HH} = 8.2 Hz, *m*-C₆H₄F), 6.06 (2 H, br. m, *o*-C₆H₄F), 2.86 (1 H, app. d, ³J_{HH} = 9.5 Hz, NCH₂), 2.59 (2 H, br. m, H₂NCH and NCH₂), 1.65 (1 H, br. m, (CH₃)₂CH), 0.93 (6 H, app. d, ³J_{HH} = 6.1 Hz, CH(CH₃)₂), 0.04 (18 H, (N(Si(CH₃)₃)₂) ppm. ¹H NMR data (THF-d₈, 500.1 MHz, 263 K): $\delta_{\text{H}} = 8.59$ (2 H, m, *o*-C₅H₅N), 7.69 (1 H, app. tt, ³J_{HH} = 7.5 Hz, ⁴J_{HH} = 1.8 Hz, *p*-C₅H₅N), 7.29 (2 H, m, *m*-C₅H₅N), 6.53 (2 H, app. t, ³J_{HH} = 7.7 Hz, *m*-C₆H₄F), 6.04 (2 H, br. m, *o*-C₆H₄F), 2.83 (1 H, br. m, NCH₂), 2.58 (2 H, br. m, H₂NCH and NCH₂), 1.66 (1 H, br. m, (CH₃)₂CH), 0.94 (6 H, app. d, ³J_{HH} = 5.0 Hz, CH(CH₃)₂), 0.04 (18 H, (N(Si(CH₃)₃)₂) ppm. ¹³C{¹H} NMR data (THF-d₈, 75.5 MHz, 263 K): $\delta_{\text{C}} = 157.8$ (*ipso*-C₆H₄F), 150.6 (*o*-C₅H₅N), 136.2 (*p*-C₅H₅N), 127.6 (d, J_{CF} = 274.0 Hz, *p*-C₆H₄F), 124.1 (*m*-C₅H₅N), 115.3 (d, J_{CF} = 19.7 Hz, *m*-C₆H₄F), 110.7 (*o*-C₆H₄F), 60.4 (H₂NCH), 54.7 (CH₂), 34.1 ((CH₃)₂CH), 19.5 (CH₃ isopropyl), 18.6 (CH₃ isopropyl), 2.4 (N(Si(CH₃)₃)₂) ppm. ¹⁹F NMR data (THF-d₈, 282.8 MHz, 293 K): $\delta_{\text{F}} = -141.57$ (br. s, *p*-C₆H₄F) ppm. ¹⁹F NMR data (THF-d₈, 282.8 MHz, 263 K): $\delta_{\text{F}} = -141.62$ (s, *p*-C₆H₄F) ppm. IR data (KBr pellet, cm⁻¹): 3341 (br. m), 3254 (br. m), 3061 (w), 3038 (w), 2960 (s), 2874 (s), 1596 (m), 1510 (s), 1466 (m), 1441 (m), 1389 (w), 1370 (w), 1304 (w), 1261 (m), 1219 (m), 1156 (w), 1101 (m), 1016 (br. m), 820 (s), 736 (w).

6.3.2.2 [Ca(NN^{ArOMe}){N(SiMe₃)₂}(py)] [6b]

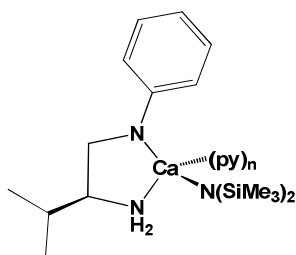
¹H NMR data (THF-d₈, 300.5 MHz, 293 K): δ_H = 8.52 (2 H, m, *o*-C₅H₅N), 7.62 (1 H, app. tt, ³J_{HH} = 7.6 Hz, ⁴J_{HH} = 1.6 Hz, *p*-C₅H₅N), 7.23 (2 H, m, *m*-C₅H₅N), 6.80-6.58 (3 H, m, ArH), 6.43 (1 H, br. s, ArH), 3.62 (3 H, br. s C₆H₄OCH₃), 2.99 (1 H, br. s NCH₂), 2.77-2.48 (2 H, m, H₂NCH and NCH₂), 1.59 (1 H, br. s, (CH₃)₂CH), 0.98-0.79 (6 H, br. s, CH(CH₃)₂), 0.04 (18 H, s, (N(Si(CH₃)₃)₂) ppm. ¹³C{¹H} NMR data (THF-d₈, 75.5 MHz, 293 K): δ_C = 151.7 (*p*-C₆H₄OCH₃), 150.6 (*o*-C₅H₅N), 143.8 (*ipso*-C₆H₄OCH₃), 136.3 (*p*-C₅H₅N), 124.1 (*m*-C₅H₅N), 115.4 (*m*-C₆H₄OCH₃), 113.8 (*o*-C₆H₄OCH₃), 57.5 (H₂NCH), 55.9 (C₆H₄OCH₃) 50.7 (CH₂), 33.7 ((CH₃)₂CH), 19.8 (CH₃ isopropyl), 18.1 (CH₃ isopropyl), 2.7 (N(Si(CH₃)₃)₂) ppm. IR data (KBr pellet, cm⁻¹): 3353 (br. m), 2961 (s), 2870 (m), 2826 (m), 2179 (w), 2065 (w), 1590 (w), 1513 (s), 1464 (w), 1415 (w), 1392 (w), 1365 (w), 1298 (w), 1260 (m), 1238 (m), 1178 (w), 1103 (m), 1036 (m), 869 (w), 819 (m), 745 (w), 731 (w), 708 (w), 519 (w).

6.3.2.3 [Ca(NN^{ArMe}){N(SiMe₃)₂}(py)] [6c]

¹H NMR data (THF-d₈, 300.5 MHz, 293 K): δ_H = 8.53 (2 H, m, *o*-C₅H₅N), 7.64 (1 H, app. tt, ³J_{HH} = 7.6 Hz, ⁴J_{HH} = 1.8 Hz, *p*-C₅H₅N), 7.23 (2 H, m, *m*-C₅H₅N), 6.74-6.54 (2 H, m, ArH), 6.35 (2 H, m, ArH), 3.00-2.88 (1 H, m, NCH₂), 2.72-2.56 (2 H, m, H₂NCH and NCH₂), 2.07 (3 H, br. s C₆H₄CH₃), 1.66-1.55 (1 H, br. s, (CH₃)₂CH), 0.93 (3 H, app. dd,

$^3J_{\text{HH}} = 6.2 \text{ Hz}$, $^3J_{\text{HH}} = 6.2 \text{ Hz}$, $\text{CH}(\underline{\text{CH}_3})_2$, 0.92 (3 H, app. dd, $^3J_{\text{HH}} = 8.0 \text{ Hz}$, $^3J_{\text{HH}} = 6.9 \text{ Hz}$, $\text{CH}(\underline{\text{CH}_3})_2$), 0.04 (18 H, s, $\text{N}(\text{Si}(\underline{\text{CH}_3})_3)_2$) ppm. $^{13}\text{C}\{^1\text{H}\}$ NMR data (THF- d_8 , 75.5 MHz, 293 K): $\delta_{\text{C}} = 150.8$ ($o\text{-C}_5\text{H}_5\text{N}$), 147.2 (*is* $po\text{-C}_6\text{H}_4\text{CH}_3$), 136.3 ($p\text{-C}_5\text{H}_5\text{N}$), 130.1 ($m\text{-C}_6\text{H}_4\text{CH}_3$), 128.9 ($p\text{-C}_6\text{H}_4\text{CH}_3$), 124.3 ($m\text{-C}_5\text{H}_5\text{N}$), 112.4 ($o\text{-C}_6\text{H}_4\text{CH}_3$), 59.0 (H_2NCH), 53.2 ($\underline{\text{CH}_2}$), 34.3 ($(\text{CH}_3)_2\text{CH}$), 20.7 ($\text{C}_6\text{H}_4\underline{\text{CH}_3}$) 20.5 ($\underline{\text{CH}_3}$ isopropyl), 19.8 ($\underline{\text{CH}_3}$ isopropyl), 2.7 ($\text{N}(\text{Si}(\underline{\text{CH}_3})_3)_2$) ppm. IR data (KBr pellet, cm^{-1}): 3347 (w), 3275 (w), 2959 (s), 2871 (m), 2239 (w), 2179 (w), 2096 (w), 1607 (m), 1579 (m), 1516 (s), 1501 (s), 1465 (m), 1388 (w), 1302 (m), 1260 (s), 1181 (m), 1095 (m), 1017 (s), 976 (br. m), 882 (w), 805 (s), 755 (w), 702 (w) 445 (w).

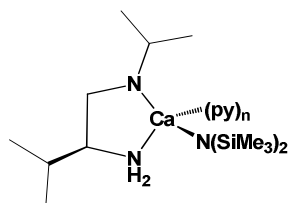
6.3.2.4 $[\text{Ca}(\text{NN}^{\text{Ph}})\{\text{N}(\text{SiMe}_3)_2\}(\text{py})]$ [6d]



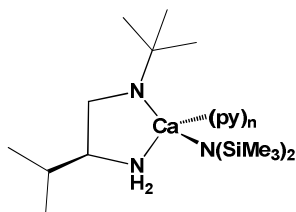
^1H NMR data (THF- d_8 , 300.5 MHz, 293 K): $\delta_{\text{H}} = 8.54$ (2 H, m, $o\text{-C}_5\text{H}_5\text{N}$), 7.66 (1 H, m, $p\text{-C}_5\text{H}_5\text{N}$), 7.25 (2 H, m, $m\text{-C}_5\text{H}_5\text{N}$), 6.76 (2 H, br. m, $o\text{-C}_6\text{H}_5$), 6.13 (2 H, br. m, $m\text{-C}_6\text{H}_5$), 5.89 (1 H, br. m, $p\text{-C}_6\text{H}_5$), 2.92 (1 H, br. m, NCH_2), 2.63 (2 H, br. m, H_2NCH and NCH_2), 1.58 (1 H, br. m, $(\text{CH}_3)_2\text{CH}$), 0.91 (6 H, br. m, $\text{CH}(\underline{\text{CH}_3})_2$), 0.04 (18 H, s, $\text{N}(\text{Si}(\underline{\text{CH}_3})_3)_2$) ppm. ^1H NMR data (THF- d_8 , 300.5 MHz, 243 K): $\delta_{\text{H}} = 8.56$ (2 H, m, $o\text{-C}_5\text{H}_5\text{N}$), 7.73 (1 H, m, $p\text{-C}_5\text{H}_5\text{N}$), 7.31 (2 H, m, $m\text{-C}_5\text{H}_5\text{N}$), 6.78 (2 H, br. m, $o\text{-C}_6\text{H}_5$), 6.78-5.97 (2 H, br. m, $m\text{-C}_6\text{H}_5$), 5.87 (1 H, br. m, $p\text{-C}_6\text{H}_5$), 2.87 (1 H, br. m, NCH_2), 2.75 (1 H, br. m, H_2NCH), 2.63 (1 H, br. m, and NCH_2), 1.50 (1 H, br. m, $(\text{CH}_3)_2\text{CH}$), 0.97 (6 H, br. m, $\text{CH}(\underline{\text{CH}_3})_2$), 0.04 (18 H, s, $\text{N}(\text{Si}(\underline{\text{CH}_3})_3)_2$) ppm. $^{13}\text{C}\{^1\text{H}\}$ NMR data (THF- d_8 , 75.5 MHz, 293 K): $\delta_{\text{C}} = 160.1$ (*is* $po\text{-C}_6\text{H}_5$), 150.7 ($o\text{-C}_5\text{H}_5\text{N}$), 136.2 ($p\text{-C}_5\text{H}_5\text{N}$), 129.2 ($o\text{-C}_6\text{H}_5$), 124.1 ($m\text{-C}_5\text{H}_5\text{N}$), 111.6 ($m\text{-C}_6\text{H}_5$), 107.7 ($p\text{-C}_6\text{H}_5$), 60.4 (H_2NCH), 54.1 ($\underline{\text{CH}_2}$), 34.2 ($(\text{CH}_3)_2\text{CH}$), 20.1 ($\underline{\text{CH}_3}$ isopropyl), 19.5 ($\underline{\text{CH}_3}$ isopropyl), 1.8 ($\text{N}(\text{Si}(\underline{\text{CH}_3})_3)_2$) ppm. $^{13}\text{C}\{^1\text{H}\}$ NMR data (THF- d_8 , 75.5 MHz, 243 K): $\delta_{\text{C}} = 160.6$ (*is* $po\text{-C}_6\text{H}_5$), 150.6 ($o\text{-C}_5\text{H}_5\text{N}$), 136.5 ($p\text{-C}_5\text{H}_5\text{N}$), 129.9 ($o\text{-C}_6\text{H}_5$), 124.4 ($m\text{-C}_5\text{H}_5\text{N}$), 116.8 ($m\text{-C}_6\text{H}_5$), 106.9 ($p\text{-C}_6\text{H}_5$), 60.7 (H_2NCH), 54.3 ($\underline{\text{CH}_2}$), 34.1 ($(\text{CH}_3)_2\text{CH}$), 20.2 ($\underline{\text{CH}_3}$ isopropyl), 19.5 ($\underline{\text{CH}_3}$ isopropyl), 2.1 ($\text{N}(\text{Si}(\underline{\text{CH}_3})_3)_2$) ppm. IR data (KBr pellet, cm^{-1}): 3339 (br. m), 3257 (m), 3051 (m), 3022 (w), 2957 (s), 2931 (s), 2869

(s), 2498 (w), 1927 (w), 1596 (s), 1552 (w), 1484 (s), 1441 (s), 1369 (m), 1303 (m), 1261 (s), 1182 (m), 1150 (m), 1100 (br. s), 1035 (s), 1010 (s), 879 (w), 804 (m), 750 (s).

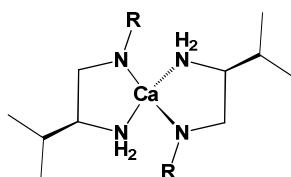
6.3.2.5 [Ca(NN^{iPr}){N(SiMe₃)₂}(py)] [6e]



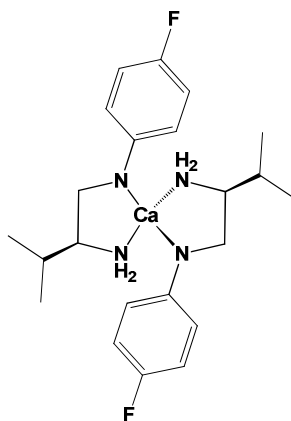
¹H NMR data (THF-d₈, 300.5 MHz, 293 K): δ_H = 8.58 (2 H, m, *o*-C₅H₅N), 7.66 (1 H, m, *p*-C₅H₅N), 7.26 (2 H, m, *m*-C₅H₅N), 2.90 (1 H, br. m, NCH₂), 2.66 (1 H, br. m, H₂NCH), 2.52 (1 H, br. m, NCH₂), 1.67-1.47 (2 H, br. m, (CH₃)₂CH), 1.24-1.03 (6 H, br. m, CH(CH₃)₂), 0.94-0.76 (6 H, br. m, CH(CH₃)₂) 0.03 (18 H, s, N(Si(CH₃)₃)₂) ppm. ¹H NMR data (THF-d₈, 300.5 MHz, 263 K): δ_H = 8.55 (2 H, m, *o*-C₅H₅N), 7.69 (1 H, app. tt, ³J_{HH} = 7.6 Hz, ⁴J_{HH} = 1.8 Hz, *p*-C₅H₅N), 7.28 (2 H, m, *m*-C₅H₅N), 3.10-2.80 (2 H, br. m, H₂NCH and NCH₂), 2.65 (1 H, br. m, NCH₂), 1.67 (1 H, br. m, (CH₃)₂CH), 1.37 (1 H, br. m, (CH₃)₂CH), 1.19-1.06 (6 H, br. m, CH(CH₃)₂), 0.93-0.80 (6 H, br. m, CH(CH₃)₂) 0.03 (18 H, s, N(Si(CH₃)₃)₂) ppm. ¹³C{¹H} NMR data (THF-d₈, 75.5 MHz, 293 K): δ_C = 150.6 (*o*-C₅H₅N), 136.2 (*p*-C₅H₅N), 124.1 (*m*-C₅H₅N), 58.3 (H₂NCH), 55.8 (NCH(CH₃)₂), 49.0 (CH₂), 36.7 ((CH₃)₂CH), 23.0 (CH₃ isopropyl), 22.1 (CH₃ isopropyl), 19.9 (CH₃ isopropyl), 18.7 (CH₃ isopropyl), 2.4 (N(Si(CH₃)₃)₂) ppm. IR data (KBr pellet, cm⁻¹): 3248 (br. w), 2959 (s), 2870 (m), 1597 (m), 1553 (m), 1465 (m), 1442 (m), 1386 (m), 1368 (m), 1324 (w), 1259 (br. m), 1165 (w), 1057 (br. s), 950 (w), 931 (w), 881 (m), 822 (s), 750 (w), 702 (w).

6.3.2.6 [Ca(NN^{tBu}){N(SiMe₃)₂}(py)] [6f]

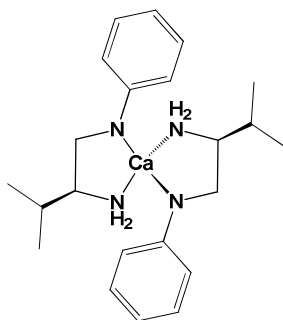
¹H NMR data (THF-d₈, 300.5 MHz, 293 K): δ_H = 8.54 (2 H, m, *o*-C₅H₅N), 7.66 (1 H, app. tt, ³J_{HH} = 7.6 Hz, ⁴J_{HH} = 1.9 Hz, *p*-C₅H₅N), 7.25 (2 H, m, *m*-C₅H₅N), 2.80 (1 H, br. m, NCH₂), 2.60 (1 H, br. m, H₂NCH), 2.45 (1 H, br. m, NCH₂), 1.57 (1 H, m, (CH₃)₂CH), 1.07 (9 H, br. s, C(CH₃)₃), 0.88 (6 H, br. t, ³J_{HH} = 6.6 Hz, CH(CH₃)₂), 0.10 (18 H, s, N(Si(CH₃)₃)₂) ppm. ¹H NMR data (THF-d₈, 300.5 MHz, 263 K): δ_H = 8.55 (2 H, m, *o*-C₅H₅N), 7.68 (1 H, app. tt, ³J_{HH} = 7.6 Hz, ⁴J_{HH} = 1.9 Hz, *p*-C₅H₅N), 7.28 (2 H, m, *m*-C₅H₅N), 2.79 (1 H, br. m, NCH₂), 2.59 (1 H, br. m, H₂NCH), 2.45 (1 H, br. m, NCH₂), 1.57 (1 H, m, (CH₃)₂CH), 1.08 (9 H, br. s, C(CH₃)₃), 0.88 (6 H, br. t, ³J_{HH} = 6.6 Hz, CH(CH₃)₂), 0.10 (18 H, s, N(Si(CH₃)₃)₂) ppm. ¹³C{¹H} NMR data (THF-d₈, 75.5 MHz, 263 K): δ_C = 150.6 (*o*-C₅H₅N), 136.2 (*p*-C₅H₅N), 124.2 (*m*-C₅H₅N), 58.1 (H₂NCH), 50.6 (NC(CH₃)₃), 47.2 (CH₂), 33.2 ((CH₃)₂CH), 29.3 ((CH₃)₃CN), 19.7 (CH₃ isopropyl), 17.9 (CH₃ isopropyl), 1.2 (N(Si(CH₃)₃)₂) ppm. IR data (KBr pellet, cm⁻¹): 3338 (br. w), 3247 (br. w), 2962 (s), 2871 (m), 1597 (w), 1466 (m), 1442 (w), 1393 (w), 1367 (m), 1261 (s), 1234 (w), 1218 (w), 1098 (br. s), 1021 (br. s), 894 (w), 859 (w), 803 (s), 749 (w).

6.3.3 Preparation of [Ca(NN^R)₂] [7a-c]

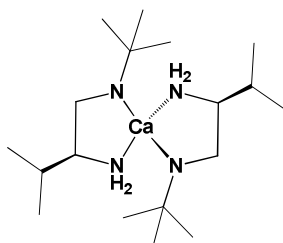
The selected diamine **4a**, **d** or **i** (50 mg, 0.31 mmol) pre-dissolved in toluene (0.5 ml) was added to [Ca{N(SiMe₃)₂]₂(THF)₂] (82.0 mg, 0.16 mmol). The solution was agitated briefly and allowed to react for 18 hours at ambient temperature. The resulting complex was typically realised as a dark orange/magenta powder when dried *in vacuo* to approximately 4 × 10⁻² mbar.

6.3.3.1 [Ca(NN^{ArF})₂] [7a]

¹H NMR data (THF-d₈, 300.5 MHz, 293 K): $\delta_{\text{H}} = 6.70$ (4 H, br. m, *m*-C₆H₅F), 6.42 (4 H, br. m, *o*-C₆H₄F), 2.99 (2 H, br. m NCH₂), 2.67 (4 H, br. m, NCH₂ and H₂NCH), 1.63 (2 H, br. m, (CH₃)₂CH), 0.92 (12 H, br. m, CH(CH₃)₂) ppm. ¹H NMR data (THF-d₈, 300.5 MHz, 183 K): $\delta_{\text{H}} = 6.89$ (3 H, br. m, C₆H₄F), 6.69 (2 H, br. m, C₆H₄F), 6.57 (2 H, br. m, C₆H₄F), 6.38 (1 H, br. m, C₆H₄F), 3.02 (2 H, br. m NCH₂), 2.73 (2 H, br. m, NCH₂), 2.55 (2 H, br. m, H₂NCH), 1.67 (2 H, br. m, (CH₃)₂CH partially obscured by solvent peak), 0.91 (12 H, br. m, CH(CH₃)₂) ppm. ¹³C{¹H} NMR data (THF-d₈, 75.5 MHz, 293 K): $\delta_{\text{C}} = 129.4$ (*ipso*-C₆H₄F), 127.2 (d, $J_{\text{CF}} = 216.9$ Hz, *p*-C₆H₄F), 115.4 (d, $J_{\text{CF}} = 21.6$, *m*-C₆H₄F), 113.3 (*o*-C₆H₄F), 59.6* (br. s, H₂NCH), 50.5* (br. s, CH₂), 33.6 ((CH₃)₂CH), 19.6 (CH₃ isopropyl), 18.0 (CH₃ isopropyl) ppm. *Resonances are broad but comparable to low temperature ¹³C{¹H} NMR of the homoleptic species. ¹³C{¹H} NMR data (THF-d₈, 75.5 MHz, 183 K): $\delta_{\text{C}} = 129.5$ (*ipso*-C₆H₄F), 127.4 (d, $J_{\text{CF}} = 217.4$ Hz, *p*-C₆H₄F), 115.7 (d, $J_{\text{CF}} = 21.8$, *m*-C₆H₄F), 115.0 (*o*-C₆H₄F partially obscured *m*-C₆H₄F), 56.5 (H₂NCH), 49.2 (CH₂), 33.3 ((CH₃)₂CH), 19.4 (CH₃ isopropyl), 17.8 (CH₃ isopropyl) ppm. ¹⁹F NMR data (THF-d₈, 282.8 MHz, 293 K): $\delta_{\text{F}} = -141.57$ (br. s, *p*-C₆H₄F), -130.64 (br. s, *p*-C₆H₄F) ppm. ¹⁹F NMR data (THF-d₈, 282.8 MHz, 183 K): $\delta_{\text{F}} = -141.09$ (s, *p*-C₆H₄F), -130.37 (br. s, *p*-C₆H₄F) ppm. IR data (KBr disc, cm⁻¹): 3343 (br. m), 3234 (br. m), 3058 (m), 3035 (m), 2960 (s), 2931 (s), 2871 (s), 2045 (w), 1851 (br. w), 1735 (br. w), 1609 (m), 1584 (m), 1510 (s), 1389 (m), 1369 (m), 1307 (w), 1260 (m), 1218 (s), 1157 (m), 1101 (br. m), 1017 (m), 884 (w), 820 (s), 736 (m).

6.3.3.2 [Ca(NN^{Ar})₂] [7b]

¹H NMR data (THF-d₈, 300.5 MHz, 293 K): $\delta_{\text{H}} = 6.94$ (6 H, br. m, C₆H₅), 6.43 (4 H, br. m, C₆H₅), 3.04 (2 H, br. m, NCH₂), 2.68 (4 H, br. m, H₂NCH and NCH₂), 1.52 (2 H, br. m, (CH₃)₂CH partially obscured by other signal), 0.91 (12 H, br. m, CH(CH₃)₂) ppm. Low temperature ¹H NMR studies between 273-193 K failed to give additional information. ¹³C{¹H} NMR data (THF-d₈, 75.5 MHz, 293 K): $\delta_{\text{C}} = 160.1$ (C₆H₅), 129.3 (C₆H₅), 128.8 (C₆H₅), 116.7 (C₆H₅), 113.1 (C₆H₅), 57.9 (H₂NCH), 50.44 (CH₂), 33.6 ((CH₃)₂CH), 19.6 (CH₃ isopropyl), 18.0 (CH₃ isopropyl) ppm. ¹³C{¹H} NMR data (THF-d₈, 75.5 MHz, 263 K): $\delta_{\text{C}} = 160.1$ (C₆H₅), 129.3 (C₆H₅), 128.8 (C₆H₅), 116.5 (C₆H₅), 112.9 (C₆H₅), 56.9 (H₂NCH), 49.9 (CH₂), 33.4 ((CH₃)₂CH), 19.6 (CH₃ isopropyl), 17.9 (CH₃ isopropyl) ppm. IR data (KBr pellet, cm⁻¹): 3646 (w), 3346 (br. m), 3272 (m), 3050 (m), 3020 (m), 2956 (br. s), 2869 (s), 2494 (w), 1916 (w), 1823 (w), 1766 (w), 1603 (s), 1549 (m), 1505 (s), 1387 (m), 1368 (m), 1306 (s), 1262 (s), 1180 (s), 1152 (m), 1109 (s), 1011 (m), 977 (m), 882 (m), 833 (m), 787 (m), 787 (m), 749 (s), 693 (s), 619 (w), 608 (w), 590 (w), 509 (m), 421 (m), 406 (m).

6.3.3.3 [Ca(NN^{tBu})₂] [7c]

¹H NMR data (THF-d₈, 300.5 MHz, 293 K): $\delta_{\text{H}} = 2.60$ (2 H, br. m, NCH₂), 2.43 (2 H, br. m, H₂NCH), 2.30 (2 H, m, NCH₂), 1.57 (2 H, m, (CH₃)₂CH), 1.07 (18 H, br. s, NC(CH₃)₃), 0.88 (12 H, app. t, ³J_{HH} = 6.3 Hz, CH(CH₃)₂) ppm. ¹H NMR data (THF-d₈, 300.5 MHz,

263 K): $\delta_{\text{H}} = 2.59$ (2 H, m, NCH_2), 2.44 (2 H, br. m, H_2NCH), 2.29 (m, 2 H, NCH_2), 1.57 (2 H, m, $(\text{CH}_3)_2\text{CH}$), 1.07 (18 H, br. s, $\text{NC}(\text{CH}_3)_3$), 0.88 (12 H, app. t, $^3J_{\text{HH}} = 6.5$ Hz, $\text{CH}(\text{CH}_3)_2$) ppm. $^{13}\text{C}\{^1\text{H}\}$ NMR data (THF- d_8 , 62.9 MHz, 293 K): $\delta_{\text{C}} = 58.3$ (H_2NCH), 50.5 ($\text{NC}(\text{CH}_3)_3$), 47.4 (CH_2), 33.1 ($(\text{CH}_3)_2\text{CH}$), 29.4 ($(\text{CH}_3)_3\text{CN}$), 19.7 (CH_3 isopropyl), 17.9 (CH_3 isopropyl) ppm. IR data (KBr pellet, cm^{-1}): 3295 (m), 3241 (m), 2962 (br. m), 2866 (br. m), 1586 (br. m), 1470 (m), 1388 (w), 1365 (m), 1257 (br. m), 1232 (m), 1078 (m), 1023 (w), 898 (w), 824 (w), 746 (w).

6.3.4 General Procedure for Hydroamination Catalysis:

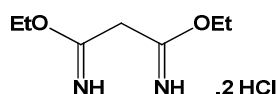
Both 1-amino 2,2-dimethylpent-4-ene and 1-amino 2,2-diphenylpent-4-ene were prepared according to literature methods.^{9, 10} In a dinitrogen filled glovebox LH (LH = HNN^{R} or R-BIM) (0.04 mmol) was predissolved in C_6D_6 (0.5 ml) and successively added to $[\text{Ca}\{\text{N}(\text{SiMe})_2\}_2(\text{THF})_2]$ (0.04 mmol). The resulting mixture was agitated by hand and left for two minutes. To this solution was added the corresponding amino olefin (0.4 mmol). The solution was transferred to a J. Young Teflon valve equipped NMR tube and sealed. All catalyst reactions were monitored via ^1H NMR periodically to check conversion (conversion was determined from notable resonances in the spectra corresponding to the pyrrolidine product).¹¹ Upon conversion ceasing, a solution of *R*-(-)- α -acetylmandelic acid **2.21** (0.41 mmol) predissolved in a minimal amount of CDCl_3 was added to the reaction mixture producing the diastereomeric salts. The resulting enantioexcess was then determined from ^1H NMR spectroscopy.¹²

6.3.5 Determination of Rate Constants from Conversion Curves:

The conversion curves were curve fitted to an exponential decay function $y = Ae^{-bx}$. The initial rate, given by the slope at the origin ($x=0$), were determined by differentiation of the equation: $dy/dx = -A/b$ (see Appendix A for data).

6.4 Experimental and Characterisation Data for Chapter Four

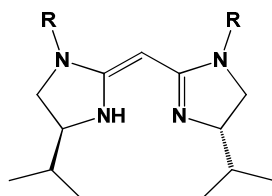
6.4.1 Preparation of diethyl malonimidate dihydrochloride [4.7]



Prepared from a modified literature procedure.¹³ To a solution of malononitrile (10 g, 0.15 mol), in dry 1,4-dioxane (200 ml), ethanol (19.70 ml, 0.33 mol) was added. Dry $\text{HCl}_{(g)}$ was then passed through the solution for 6 hours where upon the system was sealed and allowed to stir under an HCl atmosphere for a further 18 hours. The solution was filtered away from the resulting diethyl malonimidate dihydrochloride precipitate. The precipitate was washed with dry 1,4 dioxane (2×20 mls) and dry diethyl ether (20 ml). The desired product was then dried *in vacuo* and stored in a glove box, giving near quantitative yields. Data were consistent with those previously reported.¹³

^1H NMR data ($(\text{CD}_3)_2\text{SO}$, 400.1 MHz, 293 K): $\delta_{\text{H}} = 8.40$ (4 H, br. s, NH_2), 4.46 (2 H, s, $\text{H}_2\text{NCCH}_2\text{CNH}_2$), 4.21 (4 H, app. s, $\text{CH}_3\text{CH}_2\text{O}$), 1.32 (6 H, t, $^3J_{\text{HH}} = 6.7$ Hz, $\text{CH}_3\text{CH}_2\text{O}$) ppm. $^{13}\text{C}\{^1\text{H}\}$ NMR data ($(\text{CD}_3)_2\text{SO}$, 62.9 MHz, 293 K): $\delta_{\text{C}} = 166.5$ ($\text{C}=\text{N}$), 60.8 ($\text{CH}_3\text{CH}_2\text{O}$), 41.2 (CH_2 bridge), 13.9 ($\text{CH}_3\text{CH}_2\text{O}$) ppm. IR data (KBr pellet, cm^{-1}): 2853 (s), 2644 (s), 2521 (w), 2395 (w), 2363 (w), 2345 (w), 2268 (w), 2224 (w), 2189 (w), 2024 (w), 1959 (w), 1897 (w), 1738 (s), 1662 (s, $\nu_{\text{C}=\text{N}}$), 1565 (m), 1464 (m), 1442 (m), 1390 (s), 1360 (s), 1300 (m), 1262 (w), 1206 (m), 1133 (s), 1092 (s), 1004 (s), 952 (s), 901 (m), 868 (s), 822 (s), 798 (m), 725 (m), 632(s). Accurate mass ES-MS: no identifiable peaks obtained.

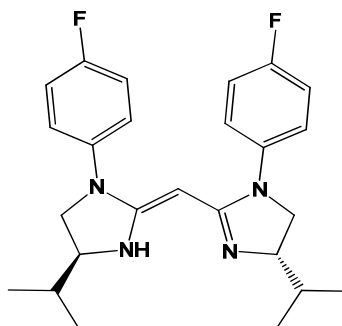
6.4.2 Procedure for Bisimidazoline Preparation R-BIM [8a-j]



Prepared according to modified literature procedures.¹⁴ Under an inert atmosphere, diethyl malonimidate dihydrochloride **4.7** (ca. 0.6 g, 26 mmol) and HNN^{R} **4a-j** (1 g, 52 mmol)

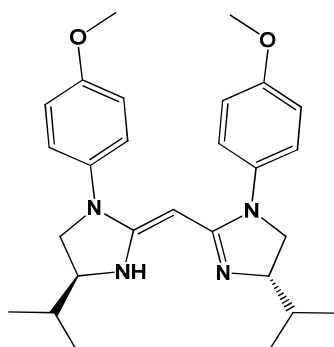
were dissolved in dry dichloromethane and heated at vigorous reflux for 4 days. Proceeding such time the solution was allowed to cool and washed with NaHCO₃ (10%, 2 × 25 ml). The organic solution was subsequently reduced in volume under reduced pressure. The relevant R-BIM was realized by column chromatography over silica gel (typical solvent systems were composed of ethyl acetate or dichloromethane with methanol and Et₃N (9:1:1 v/v)) to yield the desired R-BIM as a white solid in approximately 35-45% yield. Exceptions to this were compounds **8e** (Ar^{NO₂}-BIM) and **8h** (iPr-BIM), which were crystallised out from hot toluene and from a warm dichloromethane/hexane mixture which was subsequently cooled to -18°C respectively.

6.4.2.1 [8a]



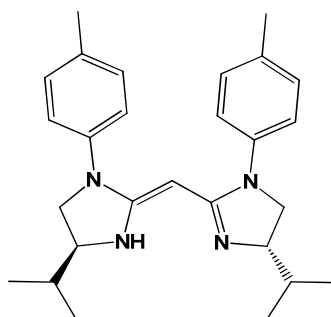
¹H NMR data (CDCl₃, 500.1 MHz, 293 K): δ_H = 7.06 (4 H, dd, ³J_{HH} = 8.5 Hz, *o*-C₆H₄F), 6.93 (4 H, app. t, ³J_{HH} = 8.5 Hz, *m*-C₆H₄F), 3.75 (2 H, m, NCH₂), 3.64 (2 H, m, NCH₂CH), 3.39 (2 H, m, NCH₂), 1.72 (2 H, m, (CH₃)₂CH), 1.09 (6 H, br. d, ³J_{HH} = 6.3 Hz, CH(CH₃)₂), 0.93 (6 H, dd, ³J_{HH} = 6.3 Hz, CH(CH₃)₂), (CH_{bridge} not observed) ppm. ¹⁹F NMR data (CDCl₃, 282.8 MHz, 293 K): δ_F = -118.45 (br. s, *p*-C₆H₄F) ppm. ¹³C{¹H} NMR data (CDCl₃, 125.7 MHz, 293 K): δ_C = 160.3 (C=N), 159.1 (d, ¹J_{CF} = 243.1 Hz, *p*-C₆H₄F), 138.4 (*ipso*-C₆H₄F), 124.3 (d, ³J_{CF} = 7.5 Hz, *o*-C₆H₄F), 115.5 (d, ²J_{CF} = 22.4 Hz, *m*-C₆H₄F), 65.2 (C=NCH imidazoline), 55.8 (CH₂ imidazoline), 33.8 ((CH₃)₂CH), 19.6 (CH₃ isopropyl), 19.1 (CH₃ isopropyl), (CH_{bridge} not observed) ppm. IR data (KBr disc, cm⁻¹): 3111 (w), 3078 (w), 3051 (w), 2959 (s), 2831 (s), 2608 (w), 1876 (w), 1616 (s), 1593 (s), 1536 (s), 1504 (s), 1469 (m), 1425 (m), 1390 (m), 1363 (m), 1306 (s), 1256 (s), 1232 (s), 1194 (s), 1168 (m), 1119 (s), 1090 (m), 1046 (m), 1010 (m), 904 (w), 832 (s), 799 (s), 723 (s), 638 (m), 593 (m), 564 (m), 551 (s), 503 (m), 435 (m). Accurate mass ES-MS for [Ar^F-BIM+H]⁺: m/z = 425.2509 (calc. for C₂₅H₃₁N₂F₂: 425.2517).

6.4.2.2 [8b]



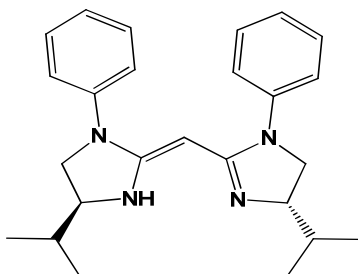
^1H NMR data (CDCl_3 , 500.1 MHz, 293 K): $\delta_{\text{H}} = 7.06$ (4 H, d, $^3J_{\text{HH}} = 8.9$ Hz, $m\text{-C}_6\text{H}_4\text{OCH}_3$), 6.77 (4 H, d, $^3J_{\text{HH}} = 8.9$ Hz, $o\text{-C}_6\text{H}_4\text{OCH}_3$), 3.75 (6 H, br. s, $\text{C}_6\text{H}_4\text{OCH}_3$), 3.73 (2 H, app. t, $^3J_{\text{HH}} = 8.3$ Hz, NCH_2), 3.62 (2 H, app. q, $^3J_{\text{HH}} = 8.5$ Hz, NCH_2CH), 3.36 (2 H, app. t, $^3J_{\text{HH}} = 8.7$ Hz, NCH_2), 1.71 (2 H, m, $(\text{CH}_3)_2\text{CH}$), 1.10 (6 H, d, $^3J_{\text{HH}} = 6.6$ Hz, $\text{CH}(\text{CH}_3)_2$), 0.92 (6 H, d, $^3J_{\text{HH}} = 6.6$ Hz, $\text{CH}(\text{CH}_3)_2$), ($\text{CH}_{\text{bridge}}$ not observed) ppm. $^{13}\text{C}\{^1\text{H}\}$ NMR data (CDCl_3 , 125.7 MHz, 293 K): $\delta_{\text{C}} = 160.8$ ($\text{C}=\text{N}$), 156.0 ($p\text{-C}_6\text{H}_4\text{OCH}_3$), 135.7 ($ipso\text{-C}_6\text{H}_4\text{OCH}_3$), 124.5 ($m\text{-C}_6\text{H}_4\text{OCH}_3$), 114.1 ($o\text{-C}_6\text{H}_4\text{CH}_3$), 65.2 ($\text{C}=\text{NCH}$ imidazoline), 56.2 (CH_2 imidazoline), 55.4 ($\text{C}_6\text{H}_4\text{OCH}_3$), 33.8 ($(\text{CH}_3)_2\text{CH}$), 19.7 (CH_3 isopropyl), 19.1 (CH_3 isopropyl), ($\text{CH}_{\text{bridge}}$ not observed) ppm. IR data (KBr disc, cm^{-1}): 3447 (br. w), 2992 (w), 2961 (s), 2866 (w), 2837 (w), 2068 (w), 1917 (w), 1887 (w), 1845 (w), 1607 (s), 1577 (m), 1538 (s), 1515 (s), 1461 (m), 1438 (w), 1431 (w), 1385 (m), 1365 (w), 1359 (w), 1326 (w), 1307 (w), 1294 (m), 1277 (m), 1248 (s), 1205 (m), 1177 (m), 1139 (m), 1126 (m), 1103 (m), 1077 (w), 1039 (s), 973 (w), 962 (w), 917 (w), 904 (w), 835 (s), 808 (m), 783 (m), 724 (m), 716 (m), 692 (w), 661 (w), 619 (w), 600 (m), 570 (w), 552 (m), 514 (w), 467 (w), 436 (w), 421 (w), 404 (w). Accurate mass ES-MS for $[\text{Ar}^{\text{OMe}}\text{BIM}+\text{H}]^+$: $m/z = 449.2906$ (calc. for $\text{C}_{27}\text{H}_{37}\text{N}_4\text{O}_2$: 449.2917).

6.4.2.3 [8c]



^1H NMR data (CDCl_3 , 500.1 MHz, 293 K): $\delta_{\text{H}} = 7.04$ (8 H, app. d, $^3J_{\text{HH}} = 1.5$ Hz, *m*- $\text{C}_6\text{H}_4\text{CH}_3$ and *o*- $\text{C}_6\text{H}_4\text{CH}_3$), 3.79 (2 H, m, NCH_2), 3.63 (2 H, m, NCH_2CH), 3.44 (2 H, m, NCH_2), 2.28 (6 H, s, $\text{C}_6\text{H}_4\text{CH}_3$), 1.72 (2 H, m, $(\text{CH}_3)_2\text{CH}$), 1.09 (6 H, br. d, $^3J_{\text{HH}} = 6.5$ Hz, $\text{CH}(\text{CH}_3)_2$), 0.93 (6 H, dd, $^3J_{\text{HH}} = 6.5$ Hz, $\text{CH}(\text{CH}_3)_2$), ($\text{CH}_{\text{bridge}}$ not observed) ppm. $^{13}\text{C}\{^1\text{H}\}$ NMR data (CDCl_3 , 125.7 MHz, 293 K): $\delta_{\text{C}} = 159.9$ ($\text{C}=\text{N}$), 139.9 (*ipso*- $\text{C}_6\text{H}_4\text{CH}_3$), 132.5 (*p*- $\text{C}_6\text{H}_4\text{CH}_3$), 129.3 (*o*- $\text{C}_6\text{H}_4\text{CH}_3$), 122.2 (*m*- $\text{C}_6\text{H}_4\text{CH}_3$), 65.0 ($\text{C}=\text{NCH}$ imidazoline), 55.5 (CH_2 imidazoline), 33.8 ($(\text{CH}_3)_2\text{CH}$), 20.7 ($\text{C}_6\text{H}_4\text{CH}_3$), 19.6 (CH_3 isopropyl), 19.1 (CH_3 isopropyl), ($\text{CH}_{\text{bridge}}$ not observed) ppm. IR data (KBr disc, cm^{-1}): 3554 (w), 3480 (w), 3413 (w), 3031 (w), 2963 (s), 2917 (m), 2867 (m), 2823 (m), 1895 (w), 1623 (s), 1601 (s), 1571 (m), 1533 (s), 1509 (s), 1471 (m), 1385 (m), 1324 (m), 1260 (s), 1194 (m), 1171 (m), 1105 (br. s), 1023 (br. s), 862 (w), 801 (s), 722 (m), 711 (m), 631 (w), 550 (m), 502 (w). Accurate mass ES-MS for $[\text{Ar}^{\text{Mc}}\text{BIM}+\text{H}]^+$: $m/z = 417.3018$ (calc. for $\text{C}_{27}\text{H}_{37}\text{N}_4$: 417.3006).

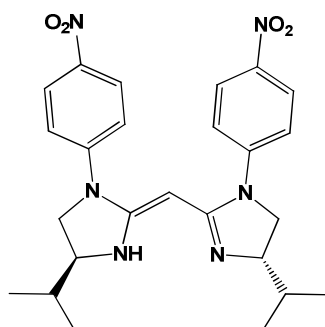
6.4.2.4 [8d]



^1H NMR data (CDCl_3 , 500.1 MHz, 293 K): $\delta_{\text{H}} = 7.23$ (4 H, m, *m*- C_6H_5), 7.14 (4 H, m, *o*- C_6H_5), 6.97 (2 H, app. t, $^3J_{\text{HH}} = 7.3$ Hz, *p*- C_6H_5), 3.82 (2 H, app. dt, $^3J_{\text{HH}} = 8.4$ Hz, $^3J_{\text{HH}} = 6.0$ Hz, $^4J_{\text{HH}} = 2.3$ Hz NCH_2), 3.65 (2 H, app. q, $^3J_{\text{HH}} = 8.4$ Hz, NCH_2CH),

3.48 (2 H, m, NCH_2), 1.73 (2 H, m, $(\text{CH}_3)_2\text{CH}$), 1.10 (6 H, dd, $^3J_{\text{HH}} = 6.6 \text{ Hz}$, $^3J_{\text{HH}} = 6.6 \text{ Hz}$, $\text{CH}(\text{CH}_3)_2$), 0.94 (6 H, dd, $^3J_{\text{HH}} = 6.6 \text{ Hz}$, $^3J_{\text{HH}} = 6.6 \text{ Hz}$, $\text{CH}(\text{CH}_3)_2$), ($\text{CH}_{\text{bridge}}$ not observed) ppm. $^{13}\text{C}\{^1\text{H}\}$ NMR data (CDCl_3 , 75.5 MHz, 293 K): $\delta_{\text{C}} = 159.8$ ($\text{C}=\text{N}$), 159.7 ($\text{C}=\text{N}$), 142.4 (*ipso*- C_6H_5), 128.9 (*m*- C_6H_5), 123.0 (*p*- C_6H_5), 122.0 (*o*- C_6H_5), 65.1 ($\text{C}=\text{NCH}_{\text{imidazoline}}$), 64.9 ($\text{C}=\text{NCH}_{\text{imidazoline}}$), 55.3 ($\text{CH}_2_{\text{imidazoline}}$), 55.2 ($\text{CH}_2_{\text{imidazoline}}$), 33.9 ($(\text{CH}_3)_2\text{CH}$), 19.7 ($\text{CH}_3_{\text{isopropyl}}$), 19.6 ($\text{CH}_3_{\text{isopropyl}}$), 19.2 ($\text{CH}_3_{\text{isopropyl}}$), ($\text{CH}_{\text{bridge}}$ not observed) ppm. IR data (KBr disc, cm^{-1}): 3393 (w), 3313 (w), 3061 (w), 3027 (w), 2960 (s), 2866 (m), 1948 (w), 1619 (s), 1592 (m), 1556 (m), 1536 (s), 1499 (s), 1458 (br. m), 1412 (w), 1378 (w), 1362 (w), 1308 (w), 1261 (s), 1201 (w), 1174 (w), 1131 (w), 1077 (w), 1043 (w), 909 (w), 802 (m), 752 (m), 725 (w), 698 (m), 645 (w), 577 (w), 550 (m), 504 (w). Accurate mass ES-MS for $[\text{Ar}^{\text{H}}\text{-BIM}+\text{H}]^+$: $m/z = 389.5563$ (calc. for $\text{C}_{25}\text{H}_{32}\text{N}_4$: 389.2702).

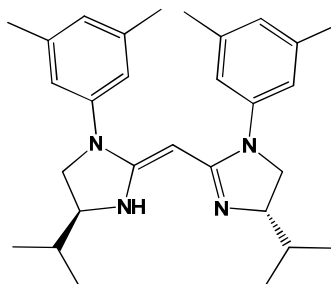
6.4.2.5 [8e]



^1H NMR data (CDCl_3 , 500.1 MHz, 293 K): $\delta_{\text{H}} = 8.16$ (4 H, app. dd, $^3J_{\text{HH}} = 9.2 \text{ Hz}$, $^3J_{\text{HH}} = 2.5 \text{ Hz}$, *m*- $\text{C}_6\text{H}_4\text{NO}_2$), 7.19 (4 H, app. dd, $^3J_{\text{HH}} = 9.2 \text{ Hz}$, $^3J_{\text{HH}} = 4.4 \text{ Hz}$, *o*- $\text{C}_6\text{H}_4\text{NO}_2$), 4.77 (1 H, app. d, $J = 9.2 \text{ Hz}$, $\text{CH}_{\text{bridge}}$), 3.93 (2 H, q, $^3J_{\text{HH}} = 8.8 \text{ Hz}$, NCH_2), 3.75 (2 H, q, $^3J_{\text{HH}} = 7.5 \text{ Hz}$, NCH_2CH), 3.60 (2 H, t, $^3J_{\text{HH}} = 8.8 \text{ Hz}$, NCH_2), 1.82-1.70 (2 H, br. m, $(\text{CH}_3)_2\text{CH}$), 1.07 (6 H, t, $^3J_{\text{HH}} = 6.6 \text{ Hz}$, $\text{CH}(\text{CH}_3)_2$), 0.97 (6 H, dd, $^3J_{\text{HH}} = 6.6 \text{ Hz}$, $^3J_{\text{HH}} = 4.2 \text{ Hz}$, $\text{CH}(\text{CH}_3)_2$) ppm. $^{13}\text{C}\{^1\text{H}\}$ NMR data (CDCl_3 , 125.7 MHz, 293 K): $\delta_{\text{C}} = 157.5$ ($\text{C}=\text{N}$), 147.5 (*p*- $\text{C}_6\text{H}_4\text{NO}_2$), 141.6 (*ipso*- $\text{C}_6\text{H}_4\text{NO}_2$), 125.1 (*m*- $\text{C}_6\text{H}_4\text{NO}_2$), 119.0 (*o*- $\text{C}_6\text{H}_4\text{NO}_2$), 64.7 ($\text{C}=\text{NCH}_{\text{imidazoline}}$), 64.7 ($\text{C}=\text{NCH}_{\text{imidazoline}}$), 61.8 ($\text{CH}_{\text{bridge}}$), 54.5 ($\text{CH}_2_{\text{imidazoline}}$), 33.5 ($(\text{CH}_3)_2\text{CH}$), 18.90 ($\text{CH}_3_{\text{isopropyl}}$), 18.87 ($\text{CH}_3_{\text{isopropyl}}$) ppm. IR data (KBr disc, cm^{-1}): 3374 (br. m), 3111 (m), 3079 (m), 2958 (s), 2934 (m), 2867 (m), 2628 (w), 2433 (w), 1623 (s), 1595 (s), 1549 (s), 1501 (s), 1467 (s), 1430 (m), 1362 (m), 1326 (s), 1275 (s), 1256 (s), 1186 (s), 1139 (m), 1112 (s), 1069 (m), 1043 (m), 1003 (m), 926 (w), 906 (w), 864 (m),

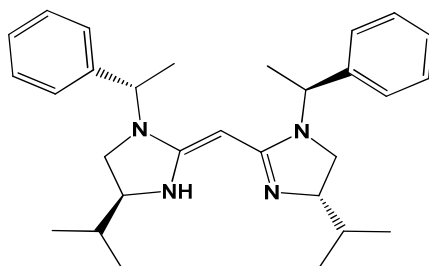
853 (m), 827 (m), 814 (m), 753 (m), 713 (m), 693 (m), 628 (w), 558 (w), 528 (w), 512 (w), 480 (w), 465 (w), 416 (w). Accurate mass ES-MS for $[\text{O}_2\text{N}(\text{C}_6\text{H}_5)\text{NCH}_2\text{CH}((\text{CH}_3)_2)\text{NH}=\text{CH}]^+$: $m/z = 234.1239$ (calc. for $\text{C}_{12}\text{H}_{16}\text{N}_3\text{O}_2$: 234.1243).

6.4.2.6 [8f]



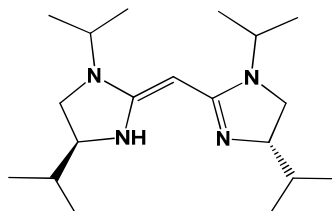
^1H NMR data (CDCl_3 , 500.1 MHz, 293 K): $\delta_{\text{H}} = 6.77$ (4 H, s, $o\text{-C}_6\text{H}_3(\text{CH}_3)_2$), 6.64 (2 H, s, $p\text{-C}_6\text{H}_3(\text{CH}_3)_2$), 3.77 (2 H, app. t, $^3J_{\text{HH}} = 8.3$ Hz, NCH_2), 3.62 (2 H, app. q, $^3J_{\text{HH}} = 8.5$ Hz, NCH_2CH), 3.43 (2 H, app. t, $^3J_{\text{HH}} = 8.3$ Hz, NCH_2), 2.34 (12 H, br. s, $\text{C}_6\text{H}_3(\text{CH}_3)_2$), 1.71 (2 H, m, $(\text{CH}_3)_2\text{CH}$), 1.10 (6 H, d, $^3J_{\text{HH}} = 6.6$ Hz, $\text{CH}(\text{CH}_3)_2$), 0.94 (6 H, d, $^3J_{\text{HH}} = 6.6$ Hz, $\text{CH}(\text{CH}_3)_2$), ($\text{CH}_{\text{bridge}}$ not observed) ppm. $^{13}\text{C}\{^1\text{H}\}$ NMR data (CDCl_3 , 100.6 MHz, 293 K): $\delta_{\text{C}} = 160.1$ ($\text{C}=\text{N}$), 142.3 ($ipso\text{-C}_6\text{H}_3(\text{CH}_3)_2$), 138.3 ($m\text{-C}_6\text{H}_3(\text{CH}_3)_2$), 124.8 ($p\text{-C}_6\text{H}_3(\text{CH}_3)_2$), 119.9 ($o\text{-C}_6\text{H}_3(\text{CH}_3)_2$), 64.9 ($\text{C}=\text{NCH}$ imidazoline), 55.5 (CH_2 imidazoline), 33.8 ($(\text{CH}_3)_2\text{CH}$), 21.4 ($\text{C}_6\text{H}_3(\text{CH}_3)_2$), 19.7 (CH_3 isopropyl), 19.1 (CH_3 isopropyl), ($\text{CH}_{\text{bridge}}$ not observed) ppm. IR data (KBr disc, cm^{-1}): 3011 (w), 2961 (s), 2917 (s), 2861 (s), 1621 (s), 1591 (s), 1541 (s), 1460 (s), 1375 (m), 1357 (m), 1334 (m), 1312 (w), 1284 (m), 1258 (s), 1227 (w), 1196 (s), 1165 (w), 1124 (s), 1096 (w), 1078 (w), 1051 (m), 971 (w), 915 (w), 878 (w), 860 (w), 834 (s), 802 (m), 767 (w), 722 (m), 698 (m), 642 (w), 604 (w), 594 (w), 534 (m), 496 (w), 477 (w), 458 (w), 418 (w). Accurate mass ES-MS for $[\text{Ar}^{3,5\text{Me}}\text{-BIM}+\text{H}]^+$: $m/z = 445.3322$ (calc. for $\text{C}_{29}\text{H}_{41}\text{N}_4$: 445.3331).

6.4.2.7 [8g]



^1H NMR data (CDCl_3 , 500.1 MHz, 293 K): $\delta_{\text{H}} = 7.34$ (4 H, app. t, $^3J_{\text{HH}} = 7.6$ Hz, $m\text{-C}_6\text{H}_5$), 7.29 (2 H, d, $^3J_{\text{HH}} = 7.3$ Hz, $p\text{-C}_6\text{H}_5$), 7.13 (4 H, d, $^3J_{\text{HH}} = 7.3$ Hz, $o\text{-C}_6\text{H}_5$), 4.53 (2 H, q, $^3J_{\text{HH}} = 6.9$ Hz, $\text{NHCH}(\text{CH}_3)(\text{C}_6\text{H}_5)$), 3.95 (2 H, m, NCH_2CH), 3.70 (1 H, br. s, $\text{CH}_{\text{bridge}}$) 3.49 (2 H, t, $^3J_{\text{HH}} = 10.0$ Hz, NCH_2), 3.03 (2 H, dd, $^3J_{\text{HH}} = 6.8$ Hz, $^3J_{\text{HH}} = 9.6$ Hz, NCH_2), 2.15 (2 H, m, $(\text{CH}_3)_2\text{CH}$), 1.42 (6 H, d, $^3J_{\text{HH}} = 7.0$ Hz, $\text{NHCH}(\text{CH}_3)(\text{C}_6\text{H}_5)$), 0.89 (6 H, d, $^3J_{\text{HH}} = 6.8$ Hz, $\text{CH}(\text{CH}_3)_2$), 0.84 (6 H, d, $^3J_{\text{HH}} = 6.8$ Hz, $\text{CH}(\text{CH}_3)_2$) ppm. $^{13}\text{C}\{^1\text{H}\}$ NMR data (CDCl_3 , 125.7 MHz, 293 K): $\delta_{\text{C}} = 160.1$ ($\text{C}=\text{N}$), 140.2 ($ipso\text{-C}_6\text{H}_5$), 128.8 ($m\text{-C}_6\text{H}_5$), 127.8 ($p\text{-C}_6\text{H}_5$), 126.2 ($o\text{-C}_6\text{H}_5$), 59.5 (NCH_2CH), 56.3 ($\text{CH}_{\text{bridge}}$), 53.3 ($\text{CH}(\text{CH}_3)(\text{C}_6\text{H}_5)$), 45.3 (NCH_2 imidazoline), 31.5 ($(\text{CH}_3)_2\text{CH}$), 18.6 (CH_3 isopropyl), 17.7 ($\text{CH}(\text{CH}_3)(\text{C}_6\text{H}_5)$), 16.2 (CH_3 isopropyl) ppm. IR data (KBr disc, cm^{-1}): 3429 (br. m), 3200 (br s), 3140 (br. s), 3059 (m), 2956 (s), 2871 (s), 2206 (w), 1972 (w), 1951 (w), 1894 (w), 1878 (w), 1807 (w), 1739 (m), 1564 (br. s) 1502 (s), 1454 (s), 1388 (m), 1378 (m), 1370 (m), 1332 (s), 1278 (s), 1231 (m), 1213 (m), 1191 (m), 1130 (m), 1090 (s), 1069 (m), 1025 (s), 990 (m), 979 (m), 914 (w), 853 (w), 818 (w), 786 (m), 773 (m), 759 (m), 731 (m), 700 (s), 649 (m), 590 (w), 555 (m), 493 (w). Accurate mass ES-MS for $[\text{NHCH}(\text{CH}_3)(\text{C}_6\text{H}_5)\text{-BIM+H}]^+$: $m/z = 445.3324$ (calc. for $\text{C}_{29}\text{H}_{41}\text{N}_4$: 445.3326).

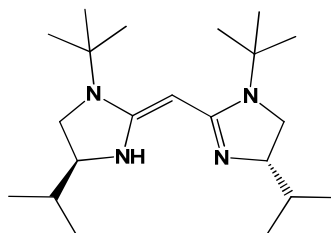
6.4.2.8 [8h]



^1H NMR data (CDCl_3 , 500.1 MHz, 293 K): $\delta_{\text{H}} = 3.91$ (2 H, m, NCH_2CH), 3.78 (2 H, sept., $^3J_{\text{HH}} = 6.7$ Hz, $(\text{CH}_3)_2\text{CHNH}$), 3.68 (1 H, br. s, $\text{CH}_{\text{bridge}}$), 3.41 (2 H, t, $^3J_{\text{HH}} = 9.7$ Hz,

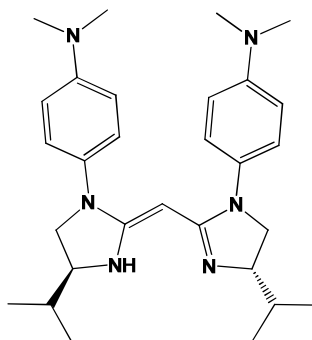
NCH₂), 3.15 (2 H, dd, ³J_{HH} = 9.5 Hz, ³J_{HH} = 6.6 Hz, NCH₂), 2.20 (2 H, m, (CH₃)₂CH), 1.18 (12 H, dd, ³J_{HH} = 6.7 Hz, ³J_{HH} = 2.5 Hz, NHCH(CH₃)₂), 0.94 (6 H, d, ³J_{HH} = 6.7 Hz, CH(CH₃)₂), 0.87 (6 H, d, ³J_{HH} = 6.7 Hz, CH(CH₃)₂) ppm. ¹³C{¹H} NMR data (CDCl₃, 125.7 MHz, 293 K): δ_C = 159.7 (C=N), 59.2 (C=NCH imidazoline), 54.7 (CH bridge), 45.7 (NHCH(CH₃)₂), 43.3 (CH₂ imidazoline), 31.6 ((CH₃)₂CH), 19.4 (NHCH(CH₃)₂), 19.3 (NHCH(CH₃)₂), 18.7 (CH₃ isopropyl), 16.0 (CH₃ isopropyl) ppm. IR data (KBr disc, cm⁻¹): 3440 (br. m), 3210 (br. m), 3144 (br. m), 2953 (s), 2868 (m), 1569 (br. s), 1503 (s), 1479 (m), 1462 (m), 1443 (m), 1389 (w), 1362 (m), 1332 (s), 1280 (s), 1224 (m), 1201 (m), 1146 (w), 1124 (m), 1111 (m), 1068 (m), 1017 (w), 984 (w), 925 (w), 884 (w), 816 (w), 736 (m), 657 (br. w), 513 (w), 453 (w), 436 (w), 404 (w). Accurate mass ES-MS for [iPr-BIM+H]⁺: m/z = 321.3015 (calc. for C₁₉H₃₇N₄: 321.3013).

6.4.2.9 [8i]

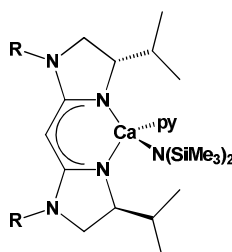


¹H NMR data (CDCl₃, 500.1 MHz, 293 K): δ_H = 3.42 (2 H, app. t, ³J_{HH} = 7.9 Hz, NCH₂), 3.25 (2 H, m, NCH₂CH) 2.85 (2 H, app. t, ³J_{HH} = 8.8 Hz, NCH₂), 1.54 (2 H, m, (CH₃)₂CH), 1.33 (9 H, s, C(CH₃)₃), 1.00 (6 H, d, ³J_{HH} = 6.5 Hz, CH(CH₃)₂), 0.83 (6 H, d, ³J_{HH} = 6.5 Hz, CH(CH₃)₂), (CH bridge not observed) ppm. ¹³C{¹H} NMR data (CDCl₃, 125.7 MHz, 293 K): δ_C = 162.2 (C=N), 63.8 (C=NCH imidazoline), 52.4 (CH₂ imidazoline), 52.0 (C(CH₃)₃), 33.7 ((CH₃)₂CH), 28.7 (C(CH₃)₃) 19.9 (CH₃ isopropyl), 19.2 (CH₃ isopropyl), (CH bridge not observed) ppm. IR data (KBr disc, cm⁻¹): 3465 (br. m), 2964 (br. s), 2867 (m), 2810 (m), 1604 (s), 1529 (s), 1469 (m), 1391 (m), 1362 (m), 1294 (m), 1264 (s), 1227 (s), 1166 (w), 1122 (m), 1095 (s), 1065 (m), 1017 (m), 973 (w), 921 (w), 802 (s), 732 (m), 698 (w), 646 (w), 547 (w), 468 (w). Accurate mass ES-MS for [tBu-BIM+H]⁺: m/z = 349.3344 (calc. for C₂₁H₄₁N₄: 349.3331).

6.4.2.10 [8j]



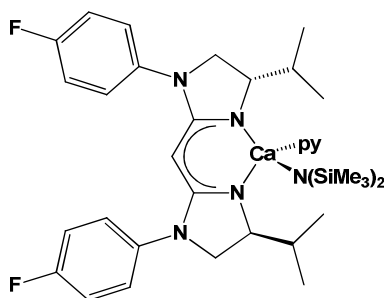
^1H NMR data (CDCl_3 , 500.1 MHz, 293 K): $\delta_{\text{H}} = 6.85$ (4 H, d, $^3J_{\text{HH}} = 9.0$ Hz, $m\text{-C}_6\text{H}_4\text{N}(\text{CH}_3)_2$), 6.51 (4 H, d, $^3J_{\text{HH}} = 9.0$ Hz, $o\text{-C}_6\text{H}_4\text{N}(\text{CH}_3)_2$), 4.02 (2 H, m, NCH_2CH), 3.76 (2 H, app. t, $^3J_{\text{HH}} = 9.6$ Hz, NCH_2), 3.58 (1 H, br. s, $\text{CH}_{\text{bridge}}$), 3.48 (2 H, app. q, $^3J_{\text{HH}} = 9.6$ Hz, $^4J_{\text{HH}} = 3.4$ Hz, NCH_2), 2.87 (12 H, br. s, $\text{C}_6\text{H}_4\text{N}(\text{CH}_3)_2$), 2.25 (2 H, m, $(\text{CH}_3)_2\text{CH}$), 0.96 (12 H, t, $^3J_{\text{HH}} = 6.7$ Hz, $\text{CH}(\text{CH}_3)_2$). $^{13}\text{C}\{^1\text{H}\}$ NMR data (CDCl_3 , 125.7 MHz, 293 K): $\delta_{\text{C}} = 159.9$ ($\text{C}=\text{N}$), 149.2 ($p\text{-C}_6\text{H}_4\text{N}(\text{CH}_3)_2$), 127.9 ($ipso\text{-C}_6\text{H}_4\text{N}(\text{CH}_3)_2$), 126.5 ($m\text{-C}_6\text{H}_4\text{N}(\text{CH}_3)_2$), 112.5 ($o\text{-C}_6\text{H}_4\text{N}(\text{CH}_3)_2$), 59.9 ($\text{C}=\text{NCH}$ imidazoline), 57.7 ($\text{CH}_{\text{bridge}}$), 52.6 (CH_2 imidazoline), 40.4 ($\text{C}_6\text{H}_4\text{N}(\text{CH}_3)_2$), 31.6 ($(\text{CH}_3)_2\text{CH}$), 18.5 (CH_3 isopropyl), 16.1 (CH_3 isopropyl) ppm. IR data (KBr disc, cm^{-1}): 3419 (br. w), 3198 (s), 3117 (br. s), 2956 (s), 2870 (w), 2805 (s), 2675 (m), 2604 (m), 2531 (w), 2497 (m), 1683 (w), 1569 (s), 1522 (s), 1446 (s), 1388 (m), 1360 (s), 1337 (s), 1308 (s), 1272 (s), 1226 (s), 1186 (m), 1169 (m), 1145 (m), 1068 (m), 1028 (m), 999 (w), 979 (w), 945 (m), 815 (s), 760 (w), 746 (w), 725 (w), 679 (m), 638 (w), 546 (m), 488 (w), 418 (w), 406 (w). Accurate mass ES-MS for $[\text{Ar}^{\text{NMe}_2}\text{-BIM}+\text{H}]^+$: $m/z = 475.3543$ (calc. for $\text{C}_{29}\text{H}_{43}\text{N}_6$: 475.3549).

6.4.3 NMR Scale Preparation of $[\text{Ca}(\text{R-BIM})\{\text{N}(\text{SiMe}_3)_2\}(\text{py})]$ [10a-j]

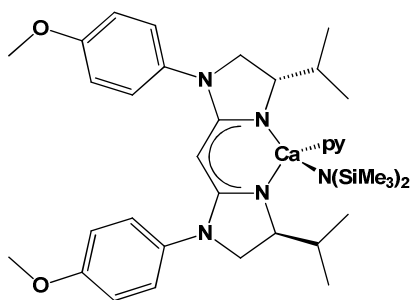
$[\text{Ca}\{\text{N}(\text{SiMe}_3)_2\}_2(\text{py})_2]$ was prepared from the corresponding analogue $[\text{Ca}\{\text{N}(\text{SiMe}_3)_2\}_2(\text{THF})_2]$ (*vide supra*) via literature procedures.⁷ R-BIM **8a-j**

(30mg, 0.07 mmol) in dry toluene (0.5ml) was added to 1 equivalent of $[\text{Ca}\{\text{N}(\text{SiMe}_3)_2\}_2(\text{py})_2]$ (ca. 0.037 g, 0.07 mmol). The solution was agitated briefly and allowed to react for 18 hours at ambient temperature under an inert atmosphere. The resulting complex was typically realised as an orange powder when dried *in vacuo* to approximately 4×10^{-2} mbar.

6.4.3.1 $[\text{Ca}(\text{Ar}^{\text{F}}\text{-BIM})\{\text{N}(\text{Si}(\text{CH}_3)_3)_2\}(\text{py})]$ [10a]



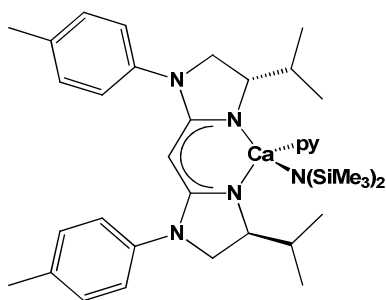
^1H NMR data (THF- d_8 , 500.1 MHz, 293 K): $\delta_{\text{H}} = 8.54$ (2 H, m, 2,6-NC $_5$ H $_5$), 7.64 (1 H, m, 4-NC $_5$ H $_5$), 7.24 (2 H, m, 3,5-NC $_5$ H $_5$), 7.10-7.02 (4 H, m, *o*-C $_6$ H $_4$ F), 6.87 (4 H, app. t, $^3\text{J} = 8.7$ Hz, *m*-C $_6$ H $_4$ F), 3.90 (2 H, m, NCH $_2$ CH), 3.52 (2 H, NCH $_2$), 3.48 (1 H, s, CH bridge), 3.40 (2 H, NCH $_2$), 2.04 (2 H, m, (CH $_3$) $_2$ CH), 0.89 (6 H, d, $^3\text{J}_{\text{HH}} = 6.8$ Hz, CH(CH $_3$) $_2$), 0.78 (6 H, d, $^3\text{J}_{\text{HH}} = 6.8$ Hz, CH(CH $_3$) $_2$), 0.10 (18 H, s, N(Si(CH $_3$) $_3$) ppm. $^{13}\text{C}\{^1\text{H}\}$ NMR data (THF- d_8 , 75.5 MHz, 293 K): $\delta_{\text{C}} = 164.4$ (C=N), 159.2 (d, $^1\text{J}_{\text{CF}} = 239.9$ Hz, *p*-C $_6$ H $_4$ F), 150.8 (2,6-NC $_5$ H $_5$), 141.9 (d, $^4\text{J}_{\text{CF}} = 2.3$ Hz, *ipso*-C $_6$ H $_4$ F), 136.3 (4-NC $_5$ H $_5$), 125.8 (d, $^3\text{J}_{\text{CF}} = 7.5$ Hz, *o*-C $_6$ H $_4$ F), 124.3 (3,5-NC $_5$ H $_5$), 115.4 (d, $^2\text{J}_{\text{CF}} = 22.5$ Hz, *m*-C $_6$ H $_4$ F), 66.5 (C=NCH imidazoline), 57.8 (CH bridge), 52.1 (CH $_2$ imidazoline), 34.2 ((CH $_3$) $_2$ CH), 20.7 (CH $_3$ isopropyl), 15.7 (CH $_3$ isopropyl), 2.7 (N(Si(CH $_3$) $_3$) $_2$) ppm. ^{19}F NMR data (THF- d_8 , 282.8 MHz, 293 K): $\delta_{\text{F}} = -121.80$ (s, *p*-C $_6$ H $_4$ F) ppm. IR data (KBr disc, cm^{-1}): 3419 (br. w) 2960 (m), 2873 (w), 2240 (w), 1621 (m) 1593 (w), 1544 (s), 1479 (w), 1428 (w), 1387 (w), 1316 (w), 1260 (m), 1222 (m), 1097 (m), 1018 (m), 837 (m), 798 (m), 720 (w), 668 (w), 594 (w), 551 (m), 422 (w), 417 (w).

6.4.3.2 [Ca(Ar^{OMe}-BIM){N(SiMe₃)₂}(py)] [10b]

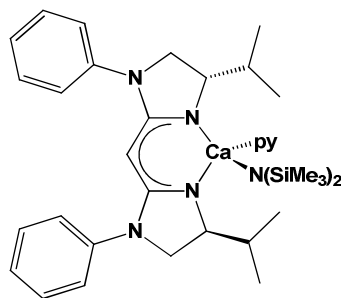
¹H NMR data (d₈-THF, 500.1 MHz, 293 K): δ_H = 8.56 (2 H, m, 2,6-NC₅H₅), 7.65 (1 H, m, 4-NC₅H₅), 7.24 (2 H, m, 3,5-NC₅H₅), 6.99 (2 H, d, ³J_{HH} = 8.8 Hz, *m*-C₆H₄OCH₃), 6.95 (2 H, d, ³J_{HH} = 8.8 Hz, *m*-C₆H₄OCH₃), 6.68 (4 H, app. dd, ³J_{HH} = 8.8 Hz, ³J_{HH} = 2.7 Hz, *o*-C₆H₄OCH₃), 3.89 (2 H, app. dt, ³J_{HH} = 9.1 Hz, ³J_{HH} = 3.1 Hz, NCH₂CH), 3.69 (6 H, br. s, C₆H₄OCH₃), 3.48 (2 H, q, ³J_{HH} = 8.8 Hz, NCH₂), 3.29 (1 H, s, CH bridge), 3.23 (2 H, m, NCH₂), 2.06 (1 H, m, (CH₃)₂CH), 1.86 (1 H, m, (CH₃)₂CH), 0.88 (4 H, app t, ³J_{HH} = 6.6 Hz, CH(CH₃)₂), 0.85 (2 H, d, ³J_{HH} = 6.9 Hz, CH(CH₃)₂), 0.80 (4 H, d, ³J_{HH} = 6.6 Hz, CH(CH₃)₂), 0.75 (2 H, d, ³J_{HH} = 6.9 Hz, CH(CH₃)₂), 0.11 (18 H, s, N(Si(CH₃)₃)₂) ppm.

¹³C{¹H} NMR data (d₈-THF, 75.5 MHz, 293 K): δ_C = 165.6 (C=N), 165.2 (C=N), 156.6 (*p*-C₆H₅OCH₃), 156.5 (*p*-C₆H₅OCH₃), 150.8 (2,6-NC₅H₅), 138.5 (*ipso*-C₆H₄OCH₃), 138.4 (*ipso*-C₆H₄OCH₃), 136.3 (4-NC₅H₅), 125.97 (*m*-C₆H₄OCH₃), 125.94 (*m*-C₆H₄OCH₃), 124.3 (3,5-NC₅H₅), 114.3 (*o*-C₆H₄OCH₃), 114.2 (*o*-C₆H₄OCH₃), 66.6 (C=NCH imidazoline), 66.5 (C=NCH imidazoline), 57.8 (CH bridge), 55.4 (C₆H₄OCH₃), 52.2 (CH₂ imidazoline), 52.3 (CH₂ imidazoline), 34.5 ((CH₃)₂CH), 34.3 ((CH₃)₂CH), 20.8 (CH₃ isopropyl), 20.2 (CH₃ isopropyl), 20.1 (CH₃ isopropyl), 2.7 (N(Si(CH₃)₃)₂) ppm.

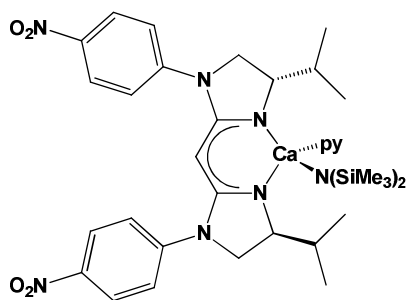
IR data (KBr disc, cm⁻¹): 3376 (br. w), 3039 (w), 2953 (s), 2868 (s), 2833 (s), 2239 (m), 2186 (w), 2122 (w), 2088 (w), 1869 (w), 1608 (s), 512 (s), 1464 (w), 1441 (w), 1383 (m), 1365 (m), 1244 (s), 1178 (m), 1144 (m), 1107 (m), 1040 (s), 970 (w), 932 (m), 882 (m), 831 (s), 783 (m), 752 (w), 721 (w), 703 (w), 660 (w), 638 (w), 752 (w), 721 (w), 555 (m), 485 (w).

6.4.3.3 [Ca(Ar^{Me}-BIM){N(SiMe₃)₂}(py)] [10c]

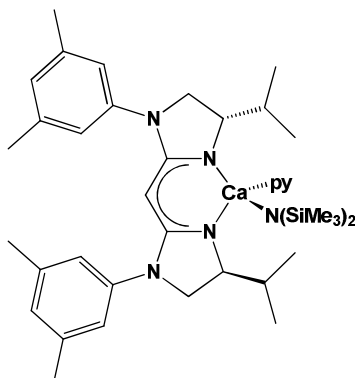
¹H NMR data (THF-d₈, 500.1 MHz, 293 K): δ_H = 8.56 (4 H, m, 2,6-NC₅H₅), 7.64 (2 H, m, 4-NC₅H₅), 7.24 (4 H, m, 3,5-NC₅H₅), 6.97-6.89 (8 H, m, *o*-C₆H₄CH₃ and *m*-C₆H₄CH₃), 3.89 (2 H, m, NCH₂CH), 3.69 (1 H, NCH₂), 3.67 (1 H, s, CH_{bridge}), 3.51 (1 H, NCH₂), 3.34 (1 H, NCH₂), 3.24 (1 H, NCH₂), 2.22 (3 H, br. s, C₆H₅CH₃), 2.20 (3 H, br. s, C₆H₅CH₃), 1.86 (2 H, m, (CH₃)₂CH), 0.87 (6 H, m, CH(CH₃)₂), 0.77 (6 H, app. t, ³J_{HH} = 6.7 Hz, CH(CH₃)₂), 0.11 (18 H, s, N(Si(CH₃)₃)₂) ppm. ¹³C{¹H} NMR data (THF-d₈, 75.5 MHz, 293 K): δ_C = 164.8 (C=N), 164.1 (C=N), 150.8 (2,6-NC₅H₅), 142.7 (*ipso*-C₆H₄CH₃), 142.1 (*ipso*-C₆H₄CH₃), 136.3 (4-NC₅H₅), 132.0 (*p*-C₆H₄CH₃), 131.3 (*p*-C₆H₄CH₃), 129.5 (*o*-C₆H₄CH₃), 129.4 (*o*-C₆H₄CH₃), 124.3 (3,5-NC₅H₅), 123.9 (*m*-C₆H₄CH₃), 123.2 (*m*-C₆H₄CH₃), 66.5 (C=NCH_{imidazoline}), 66.1 (C=NCH_{imidazoline}), 58.7 (CH_{bridge}), 51.8 (CH₂_{imidazoline}), 51.2 (CH₂_{imidazoline}), 34.9 ((CH₃)₂CH), 34.3 ((CH₃)₂CH), 20.8 (C₆H₄CH₃), 20.2 (CH₃_{isopropyl}), 15.4 (CH₃_{isopropyl}), 2.7 (N(Si(CH₃)₃)₂) ppm. IR data (KBr disc, cm⁻¹): 3027 (w), 2936 (s), 2867 (w), 2241 (w), 2179 (w), 2129 (w), 1652 (m), 1515 (s), 1455 (w), 1417 (w), 1315 (m), 1261 (s), 1100 (s), 1020 (s), 934 (w), 800 (s), 703 (w), 667 (w), 618 (w), 552 (w), 479 (m).

6.4.3.4 [Ca(Ph-BIM){N(SiMe₃)₂}(py)] [10d]

¹H NMR data (THF-d₈, 500.1 MHz, 293 K): δ_H = 8.57 (2 H, m, 2,6-NC₅H₅), 7.65 (1 H, m, 4-NC₅H₅), 7.25 (2 H, m, 3,5-NC₅H₅), 7.19-7.05 (8 H, m, *o/m*-C₆H₅), 6.85-6.73 (2 H, m, *p*-C₆H₅), 3.93-3.88 (2 H, m, NCH₂CH), 3.87 (1 H, br. s, CH bridge), 3.72-3.67 (1 H, m, NCH₂), 3.56 (2 H, dd, ³J_{HH} = 6.0 Hz, ³J_{HH} = 2.9 Hz, NCH₂), 3.28 (1 H, app. dt, ³J_{HH} = 8.8 Hz, ³J_{HH} = 2.4 Hz, NCH₂), 1.93-1.79 (2 H, m, (CH₃)₂CH), 0.91-0.86 (6 H, m, CH(CH₃)₂), 0.80-0.76 (6 H, m, CH(CH₃)₂), 0.12 (18 H, s, N(Si(CH₃)₃)₂) ppm. ¹³C{¹H} NMR data (THF-d₈, 75.5 MHz, 293 K): δ_C = 164.4 (C=N), 164.0 (C=N), 150.8 (2,6-NC₅H₅), 145.4 (*ipso*-C₆H₅), 144.3 (*ipso*-C₆H₅), 136.4 (4-NC₅H₅), 129.0 (*o*-C₆H₅), 128.96 (*o*-C₆H₅), 128.91 (*m*-C₆H₅), 128.8 (*m*-C₆H₅), 124.3 (3,5-NC₅H₅), 124.0 (*p*-C₆H₅), 123.7 (*p*-C₆H₅), 66.5 (C=NCH imidazoline), 66.3 (C=NCH imidazoline), 58.0 (CH bridge), 50.9 (CH₂ imidazoline), 50.6 (CH₂ imidazoline), 34.7 ((CH₃)₂CH), 34.3 ((CH₃)₂CH), 20.7 (CH₃ isopropyl), 20.0 (CH₃ isopropyl), 15.7 (CH₃ isopropyl), 15.3 (CH₃ isopropyl), 2.7 (N(Si(CH₃)₃)₂) ppm. IR data (KBr disc, cm⁻¹): 3060 (w), 3034 (w), 2955 (s), 2870 (m), 2238 (w), 2122 (w), 1935 (w), 1864 (w), 1594 (s), 1552 (m), 1522 (m), 1497 (s), 1399 (m), 1385 (m), 1365 (m), 1310 (m), 1261 (s), 1197 (w), 1177 (w), 1144 (w), 1106 (m), 1042 (m), 932 (w), 882 (w), 806 (m), 754 (m), 695 (m), 617 (w), 551 (w).

6.4.3.5 [Ca(Ar^{NO2}-BIM){N(SiMe₃)₂}(py)] [10e]

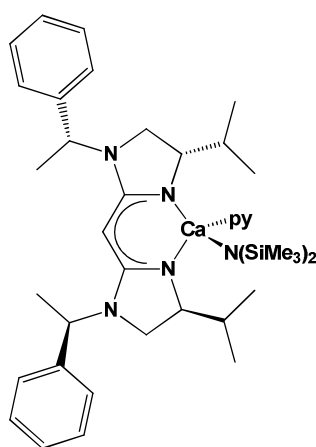
IR data (KBr disc, cm⁻¹): 3370 (br. w), 3185 (br. w), 3111 (w), 3078 (w), 2956 (m), 2869 (m), 2727 (w), 2642 (w), 2432 (w), 2233 (w), 2176 (w), 2126 (w), 1925 (w), 1821 (w), 1594 (s), 1563 (s), 1503 (s), 1429 (m), 1382 (m), 1326 (s), 1262 (s), 1231 (s), 1180 (s), 1143 (m), 1111 (s), 1073 (m), 1038 (s), 936 (m), 884 (m), 846 (m), 752 (m), 721 (w), 695 (m), 627 (w), 548 (w), 518 (w), 496 (w).

6.4.3.6 [Ca(Ar^{3,5Me}-BIM){N(SiMe₃)₂}(py)] [10f]

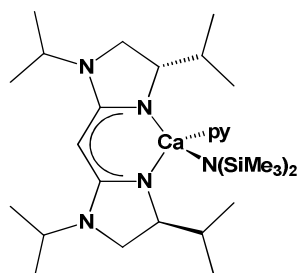
¹H NMR data (THF-d₈, 500.1 MHz, 293 K): δ_H = 8.57 (2 H, m, 2,6-NC₅H₅), 7.65 (1 H, m, 4-NC₅H₅), 7.25 (2 H, m, 3,5-NC₅H₅), 6.65 (4 H, s, *o*-C₆H₃(CH₃)₂), 6.52 (2 H, s, *p*-C₆H₃(CH₃)₂), 4.01 (1 H, br. s, CH_{bridge}), 3.90-3.86 (2 H, m, NCH₂CH), 3.66-3.64 (2 H, m, NCH₂), 3.29 (2 H, app. dt, ³J_{HH} = 8.7 Hz, ³J_{HH} = 2.0 Hz, NCH₂), 2.11 (12 H, s, C₆H₄(CH₃)₂), 1.90-1.79 (2 H, m, (CH₃)₂CH), 0.90 (6 H, d, ³J_{HH} = 6.8 Hz, CH(CH₃)₂), 0.73 (6 H, d, ³J_{HH} = 6.8 Hz, CH(CH₃)₂), 0.12 (18 H, s, N(Si(CH₃)₃) ppm. ¹³C{¹H} NMR data (THF-d₈, 75.5 MHz, 293 K): δ_C = 164.7 (C=N), 164.5 (C=N), 150.8 (2,6-NC₅H₅), 144.7 (*ipso*-C₆H₃CH₃), 144.6 (*ipso*-C₆H₄CH₃), 138.2 (*m*-C₆H₃(CH₃)₂), 136.4 (4-NC₅H₅), 124.3 (3,5-NC₅H₅), 124.0 (*p*-C₆H₃(CH₃)₂), 121.5 (*o*-C₆H₃(CH₃)₂), 66.2 (C=NCH imidazoline), 66.0 (C=NCH imidazoline) 57.7 (CH_{bridge}), 51.5 (CH₂ imidazoline), 51.4 (CH₂ imidazoline), 34.6

((CH₃)₂CH), 34.5 ((CH₃)₂CH), 21.5 (C₆H₃(CH₃)₂), 21.4 (C₆H₃(CH₃)₂), 20.3 (CH₃ isopropyl), 19.9 (CH₃ isopropyl), 15.3 (CH₃ isopropyl), 15.2 (CH₃ isopropyl), 2.7 (N(Si(CH₃)₃)₂) ppm. IR data (KBr disc, cm⁻¹): 3380 (br. w), 3011 (w), 2953 (s), 2919 (s), 2868 (s), 2237 (w), 2186 (w), 2116 (w), 2088 (w), 1595 (s), 1558 (s), 1516 (s), 1475 (s), 1383 (m), 1361 (m), 1312 (w), 1245 (s), 1201 (w), 1173 (w), 1143 (w), 1108 (w), 1043 (m), 950 (w), 931 (w), 872 (w), 837 (m), 751 (w), 727 (w), 699 (m), 618 (w), 506 (w), 464 (w), 423 (w), 413 (w).

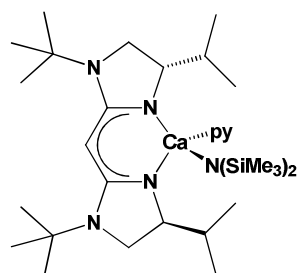
6.4.3.7 [Ca(PhMeH-BIM){N(SiMe₃)₂}(py)] [10g]



¹H NMR data (THF-d₈, 500.1 MHz, 293 K): δ_H = 8.54 (2 H, m, 2,6-NC₅H₅), 7.65 (1 H, m, 4-NC₅H₅), 7.35-7.19 (10 H, m, 3,5-NC₅H₅, *o*-C₆H₅, *m*-C₆H₅), 7.15-7.10 (2 H, m, *p*-C₅H₅), 4.67 (2 H, q, ³J_{HH} = 6.7 Hz, CH(CH₃)(C₆H₅)), 3.79 (2 H, m, NCH₂CH), 3.48 (1 H, br. s CH bridge), 2.93 (2 H, t, ³J_{HH} = 9.1 Hz, NCH₂), 2.66 (2 H, m, NCH₂), 2.05 (2 H, m, (CH₃)₂CH), 1.32 (6 H, d, ³J_{HH} = 6.8 Hz, CH(CH₃)(C₆H₅)), 0.73 (6 H, d, ³J_{HH} = 6.9 Hz, CH(CH₃)₂), 0.67 (6 H, d, ³J_{HH} = 6.9 Hz, CH(CH₃)₂) 0.04 (18 H, s, N(Si(CH₃)₃)₂) ppm. ¹³C{¹H} NMR data (THF-d₈, 75.5 MHz, 293 K): δ_C = 167.2 (C=N), 150.8 (2,6-NC₆H₅), 145.4 (*ipso*-C₆H₅), 136.3 (4-NC₆H₅), 128.9 (*o/m*-C₆H₅), 128.3 (*o/m*-C₆H₅), 127.7 (*p*-C₆H₅), 124.3 (3,5-NC₆H₅), 66.2 (C=NCH imidazoline), 55.0 (CH bridge), 54.0 (CH(CH₃)(C₆H₅)), 43.9 (CH₂ imidazoline), 34.4 ((CH₃)₂CH), 20.2 (CH₃ isopropyl), 15.8 (CH(CH₃)(C₆H₅)), 15.7 (CH₃ isopropyl), 2.7 (N(Si(CH₃)₃)₂) ppm. IR data (KBr disc, cm⁻¹): 3650 (w), 3571 (w), 3377 (w), 3088 (w), 3060 (w), 3029 (w), 2957 (s), 2870 (s), 2236 (w), 2203 (w), 2128 (w), 1948 (w), 1881 (w), 1804 (w), 1601 (s), 1494 (s), 1450 (s), 1385 (m), 1368 (m), 1261 (s), 1179 (m), 1095 (m), 1025 (s), 931 (m), 885 (m), 839 (m), 802 (m), 753 (m), 699 (s), 618 (w), 532 (w).

6.4.3.8 [Ca(iPr-BIM){N(SiMe₃)₂}(py)] [10h]

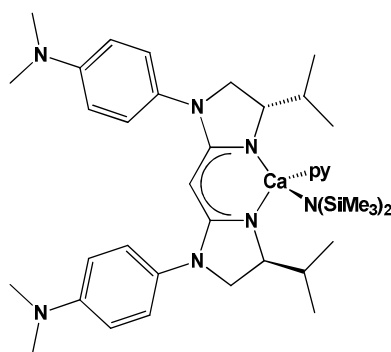
¹H NMR data (THF-d₈, 500.1 MHz, 293 K): $\delta_{\text{H}} = 8.57$ (2 H, m, 2,6-NC₆H₅), 7.65 (1 H, m, 4-NC₆H₅), 7.24 (2 H, m, 3,5-NC₆H₅), 150.8 (2,6-NC₆H₅), 136.3 (4-NC₆H₅), 3.81-3.65 (4 H, m, NCH(CH₃)₃ and NCH₂CH), 3.31 (1 H, br. s, CH_{bridge}), 2.90 (4 H, br. d, ³J_{HH} = 6.9 Hz, NCH₂), 2.07 (2 H, m, (CH₃)₂CH), 1.12 (6 H, NCH(CH₃)₂), 1.00 (6 H, NCH(CH₃)₂), 0.82 (6 H, CH(CH₃)₂), 0.68 (6 H, CH(CH₃)₂), 0.04 (18 H, s, N(Si(CH₃)₃) ppm. ¹³C{¹H} NMR data (THF-d₈, 75.5 MHz, 293 K): $\delta_{\text{C}} = 166.9$ (C=N), 150.8 (2,6-NC₆H₅), 136.3 (4-NC₆H₅), 124.3 (3,5-NC₆H₅), 65.9 (C=NCH imidazoline), 54.1 (CH_{bridge}), 46.2 (NCH(CH₃)₂), 42.2 (CH₂ imidazoline), 34.7 ((CH₃)₂CH), 21.4 (NCH(CH₃)₂), 20.4 (CH₃ isopropyl), 17.6 (NCH(CH₃)₂), 15.6 (CH₃ isopropyl), 2.7 (N(Si(CH₃)₃)₂) ppm. IR data (KBr disc, cm⁻¹): 3646 (w), 3248 (br. w), 29458 (s), 2870 (s), 1608 (s), 1540 (m), 1487 (m), 1456 (m), 1386 (w), 1366 (m), 1262 (m), 1177 (w), 1121 (w), 1109 (w), 1077 (w), 1060 (w), 1029 (m), 974 (w), 953 (w), 930 (w), 886 (w), 837 (w), 822 (w), 741 (w), 618 (w), 514 (w).

6.4.3.9 [Ca(tBu-BIM){N(SiMe₃)₂}(py)] [10i]

¹H NMR data (THF-d₈, 500.1 MHz, 293 K): $\delta_{\text{H}} = 8.55$ (2 H, m, 2,6-NC₅H₅), 7.64 (1 H, m, 4-NC₅H₅), 7.23 (2 H, m, 3,5-NC₅H₅), 3.83 (1 H, s, CH_{bridge}), 3.63-3.56 (2 H, m, partially obscured by solvent peak, NCH₂CH), 3.20-3.12 (2 H, m, NCH₂), 3.10-3.02 (2 H, m, NCH₂), 1.84-1.70 (2 H, m, partially obscured by solvent peak (CH₃)₂CH), 1.37 (18 H, s,

$C(\underline{CH}_3)_3$, 0.85 (3 H, d, $^3J_{HH} = 6.9$ Hz, $CH(\underline{CH}_3)_2$), 0.81 (3 H, app. t, $^3J_{HH} = 6.9$ Hz, $CH(\underline{CH}_3)_2$), 0.78 (3 H, d, $^3J_{HH} = 6.9$ Hz, $CH(\underline{CH}_3)_2$), 0.74 (3 H, app. t, $^3J_{HH} = 6.9$ Hz, $CH(\underline{CH}_3)_2$), 0.10 (18 H, $N(\underline{Si}(\underline{CH}_3)_2)$ ppm. $^{13}C\{^1H\}$ NMR data (THF- d_8 , 75.5 MHz, 293 K): $\delta_C = 167.0$ ($\underline{C}=\underline{N}$), 150.8 (2,6- \underline{NC}_5H_5), 136.3 (4- \underline{NC}_5H_5), 124.3 (3,5- \underline{NC}_5H_5), 64.5 ($\underline{C}=\underline{NCH}$ imidazoline), 62.5 (\underline{CH} bridge), 53.0 ($\underline{C}(\underline{CH}_3)_3$), 47.7 (\underline{CH}_2 imidazoline), 35.9 ($(\underline{CH}_3)_2\underline{CH}$), 29.87 ($\underline{C}(\underline{CH}_3)_2$), 20.2 (\underline{CH}_3 isopropyl), 15.8 (\underline{CH}_3 isopropyl), 2.7 ($N(\underline{Si}(\underline{CH}_3)_3)_2$) ppm. IR data (KBr disc, cm^{-1}): 2960 (s), 2871 (m), 1597 (s), 1528 (m), 1503 (w), 1464 (m), 1444 (w), 1396 (m), 1361 (m), 1312 (w), 1258 (s), 1229 (s), 1175 (w), 1101 (s), 1047 (s), 1018 (s), 929 (w), 861 (w), 802 (s), 748 (w), 699 (w), 670 (m), 640 (w), 615 (w), 527 (w), 473 (w).

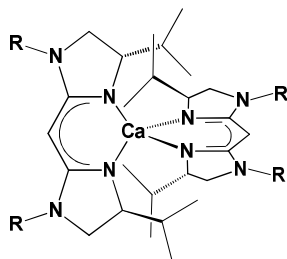
6.4.3.10 [$Ca(\text{Ar}^{\text{NMe}_2}\text{-BIM})\{N(\text{SiMe}_3)_2\}(\text{py})$] [10j]



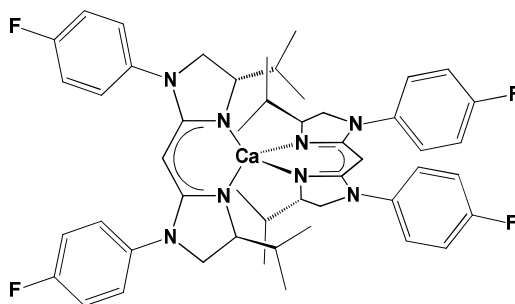
1H NMR data (THF- d_8 , 500.1 MHz, 293 K): $\delta_H = 8.56$ (2 H, m, 2,6- \underline{NC}_5H_5), 7.65 (1 H, m, 4- \underline{NC}_5H_5), 7.24 (2 H, m, 3,5- \underline{NC}_5H_5), 6.98 (4 H, d, $^3J_{HH} = 6.7$ Hz, $m\text{-C}_6H_4N(\underline{CH}_3)_2$), 6.60 (4 H, d, $^3J_{HH} = 6.7$ Hz, $o\text{-C}_6H_4N(\underline{CH}_3)_2$), 3.94 (1 H, br. s \underline{CH} bridge), 3.67 (2 H, t, $^3J_{HH} = 8.5$ Hz, NCH_2), 3.60-3.52 (2 H, br. m, partially obscured by solvent peak, $NCH_2\underline{CH}$), 3.32-3.25 (2 H, br. t, $^3J_{HH} = 8.2$ Hz, NCH_2), 2.83 (12 H, br. s, $C_6H_4N(\underline{CH}_3)_2$), 1.63 (2 H, m, $(\underline{CH}_3)_2\underline{CH}$), 1.04 (6 H, br. d, $^3J_{HH} = 6.6$ Hz, $CH(\underline{CH}_3)_2$), 0.91 (6 H, br. d, $^3J_{HH} = 6.6$ Hz, $CH(\underline{CH}_3)_2$) 0.04 (18 H, s, $N(\underline{Si}(\underline{CH}_3)_3)$ ppm. $^{13}C\{^1H\}$ NMR data (THF- d_8 , 75.5 MHz, 293 K): $\delta_C = 161.7$ ($\underline{C}=\underline{N}$), 150.4 (2,6- \underline{NC}_5H_5), 148.4 ($p\text{-C}_6H_4N(\underline{CH}_3)_2$), 136.4 (4- \underline{NC}_5H_5), 129.1 ($ipso\text{-C}_6H_4N(\underline{CH}_3)_2$), 124.5 (3,5- \underline{NC}_6H_5), 123.9 ($m\text{-C}_6H_4N(\underline{CH}_3)_2$), 113.5 ($o\text{-C}_6H_4N(\underline{CH}_3)_2$), 65.3 ($\underline{C}=\underline{NCH}$ imidazoline), 59.5 (\underline{CH} bridge), 56.3 (\underline{CH}_2 imidazoline), 40.7 ($C_6H_4N(\underline{CH}_3)_2$), 34.3 ($(\underline{CH}_3)_2\underline{CH}$), 19.4 (\underline{CH}_3 isopropyl), 19.1 (\underline{CH}_3 isopropyl), 2.2 ($N(\underline{Si}(\underline{CH}_3)_3)_2$) ppm. IR data (KBr disc, cm^{-1}): 3383 (br. w), 3229 (br. w), 3043 (s), 2953 (s), 2867 (s), 2813 (m), 2235 (w), 2103 (w), 1868 (w), 1611 (s), 1522 (s), 1481 (m), 1386 (m), 1356 (m), 1315 (m), 1273 (w), 1258 (m), 1187 (w), 1168 (m), 1139 (m), 1110 (m), 1083 (w), 1057

(w), 1019 (m), 944 (m), 885 (w), 819 (s), 752 (w), 725 (w), 701 (w), 641 (w), 618 (w), 553 (m), 496 (w), 469 (w).

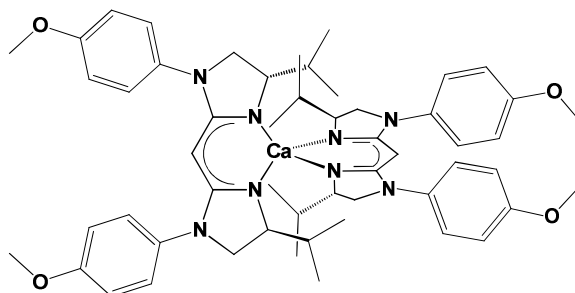
6.4.4 NMR Scale Preparation of [Ca(R-BIM)₂] [11a-j]



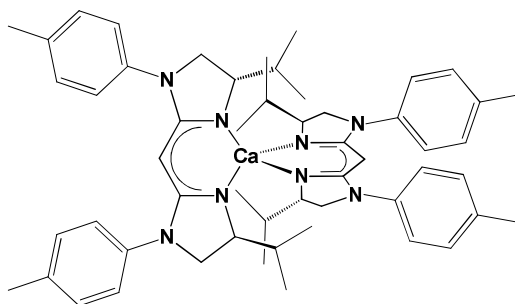
R-BIM **10a-j** (50mg, 0.31 mmol) in dry toluene (0.5 ml) was added to [Ca{N(SiMe₃)₂}(py)₂] (82.0mg, 0.16 mmol). The solution was agitated briefly and allowed to react for 18 hours at ambient temperature under an inert atmosphere. The resulting complex was typically realised as a dark orange powder when dried *in vacuo* to approximately 4×10^{-2} mbar. Despite obtaining spectroscopically pure complexes, and repeated recrystallization attempts, satisfactory elemental analyses could not be obtained. Given the highly air and moisture sensitive nature of these compounds, and literature precedence this is unsurprising.^{12,15}

6.4.4.1 [Ca(Ar^F-BIM)₂] [11a]

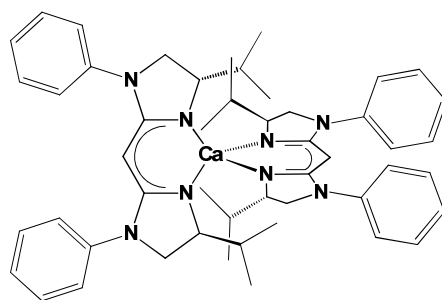
¹H NMR data (THF-d₈, 500.1 MHz, 293 K): δ_H = 7.07 (6 H, m, *m*-C₆H₄F), 6.97 (4 H, m, *o*-C₆H₄F), 6.88 (6 H, m, *m*-C₆H₄F and *o*-C₆H₄F), 4.10 (1 H, s, CH_{bridge}), 3.90 (2 H, m, NCH₂CH), 3.63 (2 H, m, NCH₂CH), 3.52 (4 H, NCH₂), 3.48 (1 H, s, CH_{bridge}), 3.39 (4 H, m, NCH₂), 2.05 (2 H, m, (CH₃)₂CH), 1.66 (2 H, m, (CH₃)₂CH), 1.04 (6 H, d, ³J_{HH} = 6.7 Hz, CH(CH₃)₂), 0.93 (6 H, d, ³J_{HH} = 6.7 Hz, CH(CH₃)₂), 0.89 (6 H, d, ³J_{HH} = 6.7 Hz, CH(CH₃)₂), 0.79 (6 H, d, ³J_{HH} = 6.7 Hz, CH(CH₃)₂) ppm. ¹³C{¹H} NMR data (THF-d₈, 75.5 MHz, 293 K): δ_C = 164.4 (C=N), 160.6 (C=N), 159.7 (d, ¹J_{CF} = 241.7 Hz, *p*-C₆H₄F), 159.2 (d, ¹J_{CF} = 239.4 Hz, *p*-C₆H₄F), 141.9 (d, ⁴J_{CF} = 2.3 Hz, *ipso*-C₆H₄F), 140.0 (d, ⁴J_{CF} = 2.3 Hz, *ipso*-C₆H₄F), 125.8 (d, ³J_{CF} = 8.0 Hz, *o*-C₆H₄F), 124.7 (d, ³J_{CF} = 8.0 Hz, *o*-C₆H₄F), 116.1 (d, ²J_{CF} = 22.5 Hz, *m*-C₆H₄F), 115.4 (d, ²J_{CF} = 22.5 Hz, *m*-C₆H₄F), 66.7 (C=NCH imidazoline), 66.5 (C=NCH imidazoline), 57.8 (CH_{bridge}), 57.7 (CH_{bridge}), 55.9 (CH₂ imidazoline), 52.1 (CH₂ imidazoline), 34.7 ((CH₃)₂CH), 34.2 ((CH₃)₂CH), 20.7 (CH₃ isopropyl), 19.5 (CH₃ isopropyl), 15.7 (CH₃ isopropyl), 15.2 (CH₃ isopropyl) ppm. ¹⁹F NMR data (THF-d₈, 282.8 MHz, 293 K): δ_F = -122.29 and -120.80 (s, *p*-C₆H₄F) ppm. IR data (KBr disc, cm⁻¹): 3104 (w), 3051 (w), 2959 (s), 2870 (m), 2238 (m), 2119 (w), 2098 (w), 1886 (w), 1619 (s), 1591 (m), 1542 (m), 1509 (s), 1427 (m), 1384 (m), 1362 (m), 1309 (m), 1260 (s), 1229 (s), 1171 (w), 1138 (m), 1122 (m), 1091 (m), 1041 (m), 1011 (m), 836 (s), 797 (s), 719 (m), 664 (w), 632 (w), 596 (w), 549 (s), 524 (w), 505 (w), 482 (w), 434 (w).

6.4.4.2 [Ca(Ar^{OMe}-BIM)₂] [11b]

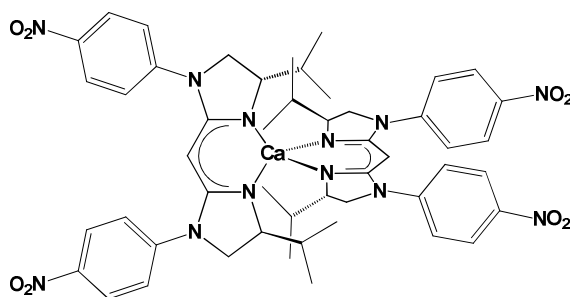
¹H NMR data (THF-d₈, 500.1 MHz, 293 K): δ_H = 7.05 (4 H, d, ³J_{HH} = 8.9 Hz, *m*-C₆H₄OCH₃), 6.99 (4 H, d, ³J_{HH} = 8.9 Hz, *m*-C₆H₄OCH₃), 6.77 (4 H, d, ³J_{HH} = 8.9 Hz, *o*-C₆H₄OCH₃), 6.67 (4 H, d, ³J_{HH} = 8.9 Hz, *o*-C₆H₄OCH₃), 3.99 (1 H, s, CH bridge), 3.89 (2 H, app. dt, ³J_{HH} = 8.9 Hz, ³J_{HH} = 2.7 Hz, NCH₂CH), 3.71 (2 H, t, ³J_{HH} = 8.4 Hz, NCH₂), 3.69 (12 H, br. s, C₆H₄OCH₃), 3.60 (2 H, app. q, ³J_{HH} = 7.8 Hz, NCH₂CH), 3.48 (2 H, t, ³J_{HH} = 8.6 Hz, NCH₂), 3.39 (1 H, s, CH bridge), 3.34 (4 H, m, NCH₂), 2.05 (2 H, m, (CH₃)₂CH), 1.65 (1 H, m, (CH₃)₂CH), 1.04 (6 H, t, ³J_{HH} = 6.7 Hz, CH(CH₃)₂), 0.92 (6 H, d, ³J_{HH} = 6.7 Hz, CH(CH₃)₂), 0.89 (6 H, t, ³J_{HH} = 6.7 Hz, CH(CH₃)₂), 0.80 (6 H, d, ³J_{HH} = 6.7 Hz, CH(CH₃)₂) ppm. ¹³C{¹H} NMR data (THF-d₈, 75.5 MHz, 293 K): δ_C = 165.2 (C=N), 161.3 (C=N), 157.6 (*p*-C₆H₅OCH₃), 156.3 (*p*-C₆H₅OCH₃), 139.1 (*ipso*-C₆H₄OCH₃), 136.9 (*ipso*-C₆H₄OCH₃), 126.0 (*m*-C₆H₄OCH₃), 124.9 (*m*-C₆H₄OCH₃), 114.7 (*o*-C₆H₄OCH₃), 114.2 (*o*-C₆H₄OCH₃), 67.2 (C=NCH imidazoline), 65.8 (C=NCH imidazoline), 59.8 (CH bridge), 57.8 (CH bridge), 56.2 (CH₂ imidazoline), 56.4 (CH₂ imidazoline), 55.4 (C₆H₄OCH₃), 52.5 (CH₂ imidazoline), 52.2 (CH₂ imidazoline), 34.8 ((CH₃)₂CH), 34.3 ((CH₃)₂CH), 20.7 (CH₃ isopropyl), 19.6 (CH₃ isopropyl), 19.3 (CH₃ isopropyl), 15.8 (CH₃ isopropyl), 2.7 (N(Si(CH₃)₃)₂) ppm. IR data (KBr disc, cm⁻¹): 3043 (w), 2957 (m), 2867 (m), 2835 (m), 2237 (w), 2086 (w), 1607 (s), 1578 (m), 1537 (s), 1512 (s), 1463 (m), 1441 (w), 1384 (w), 1365 (w), 1277 (w), 1246 (s), 1206 (w), 1178 (m), 1139 (w), 1103 (w), 1080 (w), 1039 (s), 834 (m), 808 (w), 783 (w), 724 (w), 691 (w), 600 (w), 554 (m), 513 (w).

6.4.4.3 [Ca(Ar^{Me}-BIM)₂] [11c]

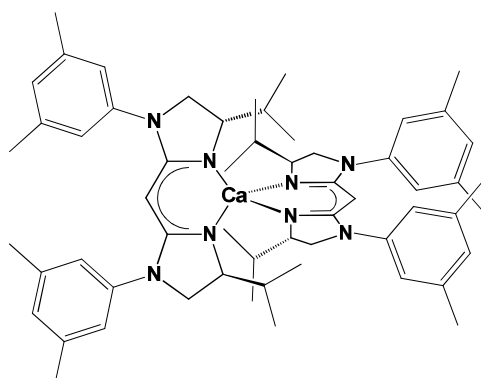
¹H NMR data (THF-d₈, 500.1 MHz, 293 K): δ_H = 7.04-6.97 (8 H, m, *o*-C₆H₄CH₃), 6.96-6.89 (8 H, m, *m*-C₆H₄CH₃), 3.96-3.82 (4 H, m, NCH₂CH), 3.72 (1 H, s, CH bridge), 3.70 (1 H, s, CH bridge), 3.68 (2 H, app. t, ³J_{HH} = 4.6 Hz, NCH₂), 3.52 (2 H, app. t, ³J_{HH} = 8.4 Hz, NCH₂), 3.35 (2 H, m, NCH₂), 3.26-3.91 (2 H, m, NCH₂), 2.21 (6 H, s, C₄H₅CH₃), 2.20 (6 H, s, C₄H₅CH₃), 2.10-1.96 (2 H, m, (CH₃)₂CH), 1.94-1.79 (2 H, m, (CH₃)₂CH), 0.89-0.82 (12 H, m, CH(CH₃)₂), 0.81-0.72 (12 H, m, CH(CH₃)₂) ppm. ¹³C{¹H} NMR data (THF-d₈, 75.5 MHz, 293 K): δ_C = 164.4 (C=N), 164.2 (C=N), 163.5 (C=N), 163.4 (C=N), 143.25 (*ipso*-C₆H₄CH₃), 143.18 (*ipso*-C₆H₄CH₃), 142.5 (*ipso*-C₆H₄CH₃), 142.3 (*ipso*-C₆H₄CH₃), 132.7 (*p*-C₆H₄CH₃), 131.3 (*p*-C₆H₄CH₃), 130.4 (*p*-C₆H₄CH₃), 130.0 (*p*-C₆H₄CH₃), 129.43 (*o*-C₆H₄CH₃), 129.40 (*o*-C₆H₄CH₃), 129.38 (*o*-C₆H₄CH₃), 129.37 (*o*-C₆H₄CH₃), 124.0 (*m*-C₆H₄CH₃), 123.9 (*m*-C₆H₄CH₃), 122.60 (*m*-C₆H₄CH₃), 122.59 (*m*-C₆H₄CH₃), 66.42 (C=NCH imidazoline), 66.40 (C=NCH imidazoline), 66.25 (C=NCH imidazoline), 66.24 (C=NCH imidazoline), 55.7 (CH bridge), 52.0 (CH bridge), 51.9 (CH₂ imidazoline), 51.6 (CH₂ imidazoline), 50.9 (CH₂ imidazoline), 50.6 (CH₂ imidazoline), 34.47 ((CH₃)₂CH), 34.42 ((CH₃)₂CH), 34.3 ((CH₃)₂CH), 34.2 ((CH₃)₂CH), 20.88 (C₆H₄CH₃), 20.80 (C₆H₄CH₃), 20.6 (CH₃ isopropyl), 20.4 (CH₃ isopropyl), 15.7 (CH₃ isopropyl), 15.4 (CH₃ isopropyl) ppm. IR data (KBr disc, cm⁻¹): 3031 (w), 2962 (m), 2868 (w), 1603 (m), 1573 (w), 1515 (m), 1478 (w), 1386 (w), 1361 (w), 1314 (w), 1260 (s), 1094 (s), 1018 (s), 798 (s), 705 (w), 614 (w), 551 (m), 499 (w).

6.4.4.4 [Ca(Ph-BIM)₂] [11d]

¹H NMR data (THF-d₈, 500.1 MHz, 293 K): δ_H = 7.22-7.09 (16 H, m, *o/m*-C₆H₅), 6.93-6.88 (2 H, m, *p*-C₆H₅), 6.84-6.71 (2 H, m, *p*-C₆H₅), 4.41 (1 H, br. s, CH_{bridge}), 3.93-3.85 (3 H, m, CH_{bridge} and NCH₂CH), 3.80 (2 H, t, ³J_{HH} = 8.4 Hz, NCH₂), 3.67-3.60 (2 H, m, NCH₂CH), 3.46 (2 H, t, ³J_{HH} = 8.4 Hz, NCH₂), 3.39 (1 H, dd, ³J_{HH} = 8.6 Hz, ³J_{HH} = 2.7 Hz, NCH₂), 3.31-3.23 (1 H, m, NCH₂) 1.95-1.80 (2 H, m, (CH₃)₂CH), 1.67 (2 H, m, (CH₃)₂CH), 1.05 (6 H, d, ³J_{HH} = 6.6 Hz, CH(CH₃)₂), 0.95 (6 H, app. t, ³J_{HH} = 6.6 Hz, CH(CH₃)₂), 0.91-0.86 (6 H, m, (CH₃)₂CH), 0.81-0.77 (6 H, m, (CH₃)₂CH). ¹³C{¹H} NMR data (THF-d₈, 75.5 MHz, 293 K): δ_C = 164.0 (C=N), 163.9 (C=N), 160.1 (C=N), 160.0 (C=N), 145.4 (*ipso*-C₆H₅), 145.3 (*ipso*-C₆H₅), 144.7 (*ipso*-C₆H₅), 144.6 (*ipso*-C₆H₅), 129.7 (C₆H₅), 129.4 (C₆H₅), 129.0 (C₆H₅), 128.95 (C₆H₅), 128.9 (C₆H₅), 128.8 (C₆H₅), 128.87 (C₆H₅), 128.9 (C₆H₅) 123.8 (*p*-C₆H₅), 123.7 (*p*-C₆H₅), 123.2 (*p*-C₆H₅), 122.4 (*p*-C₆H₅), 67.7 (C=NCH imidazoline), 66.4 (C=NCH imidazoline), 65.7 (C=NCH imidazoline), 65.4 (C=NCH imidazoline), 60.2 (CH_{bridge}), 57.9 (CH_{bridge}), 55.4 (CH₂ imidazoline), 55.3 (CH₂ imidazoline), 51.5 (CH₂ imidazoline), 50.5 (CH₂ imidazoline), 34.84 ((CH₃)₂CH), 34.80 ((CH₃)₂CH), 34.4 ((CH₃)₂CH), 34.3 ((CH₃)₂CH), 19.5 (CH₃ isopropyl), 19.4 (CH₃ isopropyl), 19.3 (CH₃ isopropyl), 19.2 (CH₃ isopropyl), 15.8 (CH₃ isopropyl), 15.6 (CH₃ isopropyl), 15.4 (CH₃ isopropyl), 15.2 (CH₃ isopropyl) ppm. IR data (KBr disc, cm⁻¹): 3056 (w), 3037 (w), 2957 (s), 2867 (m), 1938 (w), 1864 (w), 1787 (w), 1618 (s), 1592 (s), 1535 (s), 1496 (s), 1469 (m), 1405 (w), 1385 (m), 1338 (w), 1307 (m), 1260 (s), 1199 (m), 1171 (w), 1123 (w), 1107 (w), 1066 (w), 1042 (w), 903 (w), 800 (m), 752 (m), 723 (w), 695 (m), 647 (w), 553 (m), 503 (w).

6.4.4.5 [Ca(Ar^{NO2}-BIM)₂] [11e]

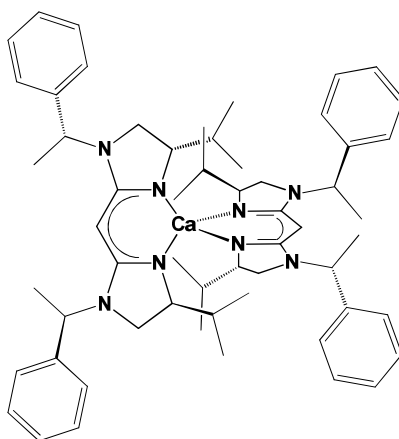
¹H NMR data (THF-d₈, 500.1 MHz, 293 K): $\delta_{\text{H}} = 8.17$ (8 H, d, $^3J_{\text{HH}} = 8.4$ Hz, *m*-C₆H₄NO₂), 7.34 (8 H, d, $^3J_{\text{HH}} = 7.6$ Hz, *o*-C₆H₄NO₂), 4.81 (1 H, s, CH_{bridge}), 4.80 (1 H, s, CH_{bridge}), 3.98 (4 H, t, $^3J_{\text{HH}} = 8.5$ Hz, NCH₂), 3.75 (4 H, m, NCH₂CH), 3.65 (4 H, m, NCH₂), 1.77 (4 H, m, (CH₃)₂CH), 1.05 (12 H, d, $^3J_{\text{HH}} = 6.6$ Hz, CH(CH₃)₂), 0.97 (12 H, d, $^3J_{\text{HH}} = 6.6$ Hz, CH(CH₃)₂) ppm. ¹³C{¹H} NMR data (THF-d₈, 75.5 MHz, 293 K): $\delta_{\text{C}} = 158.1$ (C=N), 148.6 (*p*-C₆H₄NO₂), 142.4 (*ipso*-C₆H₄NO₂), 125.7 (*m*-C₆H₄NO₂), 119.7 (*o*-C₆H₄NO₂), 65.4 (C=NCH_{imidazoline}), 65.2 (CH_{bridge}), 55.0 (CH₂_{imidazoline}), 34.6 ((CH₃)₂CH), 34.42 ((CH₃)₂CH), 19.2 (CH₃_{isopropyl}), 19.0 (CH₃_{isopropyl}) ppm. IR data (KBr disc, cm⁻¹): 3386 (br. w), 3114 (w), 3078 (w), 2949 (m), 2869 (m), 2632 (w), 2438 (w), 2293 (w), 2222 (w), 1624 (m), 1595 (s), 1549 (m), 1502 (s), 1430 (w), 1382 (w), 1365 (w), 1327 (s), 1260 (s), 1180 (m), 1140 (w), 1112 (s), 1039 (m), 851 (w), 801 (m), 752 (m), 693 (w), 661 (w), 627 (w), 547 (w), 512 (w), 483 (w).

6.4.4.6 [Ca(Ar^{3,5Me}-BIM)₂] [11f]

¹H NMR data (THF-d₈, 500.1 MHz, 293 K): $\delta_{\text{H}} = 6.78$ (4 H, s, *o*-C₆H₃(CH₃)₂), 6.70 (4 H, s, *o*-C₆H₃(CH₃)₂), 6.60 (2 H, s, *p*-C₆H₃(CH₃)₂), 6.50 (2 H, s, *p*-C₆H₃(CH₃)₂), 4.33 (1 H, s, CH_{bridge}), 4.32 (1 H, s, CH_{bridge}), 3.89 (2 H, m, NCH₂CH), 3.74 (2 H, m, NCH₂), 3.60

(2 H, m, NCH₂), 3.59 (2 H, m, NCH₂CH), 3.41 (2 H, m, NCH₂), 3.32 (2 H, dd, ³J_{HH} = 8.5 Hz, ³J_{HH} = 2.2 Hz, NCH₂), 2.21 (12 H, s, C₆H₃(CH₃)₂), 2.12 (12 H, s, C₆H₃(CH₃)₂), 2.03 (2 H, m, (CH₃)₂CH), 1.65 (2 H, m, (CH₃)₂CH), 1.04 (6 H, d, ³J_{HH} = 6.6 Hz, CH(CH₃)₂), 0.93 (6 H, d, ³J_{HH} = 6.6 Hz, CH(CH₃)₂), 0.90 (6 H, d, ³J_{HH} = 6.8 Hz, CH(CH₃)₂), 0.78 (6 H, d, ³J_{HH} = 6.8 Hz, CH(CH₃)₂), 0.11 (18 H, s, N(Si(CH₃)₃) ppm. ¹³C{¹H} NMR data (THF-d₈, 75.5 MHz, 293 K): δ_C = 164.5 (C=N), 164.3 (C=N), 160.6 (C=N), 160.5 (C=N), 145.5 (*ipso*-C₆H₃CH₃), 145.3 (*ipso*-C₆H₃CH₃), 144.6 (*ipso*-C₆H₄CH₃), 138.2 (*m*-C₆H₃(CH₃)₂), 138.0 (*m*-C₆H₃(CH₃)₂), 125.2 (*p*-C₆H₃(CH₃)₂), 124.2 (*p*-C₆H₃(CH₃)₂), 124.0 (*p*-C₆H₃(CH₃)₂), 123.6 (*o*-C₆H₃(CH₃)₂), 123.5 (*o*-C₆H₃(CH₃)₂), 123.4 (*o*-C₆H₃(CH₃)₂), 65.6 (C=NCH imidazoline), 65.4 (C=NCH imidazoline), 66.2 (C=NCH imidazoline), 66.0 (C=NCH imidazoline) 57.6 (CH bridge), 55.7 (CH bridge), 52.0 (CH₂ imidazoline), 51.8 (CH₂ imidazoline), 51.6 (CH₂ imidazoline), 51.4 (CH₂ imidazoline), 34.9 ((CH₃)₂CH), 34.8 ((CH₃)₂CH), 34.4 ((CH₃)₂CH), 34.3 ((CH₃)₂CH), 21.6 (C₆H₃(CH₃)₂), 21.58 (C₆H₃(CH₃)₂), 21.5 (C₆H₃(CH₃)₂), 21.4 (C₆H₃(CH₃)₂), 20.8 (CH₃ isopropyl), 20.5 (CH₃ isopropyl), 19.5 (CH₃ isopropyl), 19.4 (CH₃ isopropyl), 15.75 (CH₃ isopropyl), 15.71 (CH₃ isopropyl), 15.6 (CH₃ isopropyl), 15.2 (CH₃ isopropyl) ppm. IR data (KBr disc, cm⁻¹): 3011 (w), 2954 (s), 2919 (s), 2866 (s), 2729 (w), 1621 (s), 1591 (s), 1541 (s), 1470 (s), 1376 (m), 1335 (w), 1312 (w), 1283 (w), 1258 (m), 1198 (m), 1165 (w), 1124 (m), 1078 (w), 1044 (m), 950 (w), 926 (w), 871 (w), 834 (m), 722 (w), 697 (m), 640 (w), 606 (w), 594 (w), 570 (w), 534 (w), 495 (w), 418 (w).

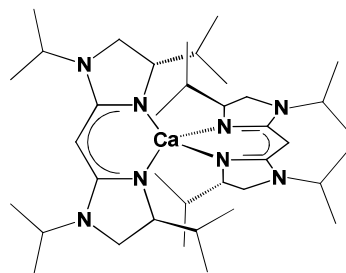
6.4.4.7 [Ca(PhMeH-BIM)₂] [11g]



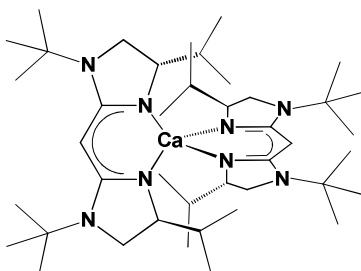
¹H NMR data (THF-d₈, 500.1 MHz, 293 K): δ_H = 7.31-7.24 (16 H, m, *o*- & *m*-C₆H₅), 7.19-7.14 (4 H, m, *p*-C₅H₅), 4.76 (4 H, q, ³J_{HH} = 6.9 Hz, CH(CH₃)(C₆H₅)), 3.96 (1 H, br. s CH bridge), 3.95 (1 H, br. s CH bridge), 3.45 (4 H, app. q, ³J_{HH} = 7.9 Hz, NCH₂CH), 3.30 (4 H,

t, $^3J_{\text{HH}} = 8.7$ Hz, NCH_2), 2.66 (4 H, t, $^3J_{\text{HH}} = 8.2$ Hz, NCH_2), 1.53 (4 H, m, $(\text{CH}_3)_2\text{CH}$ partially overlapping with adjacent peak), 1.47 (12 H, d, $^3J_{\text{HH}} = 6.9$ Hz, $\text{CH}(\text{CH}_3)(\text{C}_6\text{H}_5)$), 0.90 (12 H, d, $^3J_{\text{HH}} = 6.6$ Hz, $\text{CH}(\text{CH}_3)_2$), 0.78 (12 H, d, $^3J_{\text{HH}} = 6.6$ Hz, $\text{CH}(\text{CH}_3)_2$). $^{13}\text{C}\{^1\text{H}\}$ NMR data (THF- d_8 , 75.5 MHz, 293 K): $\delta_{\text{C}} = 163.2$ ($\text{C}=\text{N}$), 143.1 (*ipso*- C_6H_5), 128.9 (*o/m*- C_6H_5), 127.8 (*o/m*- C_6H_5), 127.5 (*p*- C_6H_5), 65.6 ($\text{C}=\text{NCH}$ imidazoline), 57.2 (CH bridge), 52.6 ($\text{CH}(\text{CH}_3)(\text{C}_6\text{H}_5)$), 48.2 (CH_2 imidazoline), 34.8 ($(\text{CH}_3)_2\text{CH}$), 19.6 (CH_3 isopropyl), 19.3 ($\text{CH}(\text{CH}_3)(\text{C}_6\text{H}_5)$), 17.6 (CH_3 isopropyl) ppm. IR data (KBr disc, cm^{-1}): 3650 (br. w), 3208 (br. m), 3086 (m), 3060 (m), 3028 (m), 2957 (s), 2869 (s), 2236 (w), 2193 (w), 1949 (w), 1877 (w), 1806 (w), 1611 (s), 1539 (s), 1494 (s), 1449 (s), 1378 (m), 1261 (s), 1221 (s), 1179 (m), 1142 (m), 1087 (m), 1065 (m), 1024 (s), 976 (w), 911 (w), 839 (w), 784 (m), 753 (w), 699 (s), 604 (w), 589 (w), 530 (w).

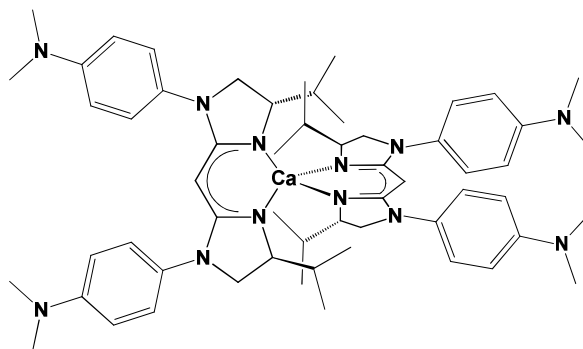
6.4.4.8 [Ca(iPr-BIM) $_2$] [11h]



^1H NMR data (THF- d_8 , 500.1 MHz, 293 K): $\delta_{\text{H}} = 3.71$ (6 H, m, $\text{NCH}(\text{CH}_3)_3$ and CH bridge), 3.41 (4 H, app. q, $^3J_{\text{HH}} = 8.4$ Hz, NCH_2CH), 3.25 (4 H, t, $^3J_{\text{HH}} = 8.4$ Hz, NCH_2), 2.82 (4 H, t, $^3J_{\text{HH}} = 8.4$ Hz, NCH_2), 1.56 (4 H, m, $(\text{CH}_3)_2\text{CH}$), 1.13 (12 H, $\text{NCH}(\text{CH}_3)_2$), 1.05 (12 H, $\text{NCH}(\text{CH}_3)_2$), 0.96 (12 H, $\text{CH}(\text{CH}_3)_2$), 0.86 (12 H, $\text{CH}(\text{CH}_3)_2$) ppm. $^{13}\text{C}\{^1\text{H}\}$ NMR data (THF- d_8 , 75.5 MHz, 293 K): $\delta_{\text{C}} = 163.2$ ($\text{C}=\text{N}$), 65.3 ($\text{C}=\text{NCH}$ imidazoline), 56.8 (CH bridge), 47.1 (CH_2 imidazoline), 45.7 ($\text{NCH}(\text{CH}_3)_2$), 34.8 ($(\text{CH}_3)_2\text{CH}$), 20.6 ($\text{NCH}(\text{CH}_3)_2$), 19.7 (CH_3 isopropyl), 19.3 (CH_3 isopropyl), 18.1 ($\text{NCH}(\text{CH}_3)_2$) ppm. IR data (KBr disc, cm^{-1}): 3329 (br. w), 3257 (br. w), 3111 (w), 2960 (s), 2868 (m), 2820 (m), 2241 (w), 2126 (w), 1612 (s), 1563 (s), 1540 (s), 1502 (m), 1469 (m), 1427 (m), 1386 (m), 1361 (m), 1282 (m), 1262 (s), 1237 (m), 1216 (m), 1177 (w), 1141 (m), 1104 (m), 1062 (s), 1032 (m), 978 (w), 918 (w), 886 (w), 801 (m), 737 (m), 713 (w), 658 (w), 618 (w), 603 (w), 549 (w), 518 (w), 465 (w), 437 (w), 417 (w).

6.4.4.9 [Ca(tBu-BIM)₂] [11i]

¹H NMR data (THF-d₈, 500.1 MHz, 293 K): δ_H = 3.70 (2 H, s, CH bridge), 3.50 (4 H, dt, ³J_{HH} = 9.1 Hz, ⁴J_{HH} = 2.7 Hz, NCH₂CH), 3.14 (4 H, dd, ³J_{HH} = 8.0 Hz, ⁴J_{HH} = 2.7 Hz, NCH₂), 3.05 (4 H, app. t, ³J_{HH} = 9.1 Hz, NCH₂), 1.83-1.75 (4 H, m, (CH₃)₂CH), 1.37 (36 H, br. s, C(CH₃)₃), 0.82 (12 H, d, ³J_{HH} = 6.9 Hz, CH(CH₃)₂), 0.73 (12 H, d, ³J_{HH} = 6.9 Hz, CH(CH₃)₂) ppm. ¹³C{¹H} NMR data (THF-d₈, 75.5 MHz, 293 K): δ_C = 166.6 (C=N), 166.4 (C=N), 65.3 (C=NCH imidazoline), 64.3 (C=NCH imidazoline), 62.0 (CH bridge), 61.8 (CH bridge), 52.9 (C(CH₃)₃), 52.7 (C(CH₃)₃), 47.9 (CH₂ imidazoline), 47.8 (CH₂ imidazoline), 35.5 ((CH₃)₂CH), 35.2 ((CH₃)₂CH), 30.0 (C(CH₃)₂), 29.82 (C(CH₃)₂), 20.9 (CH₃ isopropyl), 20.2 (CH₃ isopropyl), 16.2 (CH₃ isopropyl), 15.7 (CH₃ isopropyl) ppm. IR data (KBr disc, cm⁻¹): 2955 (s), 2866 (s), 1601 (s), 1526 (s), 1467 (m), 1442 (w), 1393 (m), 1363 (m), 1313 (w), 1259 (s), 1229 (s), 1174 (w), 1100 (s), 1016 (s), 927 (w), 863 (m), 793 (s), 734 (w), 699 (w), 659 (w), 545 (w), 520 (w), 466 (w)

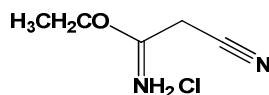
6.4.4.10 [Ca(Ar^{NMe2}-BIM)₂] [11j]

¹H NMR data (THF-d₈, 500.1 MHz, 293 K): δ_H = 6.89 (8 H, d, ³J_{HH} = 8.3 Hz, *m*-C₆H₄N(CH₃)₂), 6.54 (8 H, d, ³J_{HH} = 8.3 Hz, *o*-C₆H₄N(CH₃)₂), 3.92-3.86 (4 H, br. m, NCH₂CH), 3.48-3.41 (6 H, br. m, NCH₂ and CH bridge), 3.32-3.25 (4 H, br. t, ³J_{HH} = 8.2 Hz, NCH₂), 2.83 (24 H, br. s, C₆H₄N(CH₃)₂), 2.37-2.25 (4 H, br. m, (CH₃)₂CH), 0.85 12 H,

br. d, $^3J_{\text{HH}} = 6.7$ Hz, $\text{CH}(\text{CH}_3)_2$, 0.77 (12 H, br. d, $^3J_{\text{HH}} = 6.7$ Hz, $\text{CH}(\text{CH}_3)_2$) ppm. $^{13}\text{C}\{^1\text{H}\}$ NMR data (THF- d_8 , 75.5 MHz, 293 K): $\delta_{\text{C}} = 165.6$ ($\text{C}=\text{N}$), 147.9 ($p\text{-C}_6\text{H}_4\text{N}(\text{CH}_3)_2$), 133.9 ($ipso\text{-C}_6\text{H}_4\text{N}(\text{CH}_3)_2$), 125.86 ($m\text{-C}_6\text{H}_4\text{N}(\text{CH}_3)_2$), 113.8 ($o\text{-C}_6\text{H}_4\text{N}(\text{CH}_3)_2$), 66.3 ($\text{C}=\text{NCH}$ imidazoline), 57.6 (CH bridge), 52.1 (CH_2 imidazoline), 43.0 ($\text{C}_6\text{H}_4\text{N}(\text{CH}_3)_2$), 32.0 ($(\text{CH}_3)_2\text{CH}$), 20.4 (CH_3 isopropyl), 14.9 (CH_3 isopropyl) ppm. IR data (KBr disc, cm^{-1}): 3434 (br. m), 3222 (br. m), 2956 (m), 2890 (m), 2866 (m), 2814 (w), 2238 (w), 2116 (w), 1609 (s), 1560 (m), 1546 (s), 1522 (s), 1471 (m), 1445 (m), 1387 (w), 1375 (w), 1357 (m), 1332 (m), 1316 (m), 1273 (m), 1258 (m), 1231 (w), 1205 (m), 1188 (m), 1168 (m), 1139 (m), 1111 (m), 1083 (w), 1057 (m), 943 (w), 819 (m), 799 (m), 750 (w), 725 (w), 668 (w), 636 (w), 581 (w), 553 (w), 457 (w).

6.5 Experimental and Characterisation Data for Chapter Five

6.5.1 Preparation of ethyl 2-cyanoacetimidate hydrochloride [4.9]



Prepared from modified literature procedures.¹⁶ To a solution of malononitrile (10 g, 0.15 mol), in dry diethyl ether (300 ml), ethanol (19.70 ml, 0.33 mol) was added. Dry $\text{HCl}_{(\text{g})}$ was then passed through the solution for 6 hours where upon the system was sealed and allowed to stir under an HCl atmosphere for a further 18 hours. The solution was filtered away from the resulting white, ethyl 2-cyanoacetimidate hydrochloride precipitate. The precipitate was then washed with dry diethyl ether (20 ml) and the washings discarded. The solid product was then dried *in vacuo* and stored in a glove box, giving near quantitative yields.¹⁶

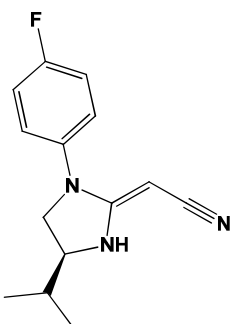
^1H NMR data ($(\text{CD}_3)_2\text{SO}$, 400.1 MHz, 293 K): $\delta_{\text{H}} = 7.77$ (2 H, br. s, NH_2), 4.15 (2 H, q, $^3J_{\text{HH}} = 7.1$ Hz, $\text{CH}_3\text{CH}_2\text{O}$), 4.01 (2 H, s, $\text{CH}_2\text{C}\equiv\text{N}$), 1.20 (3 H, t, $^3J_{\text{HH}} = 7.1$ Hz, $\text{CH}_3\text{CH}_2\text{O}$) ppm. $^{13}\text{C}\{^1\text{H}\}$ NMR data ($(\text{CD}_3)_2\text{SO}$, 62.9 MHz, 293 K): $\delta_{\text{C}} = 164.3$ ($\text{C}=\text{N}$), 115.1 ($\text{C}\equiv\text{N}$), 61.9 ($\text{CH}_3\text{CH}_2\text{O}$), 24.5 ($\text{CH}_2\text{C}\equiv\text{N}$), 13.9 ($\text{CH}_3\text{CH}_2\text{O}$) ppm. IR data (KBr pellet, cm^{-1}): 2917 (s), 2640 (s), 2392 (w), 2302 (w), 2265 (m, $\nu_{\text{C}\equiv\text{N}}$), 2210 (w), 2060 (w), 1744 (s), 1651 (s, $\nu_{\text{C}=\text{N}}$), 1560 (m), 1466 (w), 1448 (m), 1383 (s), 1361 (m), 1337 (w), 1311 (m), 1264 (w), 1200 (m), 1148 (m), 1129 (s), 1077 (s), 1027 (s), 1002 (s), 984 (w), 927 (s), 875 (w), 841

(m), 821 (s), 795 (w), 768 (w), 638 (m). Accurate mass ES-MS: no identifiable peaks obtained.

6.5.2 Preparation of Monocyclised imidazolines R-MIM [13a-f]

Prepared according to modified literature procedures.^{14,17} Under an inert atmosphere of argon, ethyl 2-cyanoacetimidate hydrochloride **4.9** (*ca.* 0.6 g, 26 mmol) and ethylene diamine analogues HNN^R **4a-f** (1 g, *ca.* 52 mmol) were dissolved in dry dichloromethane and heated at vigorous reflux for 2 days. Proceeding such time the solution was allowed to cool and was washed with NaHCO₃ (10%, 2 × 25 ml). The organic washings were combined and subsequently reduced in volume under reduced pressure. The relevant monoimidazoline R-MIM (**13a-f**) was realised by recrystallisation from dichloromethane and *n*-hexane at -20 °C.

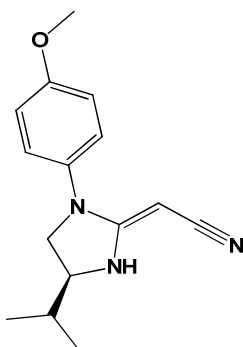
6.5.2.1 [Ar^F-MIM] [13a]



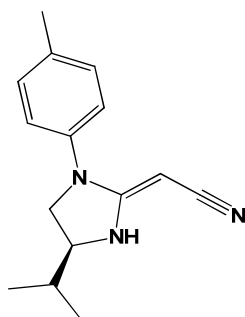
¹H NMR data (CDCl₃, 500.1 MHz, 293 K): δ_H = 7.19 (2 H, dd, ³J_{HH} = 8.9 Hz, ⁴J_{HF} = 4.7 Hz, *o*-C₆H₄F), 7.07 (2 H, app. t, ³J_{HF} = 8.3 Hz, *m*-C₆H₄F), 3.89 (1 H, t, ³J_{HH} = 8.4 Hz, NCH₂), 3.66 (1 H, m, C=NCH), 3.66 (1 H, t, ³J_{HH} = 8.5 Hz, NCH₂), 3.13 (1 H, br. s, CH_{bridge}), 1.89 (1 H, m, (CH₃)₂CH), 1.00 (3 H, d, ³J_{HH} = 6.7 Hz, CH₃ isopropyl), 0.94 (3 H, d, ³J_{HH} = 6.8 Hz, CH₃ isopropyl) ppm. ¹⁹F NMR data (CDCl₃, 282.8 MHz, 293 K): δ_F = -114.81 (s, *p*-C₆H₄F) ppm. ¹³C{¹H} NMR data (CDCl₃, 125.75 MHz, 293 K): δ_C = 162.9 (C=N), 160.5 (d, ¹J_{CF} = 246.8 Hz, *p*-C₆H₄F), 135.8 (d, ⁴J_{CF} = 2.9 Hz, *ipso*-C₆H₄F) 126.0 (d, ³J_{CF} = 8.5 Hz, *o*-C₆H₄F), 123.3 (C≡N), 116.3 (d, ²J_{CF} = 22.9 Hz, *m*-C₆H₄F), 59.9 (C=NCH imidazoline), 55.2 (CH₂ imidazoline), 37.3 (CH_{bridge}), 32.5 ((CH₃)₂CH), 18.5 (CH₃ isopropyl), 18.0 (CH₃ isopropyl) ppm. IR data (KBr pellet, cm⁻¹): 3235 (m), 3097 (w), 2963 (s),

2871 (w), 2176 (s, $\nu_{\text{C}\equiv\text{N}}$), 1893 (w), 1731 (m), 1612 (s, $\nu_{\text{C}=\text{N}}$), 1591 (s), 1508 (s), 1485 (m), 1465 (w), 1415 (w), 1386 (w), 1368 (w), 1344 (w), 1261 (s), 1216 (m), 1095 (s), 1020 (s), 940 (w), 799 (s), 719 (m), 703 (m), 660 (m), 596 (m), 576 (m), 511 (w). Accurate mass ES-MS for $[\text{Ar}^{\text{F}}\text{-MIM}+\text{H}]^+$, found (calc. for $\text{C}_{14}\text{H}_{17}\text{N}_3\text{F}$) 246.1402 (246.1407).

6.5.2.2 $[\text{Ar}^{\text{OMe}}\text{-MIM}]$ [13b]

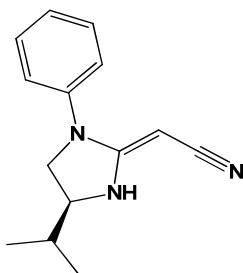


^1H NMR data (CDCl_3 , 500.1 MHz, 293 K): $\delta_{\text{H}} = 7.13$ (2 H, d, $^3J_{\text{HH}} = 8.9$ Hz, $o\text{-C}_6\text{H}_4\text{OCH}_3$), 6.89 (2 H, d, $^3J_{\text{HH}} = 8.9$ Hz, $m\text{-C}_6\text{H}_4\text{OCH}_3$), 3.86 (1 H, t, $^3J_{\text{HH}} = 8.5$ Hz, NCH_2), 3.81 (3 H, s, $\text{C}_6\text{H}_5\text{OCH}_3$), 3.63 (1 H, m, $\text{C}=\text{NCH}$), 3.52 (1 H, dd, $^2J_{\text{HH}} = 8.8$ Hz, $^3J_{\text{HH}} = 7.7$ Hz, NCH_2), 3.06 (1 H, s, $\text{CH}_{\text{bridge}}$), 1.79 (1 H, m, $(\text{CH}_3)_2\text{CH}$), 1.00 (3 H, d, $^3J_{\text{HH}} = 6.7$ Hz, CH_3 isopropyl), 0.94 (3 H, d, $^3J_{\text{HH}} = 6.7$ Hz, CH_3 isopropyl) ppm. $^{13}\text{C}\{^1\text{H}\}$ NMR data (CDCl_3 , 125.75 MHz, 293 K): $\delta_{\text{C}} = 163.4$ ($\text{C}=\text{N}$), 158.0 ($ipso\text{-C}_6\text{H}_4\text{OCH}_3$), 132.6 ($p\text{-C}_6\text{H}_4\text{OCH}_3$), 126.1 ($o\text{-C}_6\text{H}_4\text{OCH}_3$), 123.7 ($\text{C}\equiv\text{N}$), 114.7 ($m\text{-C}_6\text{H}_4\text{OCH}_3$), 66.1 ($\text{C}=\text{NCH}$ imidazoline), 55.6 (CH_2 imidazoline), 55.5 ($\text{C}_6\text{H}_4\text{OCH}_3$), 36.6 ($\text{CH}_{\text{bridge}}$), 32.6 ($(\text{CH}_3)_2\text{CH}$), 18.5 (CH_3 isopropyl), 18.2 (CH_3 isopropyl) ppm. IR data (KBr pellet, cm^{-1}): 3268 (s), 2959 (s), 2840 (m), 2350 (w), 2173 (s $\nu_{\text{C}\equiv\text{N}}$), 1889 (w), 1770 (w), 1606 (s, $\nu_{\text{C}=\text{N}}$), 1510 (s), 1463 (s), 1418 (m), 1389 (m), 1371 (m), 1352 (w), 1338 (w), 1326 (w), 1288 (m), 1247 (s), 1180 (m), 1164 (m), 1143 (w), 1101 (m), 1072 (w), 1038 (s), 937 (w), 839 (s), 822 (m), 746 (w), 727 (w), 689 (w), 639 (w), 607 (m), 582 (s), 568 (s), 515 (w). Accurate mass ES-MS for $[\text{Ar}^{\text{OMe}}\text{-MIM}+\text{H}]^+$, found (calc. for $\text{C}_{15}\text{H}_{20}\text{N}_3\text{O}_1$) 258.1600 (258.1606).

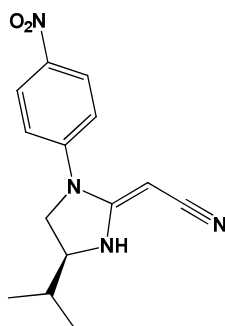
6.5.2.3 [Ar^{Me}-MIM] [13c]

¹H NMR data (CDCl₃, 500.1 MHz, 293 K): $\delta_{\text{H}} = 7.16$ (2 H, d, $^3J_{\text{HH}} = 8.1$ Hz, *m*-C₆H₄CH₃), 7.09 (2 H, d, $^3J_{\text{HH}} = 8.4$ Hz, *o*-C₆H₄CH₃), 3.89 (1 H, t, $^3J_{\text{HH}} = 8.4$ Hz, NCH₂), 3.64 (1 H, m, C=NCH), 3.54 (1 H, dd, $^2J_{\text{HH}} = 8.8$ Hz, $^3J_{\text{HH}} = 7.5$ Hz, NCH₂), 3.19 (1 H, br. s, CH bridge), 2.33 (3 H, s, C₆H₄CH₃) 1.79 (1 H, m, (CH₃)₂CH), 0.99 (3 H, d, $^3J_{\text{HH}} = 6.7$ Hz, CH₃ isopropyl), 0.93 (3 H, d, $^3J_{\text{HH}} = 6.8$ Hz, CH₃ isopropyl) ppm. ¹³C{¹H} NMR data (CDCl₃, 125.75 MHz, 293 K): $\delta_{\text{C}} = 162.7$ (C=N), 137.2 (*ipso*-C₆H₄CH₃), 135.9 (*p*-C₆H₄CH₃), 130.0 (*m*-C₆H₄CH₃), 125.2 (C≡N), 123.7 (*o*-C₆H₄CH₃), 59.8 (C=NCH imidazoline), 55.0 (CH₂ imidazoline), 32.8 (CH bridge), 32.6 ((CH₃)₂CH), 20.8 (C₆H₄CH₃) 18.4 (CH₃ isopropyl), 18.0 (CH₃ isopropyl) ppm. IR data (KBr pellet, cm⁻¹): 3311 (s), 3228 (s), 3105 (w), 3032 (w), 2962 (w), 2926 (s), 2875 (m), 2852 (m), 2185 (s), 2174 (s, $\nu_{\text{C}\equiv\text{N}}$), 1911 (w), 1802 (w), 1773 (w), 1734 (w), 1620 (s, $\nu_{\text{C}=\text{N}}$), 1598 (s, $\nu_{\text{C}=\text{N}}$), 1574 (m), 1512 (s), 1483 (s), 1459 (s), 1422 (m), 1388 (m), 1370 (m), 1338 (w), 1317 (s), 1303 (s), 1278 (m), 1241 (m), 1208 (w), 1174 (w), 1148 (w), 1121 (m), 1080 (m), 1040 (m), 1017 (m), 993 (m), 857 (w), 826 (s), 777 (w), 755 (w), 717 (m), 688 (m), 640 (w), 583 (s), 565 (s), 508 (m). Accurate mass ES-MS for [Ar^{Me}-MIM+H]⁺, found (calc. for C₁₅H₂₀N₃) 242.1660 (242.1657).

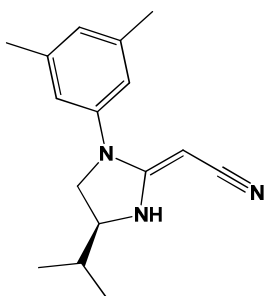
6.5.2.4 [Ph-MIM] [13d]



^1H NMR data (CDCl_3 , 500.1 MHz, 293 K): $\delta_{\text{H}} = 7.35$ (2 H, app. t, $^3J_{\text{HH}} = 7.4$ Hz, $m\text{-C}_6\text{H}_5$), 7.21 (2 H, d, $^3J_{\text{HH}} = 8.6$ Hz, $o\text{-C}_6\text{H}_5$), 7.16 (1 H, m, $p\text{-C}_6\text{H}_5$), 3.93 (1 H, t, $^3J_{\text{HH}} = 8.3$ Hz, NCH_2), 3.64 (1 H, m, $\text{C}=\text{NCH}$), 3.60 (1 H, m, NCH_2), 3.30 (1 H, br. s, $\text{CH}_{\text{bridge}}$), 1.80 (1 H, m, $(\text{CH}_3)_2\text{CH}$), 1.00 (3 H, d, $^3J_{\text{HH}} = 6.7$ Hz, CH_3 isopropyl), 0.94 (3 H, d, $^3J_{\text{HH}} = 6.8$ Hz, CH_3 isopropyl) ppm. $^{13}\text{C}\{^1\text{H}\}$ NMR data (CDCl_3 , 125.75 MHz, 293 K): $\delta_{\text{C}} = 162.3$ ($\text{C}=\text{N}$), 139.9 ($ipso\text{-C}_6\text{H}_5$), 129.4 ($m\text{-C}_6\text{H}_5$), 129.3 ($p\text{-C}_6\text{H}_5$), 125.9 ($\text{C}\equiv\text{N}$), 123.6 ($o\text{-C}_6\text{H}_5$), 59.8 ($\text{C}=\text{NCH}$ imidazole), 54.9 (CH_2 imidazole), 37.3 ($\text{CH}_{\text{bridge}}$), 32.6 ($(\text{CH}_3)_2\text{CH}$), 18.5 (CH_3 isopropyl), 18.1 (CH_3 isopropyl) ppm. IR data (KBr pellet, cm^{-1}): 3247 (s), 3097 (w), 3040 (w), 2958 (s), 2868 (s), 2350 (w), 2335 (w), 2259 (w), 2172 (s $\nu_{\text{C}=\text{N}}$), 1958 (w), 1887 (w), 1828 (w), 1667 (w), 1612 (s, $\nu_{\text{C}=\text{N}}$), 1589 (s, $\nu_{\text{C}=\text{N}}$), 1498 (s), 1463 (s), 1451 (s), 1388 (m), 1369 (m), 1343 (m), 1318 (m), 1301 (m), 1283 (m), 1243 (m), 1208 (m), 1179 (m), 1146 (m), 1130 (m), 1074 (m), 1041 (w), 1023 (w), 1002 (w), 989 (w), 916 (w), 854 (w), 769 (s), 751 (m), 702 (s), 692 (m). Accurate mass ES-MS for $[\text{Ar}^{\text{H}}\text{-MIM}+\text{H}]^+$, found (calc. for $\text{C}_{14}\text{H}_{18}\text{N}_3$) 228.1495 (228.1501).

6.5.2.5 [Ar^{NO2}-MIM] [13e]

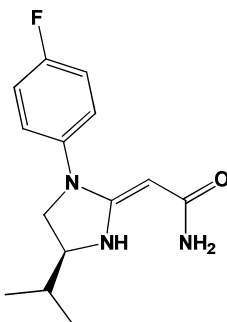
¹H NMR data (CDCl₃, 500.1 MHz, 293 K): δ_H = 8.02 (2 H, d, ³J_{HH} = 8.9 Hz, *m*-C₆H₄NO₂), 6.05 (2 H, d, ³J_{HH} = 8.9 Hz, *o*-C₆H₄NO₂), 3.28 (1 H, m, NCH₂), 2.90 (1 H, m, NCH₂), 2.74 (1 H, m, C=NCH), 2.27 (1 H, br. s, CH_{bridge}), 1.67 (1 H, m, (CH₃)₂CH), 0.96 (3 H, d, ³J_{HH} = 3.3 Hz, CH₃ isopropyl), 0.95 (3 H, d, ³J_{HH} = 3.3 Hz, CH₃ isopropyl) ppm. ¹³C{¹H} NMR data (CDCl₃, 125.75 MHz, 293 K): δ_C = 160.7 (C=N), 153.7 (*p*-C₆H₄NO₂), 137.5 (*ipso*-C₆H₄NO₂), 126.3 (*m*-C₆H₄NO₂), 125.1 (C≡N), 111.0 (*o*-C₆H₄NO₂), 60.4 (CH_{bridge}), 55.6 (C=NCH imidazoline), 46.5 (CH₂ imidazoline), 32.6 ((CH₃)₂CH), 19.1 (CH₃ isopropyl), 17.8 (CH₃ isopropyl) ppm. IR data (KBr pellet, cm⁻¹): 3349 (w), 3241 (w), 3182 (w), 3048 (w), 2936 (w), 2924 (w), 2872 (w), 2194 (s ν_{C=N}), 1598 (s, ν_{C=N}), 1506 (m), 1466 (m), 1304 (s), 1183 (m), 1113 (s), 1055 (w), 935 (w), 868 (w), 827 (m), 752 (m), 695 (w), 639 (w). Accurate mass ES-MS: no identifiable fragments observed.

6.5.2.6 [Ar^{3,5Me}-MIM] [13f]

¹H NMR data (CDCl₃, 500.1 MHz, 293 K): δ_H = 6.83 (1 H, s, *p*-C₆H₃(CH₃)₂), 6.82 (2 H, s, *m*-C₆H₃(CH₃)₂), 3.89 (2 H, app. t, ²J_{HH} = 8.4 Hz, NCH₂), 3.63 (1 H, m, C=NCH), 3.56 (1 H, d.d, ²J_{HH} = 8.4 Hz, ³J_{HH} = 7.5 Hz, NCH₂), 3.29 (1 H, br. s, CH_{bridge}), 2.30 (6 H, s, C₆H₄(CH₃)₂), 1.79 (1 H, m, (CH₃)₂CH), 1.00 (3 H, d, ³J_{HH} = 6.7 Hz, CH₃ isopropyl), 0.94 (3 H, d, ³J_{HH} = 6.7 Hz, CH₃ isopropyl) ppm. ¹³C{¹H} NMR data (CDCl₃, 125.75 MHz, 293 K): δ_C =

162.4 ($\underline{\text{C}}=\text{N}$), 139.8 (*ipso*- $\underline{\text{C}}_6\text{H}_3(\text{CH}_3)_2$), 139.2 (*m*- $\underline{\text{C}}_6\text{H}_3(\text{CH}_3)_2$), 127.6 (*p*- $\underline{\text{C}}_6\text{H}_3(\text{CH}_3)_2$), 123.6 ($\underline{\text{C}}\equiv\text{N}$), 121.3 (*o*- $\underline{\text{C}}_6\text{H}_3(\text{CH}_3)_2$), 59.8 ($\text{C}=\underline{\text{NCH}}$ imidazoline), 55.0 ($\underline{\text{CH}}_2$ imidazoline), 37.2 ($\underline{\text{CH}}$ bridge), 32.6 ($(\text{CH}_3)_2\underline{\text{CH}}$), 21.2 ($\text{C}_6\text{H}_3(\underline{\text{C}}\text{H}_3)_2$), 18.5 ($\underline{\text{C}}\text{H}_3$ isopropyl), 18.1 ($\underline{\text{C}}\text{H}_3$ isopropyl) ppm. IR data (KBr pellet, cm^{-1}): 3463 (w), 3270 (m), 3237 (m), 3112 (w), 3047 (w), 3012 (w), 2964 (m), 2915 (w), 2867 (m), 2178 (s $\nu_{\text{C}=\text{N}}$), 1614 (s, $\nu_{\text{C}=\text{N}}$), 1587 (s) 1480 (s), 1389 (m), 1369 (m), 1333 (m), 1318 (w), 1305 (w), 1284 (m), 1242 (m), 1228 (w), 1194 (w), 1179 (w), 1146 (w), 1132 (w), 1076 (w), 1053 (w), 1015 (w), 981 (w), 950 (w), 914 (w), 893 (w), 847 (s), 803 (w), 700 (m), 689 (m), 655 (w), 608 (m), 596 (m) Accurate mass ES-MS for $[\text{Ar}^{3.5\text{Me}}\text{-MIM}+\text{H}]^+$, found (calc. for $\text{C}_{29}\text{H}_{41}\text{N}_4$) 445.3343 (445.3331).

6.5.2.7 [14]



^1H NMR data ($(\text{CD}_3)_2\text{SO}$, 400.1 MHz, 293 K) $\delta_{\text{H}} = 7.55$ (2 H, d.d, $^3\text{J}_{\text{HH}} = 4.9$ Hz, $^4\text{J}_{\text{HF}} = 4.1$ Hz, *o*- $\underline{\text{C}}_6\text{H}_4\text{F}$), 7.39 (2 H, app. t, $^3\text{J}_{\text{HH}} = 8.7$ Hz, *m*- $\underline{\text{C}}_6\text{H}_4\text{F}$), 4.37 (1 H, t, $^3\text{J}_{\text{HH}} = 10.8$ Hz, NCH_2), 4.18 (1 H, m, $\text{C}=\underline{\text{NCH}}$), 4.07 (1 H, m, NCH_2), 1.90 (1 H, m, $(\text{CH}_3)_2\underline{\text{CH}}$), 0.98 (3 H, d, $^3\text{J}_{\text{HH}} = 6.7$ Hz, $\underline{\text{C}}\text{H}_3$ isopropyl), 0.95 (3 H, d, $^3\text{J}_{\text{HH}} = 6.8$ Hz, $\underline{\text{C}}\text{H}_3$ isopropyl), ($\underline{\text{CH}}$ bridge not observed) ppm. ^{19}F NMR data ($(\text{CD}_3)_2\text{SO}$, 282.8 MHz, 293 K): $\delta_{\text{F}} = -111.99$ (s, *p*- $\underline{\text{C}}_6\text{H}_4\text{F}$) ppm. $^{13}\text{C}\{^1\text{H}\}$ NMR data ($(\text{CD}_3)_2\text{SO}$, 75.5 MHz, 293 K): $\delta_{\text{C}} = 165.4$ ($\text{C}=\text{O}$) 163.6 ($\underline{\text{C}}=\text{N}$), 161.6 (d, $^1\text{J}_{\text{CF}} = 246.3$ Hz, *p*- $\underline{\text{C}}_6\text{H}_4\text{F}$), 131.9 (d, $^4\text{J}_{\text{CF}} = 2.6$ Hz, *ipso*- $\underline{\text{C}}_6\text{H}_4\text{F}$) 128.0 (d, $^3\text{J}_{\text{CF}} = 9.0$ Hz, *o*- $\underline{\text{C}}_6\text{H}_4\text{F}$), 116.6 (d, $^2\text{J}_{\text{CF}} = 22.9$ Hz, *m*- $\underline{\text{C}}_6\text{H}_4\text{F}$), 60.9 ($\text{C}=\underline{\text{NCH}}$ imidazoline), 55.5 ($\underline{\text{CH}}_2$ imidazoline), 32.9 ($\underline{\text{CH}}$ bridge), 31.5 ($(\text{CH}_3)_2\underline{\text{CH}}$), 17.28 ($\underline{\text{C}}\text{H}_3$ isopropyl), 17.23 ($\underline{\text{C}}\text{H}_3$ isopropyl) ppm. IR data (KBr pellet, cm^{-1}): 3335 (br. s), 3185 (br. s), 2964 (s), 2209 (w), 1739 (w), 1668 (s $\nu_{\text{C}=\text{O}}$), 1611 (s, $\nu_{\text{C}=\text{N}}$), 1510 (s), 1466 (m), 1395 (m), 1348 (w), 1320 (m), 1286 (m), 1261 (m), 1225 (s), 1158 (m), 1098 (m), 1070 (w), 1017 (m), 926 (w), 845 (m), 826 (w), 803 (m), 714 (w), 606 (m), 552 (m). Accurate mass ES-MS $[\text{Ar}^{\text{F}}\text{-M}+\text{H}]^+$, found (calc. for $\text{C}_{14}\text{H}_{19}\text{N}_3\text{OF}$) 264.1518 (264.1512).

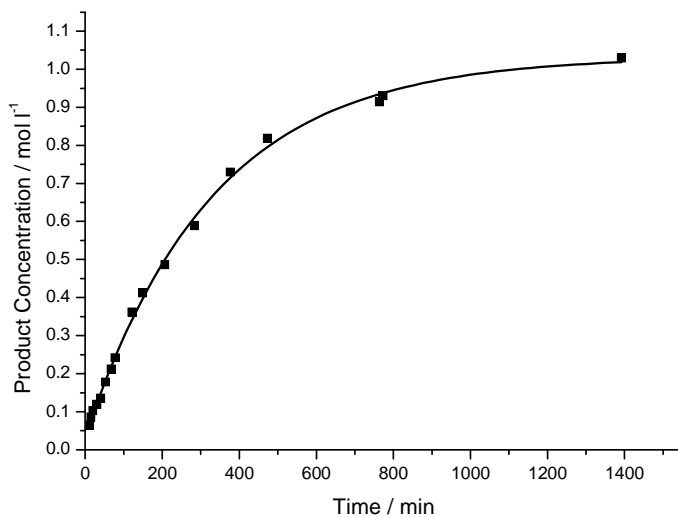
6.6 References

1. D. M. Shendage, R. Fuhlich and G. Haufe, *Org. Lett.*, **2004**, 6, 3675.
2. J. S. Wixey and B. D. Ward, *Chem. Commun.*, **2011**, 47, 5449.
3. D. Rix, S. Labat, L. Toupet, C. Crévisy and M. Mauduit, *Eur. J. Inorg. Chem.*, **2009**, 1989.
4. A. J. Davenport, D. L. Davies, J. Fawcett and D. R. Russell, *J. Organomet. Chem.*, **2006**, 691, 3445.
5. J. S. Alexander and K. Ruhlandt-Senge, *Eur. J. Inorg. Chem.*, **2002**, 2761.
6. W. D. Buchanan, D. G. Allis and K. Ruhlandt-Senge, *Chem. Commun.*, **2010**, 46, 4449.
7. D. C. Bradley, M. B. Hursthouse, A. A. Ibrahim, K. M. Abdul Malik, M. Motevalli, R. Moseler, H. Powell, J. D. Runnacles and A. C. Sullivan, *Polyhedron*, **1990**, 9, 2959.
8. M. Westerhausen, *Inorg. Chem.*, **1991**, 30, 96.
9. J. Y. Kim and L. Tom, *Org. Lett.*, **2005**, 7, 1737.
10. S. Hong, S. Tian, M. V. Metz and T. J. Marks, *J. Am. Chem. Soc.*, **2003**, 125, 14768.
11. M. R. Crimmin, I. J. Casely and M. S. Hill, *J. Am. Chem. Soc.*, **2005**, 127, 2042.
12. G. Zi, F. Zhang, L. Xiang, Y. Chen, W. Fang and H. Song, *Dalton Trans.*, **2010**, 39, 4048.
13. D. Akalay, G. Durner, J. W. Bats, M. Bolte and M. W. Gobel, *J. Org. Chem.*, **2007**, 72, 5618.
14. C. Mazet, V. Kohler and A. Pfaltz, *Angew. Chem. Int. Ed.*, **2005**, 44, 4888.
15. P. Jochmann, S. Maslek, T. P. Spaniol and J. Okuda, *Organometallics*, **2011**, 30, 1991.
16. *United States Pat.*, 2003.
17. J. S. Wixey and B. D. Ward, *Dalton Trans.*, **2011**, 40, 7693.

Appendices

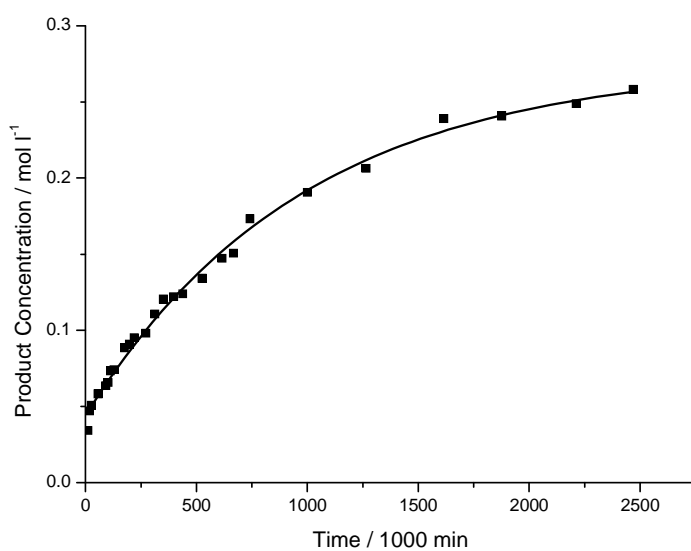
Appendix A: Product Conversion Curves for Chapter Three

1. $[\text{Ca}\{\text{N}(\text{SiMe}_3)_2\}_2(\text{THF})_2]$



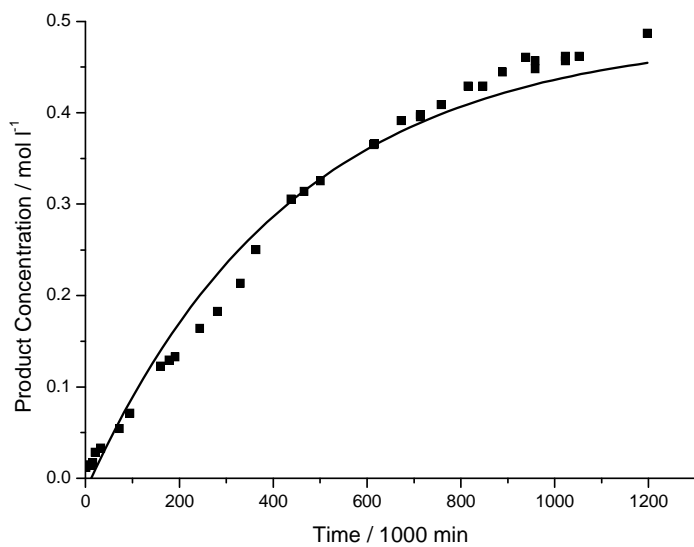
293 K, 10 mol% catalyst, substrate A, initial rate: $5.0(2) \times 10^{-5} \text{ mol dm}^{-3} \text{ s}^{-1}$.

2. $[\text{Ca}(\text{NN}^{\text{ArOMe}})\{\text{N}(\text{SiMe}_3)_2\}(\text{THF})_n]$ [5b]



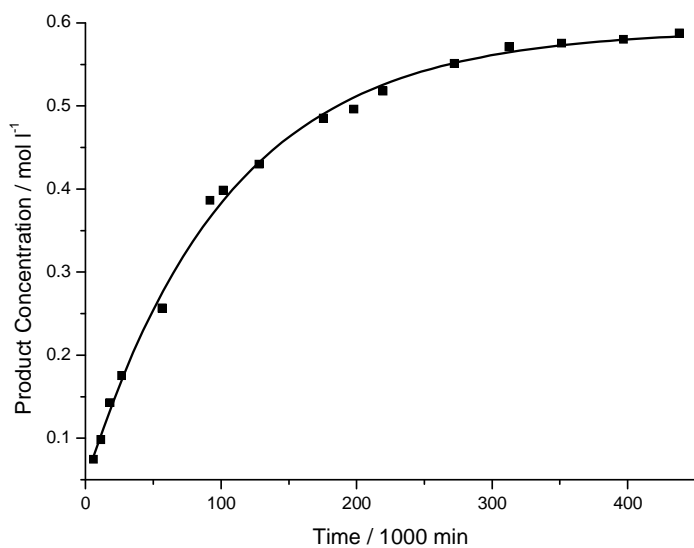
323 K, 10 mol% catalyst, substrate A, initial rate: $2.4(1) \times 10^{-7} \text{ mol dm}^{-3} \text{ s}^{-1}$.

3. $[\text{Ca}(\text{NN}^{\text{ArMe}})\{\text{N}(\text{SiMe}_3)_2\}(\text{THF})_n]$ [5c]



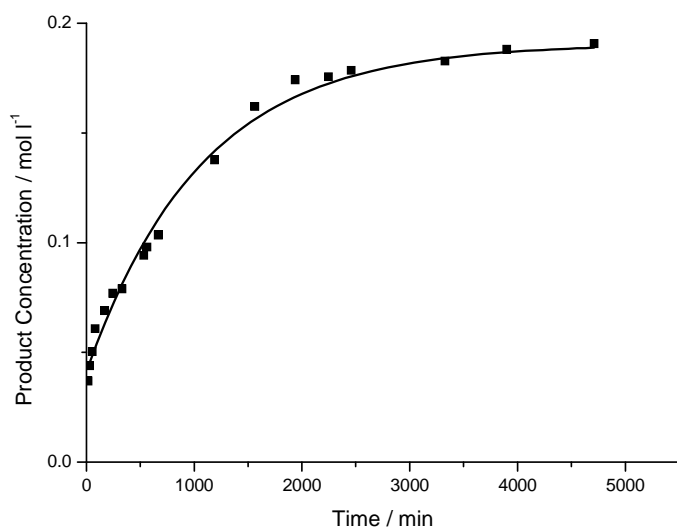
293 K, 10 mol% catalyst, substrate A, initial rate: $1.1(1) \times 10^{-6} \text{ mol dm}^{-3} \text{ s}^{-1}$.

4. $[\text{Ca}(\text{NN}^{\text{Ph}})\{\text{N}(\text{SiMe}_3)_2\}(\text{THF})_n]$ [5d]



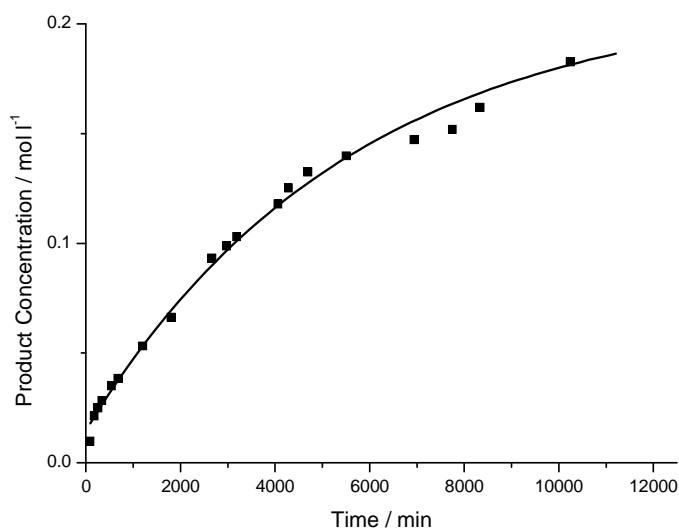
323 K, 10 mol% catalyst, substrate A, initial rate: $5.2(2) \times 10^{-6} \text{ mol dm}^{-3} \text{ s}^{-1}$.

5. $[\text{Ca}(\text{NN}^{\text{iPr}})\{\text{N}(\text{Si}(\text{CH}_3)_3)_2\}(\text{THF})_n]$ [5e]



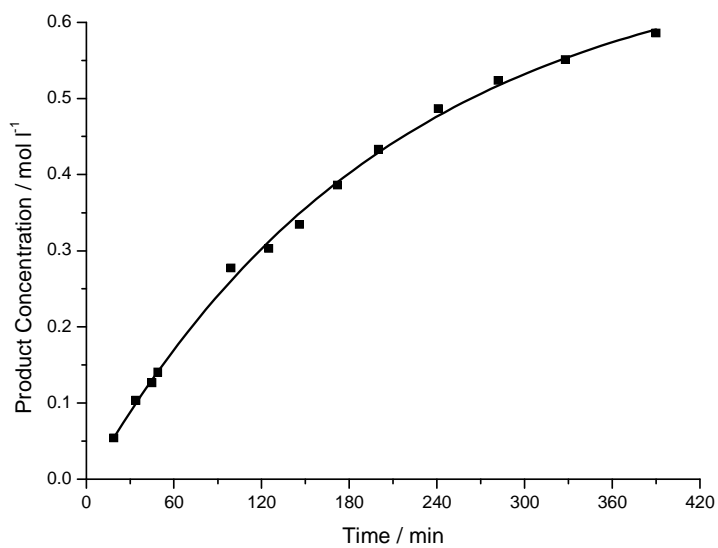
293 K, 10 mol% catalyst, substrate A, initial rate: $2.3(1) \times 10^{-6} \text{ mol dm}^{-3} \text{ s}^{-1}$.

6. $[\text{Ca}(\text{NN}^{\text{tBu}})\{\text{N}(\text{SiMe}_3)_2\}(\text{THF})_n]$ [5f]



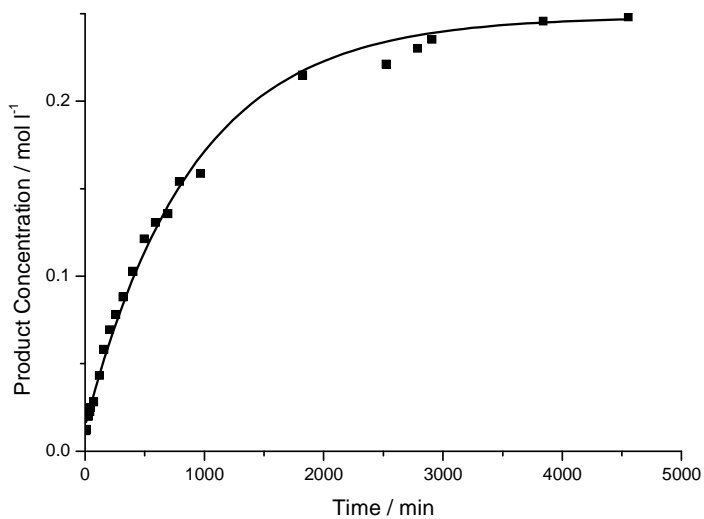
293 K, 10 mol% catalyst, substrate A, initial rate: $5.9(8) \times 10^{-7} \text{ mol dm}^{-3} \text{ s}^{-1}$.

7. $[\text{Ca}(\text{NN}^{\text{ArOMe}})\{\text{N}(\text{SiMe}_3)_2\}(\text{THF})_n]$ [5b]



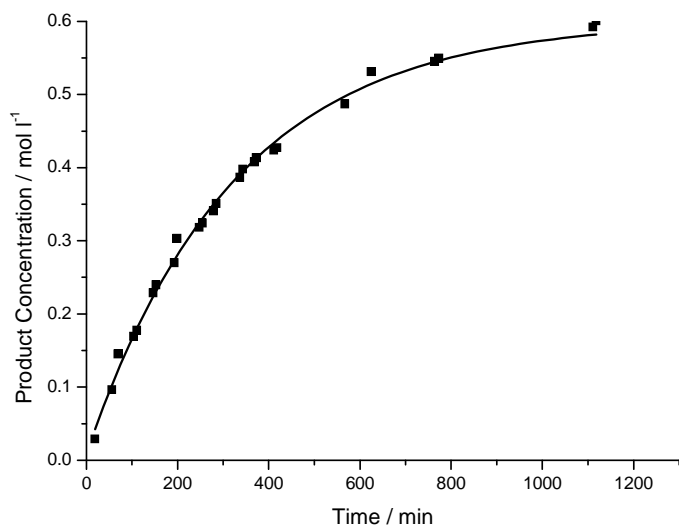
293 K, 10 mol% catalyst, substrate B, initial rate: $5.6(3) \times 10^{-5} \text{ mol dm}^{-3} \text{ s}^{-1}$.

8. $[\text{Ca}(\text{NN}^{\text{ArMe}})\{\text{N}(\text{SiMe}_3)_2\}(\text{THF})_n]$ [5c]



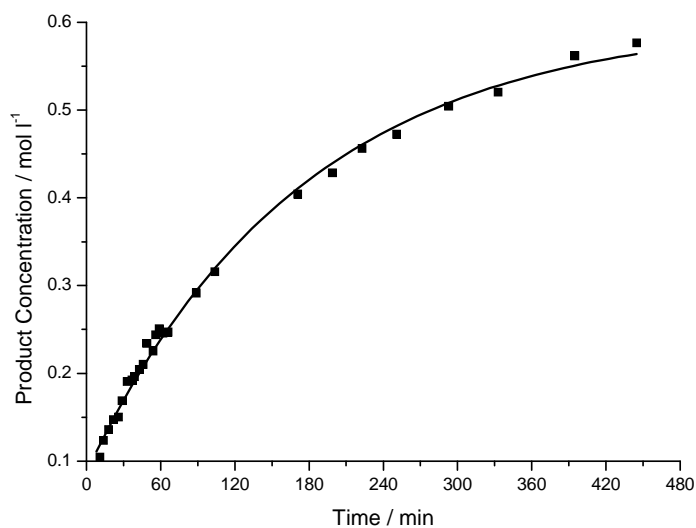
293 K, 10 mol% catalyst, substrate B, initial rate: $4.3(2) \times 10^{-6} \text{ mol dm}^{-3} \text{ s}^{-1}$.

9. $[\text{Ca}(\text{NN}^{\text{Ph}})\{\text{N}(\text{SiMe}_3)_2\}(\text{THF})_n]$ [5d]



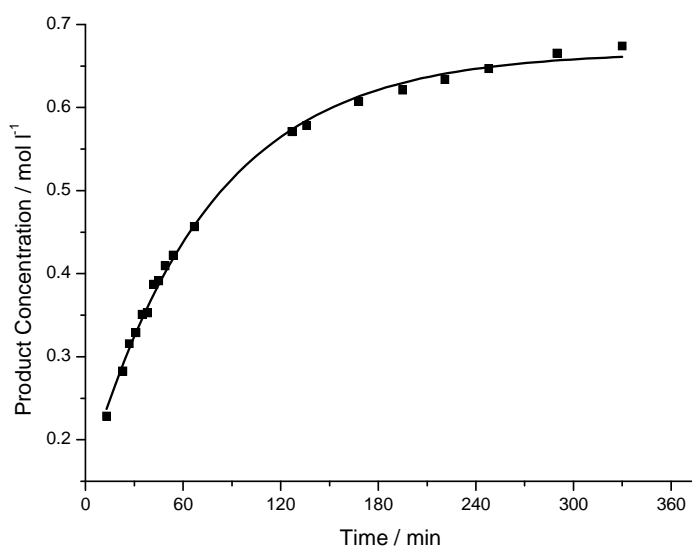
293 K, 10 mol% catalyst, substrate B, initial rate: $3.0(1) \times 10^{-5} \text{ mol dm}^{-3} \text{ s}^{-1}$.

10. $[\text{Ca}(\text{NN}^{\text{iPr}})\{\text{N}(\text{SiMe}_3)_2\}(\text{THF})_n]$ [5e]



293 K, 10 mol% catalyst, substrate B, initial rate: $4.9(2) \times 10^{-5} \text{ mol dm}^{-3} \text{ s}^{-1}$.

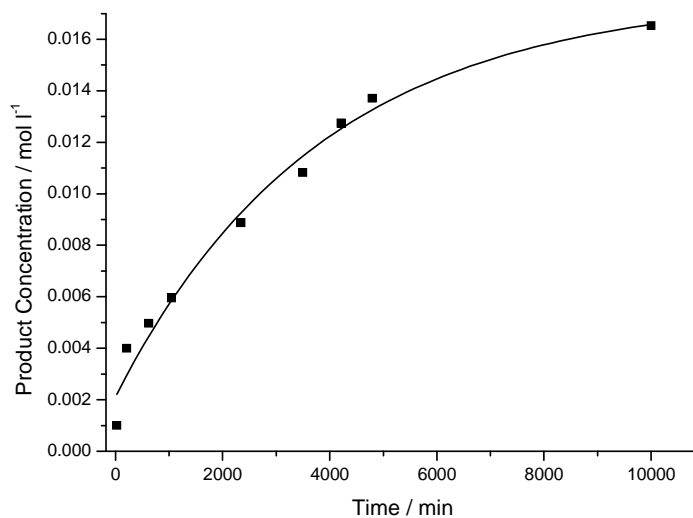
11. $[\text{Ca}(\text{NN}^{\text{tBu}})\{\text{N}(\text{SiMe}_3)_2\}(\text{THF})_n]$ [5f]



293 K, 10 mol% catalyst, substrate B, initial rate: $1.1(1) \times 10^{-4} \text{ mol dm}^{-3} \text{ s}^{-1}$.

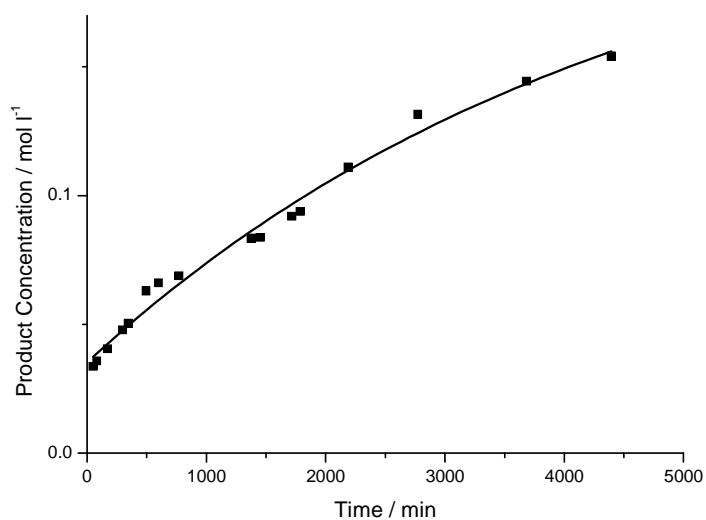
Appendix B: Product Conversion Curves for Chapter Four

1. $[\text{Ca}(\text{Ar}^{\text{F}}\text{-BIM})\{\text{N}(\text{SiMe}_3)_2\}(\text{THF})]$ [9a]



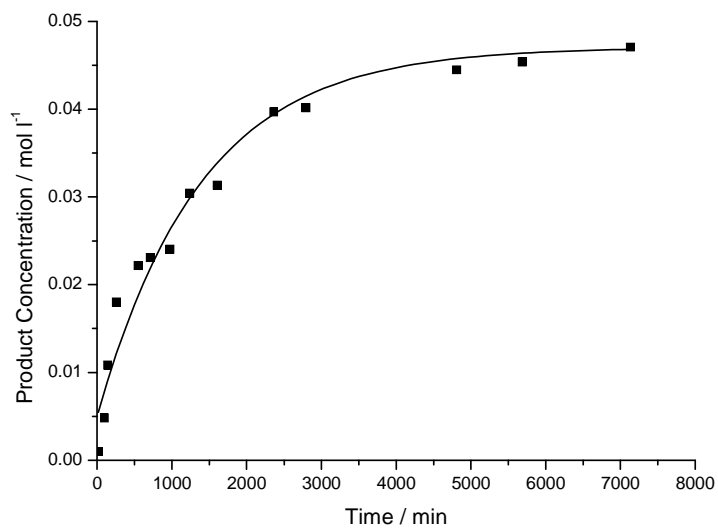
293 K, 10 mol% catalyst, substrate A, initial rate: $6.8(3) \times 10^{-8} \text{ mol dm}^{-3} \text{ s}^{-1}$.

2. $[\text{Ca}(\text{Ar}^{\text{OMe}}\text{-BIM})\{\text{N}(\text{SiMe}_3)_2\}(\text{THF})]$ [9b]



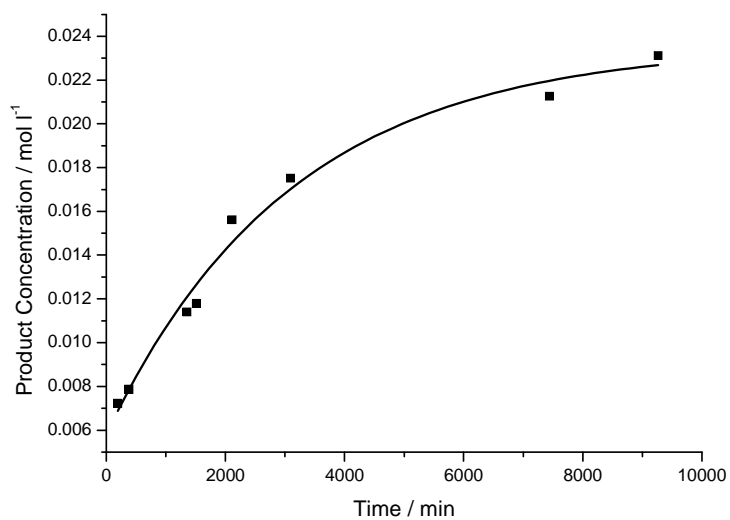
293 K, 10 mol% catalyst, substrate A, initial rate: $7.2(3) \times 10^{-6} \text{ mol dm}^{-3} \text{ s}^{-1}$.

3. [Ca(Ar^{Me}-BIM){N(SiMe₃)₂}(THF)] [9c]



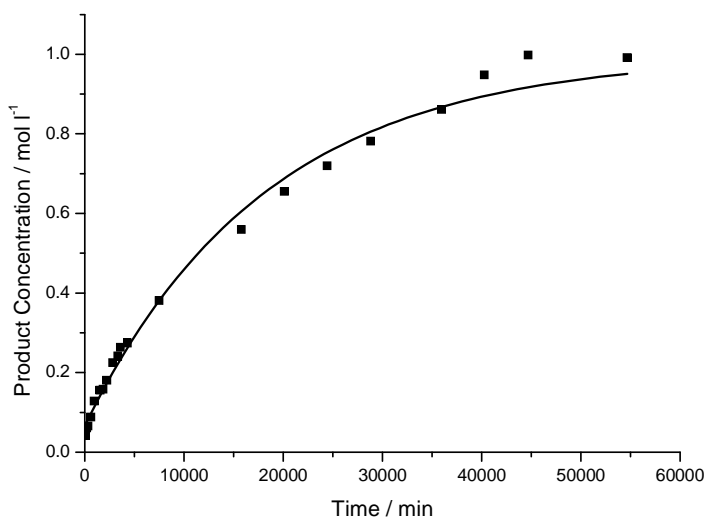
293 K, 10 mol% catalyst, substrate A, initial rate: $5.1(5) \times 10^{-7} \text{ mol dm}^{-3} \text{ s}^{-1}$.

4. [Ca(Ph-BIM){N(SiMe₃)₂}(THF)] [9d]



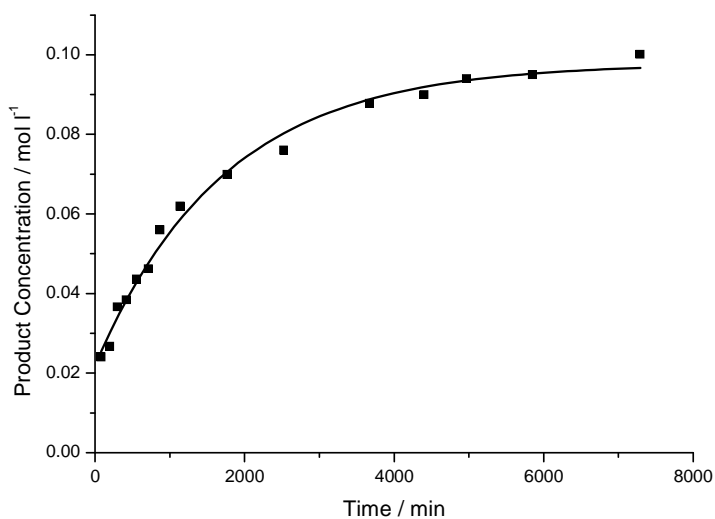
293 K, 10 mol% catalyst, substrate A, initial rate: $9.5(4) \times 10^{-8} \text{ mol dm}^{-3} \text{ s}^{-1}$.

5. $[\text{Ca}(\text{Ar}^{3,5\text{Me}}\text{-BIM})\{\text{N}(\text{SiMe}_3)_2\}(\text{THF})]$ [9f]



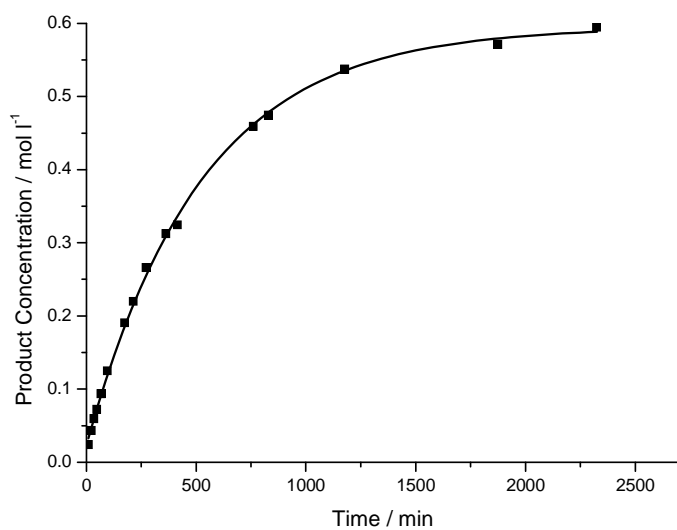
293 K, 10 mol% catalyst, substrate A, initial rate: $8.5(4) \times 10^{-7} \text{ mol dm}^{-3} \text{ s}^{-1}$.

6. $[\text{Ca}(\text{tBu-BIM})\{\text{N}(\text{SiMe}_3)_2\}(\text{THF})]$ [9i]



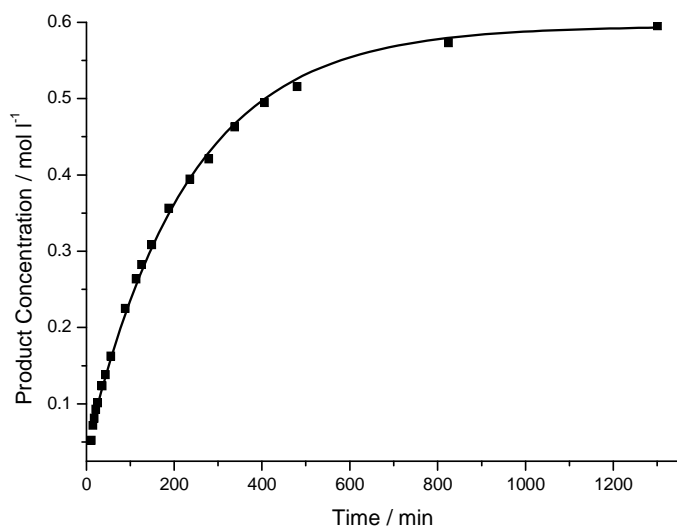
293 K, 10 mol% catalyst, substrate A, initial rate: $7.3(4) \times 10^{-7} \text{ mol dm}^{-3} \text{ s}^{-1}$.

7. [Ca(Ar^F-BIM){N(SiMe₃)₂}(THF)] [9a]



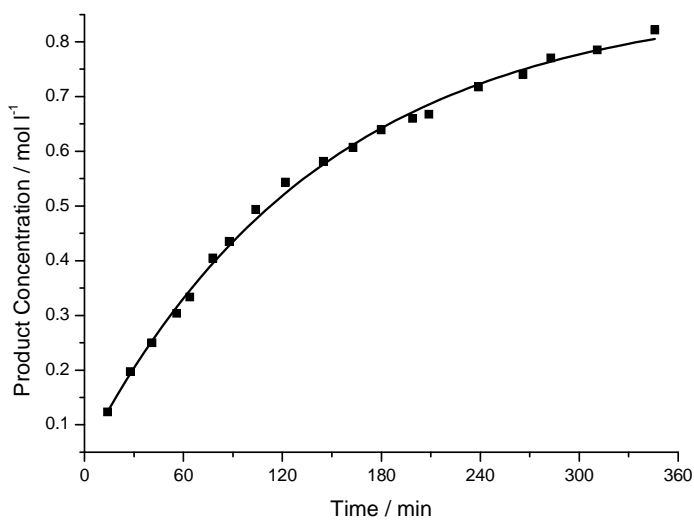
293 K, 10 mol% catalyst, substrate B, initial rate: $1.8(1) \times 10^{-5} \text{ mol dm}^{-3} \text{ s}^{-1}$.

8. [Ca(Ar^F-BIM){N(SiMe₃)₂}(THF)] [9a]



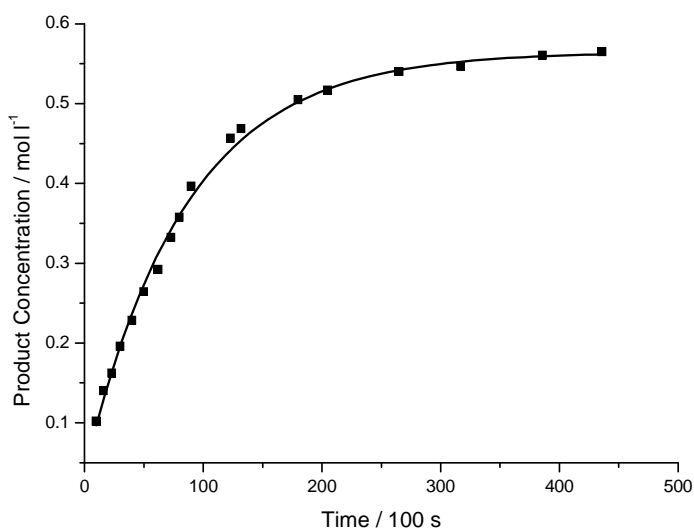
293 K, 20 mol% catalyst, substrate B, initial rate: $4.0(3) \times 10^{-5} \text{ mol dm}^{-3} \text{ s}^{-1}$.

9. $[\text{Ca}(\text{Ar}^{\text{OMe}}\text{-BIM})\{\text{N}(\text{SiMe}_3)_2\}(\text{THF})]$ [9b]



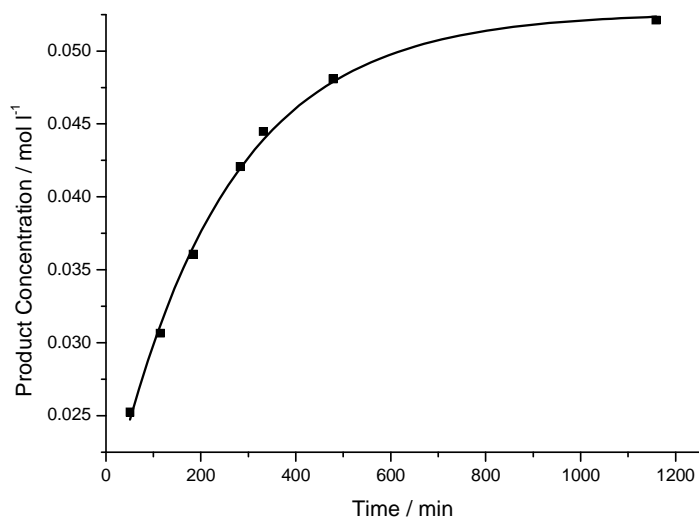
293 K, 10 mol% catalyst, substrate B, initial rate: $9.7(4) \times 10^{-5} \text{ mol dm}^{-3} \text{ s}^{-1}$.

10. $[\text{Ca}(\text{Ar}^{\text{Me}}\text{-BIM})\{\text{N}(\text{SiMe}_3)_2\}(\text{THF})]$ [9c]



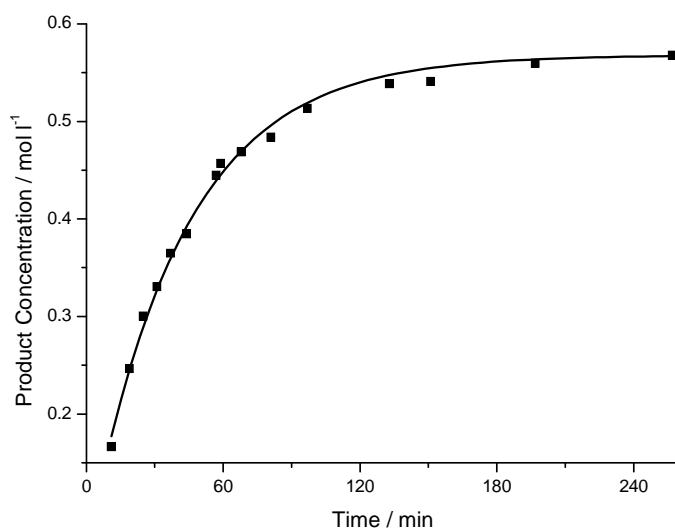
293 K, 10 mol% catalyst, substrate B, initial rate: $1.0(1) \times 10^{-4} \text{ mol dm}^{-3} \text{ s}^{-1}$.

11. $[\text{Ca}(\text{Ar}^{\text{Me}}\text{-BIM})\{\text{N}(\text{SiMe}_3)_2\}(\text{THF})]$ [9c]



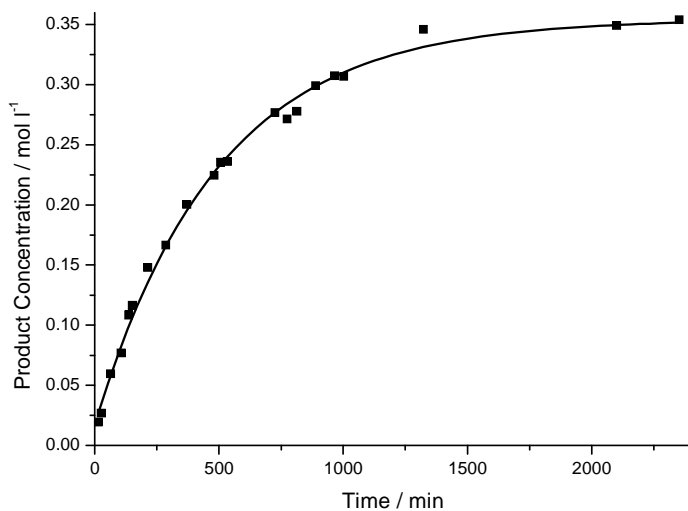
293 K, 5 mol% catalyst, substrate B, initial rate: $2.5(1) \times 10^{-6} \text{ mol dm}^{-3} \text{ s}^{-1}$.

12. $[\text{Ca}(\text{Ar}^{\text{Me}}\text{-BIM})\{\text{N}(\text{SiMe}_3)_2\}(\text{THF})]$ [9c]



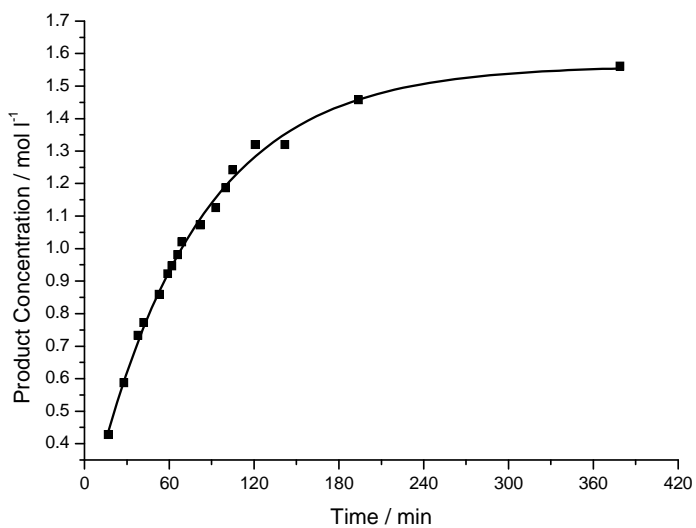
293 K, 20 mol% catalyst, substrate B, initial rate: $2.2(4) \times 10^{-4} \text{ mol dm}^{-3} \text{ s}^{-1}$.

13. [Ca(Ph-BIM){N(SiMe₃)₂}(THF)] [9d]



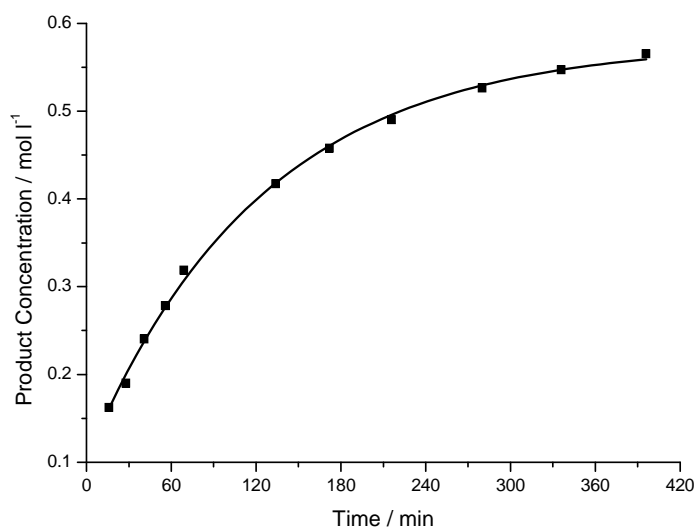
293 K, 10 mol% catalyst, substrate B, initial rate: $1.1(1) \times 10^{-5} \text{ mol dm}^{-3} \text{ s}^{-1}$.

14. [Ca(Ar^{3,5Me}-BIM){N(SiMe₃)₂}(THF)] [9f]



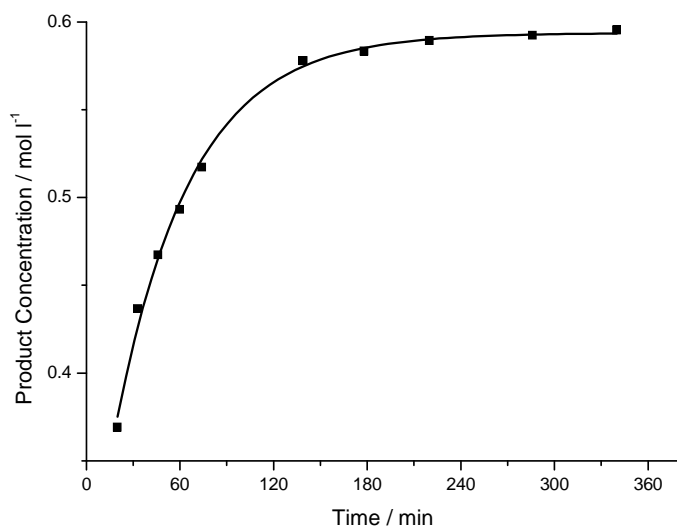
293 K, 10 mol% catalyst, substrate B, initial rate: $3.1(1) \times 10^{-4} \text{ mol dm}^{-3} \text{ s}^{-1}$.

15. [Ca(tBu-BIM){N(SiMe₃)₂}(THF)] [9i]



293 K, 10 mol% catalyst, substrate B, initial rate: $6.4(3) \times 10^{-6} \text{ mol dm}^{-3} \text{ s}^{-1}$.

16. [Ca(tBu-BIM){N(SiMe₃)₂}(THF)] [9i]



293 K, 20 mol% catalyst, substrate B, initial rate: $1.1(1) \times 10^{-4} \text{ mol dm}^{-3} \text{ s}^{-1}$.

Appendix C: X-ray Structure Analysis of [1]

1. Crystal data and structure refinement

Empirical formula	C ₁₃ H ₁₂ ClNO ₃
Formula weight	265.69
Crystal description	colourless needle
Crystal size	0.25 x 0.15 x 0.10 mm
Temperature	150 K
Crystal system	Hexagonal
Space group	P6 ₁
Unit cell dimensions	$a = 10.670(2) \text{ \AA}$ $\alpha = 90^\circ$ $b = 10.670(2) \text{ \AA}$ $\beta = 90^\circ$ $c = 19.506(4) \text{ \AA}$ $\gamma = 120^\circ$
Reflections for cell refinement	1971
Range in theta	4 to 24 °
Volume, Z	1923.0(5) A ³ , 6
Density (calculated)	1.377 mg/m ³
Absorption coefficient	0.297 mm ⁻¹
F(000)	828
Diffractometer type	Area
Wavelength	0.71073 A
Scan type	φ & ω scans
Theta range for data collection	4 to 24 deg.
Index ranges	-9<=h<=0, 0<=k<=12, -22<=l<=22
Reflections collected	9106
Independent reflections	1971 [R(merge) = 0.097]
Observed reflections	1183
Absorption correction	Multi-scan (T _{min} = 0.96, T _{max} = 0.97)
Structure solution by	direct and Fourier difference maps
Hydrogen atom location	geometric
Hydrogen atom treatment	Riding model
Refinement method	Full-matrix least-squares on F ²
Weighting scheme	Modified ShelX

Data / restraints / parameters	1961 / 24/ 164
Goodness-of-fit on F^2	0.9353
Final R indices [$I > 2\sigma(I)$]	$R_1 = 0.0842$, $R_w = 0.2066$
Final R indices [all data]	$R_1 = 0.1271$, $R_w = 0.2297$
Absolute structure parameter	0.1(2)
Final maximum delta/sigma	0.000621
Largest diff. peak and hole	1.90 and -1.16 e. \AA^{-3}

2. Bond lengths (\AA) and angles ($^\circ$)

Cl(1)-C(1)	1.812(10)	C(3)-C(5)	1.43(2)
O(1)-C(1)	1.170(9)	C(6)-C(7)	1.489(12)
O(2)-C(6)	1.187(9)	C(7)-C(8)	1.311(12)
O(3)-C(13)	1.214(10)	C(7)-C(12)	1.383(11)
N(1)-C(2)	1.467(10)	C(8)-C(9)	1.468(14)
N(1)-C(6)	1.409(10)	C(9)-C(10)	1.315(13)
N(1)-C(13)	1.375(10)	C(10)-C(11)	1.391(12)
C(1)-C(2)	1.495(12)	C(11)-C(12)	1.377(12)
C(2)-C(3)	1.53(2)	C(12)-C(13)	1.505(12)
C(3)-C(4)	1.57(2)		
C(2)-N(1)-C(6)	122.9(6)	C(4)-C(3)-C(5)	115.2(12)
C(2)-N(1)-C(13)	123.6(6)	N(1)-C(6)-O(2)	123.4(8)
C(6)-N(1)-C(13)	113.1(7)	N(1)-C(6)-C(7)	104.9(7)
Cl(1)-C(1)-O(1)	118.7(8)	O(2)-C(6)-C(7)	131.7(8)
Cl(1)-C(1)-C(2)	112.1(7)	C(6)-C(7)-C(8)	130.4(8)
O(1)-C(1)-C(2)	129.2(9)	C(6)-C(7)-C(12)	108.5(7)
C(1)-C(2)-N(1)	111.9(7)	C(8)-C(7)-C(12)	121.1(8)
C(1)-C(2)-C(3)	112.4(8)	C(7)-C(8)-C(9)	117.7(9)
N(1)-C(2)-C(3)	114.7(8)	C(8)-C(9)-C(10)	119.4(9)
C(2)-C(3)-C(4)	105.3(9)	C(9)-C(10)-C(11)	123.5(9)
C(2)-C(3)-C(5)	119.0(10)	C(10)-C(11)-C(12)	115.4(9)
C(7)-C(12)-C(11)	122.8(8)	C(12)-C(13)-N(1)	105.3(7)

C(7)-C(12)-C(13)	108.1(7)	C(12)-C(13)-O(3)	129.6(8)
C(11)-C(12)-C(13)	129.1(8)	N(1)-C(13)-O(3)	125.1(8)

Appendix D: X-ray Structure Analysis of [13a]

1. Crystal data and structure refinement

Empirical formula	C ₁₄ H ₁₆ FN ₃
Formula weight	245.30
Crystal description	colourless regular
Crystal size	0.50 × 0.40 × 0.08 mm
Temperature	150 K
Crystal system	Triclinic
Space group	P 1
Unit cell dimensions	a = 7.675(2) Å α = 81.66(3) ° b = 9.359(2) Å β = 87.70(3) ° c = 9.395(2) Å γ = 77.93(3) °
Reflections for cell refinement	4205
Range in theta	4 to 28 °
Volume, Z	652.9(2) Å ³ , 2
Density (calculated)	1.248 mg/m ³
Absorption coefficient	0.086 mm ⁻¹
F(000)	260
Diffractometer type	Area
Wavelength	0.71073 Å
Scan type	φ & ω scans
Theta range for data collection	4 to 28 °
Index ranges	-9 ≤ h ≤ 9, -11 ≤ k ≤ 12, 0 ≤ l ≤ 12
Reflections collected	4205
Independent reflections	2900 [R(merge) = 0.030]
Observed reflections	2433
Absorption correction	Multi-scan (T _{min} = 0.97, T _{max} = 0.99)
Structure solution by	direct and Fourier difference maps
Hydrogen atom location	geometrical
Hydrogen atom treatment	riding model
Refinement method	Full-matrix least-squares on F ²
Weighting scheme	modified ShelX
Data / restraints / parameters	2893 / 39 / 325

Goodness-of-fit on F	0.9971
Final R indices [$I > 2\sigma(I)$]	$R_1 = 0.0658$, $R_w = 0.1644$
Final R indices [all data]	$R_1 = 0.0766$, $R_w = 0.1749$
Final maximum delta/sigma	0.000707
Largest diff. peak and hole	0.72 and -0.40 e.Å ⁻³

2. Bond lengths (Å) and angles (°)

F(1)-C(12)	1.349(5)	C(6)-C(8)	1.548(6)
F(2)-C(26)	1.367(6)	C(9)-C(10)	1.396(6)
N(1)-C(1)	1.155(6)	C(9)-C(14)	1.386(6)
N(2)-C(3)	1.353(6)	C(10)-C(11)	1.375(7)
N(2)-C(5)	1.480(5)	C(11)-C(12)	1.382(7)
N(3)-C(3)	1.374(6)	C(12)-C(13)	1.382(7)
N(3)-C(4)	1.456(6)	C(13)-C(14)	1.383(7)
N(3)-C(9)	1.435(6)	C(15)-C(16)	1.416(6)
N(4)-C(15)	1.153(6)	C(16)-C(17)	1.374(6)
N(5)-C(17)	1.357(6)	C(18)-C(19)	1.539(8)
N(5)-C(19)	1.461(6)	C(19)-C(20)	1.407(8)
N(6)-C(17)	1.366(6)	C(20)-C(21)	1.527(9)
N(6)-C(18)	1.463(6)	C(20)-C(22)	1.501(8)
N(6)-C(23)	1.415(6)	C(23)-C(24)	1.394(7)
C(1)-C(2)	1.389(6)	C(23)-C(28)	1.377(7)
C(2)-C(3)	1.375(6)	C(24)-C(25)	1.397(8)
C(4)-C(5)	1.531(6)	C(25)-C(26)	1.366(8)
C(5)-C(6)	1.541(6)	C(26)-C(27)	1.357(8)
C(6)-C(7)	1.546(7)	C(27)-C(28)	1.386(7)
C(3)-N(2)-C(5)	111.1(3)	C(11)-C(12)-C(13)	122.4(4)
C(3)-N(3)-C(4)	110.1(4)	C(12)-C(13)-C(14)	118.2(4)
C(3)-N(3)-C(9)	124.5(4)	C(9)-C(14)-C(13)	120.5(4)
C(4)-N(3)-C(9)	120.1(4)	N(4)-C(15)-C(16)	177.6(5)
C(17)-N(5)-C(19)	112.3(4)	C(15)-C(16)-C(17)	121.7(4)
C(17)-N(6)-C(18)	111.3(4)	C(16)-C(17)-N(6)	124.4(4)

C(17)-N(6)-C(23)	125.4(4)	C(16)-C(17)-N(5)	127.1(4)
C(18)-N(6)-C(23)	123.3(4)	N(6)-C(17)-N(5)	108.5(4)
N(1)-C(1)-C(2)	177.3(5)	N(6)-C(18)-C(19)	103.2(4)
C(1)-C(2)-C(3)	121.9(4)	C(18)-C(19)-N(5)	101.8(4)
C(2)-C(3)-N(3)	124.3(4)	C(18)-C(19)-C(20)	120.7(5)
C(2)-C(3)-N(2)	127.0(4)	N(5)-C(19)-C(20)	121.4(5)
N(3)-C(3)-N(2)	108.7(4)	C(19)-C(20)-C(21)	112.6(5)
N(3)-C(4)-C(5)	102.8(4)	C(19)-C(20)-C(22)	115.6(6)
C(4)-C(5)-N(2)	100.7(3)	C(21)-C(20)-C(22)	110.7(5)
C(4)-C(5)-C(6)	112.0(4)	N(6)-C(23)-C(24)	119.8(4)
N(2)-C(5)-C(6)	110.9(3)	N(6)-C(23)-C(28)	120.0(4)
C(5)-C(6)-C(7)	108.8(4)	C(24)-C(23)-C(28)	120.2(4)
C(5)-C(6)-C(8)	109.8(4)	C(23)-C(24)-C(25)	119.4(5)
C(7)-C(6)-C(8)	108.9(4)	C(24)-C(25)-C(26)	118.3(4)
N(3)-C(9)-C(10)	120.8(4)	F(2)-C(26)-C(25)	118.3(5)
N(3)-C(9)-C(14)	119.3(4)	F(2)-C(26)-C(27)	118.7(5)
C(10)-C(9)-C(14)	119.9(4)	C(25)-C(26)-C(27)	123.0(5)
C(9)-C(10)-C(11)	120.2(4)	C(26)-C(27)-C(28)	119.1(5)
C(10)-C(11)-C(12)	118.7(4)	C(27)-C(28)-C(23)	119.9(4)
F(1)-C(12)-C(13)	118.7(4)		

Appendix E: X-ray Structure Analysis of [13b]

1. Crystal data and structure refinement

Empirical formula	C ₁₅ H ₁₉ N ₃ O
Formula weight	257.33
Crystal description	colourless prism
Crystal size	0.40 x 0.40 x 0.40 mm
Temperature	150 K
Crystal system	Triclinic
Space group	P 1
Unit cell dimensions	a = 9.867(2) Å α = 63.10(3) ° b = 13.137(3) Å β = 70.19(3) ° c = 13.140(3) Å γ = 77.15(3) °
Reflections for cell refinement	9147
Range in theta	4 to 27 deg.
Volume, Z	1424.3(7) Å ³ , 4
Density (calculated)	1.200 mg/m ³
Absorption coefficient	0.077 mm ⁻¹
F(000)	552
Diffractometer type	Area
Wavelength	0.71073 Å
Scan type	φ & ω scans
Theta range for data collection	4 to 27 °
Index ranges	-11 ≤ h ≤ 12, -14 ≤ k ≤ 17, 0 ≤ l ≤ 17
Reflections collected	9147
Independent reflections	6440 [R(merge) = 0.043]
Observed reflections	4476
Absorption correction	Multi-scan (T _{min} = 0.97, T _{max} = 0.97)
Structure solution by	direct and Fourier difference maps
Hydrogen atom location	geometrical
Hydrogen atom treatment	riding model
Refinement method	Full-matrix least-squares on F ²
Weighting scheme	modified ShelX
Data / restraints / parameters	6431 / 3/ 685

Goodness-of-fit on F	0.9862
Final R indices [$I > 2\sigma(I)$]	$R_1 = 0.0728$, $R_w = 0.1586$
Final maximum delta/sigma	0.000324
Largest diff. peak and hole	0.67 and -0.50 e. \AA^{-3}

2. Bond lengths (\AA) and angles ($^\circ$)

N(1)-C(1)	1.159(7)	C(10)-C(11)	1.372(8)
N(2)-C(3)	1.365(7)	C(11)-C(12)	1.388(8)
N(2)-C(5)	1.471(6)	C(12)-C(13)	1.376(7)
N(3)-C(3)	1.373(6)	C(13)-C(14)	1.388(8)
N(3)-C(4)	1.468(7)	C(16)-C(17)	1.405(8)
N(3)-C(9)	1.420(6)	C(17)-C(18)	1.372(8)
N(4)-C(16)	1.146(7)	C(19)-C(20)	1.526(7)
N(5)-C(18)	1.351(7)	C(20)-C(21)	1.520(7)
N(5)-C(20)	1.467(7)	C(21)-C(22)	1.518(8)
N(6)-C(18)	1.370(6)	C(21)-C(23)	1.515(8)
N(6)-C(19)	1.452(7)	C(24)-C(25)	1.380(8)
N(6)-C(24)	1.440(7)	C(24)-C(29)	1.379(8)
N(7)-C(31)	1.143(7)	C(25)-C(26)	1.399(8)
N(8)-C(33)	1.361(7)	C(26)-C(27)	1.370(8)
N(8)-C(35)	1.485(6)	C(27)-C(28)	1.383(9)
N(9)-C(33)	1.371(6)	C(28)-C(29)	1.377(8)
N(9)-C(34)	1.468(7)	C(31)-C(32)	1.408(7)
N(9)-C(39)	1.433(7)	C(32)-C(33)	1.377(7)
N(10)-C(46)	1.162(7)	C(34)-C(35)	1.535(7)
N(11)-C(48)	1.340(7)	C(35)-C(36)	1.516(7)
N(11)-C(50)	1.458(7)	C(36)-C(37)	1.530(8)
N(12)-C(48)	1.373(7)	C(36)-C(38)	1.512(8)
N(12)-C(49)	1.441(8)	C(39)-C(40)	1.383(8)
N(12)-C(54)	1.416(7)	C(39)-C(44)	1.377(7)
O(1)-C(12)	1.383(6)	C(40)-C(41)	1.381(8)
O(1)-C(15)	1.406(7)	C(41)-C(42)	1.389(8)

O(2)-C(27)	1.376(7)	C(42)-C(43)	1.388(8)
O(2)-C(30)	1.436(8)	C(43)-C(44)	1.415(7)
O(3)-C(42)	1.364(7)	C(46)-C(47)	1.404(7)
O(3)-C(45)	1.419(8)	C(47)-C(48)	1.341(8)
O(4)-C(57)	1.367(7)	C(49)-C(50)	1.556(9)
O(4)-C(60)	1.427(8)	C(50)-C(51)	1.465(9)
C(1)-C(2)	1.395(8)	C(51)-C(52)	1.497(9)
C(9)-C(14)	1.365(8)	C(51)-C(53)	1.520(9)
C(9)-C(10)	1.528(7)	C(54)-C(55)	1.401(7)
C(6)-C(8)	1.511(7)	C(54)-C(59)	1.393(9)
C(6)-C(7)	1.533(8)	C(55)-C(56)	1.382(8)
C(5)-C(6)	1.525(8)	C(56)-C(57)	1.384(8)
C(4)-C(5)	1.384(7)	C(57)-C(58)	1.387(8)
C(2)-C(3)	1.378(7)	C(58)-C(59)	1.369(8)
C(3)-N(2)-C(5)	111.0(4)	N(6)-C(24)-C(25)	119.9(5)
C(3)-N(3)-C(4)	110.0(4)	N(6)-C(24)-C(29)	119.5(5)
C(3)-N(3)-C(9)	124.4(5)	C(25)-C(24)-C(29)	120.6(5)
C(4)-N(3)-C(9)	122.1(4)	C(24)-C(25)-C(26)	119.7(5)
C(18)-N(5)-C(20)	111.2(4)	C(25)-C(26)-C(27)	119.4(5)
C(18)-N(6)-C(19)	110.7(4)	O(2)-C(27)-C(26)	124.8(6)
C(18)-N(6)-C(24)	124.1(5)	O(2)-C(27)-C(28)	114.7(6)
C(19)-N(6)-C(24)	122.5(4)	C(26)-C(27)-C(28)	120.5(5)
C(33)-N(8)-C(35)	110.8(4)	C(27)-C(28)-C(29)	120.3(6)
C(33)-N(9)-C(34)	109.2(4)	C(24)-C(29)-C(28)	119.6(5)
C(33)-N(9)-C(39)	125.1(5)	N(7)-C(31)-C(32)	179.3(6)
C(34)-N(9)-C(39)	120.3(4)	C(31)-C(32)-C(33)	120.6(5)
C(48)-N(11)-C(50)	110.9(5)	C(32)-C(33)-N(9)	124.4(5)
C(48)-N(12)-C(49)	111.4(5)	C(32)-C(33)-N(8)	126.0(5)
C(48)-N(12)-C(54)	126.7(5)	N(9)-C(33)-N(8)	109.6(5)
C(49)-N(12)-C(54)	121.9(5)	N(9)-C(34)-C(35)	103.7(4)
C(12)-O(1)-C(15)	117.8(4)	C(34)-C(35)-N(8)	100.4(4)
C(27)-O(2)-C(30)	116.8(6)	C(34)-C(35)-C(36)	111.7(4)

C(42)-O(3)-C(45)	118.0(5)	N(8)-C(35)-C(36)	112.7(4)
C(57)-O(4)-C(60)	116.6(5)	C(35)-C(36)-C(37)	108.7(4)
N(1)-C(1)-C(2)	179.2(7)	C(35)-C(36)-C(38)	112.3(4)
C(1)-C(2)-C(3)	121.4(6)	C(37)-C(36)-C(38)	108.9(5)
N(3)-C(3)-N(2)	107.6(5)	N(9)-C(39)-C(40)	121.4(5)
N(3)-C(3)-C(2)	124.5(5)	N(9)-C(39)-C(44)	117.5(5)
N(2)-C(3)-C(2)	127.9(5)	C(40)-C(39)-C(44)	121.1(5)
N(3)-C(4)-C(5)	101.9(4)	C(39)-C(40)-C(41)	119.5(5)
C(4)-C(5)-N(2)	100.1(4)	C(40)-C(41)-C(42)	120.6(6)
C(4)-C(5)-C(6)	115.6(4)	C(41)-C(42)-O(3)	115.5(5)
N(2)-C(5)-C(6)	114.2(4)	C(41)-C(42)-C(43)	120.2(5)
C(5)-C(6)-C(7)	110.0(4)	O(3)-C(42)-C(43)	124.2(5)
C(5)-C(6)-C(8)	110.3(4)	C(42)-C(43)-C(44)	119.0(5)
C(7)-C(6)-C(8)	110.3(5)	C(43)-C(44)-C(39)	119.6(6)
N(3)-C(9)-C(10)	121.7(5)	N(10)-C(46)-C(47)	178.8(6)
N(3)-C(9)-C(14)	119.3(4)	C(46)-C(47)-C(48)	120.4(5)
C(10)-C(9)-C(14)	119.0(5)	N(12)-C(48)-C(47)	125.9(5)
C(9)-C(10)-C(11)	120.3(5)	N(12)-C(48)-N(11)	107.9(5)
C(10)-C(11)-C(12)	120.5(5)	C(47)-C(48)-N(11)	126.2(5)
C(11)-C(12)-O(1)	115.4(5)	N(12)-C(49)-C(50)	99.8(5)
C(11)-C(12)-C(13)	119.8(5)	C(49)-C(50)-N(11)	101.0(5)
O(1)-C(12)-C(13)	124.8(5)	C(49)-C(50)-C(51)	114.9(6)
C(12)-C(13)-C(14)	119.1(5)	N(11)-C(50)-C(51)	115.9(6)
C(13)-C(14)-C(9)	121.3(5)	C(50)-C(51)-C(52)	111.8(6)
N(4)-C(16)-C(17)	178.8(6)	C(50)-C(51)-C(53)	113.0(6)
C(16)-C(17)-C(18)	121.0(5)	C(52)-C(51)-C(53)	111.0(6)
C(17)-C(18)-N(6)	124.8(5)	N(12)-C(54)-C(55)	120.6(6)
C(17)-C(18)-N(5)	127.2(5)	N(12)-C(54)-C(59)	120.8(5)
N(6)-C(18)-N(5)	107.9(5)	C(55)-C(54)-C(59)	118.5(5)
N(6)-C(19)-C(20)	102.2(4)	C(54)-C(55)-C(56)	120.8(6)
C(19)-C(20)-N(5)	100.8(4)	C(55)-C(56)-C(57)	119.6(5)
C(19)-C(20)-C(21)	113.9(4)	C(56)-C(57)-O(4)	125.4(5)
N(5)-C(20)-C(21)	114.2(4)	C(56)-C(57)-C(58)	120.1(5)

C(20)-C(21)-C(22)	111.1(4)	O(4)-C(57)-C(58)	114.5(6)
C(20)-C(21)-C(23)	110.9(4)	C(57)-C(58)-C(59)	120.4(6)
C(22)-C(21)-C(23)	110.6(5)	C(54)-C(59)-C(58)	120.7(5)

Appendix F: X-ray Structure Analysis of [13c]

1. Crystal data and structure refinement

Empirical formula	C ₁₅ H ₁₉ N ₃
Formula weight	241.34
Crystal description	colourless regular
Crystal size	0.50 × 0.40 × 0.08 mm
Temperature	150 K
Crystal system	Triclinic
Space group	P 1
Unit cell dimensions	a = 9.604(2) Å α = 105.03(3) ° b = 13.097(3) Å β = 109.34(3) ° c = 13.115(3) Å γ = 106.40(3) °
Reflections for cell refinement	9739
Range in theta	4 to 28 °
Volume, Z	1375.0(8) Å ³ , 4
Density (calculated)	1.166 mg/m ³
Absorption coefficient	0.071 mm ⁻¹
F(000)	520
Diffractometer type	Area
Wavelength	0.71073 Å
Scan type	φ & ω scans
Theta range for data collection	4 to 28 °
Index ranges	-12 ≤ h ≤ 11, -16 ≤ k ≤ 16, 0 ≤ l ≤ 17
Reflections collected	9739
Independent reflections	6243 [R(merge) = 0.039]
Observed reflections	4269
Absorption correction	Multi-scan (T _{min} = 0.97, T _{max} = 0.99)
Structure solution by	direct and Fourier difference maps
Hydrogen atom location	geometrical
Hydrogen atom treatment	riding model
Refinement method	Full-matrix least-squares on F ²
Weighting scheme	Modified ShelX
Data / restraints / parameters	6227 / 3/ 649

Goodness-of-fit on F	0.9800
Final R indices [$I > 2\sigma(I)$]	$R_1 = 0.0706$, $R_w = 0.1604$
Final R indices [all data]	$R_1 = 0.1034$, $R_w = 0.1829$
Final maximum Δ/σ	0.008134
Largest diff. peak and hole	0.79 and -0.55 e. \AA^{-3}

2. Bond lengths (\AA) and angles ($^\circ$)

N(1)-C(1)	1.140(8)	C(17)-C(18)	1.364(8)
N(2)-C(3)	1.368(7)	C(19)-C(20)	1.548(9)
N(2)-C(5)	1.475(7)	C(20)-C(21)	1.526(7)
N(3)-C(3)	1.363(8)	C(21)-C(22)	1.517(9)
N(3)-C(4)	1.456(8)	C(21)-C(23)	1.503(9)
N(3)-C(9)	1.425(8)	C(24)-C(25)	1.389(8)
N(4)-C(16)	1.165(8)	C(24)-C(29)	1.391(8)
N(5)-C(18)	1.349(7)	C(25)-C(26)	1.399(9)
N(5)-C(20)	1.470(7)	C(26)-C(27)	1.392(9)
N(6)-C(18)	1.375(8)	C(27)-C(28)	1.379(9)
N(6)-C(19)	1.473(8)	C(27)-C(30)	1.508(8)
N(6)-C(24)	1.411(7)	C(28)-C(29)	1.378(9)
N(7)-C(31)	1.155(8)	C(31)-C(32)	1.415(9)
N(8)-C(33)	1.352(7)	C(32)-C(33)	1.375(8)
N(8)-C(35)	1.489(7)	C(34)-C(35)	1.523(8)
N(9)-C(33)	1.372(7)	C(35)-C(36)	1.536(7)
N(9)-C(34)	1.470(7)	C(36)-C(37)	1.537(7)
N(9)-C(39)	1.408(7)	C(36)-C(38)	1.539(8)
N(10)-C(46)	1.158(8)	C(39)-C(40)	1.405(8)
N(11)-C(48)	1.359(7)	C(39)-C(44)	1.371(8)
N(11)-C(50)	1.454(7)	C(40)-C(41)	1.393(8)
N(12)-C(48)	1.353(8)	C(41)-C(42)	1.398(9)
N(12)-C(49)	1.451(7)	C(42)-C(43)	1.388(9)
N(12)-C(54)	1.439(7)	C(42)-C(45)	1.496(9)
C(1)-C(2)	1.397(9)	C(43)-C(44)	1.405(9)

C(2)-C(3)	1.377(8)	C(46)-C(47)	1.381(9)
C(4)-C(5)	1.494(8)	C(47)-C(48)	1.383(7)
C(5)-C(6)	1.503(8)	C(49)-C(50)	1.521(9)
C(6)-C(7)	1.540(9)	C(50)-C(51)	1.417(9)
C(6)-C(8)	1.519(10)	C(51)-C(52)	1.541(9)
C(9)-C(10)	1.386(8)	C(51)-C(53)	1.519(10)
C(9)-C(14)	1.394(8)	C(54)-C(55)	1.404(8)
C(10)-C(11)	1.382(9)	C(54)-C(59)	1.372(7)
C(11)-C(12)	1.373(8)	C(55)-C(56)	1.358(8)
C(12)-C(13)	1.403(8)	C(56)-C(57)	1.399(8)
C(12)-C(15)	1.498(8)	C(57)-C(58)	1.385(9)
C(13)-C(14)	1.384(8)	C(57)-C(60)	1.531(9)
C(16)-C(17)	1.404(9)	C(58)-C(59)	1.380(9)
C(3)-N(2)-C(5)	109.9(5)	C(25)-C(24)-C(29)	118.8(6)
C(3)-N(3)-C(4)	110.5(5)	C(24)-C(25)-C(26)	119.9(6)
C(3)-N(3)-C(9)	125.3(5)	C(25)-C(26)-C(27)	121.1(6)
C(4)-N(3)-C(9)	124.0(5)	C(26)-C(27)-C(28)	117.8(6)
C(18)-N(5)-C(20)	112.3(5)	C(26)-C(27)-C(30)	120.4(6)
C(18)-N(6)-C(19)	109.6(5)	C(28)-C(27)-C(30)	121.8(6)
C(18)-N(6)-C(24)	125.3(5)	C(27)-C(28)-C(29)	121.9(5)
C(19)-N(6)-C(24)	120.7(5)	C(24)-C(29)-C(28)	120.5(6)
C(33)-N(8)-C(35)	111.0(5)	N(7)-C(31)-C(32)	177.6(6)
C(33)-N(9)-C(34)	109.4(5)	C(31)-C(32)-C(33)	119.3(6)
C(33)-N(9)-C(39)	128.5(5)	C(32)-C(33)-N(9)	124.4(5)
C(34)-N(9)-C(39)	121.3(5)	C(32)-C(33)-N(8)	126.0(5)
C(48)-N(11)-C(50)	110.8(5)	N(9)-C(33)-N(8)	109.7(5)
C(48)-N(12)-C(49)	110.9(5)	N(9)-C(34)-C(35)	104.4(5)
C(48)-N(12)-C(54)	126.7(5)	C(34)-C(35)-N(8)	100.7(5)
C(49)-N(12)-C(54)	122.0(5)	C(34)-C(35)-C(36)	110.3(5)
N(1)-C(1)-C(2)	177.8(6)	N(8)-C(35)-C(36)	111.4(4)
C(1)-C(2)-C(3)	121.6(6)	C(35)-C(36)-C(37)	108.1(4)
C(2)-C(3)-N(2)	126.6(6)	C(35)-C(36)-C(38)	111.2(4)

C(2)-C(3)-N(3)	125.3(6)	C(37)-C(36)-C(38)	109.3(5)
N(2)-C(3)-N(3)	108.0(5)	N(9)-C(39)-C(40)	120.6(5)
N(3)-C(4)-C(5)	103.6(5)	N(9)-C(39)-C(44)	119.6(5)
C(4)-C(5)-N(2)	101.4(5)	C(40)-C(39)-C(44)	119.8(6)
C(4)-C(5)-C(6)	116.4(5)	C(39)-C(40)-C(41)	119.4(5)
N(2)-C(5)-C(6)	114.2(4)	C(40)-C(41)-C(42)	121.7(5)
C(5)-C(6)-C(7)	109.9(5)	C(41)-C(42)-C(43)	117.6(6)
C(5)-C(6)-C(8)	112.3(5)	C(41)-C(42)-C(45)	121.0(6)
C(7)-C(6)-C(8)	110.0(5)	C(43)-C(42)-C(45)	121.4(6)
N(3)-C(9)-C(10)	122.7(6)	C(42)-C(43)-C(44)	121.5(6)
N(3)-C(9)-C(14)	118.2(5)	C(43)-C(44)-C(39)	120.0(6)
C(10)-C(9)-C(14)	119.0(6)	N(10)-C(46)-C(47)	178.9(6)
C(9)-C(10)-C(11)	120.7(6)	C(46)-C(47)-C(48)	121.9(6)
C(10)-C(11)-C(12)	121.2(6)	C(47)-C(48)-N(11)	124.4(5)
C(11)-C(12)-C(13)	118.1(6)	C(47)-C(48)-N(12)	126.7(6)
C(11)-C(12)-C(15)	121.9(5)	N(11)-C(48)-N(12)	108.8(5)
C(13)-C(12)-C(15)	120.1(5)	N(12)-C(49)-C(50)	102.3(5)
C(12)-C(13)-C(14)	121.4(5)	C(49)-C(50)-N(11)	102.5(5)
C(9)-C(14)-C(13)	119.5(5)	C(49)-C(50)-C(51)	121.3(6)
N(4)-C(16)-C(17)	179.8(7)	N(11)-C(50)-C(51)	118.5(6)
C(16)-C(17)-C(18)	121.9(6)	C(50)-C(51)-C(52)	112.4(6)
N(6)-C(18)-C(17)	124.8(6)	C(50)-C(51)-C(53)	115.5(6)
N(6)-C(18)-N(5)	108.3(5)	C(52)-C(51)-C(53)	110.4(6)
C(17)-C(18)-N(5)	126.9(6)	N(12)-C(54)-C(55)	119.3(5)
N(6)-C(19)-C(20)	102.1(5)	N(12)-C(54)-C(59)	121.9(5)
C(19)-C(20)-N(5)	99.5(4)	C(55)-C(54)-C(59)	118.6(5)
C(19)-C(20)-C(21)	114.8(4)	C(54)-C(55)-C(56)	120.9(6)
N(5)-C(20)-C(21)	114.3(4)	C(55)-C(56)-C(57)	120.9(6)
C(20)-C(21)-C(22)	110.8(5)	C(56)-C(57)-C(58)	117.8(6)
C(20)-C(21)-C(23)	109.5(5)	C(56)-C(57)-C(60)	120.5(6)
C(22)-C(21)-C(23)	110.3(5)	C(58)-C(57)-C(60)	121.7(6)
N(6)-C(24)-C(25)	119.6(5)	C(57)-C(58)-C(59)	121.5(5)
N(6)-C(24)-C(29)	121.6(5)	C(58)-C(59)-C(54)	120.3(6)

Appendix G: X-ray Structure Analysis of [13f]

1. Crystal data and structure refinement

Empirical formula	C ₁₆ H ₂₁ N ₃
Formula weight	255.36
Crystal description	colourless regular
Crystal size	0.35 x 0.30 x 0.25 mm
Temperature	150 K
Crystal system	Triclinic
Space group	P 1
Unit cell dimensions	a = 8.270(2) Å α = 92.88(3) ° b = 8.574(2) Å β = 107.69(3) ° c = 12.369(3) Å γ = 115.03(3) °
Reflections for cell refinement	4737
Range in theta	4 to 28 °
Volume, Z	740.7(4) Å ³ , 2
Density (calculated)	1.145 mg/m ³
Absorption coefficient	0.069 mm ⁻¹
F(000)	276
Diffractometer type	Area
Wavelength	0.71073 Å
Scan type	φ & ω scans
Theta range for data collection	4 to 28 °
Index ranges	-10 ≤ h ≤ 9, -11 ≤ k ≤ 11, 0 ≤ l ≤ 16
Reflections collected	4737
Independent reflections	3369 [R(merge) = 0.032]
Observed reflections	2722
Absorption correction	Multi-scan (T _{min} = 0.98, T _{max} = 0.98)
Structure solution by	direct and Fourier difference maps
Hydrogen atom location	Geometrical
Hydrogen atom treatment	Riding model
Refinement method	Full-matrix least-squares on F ²
Weighting scheme	Modified ShelX
Data / restraints / parameters	3360 / 3 / 343

Goodness-of-fit on F	0.9684
Final R indices [$I > 2\sigma(I)$]	$R_1 = 0.0652$, $R_w = 0.1614$
Final R indices [all data]	$R_1 = 0.0800$, $R_w = 0.1763$
Final maximum Δ/σ	0.000624
Largest diff. peak and hole	0.68 and -0.46 e. \AA^{-3}

2. Bond lengths (\AA) and angles ($^\circ$)

N(1)-C(1)	1.158(6)	C(10)-C(11)	1.389(6)
N(2)-C(3)	1.359(5)	C(11)-C(12)	1.395(7)
N(2)-C(5)	1.453(6)	C(11)-C(15)	1.512(7)
N(3)-C(3)	1.360(6)	C(12)-C(13)	1.398(7)
N(3)-C(4)	1.466(6)	C(13)-C(14)	1.376(6)
N(3)-C(9)	1.411(6)	C(13)-C(16)	1.523(7)
N(4)-C(17)	1.150(6)	C(17)-C(18)	1.412(7)
N(5)-C(19)	1.350(5)	C(18)-C(19)	1.386(7)
N(5)-C(21)	1.491(5)	C(20)-C(21)	1.517(6)
N(6)-C(19)	1.380(6)	C(21)-C(22)	1.532(5)
N(6)-C(20)	1.458(6)	C(22)-C(23)	1.537(6)
N(6)-C(25)	1.426(6)	C(22)-C(24)	1.547(6)
C(1)-C(2)	1.387(6)	C(25)-C(26)	1.392(6)
C(2)-C(3)	1.375(7)	C(25)-C(30)	1.392(6)
C(4)-C(5)	1.536(6)	C(26)-C(27)	1.404(6)
C(5)-C(6)	1.456(7)	C(27)-C(28)	1.389(6)
C(6)-C(7)	1.537(8)	C(27)-C(31)	1.499(7)
C(6)-C(8)	1.520(7)	C(28)-C(29)	1.393(7)
C(9)-C(10)	1.403(6)	C(29)-C(30)	1.395(7)
C(9)-C(14)	1.400(7)	C(29)-C(32)	1.510(7)
C(3)-N(2)-C(5)	112.5(4)	C(12)-C(13)-C(14)	119.7(4)
C(3)-N(3)-C(4)	110.8(4)	C(12)-C(13)-C(16)	120.2(5)
C(3)-N(3)-C(9)	127.4(4)	C(14)-C(13)-C(16)	120.1(5)
C(4)-N(3)-C(9)	121.3(4)	C(9)-C(14)-C(13)	121.0(4)

C(19)-N(5)-C(21)	110.6(4)	N(4)-C(17)-C(18)	176.2(5)
C(19)-N(6)-C(20)	109.5(4)	C(17)-C(18)-C(19)	120.6(5)
C(19)-N(6)-C(25)	126.8(4)	C(18)-C(19)-N(6)	124.0(4)
C(20)-N(6)-C(25)	122.4(4)	C(18)-C(19)-N(5)	127.5(4)
N(1)-C(1)-C(2)	177.6(5)	N(6)-C(19)-N(5)	108.5(4)
C(1)-C(2)-C(3)	124.2(4)	N(6)-C(20)-C(21)	102.9(4)
C(2)-C(3)-N(3)	126.2(4)	C(20)-C(21)-N(5)	100.0(3)
C(2)-C(3)-N(2)	125.2(4)	C(20)-C(21)-C(22)	114.3(3)
N(3)-C(3)-N(2)	108.4(4)	N(5)-C(21)-C(22)	112.0(3)
N(3)-C(4)-C(5)	103.8(4)	C(21)-C(22)-C(23)	109.0(3)
C(4)-C(5)-N(2)	101.3(4)	C(21)-C(22)-C(24)	110.4(3)
C(4)-C(5)-C(6)	116.9(4)	C(23)-C(22)-C(24)	109.5(4)
N(2)-C(5)-C(6)	118.7(4)	N(6)-C(25)-C(26)	119.2(4)
C(5)-C(6)-C(7)	111.2(4)	N(6)-C(25)-C(30)	120.3(4)
C(5)-C(6)-C(8)	113.8(5)	C(26)-C(25)-C(30)	120.4(4)
C(7)-C(6)-C(8)	109.6(5)	C(25)-C(26)-C(27)	120.1(4)
N(3)-C(9)-C(10)	121.7(4)	C(26)-C(27)-C(28)	118.3(4)
N(3)-C(9)-C(14)	119.4(4)	C(26)-C(27)-C(31)	120.9(4)
C(10)-C(9)-C(14)	118.9(4)	C(28)-C(27)-C(31)	120.7(4)
C(9)-C(10)-C(11)	120.5(4)	C(27)-C(28)-C(29)	122.4(4)
C(10)-C(11)-C(12)	119.6(5)	C(28)-C(29)-C(30)	118.4(4)
C(10)-C(11)-C(15)	119.7(5)	C(28)-C(29)-C(32)	121.5(4)
C(12)-C(11)-C(15)	120.7(5)	C(30)-C(29)-C(32)	120.1(5)
C(11)-C(12)-C(13)	120.3(5)	C(29)-C(30)-C(25)	120.3(4)

Appendix H: X-ray Structure Analysis of [15]

1. Crystal data and structure refinement

Empirical formula	C5 H8 N2 O1
Formula weight	112.13
Crystal description	colourless regular
Crystal size	0.30 x 0.30 x 0.20 mm
Temperature	150 K
Crystal system	Triclinic
Space group	P -1
Unit cell dimensions	a = 5.7473(11) Å $\alpha = 96.45(3)^\circ$ b = 6.3554(13) Å $\beta = 100.48(3)^\circ$ c = 8.963(2) Å $\gamma = 109.76(3)^\circ$
Reflections for cell refinement	1326
Range in theta	2.353 to 27.458°
Volume, Z	297.57(13) Å ³ , 2
Density (calculated)	1.251 Mg/m ³
Absorption coefficient	0.090 mm ⁻¹
F(000)	120
Diffractometer type	Area
Wavelength	0.71073 Å
Scan type	φ and ω
Theta range for data collection	2.353 to 27.458°
Index ranges	-7 ≤ h ≤ 7, -8 ≤ k ≤ 8, 0 ≤ l ≤ 11
Reflections collected	1934
Independent reflections	1326 [R(merge) = 0.025]
Observed reflections	1157 [I > 2σ(I)]
Absorption correction	Multi-scan (T _{min} = 0.97, T _{max} = 0.98)
Structure solution by	direct and Fourier difference maps
Hydrogen atom location	geometrical
Hydrogen atom treatment	riding model
Refinement method	Full-matrix least-squares on F ²
Weighting scheme	calc
Data / restraints / parameters	1323 / 0 / 73

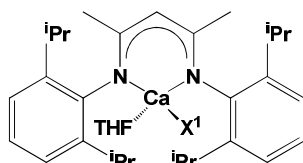
Goodness-of-fit on F	1.0037
Final R indices [all data]	R1 = 0.0557, Rw = 0.1253
Final R indices [$I > 2\sigma(I)$]	R1 = 0.0488, Rw = 0.1201
Final maximum delta/sigma	0.000153
Largest diff. peak and hole	0.30 and -0.30 e.A ⁻³

2. Bond lengths (Å) and angles (°)

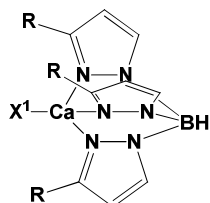
O(1)-C(1)	1.231(2)	C(2)-C(3)	1.478(2)
N(1)-C(1)	1.332(2)	C(2)-C(4)	1.546(2)
N(2)-C(3)	1.145(2)	C(2)-C(5)	1.536(2)
C(1)-C(2)	1.543(2)		
N(1)-C(1)-O(1)	123.12(12)	C(3)-C(2)-C(4)	109.09(11)
N(1)-C(1)-C(2)	118.58(12)	C(1)-C(2)-C(5)	110.56(11)
O(1)-C(1)-C(2)	118.20(12)	C(3)-C(2)-C(5)	108.79(11)
C(1)-C(2)-C(3)	111.17(11)	C(4)-C(2)-C(5)	110.36(11)
C(1)-C(2)-C(4)	106.85(11)	C(2)-C(3)-N(2)	179.09(14)

Appendix I: Summary Sheet of Literature Compounds Included in this Thesis

Chapter One

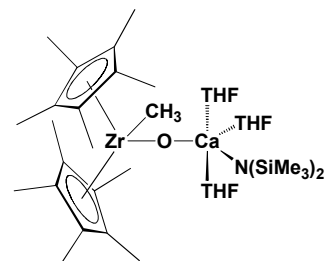


1.1

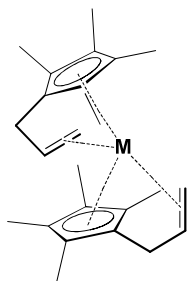


R = *i*Pr, X¹ = N(SiMe₃)₂
 R = *t*Bu, X¹ = N(SiMe₃)₂
 R = *t*Bu, X¹ = O(2,6-*i*PrC₆H₃)

1.2

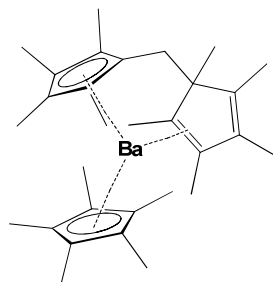


1.3

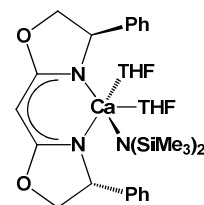


M = Mg, Ca, Sr, Ba

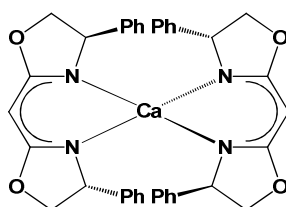
1.4



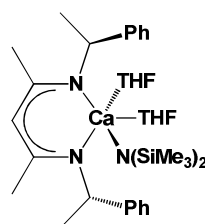
1.5



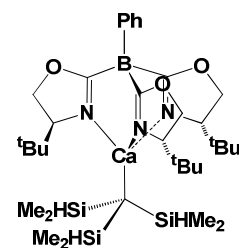
1.6



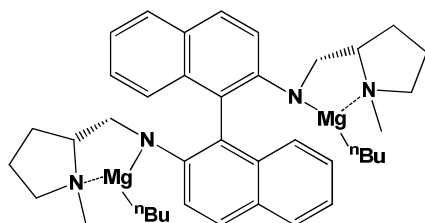
1.7



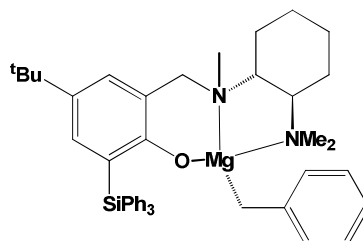
1.8



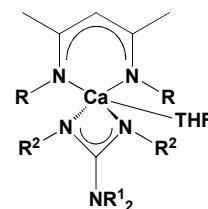
1.9



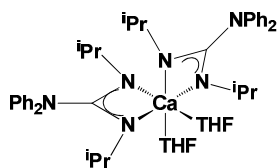
1.10



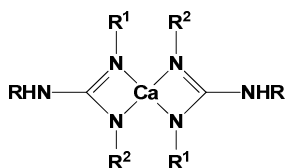
1.11



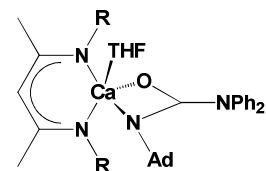
1.12



1.13

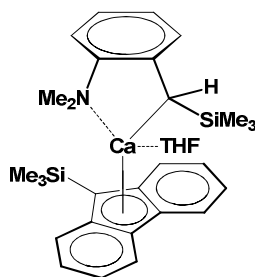


1.14

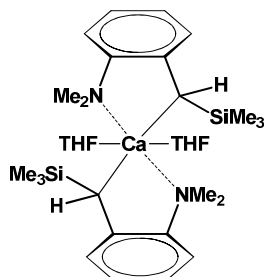


R = 2,6-di-*iso*-propylphenyl
Ad = adamantyl

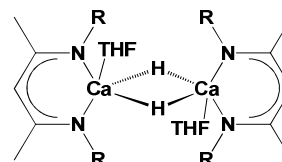
1.15



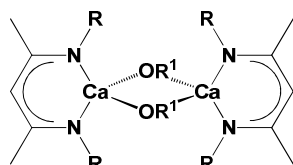
1.16



1.17



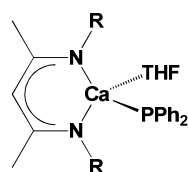
1.18



R = 2,6-di-*iso*-propylphenyl

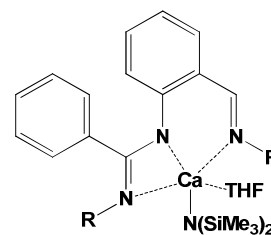
R¹ = CH(Ph)₂, CH(CH₃)(Ph), CH(CH₃)₂,
-(CH₂)₅-, CH(CH₂Ph), adamantyl

1.19



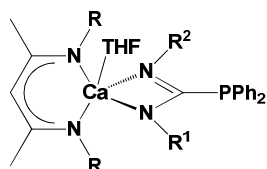
R = 2,6-di-*iso*-propylphenyl

1.20



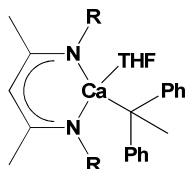
R = 2,6-di-*iso*-propylphenyl

1.21



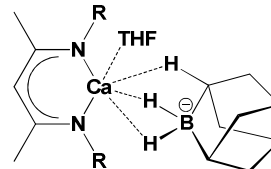
R = 2,6-di-*iso*-propylphenyl

1.22



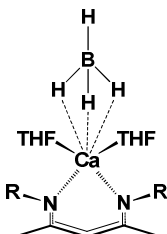
R = 2,6-di-*iso*-propylphenyl

1.23



R = 2,6-di-*iso*-propylphenyl

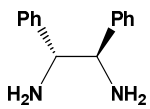
1.24



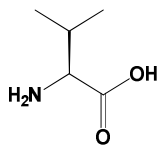
R = 2,6-di-*iso*-propylphenyl

1.25

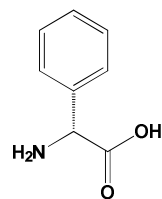
Chapter Two



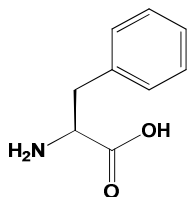
2.1



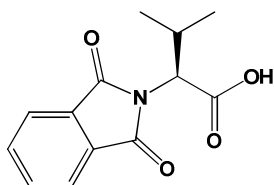
2.2



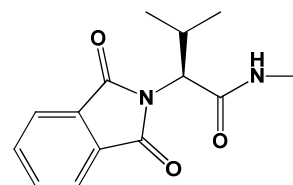
2.3



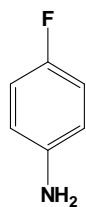
2.4



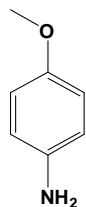
2.5



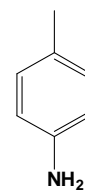
2.6



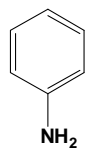
2.7



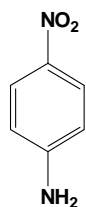
2.8



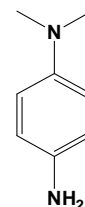
2.9



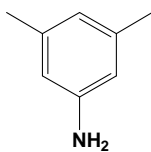
2.10



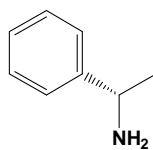
2.11



2.12



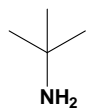
2.13



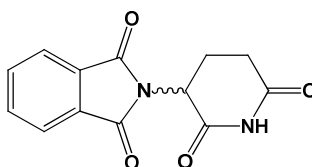
2.14



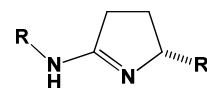
2.15



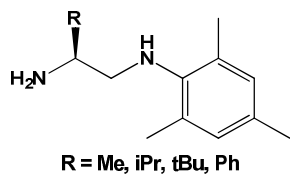
2.16



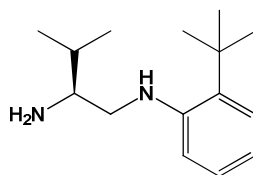
2.17



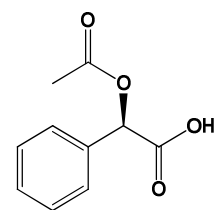
2.18



2.19

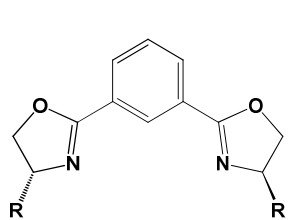


2.20

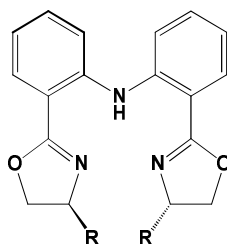


2.21

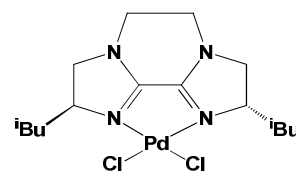
Chapter Four



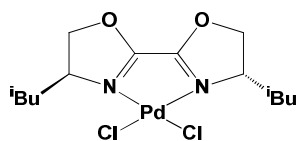
4.1



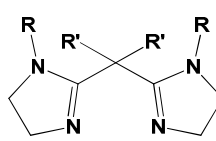
4.2



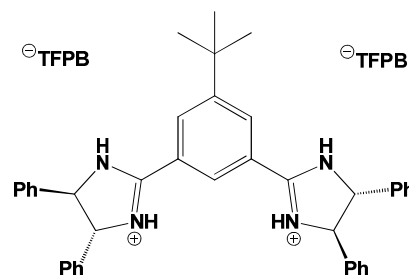
4.3



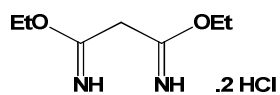
4.4



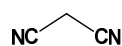
4.5



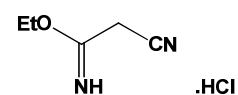
4.6



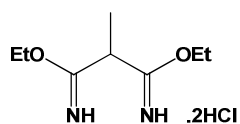
4.7



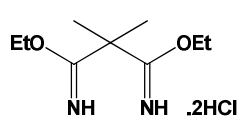
4.8



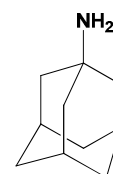
4.9



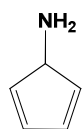
4.10



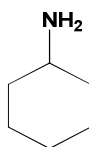
4.11



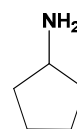
4.12



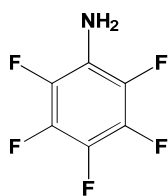
4.13



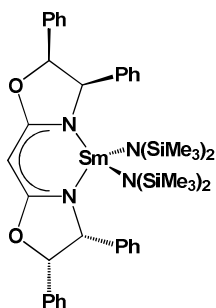
4.14



4.15



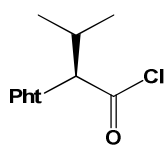
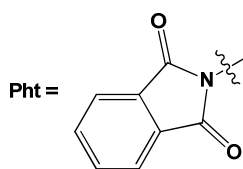
4.16



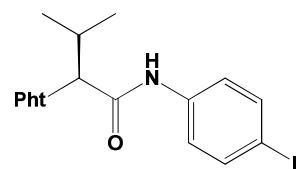
4.17

Appendix J: Summary Sheet of Novel Compounds Presented in this Thesis

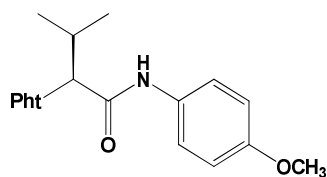
Chapter Two



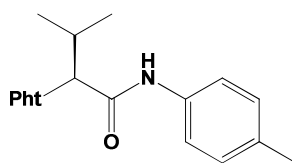
1



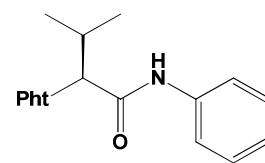
2a



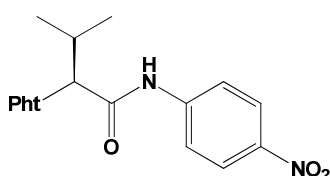
2b



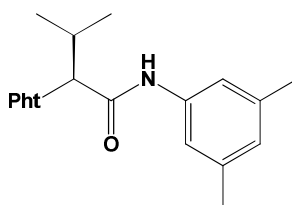
2c



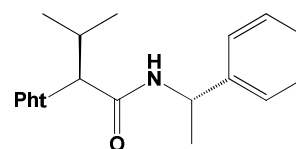
2d



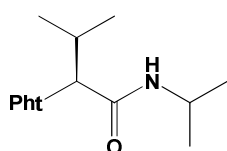
2e



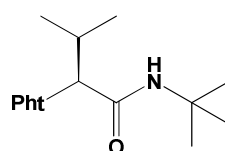
2f



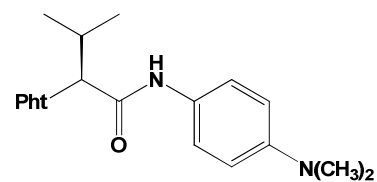
2g



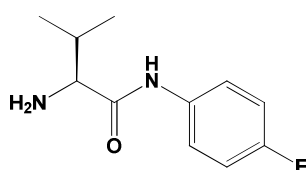
2h



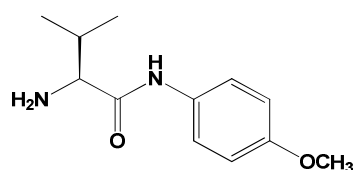
2i



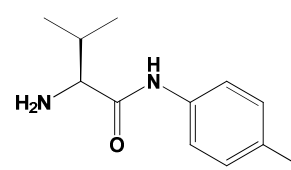
2j



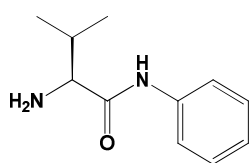
3a



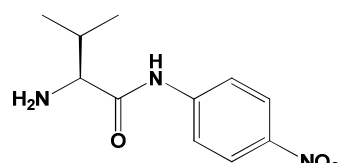
3b



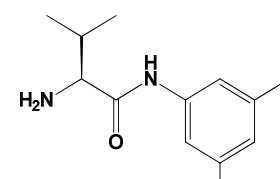
3c



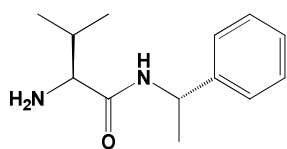
3d



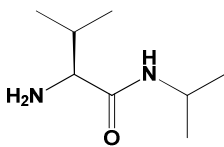
3e



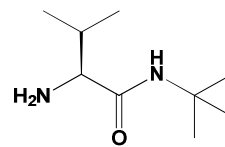
3f



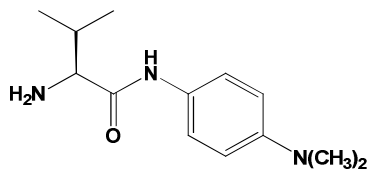
3g



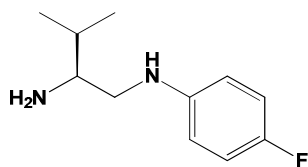
3h



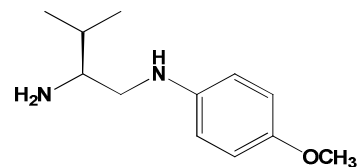
3i



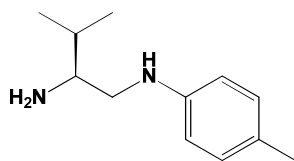
3j



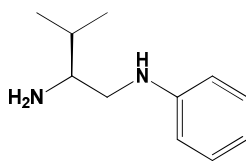
4a



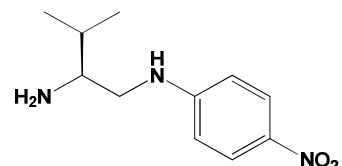
4b



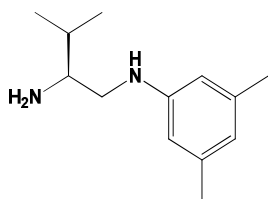
4c



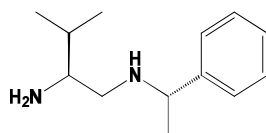
4d



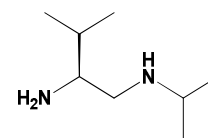
4e



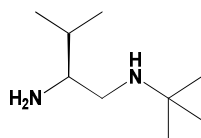
4f



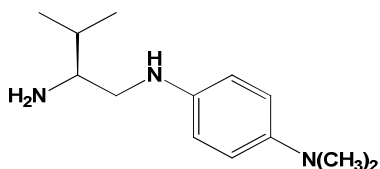
4g



4h



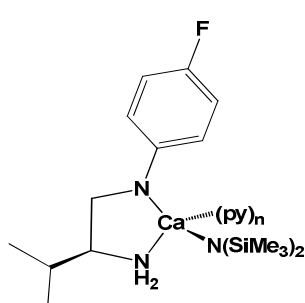
4i



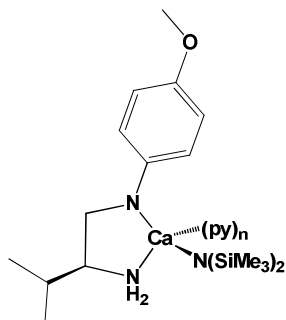
4j

Chapter Three

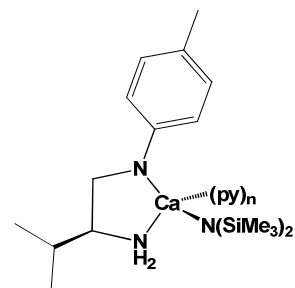
Compounds **5a-f** are the THF analogues $[\text{Ca}(\text{NN}^{\text{R}})\{\text{N}(\text{SiMe}_3)_2\}(\text{THF})_n]$ of **6a-f** $[\text{Ca}(\text{NN}^{\text{R}})\{\text{N}(\text{SiMe}_3)_2\}(\text{py})_n]$



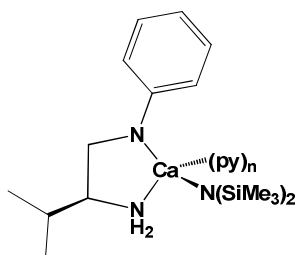
6a



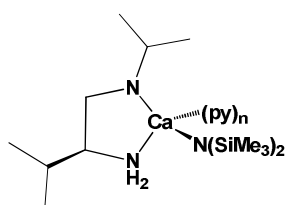
6b



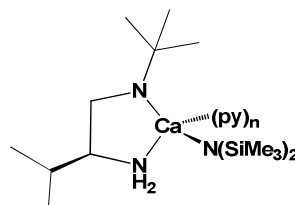
6c



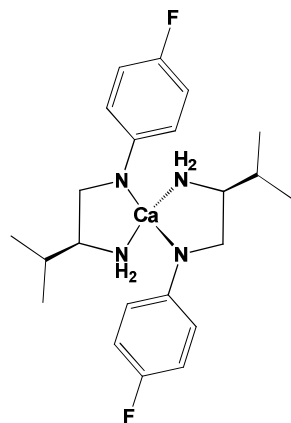
6d



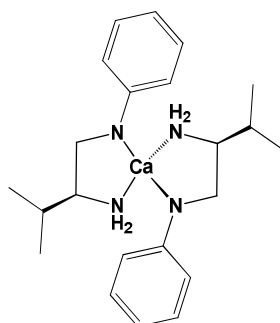
6e



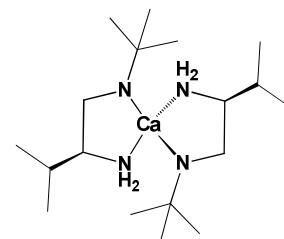
6f



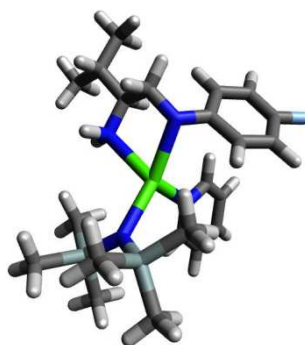
7a



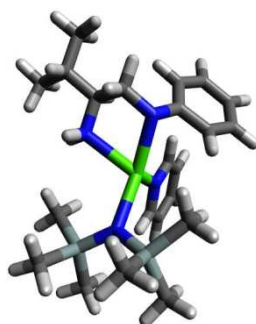
7b



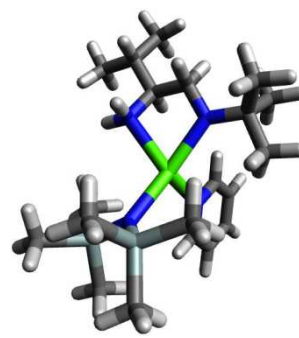
7c



7a_{calc}

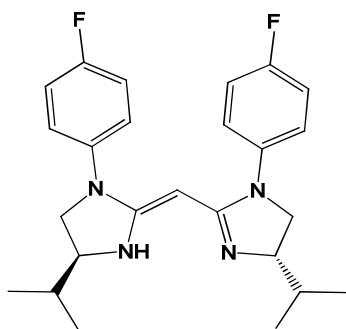


7b_{calc}

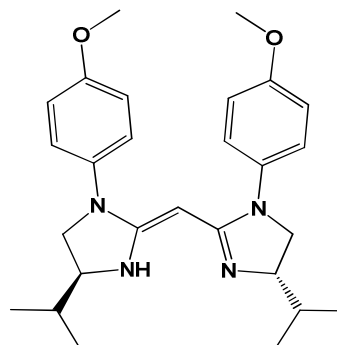


7c_{calc}

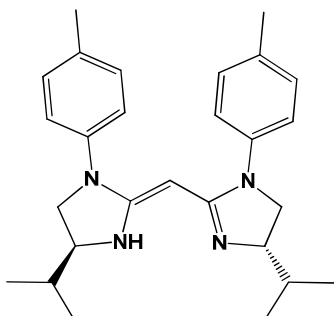
Chapter Four



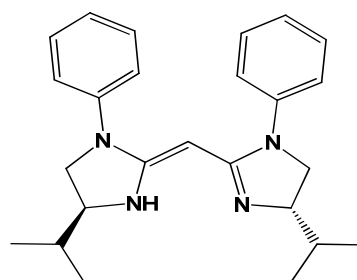
8a



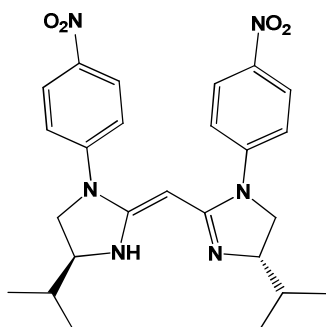
8b



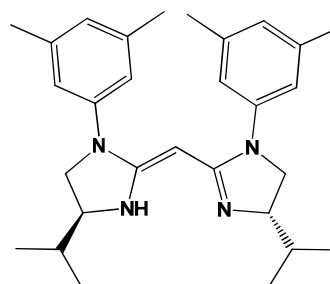
8c



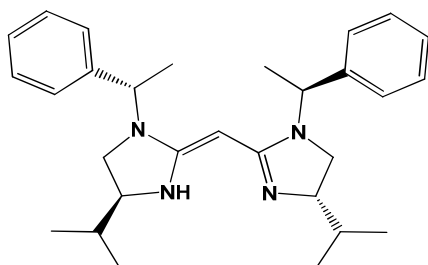
8d



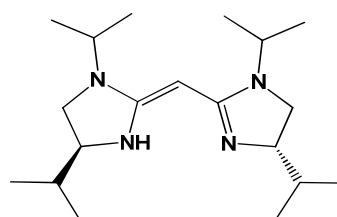
8e



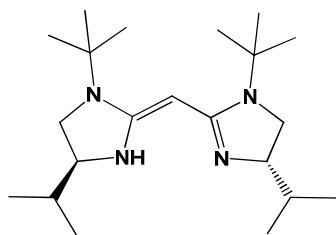
8f



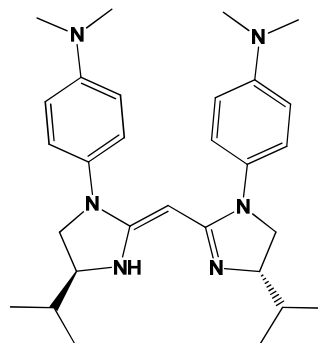
8g



8h

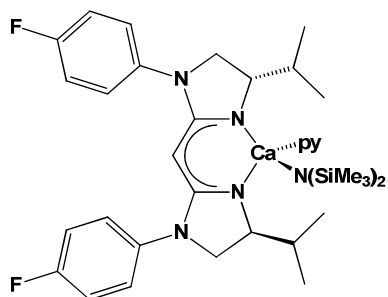


8i

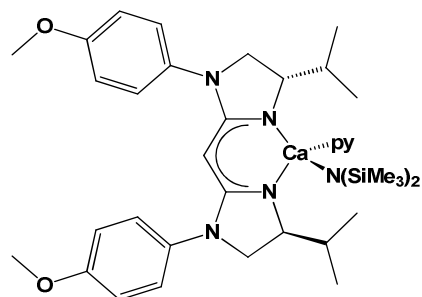


8j

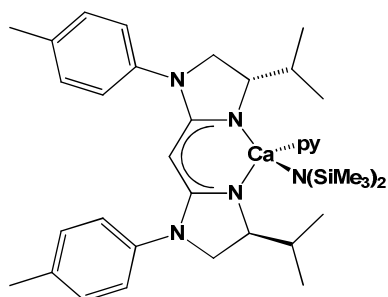
Compounds **9a-j** are the THF analogues $[\text{Ca}(\text{R-BIM})\{\text{N}(\text{Si}(\text{Me}_3)_2)(\text{THF})_n\}]$ of **10a-j** $[\text{Ca}(\text{R-BIM})\{\text{N}(\text{Si}(\text{Me}_3)_2)(\text{py})_n\}]$.



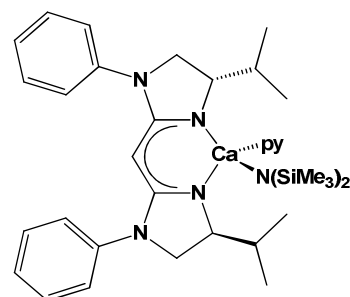
10a



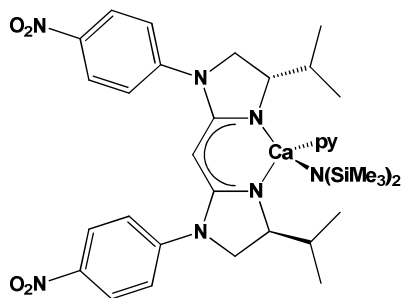
10b



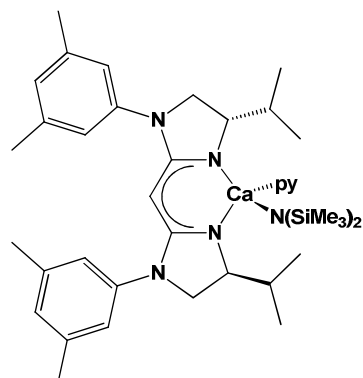
10c



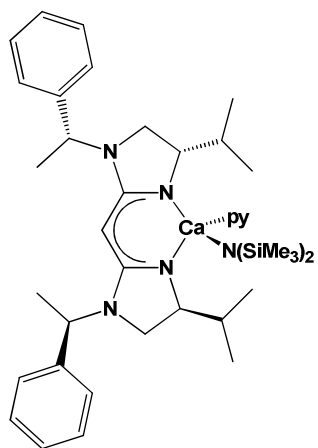
10d



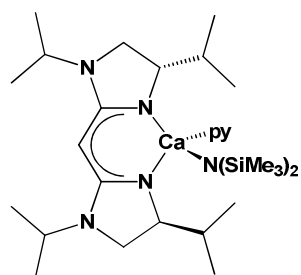
10e



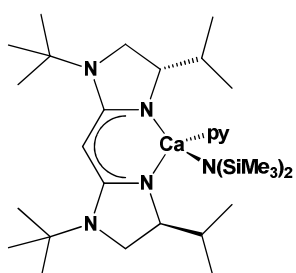
10f



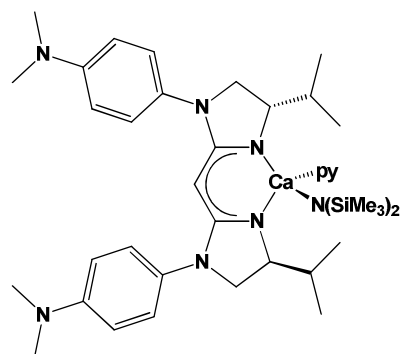
10g



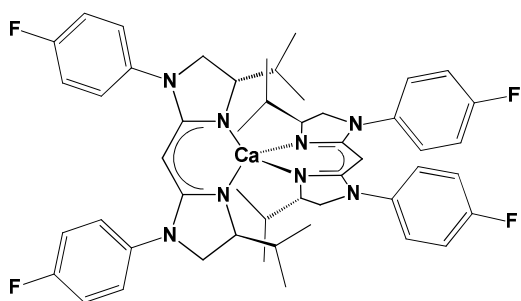
10h



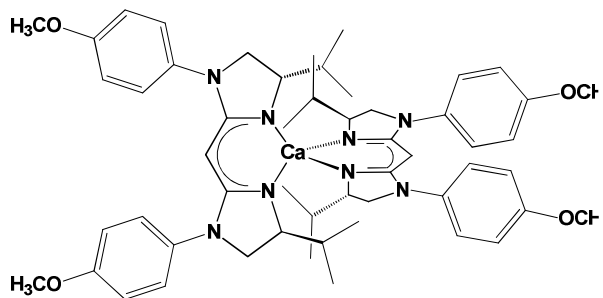
10i



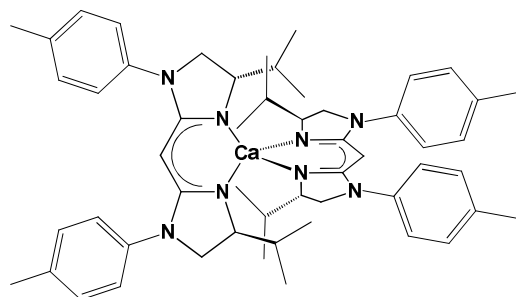
10j



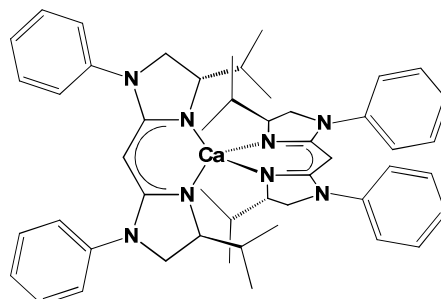
11a



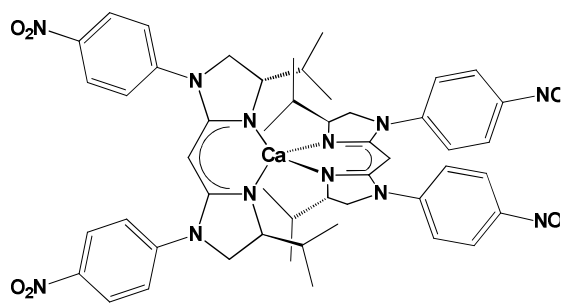
11b



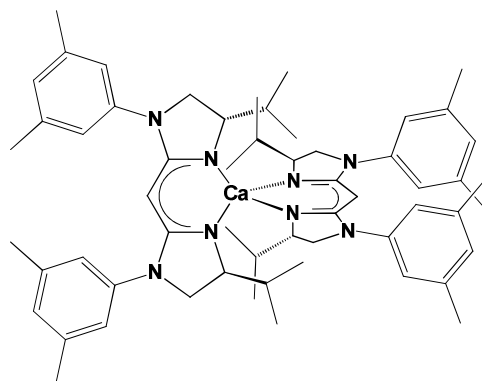
11c



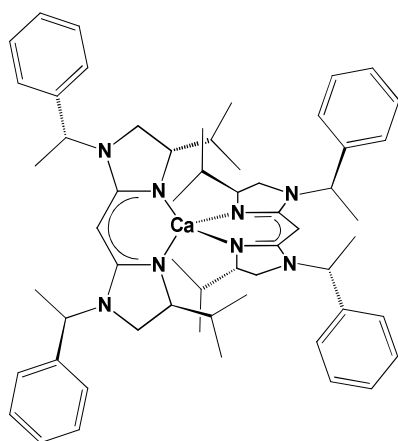
11d



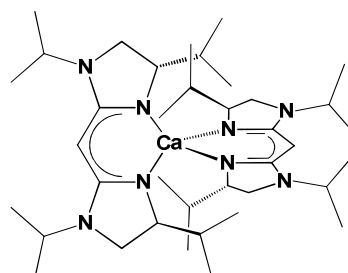
11e



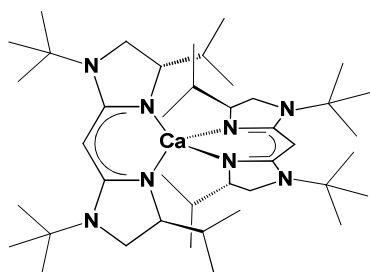
11f



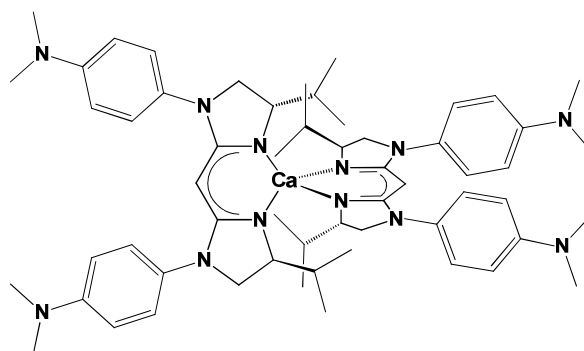
11g



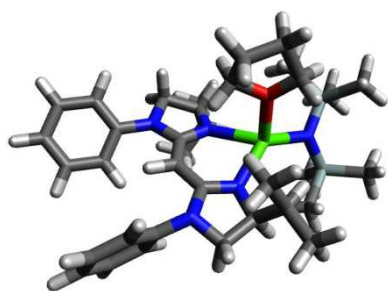
11h



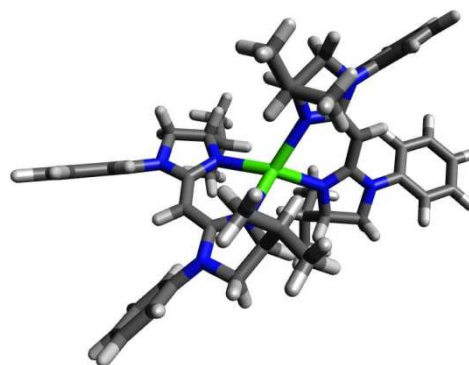
11i



11j

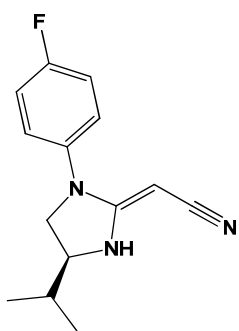


12a

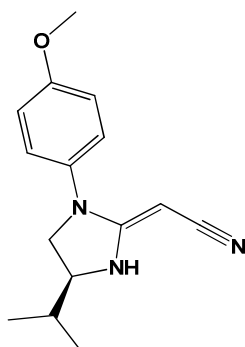


12b

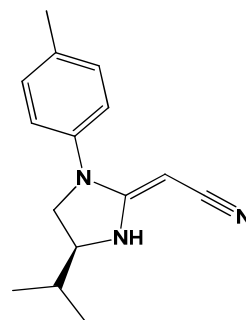
Chapter Five



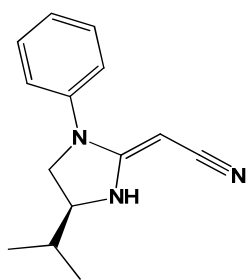
13a



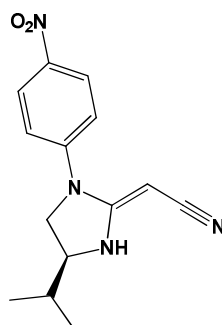
13b



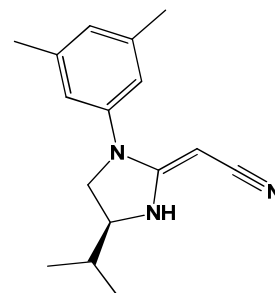
13c



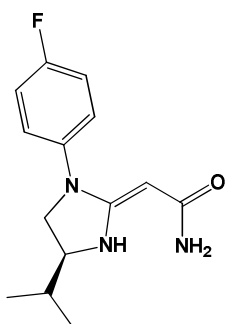
13d



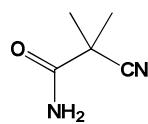
13e



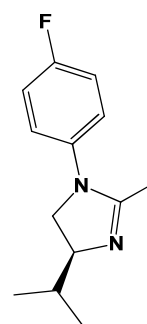
13f



14



15



16

Appendix K: Publications Resulting from This Thesis

- a) J. S. Wixey and B. D. Ward, *Chem. Commun.*, **2011**, 47, 5449.
- b) J. S. Wixey and B. D. Ward, *Dalton Trans.*, **2011**, 40, 7693.

The relevant documents follow overleaf...

Cite this: *Chem. Commun.*, 2011, **47**, 5449–5451

www.rsc.org/chemcomm

COMMUNICATION

Chiral calcium catalysts for asymmetric hydroamination/cyclisation†

James S. Wixey and Benjamin D. Ward*

Received 1st March 2011, Accepted 22nd March 2011

DOI: 10.1039/c1cc11229e

Calcium complexes supported by chiral 1,2-diamines have been shown to be efficient catalysts for the asymmetric hydroamination of amino-olefin substrates; the calcium complexes $[\text{Ca}(\text{NN}^{\text{R}})\{\text{N}(\text{SiMe}_3)_2\}(\text{THF})]$ ($\text{R} = \text{}^t\text{Bu}$, $\text{}^i\text{Pr}$, Ph , $4\text{-C}_6\text{H}_4\text{F}$) give enantioselectivities of up to 26% which marks a significant increase based upon literature precedence. The structure of $[\text{Ca}(\text{NN}^{\text{Ph}})\{\text{N}(\text{SiMe}_3)_2\}(\text{py})]$ has been computed with density functional methods.

Whilst the coordination chemistry of the alkaline earth (AE) metals is well established, the development of well-defined complexes which can be successfully adapted to catalysis has only become apparent in the last few years.¹ The primary reason behind this late development of AE metals in catalysis is their propensity to undergo rapid Schlenk-type ligand redistribution processes,² thus rendering catalytically active species either inactive, or else removing the possibility of regio- or stereoselectivity. As such, the rich chemistry associated with the AE metals has been somewhat neglected outside the context of stoichiometric reagents.

Advances in the last five years have demonstrated that a further understanding of their coordination chemistry is likely to propel the catalytic applications of the AE metals, particularly calcium, into new and exciting directions. In this regard, remarkable advances in the area have been made, particularly with β -diketiminato ligands which have proven remarkably successful in supporting well-defined calcium complexes (Fig. 1a).³ These, and related, AE complexes have been shown to be active in hydroamination,⁴ hydrosilylation,⁵

hydrogenation,⁶ and ring opening polymerisation^{3,7} catalysis. Despite the significant advances in this area, the use of chiral ligands to effect asymmetric catalysis remains much less developed, particularly in complexes in which strongly basic amide- or alkyl co-ligands are present.⁸ Recently Buch and Harder prepared calcium amide complexes supported by the ubiquitous bisoxazoline (BOX) ligands, $[\text{Ca}(\text{BOX})\{\text{N}(\text{SiMe}_3)_2\}(\text{THF})]$ (Fig. 1b).⁹ These complexes were screened in asymmetric hydroamination and hydrosilylation catalysis; despite being able to prepare and structurally characterise these complexes, ligand redistribution proved to be rapid in solution, reforming the achiral homoleptic complex $\text{Ca}\{\text{N}(\text{SiMe}_3)_2\}(\text{THF})_2$ alongside the catalytically inactive $[\text{Ca}(\text{BOX})_2]$, thus rendering the enantioselectivities low (5–10% ee). Such observations have led to the hypothesis that ligand redistribution must be completely suppressed in order to generate acceptable enantioselectivities. Even more recently, Sadow *et al.* have reported somewhat higher enantioselectivities when using trisoxazoline magnesium and calcium complexes,¹⁰ with the highest enantioselectivities being obtained with the magnesium complexes at elevated temperatures. It is in this context that we have sought to prepare simple and readily available chiral ligands that provide greater stereocontrol in hydroamination catalysis with calcium.

A series of chiral ethylene diamine derivatives $\text{H}_2\text{NCH}(\text{}^i\text{Pr})\text{CH}_2\text{NHR}$ (HNN^{R} , $\text{R} = \text{}^t\text{Bu}$ **1a**, $\text{}^i\text{Pr}$ **1b**, Ph **1c** and $4\text{-C}_6\text{H}_4\text{F}$ **1d**) have been prepared from L-valine according to Scheme 1. This route utilises the amidation of an acid chloride with a series of primary amines or anilines. We have found that using thionyl chloride is the most convenient method of converting phthalimide-protected valine into the acid chloride, and does not give rise to epimerisation of the chiral acid; the protected valinoyl chloride can be readily prepared on a 100 g scale and is therefore convenient for the preparation of large quantities of diamines. The acid chloride can be converted into an N-substituted amide by adding a primary amine or aniline in THF. The addition of triethylamine allows this reaction to proceed under ambient conditions, although the yields are often much improved with the addition of catalytic *N,N*-dimethylaminopyridine (DMAP). The reduction of the amides to afford diamines was effected on a small scale with $\text{BH}_3(\text{THF})$ (using commercial 1 M solution). However, on increasing the scale of the reaction, this required the use of excessively large quantities of solvent, causing problems with heat transfer and unnecessary dilution. The reaction was less effective with $\text{BH}_3(\text{SMe}_2)$ (10 M), whilst this enabled the

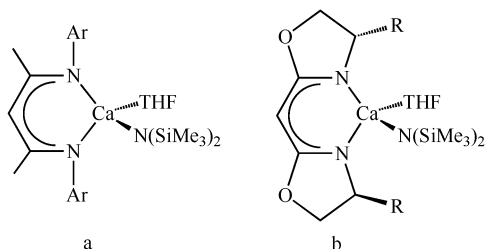
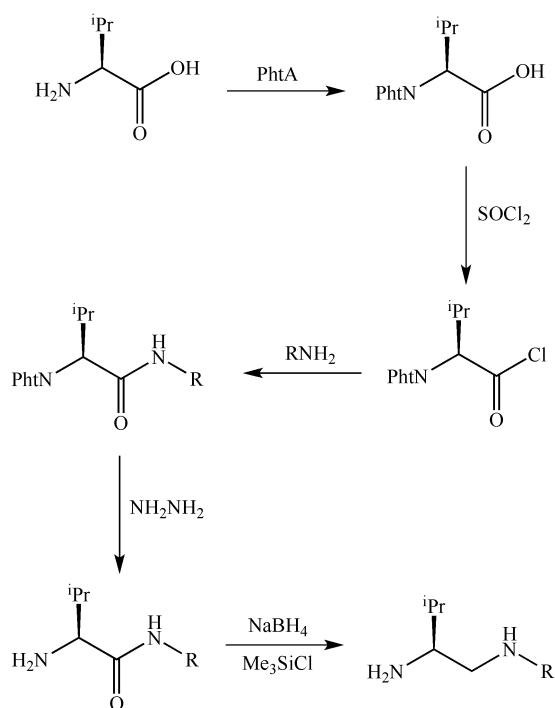


Fig. 1 Calcium complexes used in hydroamination catalysis.

School of Chemistry, Cardiff University, Main Building, Park Place, Cardiff CF10 3AT, UK. E-mail: WardBD@Cardiff.ac.uk; Fax: +44 (0)29 208 74030; Tel: +44 (0)29 208 70302

† Electronic supplementary information (ESI) available: Experimental procedures, characterising data, and computational methods. See DOI: 10.1039/c1cc11229e



Scheme 1 Synthesis of chiral diamines **1a–d**.

reaction to be scaled up safely, these conditions resulted in significantly lower yields, in addition to by-products arising from the degradation of the THF solvent. Conversely, the use of $\text{NaBH}_4/\text{Me}_3\text{SiCl}$ was found to give excellent yields,¹¹ with much more control over the reaction concentration; this procedure has been demonstrated to be successful on a scale of up to 12 g in 250 ml solvent. This simple multistep method allows a series of diamines (HNN^{R}) to be prepared in which the R substituent can be varied in a modular fashion, without introducing additional synthetic complexity.

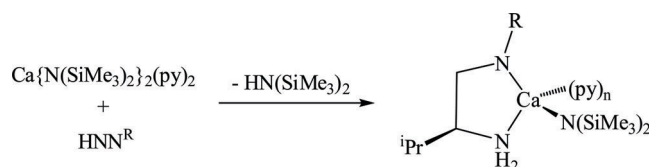
Reaction of the protio-ligands **1a–d** with $\text{Ca}\{\text{N}(\text{SiMe}_3)_2\}_2(\text{THF})_2$ in C_6D_6 afforded pale yellow precipitates, which although are suitable precursors for hydroamination catalysis (*vide infra*), were difficult to unambiguously characterise since they were found to be extremely labile in THF-d_8 , but are insoluble in hydrocarbon solvents and $\text{C}_6\text{D}_5\text{Cl}$, and unstable in CDCl_3 and CD_2Cl_2 . In order to determine the extent of base coordination, the complexes were prepared using the pyridine analogue $\text{Ca}\{\text{N}(\text{SiMe}_3)_2\}_2(\text{py})_2$ in the presence of an excess of pyridine.¹² These complexes are formulated as $[\text{Ca}(\text{NN}^{\text{R}})\{\text{N}(\text{SiMe}_3)_2\}(\text{py})_n]$ (**2a–d**) (Scheme 2).

As with the THF complexes, the pyridine adducts were found to be only sparingly soluble in benzene and toluene, and decomposed in chloroform and dichloromethane. The NMR spectra in THF-d_8 were broad at ambient temperature, but nevertheless showed three clear signals (albeit without fine

structure) for the diamine backbone protons. The presence of a single bis(trimethylsilyl)amide moiety was also evident from the relative integration of the signal at *ca.* 0 ppm. The fluxional process, presumably arising from the lability of the NN^{R} ligands, could not be completely “frozen out” using low temperature NMR analyses, within our instrumental capability (500 MHz, -90°C), however NMR tube scale reactions carried out *in situ* demonstrated the elimination of one molar equivalent of $\text{HN}(\text{SiMe}_3)_2$, thus supporting the formation of a heteroleptic complex containing one deprotonated diamine moiety and one remaining bis(trimethylsilyl)amide ligand. Most noteworthy was the relative intensity of the pyridine, coordinated to the calcium centre. In each case, the complexes were dried *in vacuo* to 4×10^{-2} mbar, in order to ensure a consistent level of base coordination. Remarkably, when the alkyl-substituted diamines were employed (**2a** and **2b**), the number of pyridine ligands was less reproducible, ranging from 0.3–0.6. This suggests that the pyridine is only weakly bound to the calcium, and so we attempted to prepare the base-free complex $[\text{Ca}(\text{NN}^{\text{R}})\{\text{N}(\text{SiMe}_3)_2\}]$ by subjecting the complex to vacuum overnight, but in all cases we were unable to completely remove the pyridine. In contrast, approximately one molar equivalent of coordinated pyridine was observed in complexes **2c** and **2d**, which decrease less after extended periods *in vacuo*. It is unclear as to the observed differences in pyridine coordination between alkyl and aryl systems, although we tentatively suggest that the difference may lie in the difference in steric constraints imposed by the different N-substituents. Given the different degrees to which pyridine coordinates to the calcium and the extremity of the NN^{R} lability, we cannot categorically rule out the possibility that complexes **2a–2d**, existing as dimers/oligomers; we suggest that the actual structure could be a complex mixture of monomeric and oligomeric species. Such a phenomenon is not unexpected, given the propensity of Grignard reagents to undergo such redistribution processes.² Attempts to crystallographically characterise complexes **2a–2d** were unsuccessful, yielding only redistributed calcium species without the NN^{R} ligand.

When $\text{Ca}\{\text{N}(\text{SiMe}_3)_2\}_2(\text{py})_2$ was reacted with *two* equivalents of HNN^{R} , two equivalents of $\text{HN}(\text{SiMe}_3)_2$ were eliminated, forming the homoleptic complex $[\text{Ca}(\text{NN}^{\text{R}})_2]$ (R = ^tBu **3a** or 4- $\text{C}_6\text{H}_4\text{F}$ **3b**). Again, the NMR spectra were broad at both ambient and low temperatures. Although we cannot completely rule out the possibility that the homoleptic complexes $[\text{Ca}(\text{NN}^{\text{R}})_2]$ form in solution from the redistribution of ligands in **2**, it is unlikely that this represents a major component since complexes **2** were found to be catalytically active in the hydroamination/cyclisation of amino-olefins, whereas **3a** and **3b** were found to be completely inactive.

In order to gain insight into the structure of the proposed mononuclear species, and especially to determine which of the



Scheme 2 Preparation of $[\text{Ca}(\text{NN}^{\text{R}})\{\text{N}(\text{SiMe}_3)_2\}(\text{Py})_n]$ **2a–d**.

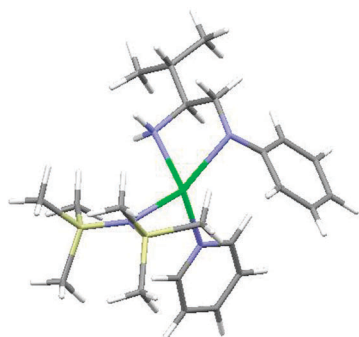
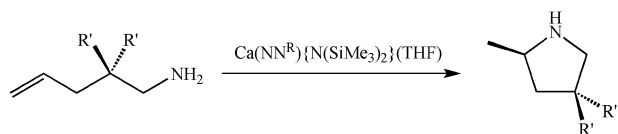


Fig. 2 Calculated structure of $[\text{Ca}(\text{NN}^{\text{Ph}})\{\text{N}(\text{SiMe}_3)_2\}(\text{py})]$ **2c_{calc}**.

amine moieties is likely to be preferentially deprotonated in the NN^{R} ligands, the structure of the $[\text{Ca}(\text{NN}^{\text{Ph}})\{\text{N}(\text{SiMe}_3)_2\}(\text{py})]$ **2c_{calc}** was calculated using density functional methods.[†] The computed structure is displayed in Fig. 2. The two possible structures, with the primary and secondary amines deprotonated, were calculated, however the structure with the secondary amine deprotonated, as shown in Fig. 2, was found to be significantly more stable, by *ca.* 13 kcal. In addition, the structure indicates a significant deviation of the amido nitrogen from the expected trigonal planar geometry; the consequence is that the phenyl ring is orientated so as to provide a chiral environment at the calcium centre, which may well explain the effective stereocontrol in hydroamination catalysis.

Complexes **2a–2d** were tested as precatalysts for the enantioselective hydroamination of the amino-olefin substrates **A** and **B** (Scheme 3). The activities and enantioselectivities of these catalytic reactions[‡] are summarised in Table 1. For each of the ligands **2a–2c** the reaction proceeded significantly slower than with the homoleptic bis amide complex $\text{Ca}\{\text{N}(\text{SiMe}_3)_2\}(\text{THF})_2$ (23 h for **A** and 20 min for **B** at ambient temperature), as is expected when adding a sterically demanding spectator ligand. Interestingly, when the *para*-fluorophenyl ligand **2d** was employed, no activity was observed at all over a two week period (entries 7 and 8). The same was true of ligand **2c**, although only with the dimethyl-substrate **A** (entry 5). Most noteworthy is catalyst **2c** (phenyl *N*-substituent) with substrate **B** (entry 6), in



Scheme 3 Hydroamination catalysis ($\text{R}' = \text{Me}$ **A** or Ph **B**).

Table 1 Catalytic hydroamination of amino-olefins using $[\text{Ca}(\text{N}_2\text{N}^{\text{R}})\{\text{N}(\text{SiMe}_3)_2\}(\text{THF})]^\ddagger$

Entry	Ligand	Substrate	Time ^a	Conv. ^a %	ee ^b %
1	1a	A	7 d	90	0
2	1a	B	24 h	>99	6
3	1b	A	5 d	>99	12
4	1b	B	1 h	>99	5
5	1c	A	21 d	0	—
6	1c	B	3 d	80	26
7	1d	A	14 d	0	—
8	1d	B	14 d	0	—

^a Determined from ^1H NMR spectra when no further conversion observed. ^b Determined by ^1H NMR using *R*-(*-*)-*O*-acetylmandelic acid.¹³

which the chiral pyrrolidine is formed in 26% ee. This level of enantioselectivity represents a remarkable increase from the 5–10% obtained with calcium BOX complexes⁸ and is also higher than the calcium complexes reported by Sadow *et al.*¹⁰ It is thus far unclear as to why the enantioselectivity in this case far exceeds the other diamine–substrate combinations tested, however the phenyl-substituted diamine/phenyl-substituted substrate combination suggests that π – π stacking may be an important feature in one of the intermediate steps of the catalytic cycle. Such interactions may well explain the lack of selectivity in the entries 2 and 4; as well as the lack of selectivity in any entry involving the methyl-substituted substrate **A**. It is clear however that further investigations into the detailed mechanism are warranted, for such studies will undoubtedly facilitate further developments in stereoselective catalysis with calcium complexes.

Chiral 1,2-diamines have been shown to be efficient stereo-directing ligands in the calcium-catalysed intramolecular hydroamination of amino-olefins. Whilst there is clearly room for improvement, the enantioselectivities described herein represent a significant advance in calcium-mediated stereoselective catalysis. Further work in this area, particularly to probe the structure of these complexes, is currently underway.

We thank the EPSRC (EP/H012109) and the Royal Society for financial support. Assistance by Dr R. L. Jenkins with NMR spectroscopic measurements is gratefully acknowledged.

Notes and references

[†] 70 μmol $[\text{Ca}(\text{NN}^{\text{R}})\{\text{N}(\text{SiMe}_3)_2\}(\text{THF})]$, 0.7 mmol substrate, 0.5 ml C_6D_6 , rt. Reaction progress monitored by ^1H NMR spectroscopy. Enantiomeric excesses determined by ^1H NMR spectroscopy after the addition of *R*-(*-*)-*O*-acetylmandelic acid. See ref. 13.

- Recent reviews: (a) M. Westerhausen, *Z. Anorg. Allg. Chem.*, 2009, **635**, 13; (b) S. Harder, *Chem. Rev.*, 2010, **110**, 3852; (c) M. Westerhausen, *Coord. Chem. Rev.*, 2008, **252**, 1516; (d) J. D. Smith, *Angew. Chem., Int. Ed.*, 2009, **48**, 6597.
- D. Seyferth, *Organometallics*, 2009, **28**, 1598.
- M. H. Chisholm, J. Gallucci and K. Phomphrai, *Inorg. Chem.*, 2004, **43**, 6717.
- (a) M. R. Crimmin, I. J. Casely and M. S. Hill, *J. Am. Chem. Soc.*, 2005, **127**, 2042; (b) S. Datta, H. W. Roesky and S. Blechert, *Organometallics*, 2007, **26**, 4392; (c) A. G. M. Barrett, M. R. Crimmin, M. S. Hill, P. B. Hitchcock, G. Kociok-Köhn and P. A. Procopiou, *Inorg. Chem.*, 2008, **47**, 7366; (d) J. R. Lachs, A. G. M. Barrett, M. R. Crimmin, G. Kociok-Köhn, M. S. Hill, M. F. Mahon and P. A. Procopiou, *Eur. J. Inorg. Chem.*, 2008, 4173; (e) A. G. M. Barrett, C. Brinkmann, M. R. Crimmin, M. S. Hill, P. A. Hunt and P. A. Procopiou, *J. Am. Chem. Soc.*, 2009, **131**, 12906; (f) M. Arrowsmith, M. S. Hill and G. Kociok-Köhn, *Organometallics*, 2009, **28**, 1730; (g) P. Horrillo-Martinez and K. C. Hultsch, *Tetrahedron Lett.*, 2009, **50**, 2054.
- J. Spielmann and S. Harder, *Eur. J. Inorg. Chem.*, 2008, 1480.
- J. Spielmann, F. Buch and S. Harder, *Angew. Chem., Int. Ed.*, 2008, **47**, 9434.
- M. G. Cushion and P. Mountford, *Chem. Commun.*, 2011, **47**, 2276.
- Group 2 metals have been used in asymmetric Lewis acid catalysis: S. Kobayashi and Y. Yamashita, *Acc. Chem. Res.*, 2011, **44**, 58.
- F. Buch and S. Harder, *Z. Naturforsch., B*, 2008, **63**, 169.
- S. R. Neal, A. Ellern and A. D. Sadow, *J. Organomet. Chem.*, 2011, **696**, 228.
- S. W. Coghlan, R. L. Giles, J. A. K. Howard, L. G. F. Patrick, M. R. Probert, G. E. Smith and A. Whiting, *J. Organomet. Chem.*, 2005, **690**, 4784.
- D. C. Bradley, M. B. Hursthouse, A. A. Ibrahim, K. M. A. Malik, M. Motevalli, R. Mösel, H. Powell, J. D. Runnacles and A. C. Sullivan, *Polyhedron*, 1990, **9**, 2959.
- G. Zi, F. Zhang, L. Xiang, Y. Chen, W. Fang and H. Song, *Dalton Trans.*, 2010, **39**, 4048.

This article is published as part of the *Dalton Transactions* themed issue entitled:

d^0 organometallics in catalysis

Guest Editors John Arnold (UC Berkeley) and Peter Scott (University of Warwick)

Published in [issue 30, 2011](#) of *Dalton Transactions*



Image reproduced with permission of Guo-Xin Jin

Articles in the issue include:

PERSPECTIVES:

[Half-titanocenes for precise olefin polymerisation: effects of ligand substituents and some mechanistic aspects](#)

Kotohiro Nomura and Jingyu Liu

Dalton Trans., 2011, DOI: 10.1039/C1DT10086F

ARTICLES:

[Stoichiometric reactivity of dialkylamine boranes with alkaline earth silylamides](#)

Michael S. Hill, Marina Hodgson, David J. Liptrot and Mary F. Mahon

Dalton Trans., 2011, DOI: 10.1039/C1DT10171D

[Synthesis and reactivity of cationic niobium and tantalum methyl complexes supported by imido and \$\beta\$ -diketiminato ligands](#)

Neil C. Tomson, John Arnold and Robert G. Bergman

Dalton Trans., 2011, DOI: 10.1039/C1DT10202H

Visit the *Dalton Transactions* website for more cutting-edge inorganic and organometallic research

www.rsc.org/dalton

Cite this: *Dalton Trans.*, 2011, **40**, 7693

www.rsc.org/dalton

Modular ligand variation in calcium bisimidazoline complexes: effects on ligand redistribution and hydroamination catalysis†

James S. Wixey and Benjamin D. Ward*

Received 21st April 2011, Accepted 16th May 2011

DOI: 10.1039/c1dt10732a

A series of calcium complexes supported by chiral bisimidazoline ligands have been studied in the catalytic intramolecular hydroamination/cyclisation of amino-olefins. The complexes $[\text{Ca}(\text{R-BIM})\{\text{N}(\text{SiMe}_3)_2\}(\text{THF})]$ ($\text{R} = 4\text{-C}_6\text{H}_4\text{Me}$, **5a**, $4\text{-C}_6\text{H}_4\text{F}$, **5b** and ^tBu , **5c**) have given competitive enantioselectivities (up to 12%) when compared to current literature studies involving calcium. Bisimidazolines offer a significant advance over similar bisoxazoline ligands, by allowing a greater structural variance through a modular synthetic pathway.

The implementation of alkaline earth (AE) metals in asymmetric hydroamination catalysis has received increasing interest over the past few years, particularly with calcium.^{1,2} Whilst most studies have involved the β -diketiminato complex (**I**, Fig. 1),³ the development of chiral derivatives is very much in its infancy. Few examples of chiral calcium complexes have emerged (**II–IV**),^{4–6} and with enantioselectivities below 30%, this is indicative of the challenging nature of calcium in asymmetric catalysis. Whilst significant developments have been made within the area, developments are often hindered by the lability of AE complexes, exemplified by the eponymous Grignard reagents.^{2a,2c,7,8} Their susceptibility to undergo rapid Schlenk-type ligand redistribution understandably renders complexes catalytically inactive or greatly inhibits regio- or stereoselectivity, ultimately leading to poor enantioselectivities. A detailed understanding of how to suppress/control such redistribution processes is crucial in order to facilitate the further development of asymmetric catalysis with the AE metals; we herein report further insight into the redistribution processes with calcium bisimidazoline complexes, and the corresponding impact on catalytic performance.

The first example of calcium employed in asymmetric hydroamination catalysis was contributed by Buch and Harder employing the bisoxazoline containing complex **II**,⁴ giving 4–6% ee. The low enantioselectivities were attributed to the rapid redistribution of the ligand in solution giving the unreactive homoleptic complex $[\text{Ca}(\text{BOX})_2]$ and the non-selective calcium amide complex, $\text{Ca}\{\text{N}(\text{SiMe}_3)_2\}_2(\text{THF})_2$. Work by Sadow *et al.*⁵

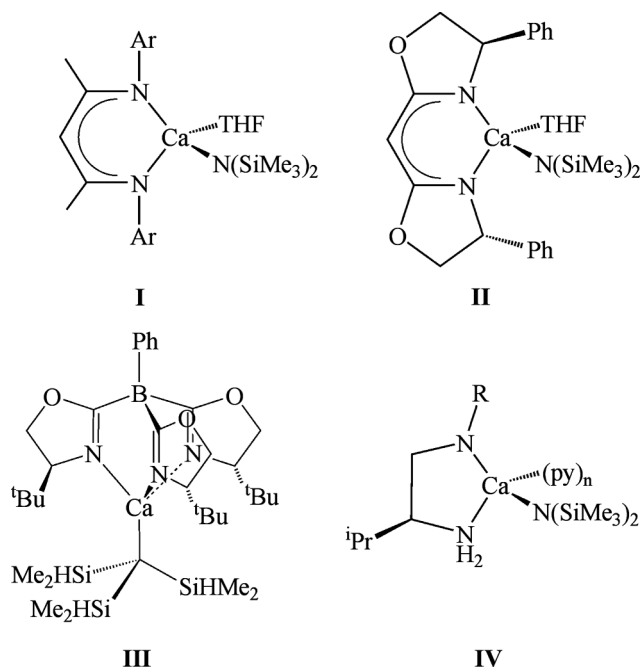
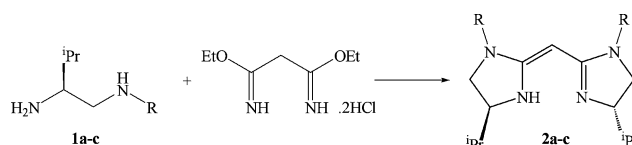


Fig. 1 Calcium complexes employed in hydroamination catalysis.

using **III** improved the selectivity to 18% ee; we recently reported selectivities of up to 26% ee using **IV**.⁶ It is apparent from this trend, that progress towards greater enantioselectivities is highly dependent on a judicious choice of supporting ligand, but may not necessarily depend on completely suppressing the ligand redistribution processes, since **IV** was highly labile in solution.

Chiral bisimidazolines (Scheme 1) offer an advantage over the aforementioned bisoxazolines as a ligand platform for the AE metals. The incorporation of an additional N–R moiety allows for alteration of electronic, in addition to the steric, properties of the ligand;^{9–11} we have therefore systematically varied the N–R



Scheme 1 Preparation of bisimidazoline ligands ($\text{R} = 4\text{-C}_6\text{H}_4\text{Me}$ **2a**, $4\text{-C}_6\text{H}_4\text{F}$ **2b**, ^tBu **2c**).

School of Chemistry, Cardiff University, Main Building, Park Place, Cardiff, UK, CF10 3AT. E-mail: WardBD@Cardiff.ac.uk; Fax: +44 (0)29 208 74030; Tel: +44 (0)29 208 70302

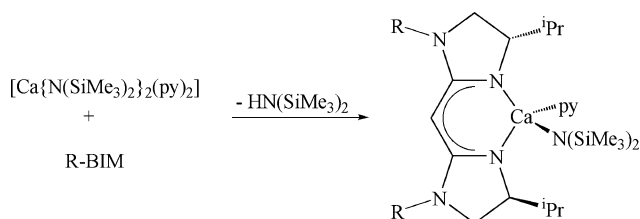
† Electronic supplementary information (ESI) available: Experimental procedures, characterising data, conversion curves, and kinetics methodology. See DOI: 10.1039/c1dt10732a

substituent in order to determine the effect on the coordination chemistry and catalytic ability of the complexes.

A series of chiral bisimidazoline derivatives (R-BIM, R = 4-C₆H₄Me, **2a**, 4-C₆H₄F, **2b** and ^tBu, **2c**) have been prepared from the condensation of the corresponding diamine (**1a–c**)⁶ and Pinner salt¹² in refluxing CH₂Cl₂ for 48 h, as reported by Pflatz *et al.*¹³ We have found this method convenient for preparing the corresponding bisimidazoline in up to 40% yield, based on starting diamine. Though typically moderate yields were obtained, higher yields were not realised by extending reaction times or conducting the reaction in higher boiling point solvents, for example chloroform or chlorobenzene. This simple method allows a series of bisimidazolines (R-BIM) to be prepared in which, in principle, the stereodirecting and R substituents can be independently varied in a modular fashion *via* the choice of amino acid and primary amine in the diamine synthesis, without introducing additional synthetic complexity. In this report we have concentrated on the isopropyl derivatives starting from L-valine.

Reaction of the protio-ligands **2a–c** with Ca{N(SiMe₃)₂}(THF)₂ in C₆D₆ afforded orange precipitates, which were found to be soluble only in THF-d₈, insoluble in hydrocarbon solvents, and unstable in chlorinated solvents. The low solubility of calcium-based complexes is well documented and therefore unsurprising.^{1b,6,14} No evidence of ether-cleavage was observed in THF, even though this has been previously reported in calcium complexes under similar conditions.¹⁴

Although the THF adducts [Ca(R-BIM){N(SiMe₃)₂}(THF)] **5a–c** were employed in hydroamination catalysis (*vide infra*), for analysis of the complexes, and in order to determine the extent of base coordination in THF-d₈, the complexes were prepared using the pyridine analogue Ca{N(SiMe₃)₂}(py)₂ in the presence of an excess of pyridine (Scheme 2).¹⁵ These complexes are formulated as [Ca(R-BIM){N(SiMe₃)₂}(py)] (**3a–c**). As with the THF complexes, the pyridine adducts were found to be only sparingly soluble in benzene and toluene, and decomposed in chloroform and dichloromethane.



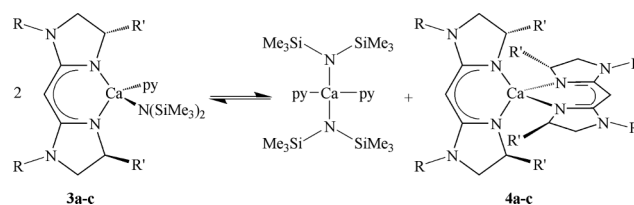
Scheme 2 Preparation of [Ca(R-BIM){N(SiMe₃)₂}(py)] (R = 4-C₆H₄Me, **3a**, 4-C₆H₄F, **3b** and ^tBu, **3c**).

The NMR spectra of **3a–c** in THF-d₈ were well-defined at ambient temperature, but nevertheless showed a mixture of the heteroleptic species **3** and homoleptic species **4** (Scheme 3). Buch and Harder report a redistribution ratio of 80:20 heteroleptic to homoleptic respectively in the related bisoxazoline complex [Ca(BOX){N(SiMe₃)₂}(THF)₂];⁴ however upon varying the N-R substituent of the bisimidazolines a strong variation in equilibrium position was observed (Table 1). ¹H NMR studies established that all complexes had reached their irrespective equilibrium positions within 10 min. Further monitoring over several hours indicated that no further deviation of the equilibrium position

Table 1 Redistribution of [Ca(R-BIM){N(SiMe₃)₂}(py)] **3** to [Ca(BIM^R)₂] **4** and Ca{N(SiMe₃)₂}(py)₂ at 293 K

Entry	Complex	3:4 ^a	K ^b	ΔG ₂₉₃ (kJ mol ⁻¹)
1	3a	64 : 36	0.31	2.8
2	3b	48 : 52	1.17	-0.4
3	3c	80 : 20	0.06	6.8

^a Determined by integration of ¹H NMR spectra. ^b Equilibrium coefficient determined at 293 K.



Scheme 3 Ligand redistribution of [Ca(R-BIM){N(SiMe₃)₂}(py)] (R' = ⁱPr, R = 4-C₆H₄Me, **3a** 4-C₆H₄F, **3b** and ^tBu, **3c**).

occurred. The values of ΔG₂₉₃ were calculated from the equilibrium coefficients, which were found to be small and almost negligible.

The presence of three bis(trimethylsilyl)amide moieties was evident from the relative integration of the resonances, at *ca.* 0 ppm. These can be attributed to the coordinated bis(trimethylsilyl)amide on the heteroleptic complex **3**, the corresponding Ca{N(SiMe₃)₂}(py)₂ redistribution product, and the liberated amine HN(SiMe₃)₂.

Although the HN(SiMe₃)₂ is expected to be a highly soluble, volatile by-product, even after repeated recrystallisation and extensive drying *in vacuo* we were unable to fully remove the residue. This could potentially be attributed to the partial reinsertion of the HN(SiMe₃)₂ into the complex when in solution, which has been previously observed by Ruhlandt-Senge *et al.*¹⁶ In each case, the complexes were dried *in vacuo* to 4 × 10⁻² mbar, in order to ensure a consistent level of base coordination, since it is known that extended exposure to vacuum can remove coordinated pyridine.⁶ There was consistently only one pyridine ligand bound to the calcium in the heteroleptic complex **3**, which contrasts the BOX complex **II** (Fig. 1), in which there were two THF ligands.⁴

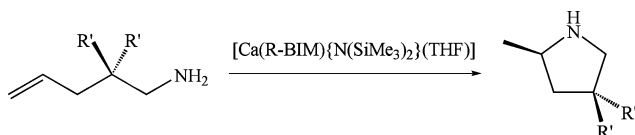
In order to clarify the identity of the homoleptic complexes **4** in the mixture obtained by the redistribution of **3**, Ca{N(SiMe₃)₂}(py)₂ was reacted with *two* equivalents of R-BIM, whereupon two equivalents of HN(SiMe₃)₂ were eliminated, forming the homoleptic complex [Ca(R-BIM)₂] (R = 4-C₆H₄Me, **4a**, 4-C₆H₄F, **4b** and ^tBu, **4c**). In each case, the complexes were again dried *in vacuo* to 4 × 10⁻² mbar, which was sufficient to remove all pyridine traces.

In order to determine the effect of the nitrogen substituent, and consequently the equilibrium position, on their catalytic performance, the THF derivatives, **5a–c** were employed in the hydroamination/cyclisation of the amino-olefins **A** and **B** (Scheme 4); the conversions, initial rates and enantioselectivities, are listed in Table 2.† Consistent with our previous observations,⁶ catalytic hydroamination of the diphenyl substrate **B** was found to be much faster than with the dimethyl substrate **A**, which mirrors the observations with Ca{N(SiMe₃)₂}(THF)₂ (23 h for **A** and

Table 2 Asymmetric hydroamination of amino-olefins using 10 mol% [Ca(R-BIM){N(SiMe₃)₂}(THF)]

Entry	Complex	Substrate	Initial Rate/mol dm ⁻³ s ⁻¹	Conv.% ^a	ee% ^b
1	5a	A	5.1(5) × 10 ⁻⁷	8	5
2	5a	B	1.0(1) × 10 ⁻⁴	95	0
3	5b	A	6.8(3) × 10 ⁻⁸	3	9
4	5b	B	1.8(1) × 10 ⁻⁵	>99	9
5	5c	A	7.3(4) × 10 ⁻⁷	18	12
6	5c	B	6.4(3) × 10 ⁻⁵	>99	12

^a Determined from ¹H NMR spectra. ^b Determined by ¹H NMR spectroscopy using (R)-(-)-*O*-acetylmandelic acid.¹⁸

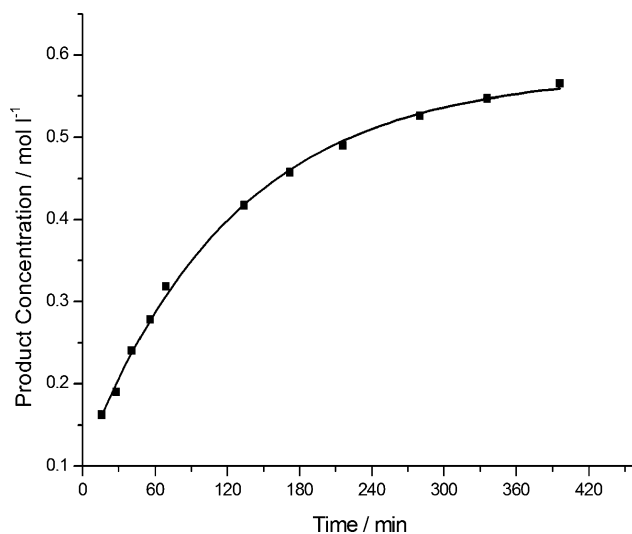
**Scheme 4** Asymmetric hydroamination catalysis (R' = Me **A**, Ph **B**).

20 min for **B** at ambient temperature with 10 mol% catalyst), although all reactions employing complexes **5a–c** were significantly slower than this, as is expected when using a sterically demanding spectator ligand. Reactions employing **B** went to completion, whereas the analogous reactions with **A** did not, reaching only <20% conversion within several days. Despite this however, the enantioselectivities with a particular catalyst complex were consistent within error, regardless of the substrate. This is in stark contrast to the bis-⁴ and trisoxazoline,⁵ and diamine⁶ complexes which are much more substrate-specific. The 4-C₆H₄Me complex **5a** gave the fastest conversion but little stereoselectivity (entries 1 and 2), whereas the 4-C₆H₄F and ^tBu complexes **5b** and **5c** gave moderate selectivities, comparable to those obtained with the trisoxazoline complex **III**, and higher than with the structurally related bisoxazoline complex **II** (entries 3–6). Based upon the measurements in Table 1, **5b** is expected to give the highest amount of Ca{N(SiMe₃)₂}(THF)₂, and yet the rate of reaction is significantly slower than those of **5a** and **5c**. This is most likely due to the nature of the equilibrium, which will be different under catalytic conditions where the liberated HN(SiMe₃)₂, catalysis substrate and pyrrolidine product can take part in the redistribution processes. **5b** still invokes a comparable stereocontrol compared to **5c**, suggesting that the equilibrium position has little effect on the stereoselectivity; this may suggest that the redistribution process may be more complex than described by Scheme 3.

The catalytic reactions using 10 and 20 mol% **5a–c** were monitored, and the initial rates are consistent with a first order reaction with respect to catalyst, in agreement with Marks *et al.*¹⁷ However, with 5 mol% catalyst loading the reactions showed little to no activity. A representative conversion curve is provided in Fig. 2.

Conclusions

Ligand redistribution is a prominent feature of calcium complexes. The bisimidazoline complexes described herein are no exception, but in contrast to the analogous bisoxazoline complexes allow a greater degree of ligand variation through the presence of

**Fig. 2** Conversion for the catalytic hydroamination of substrate **B** using [Ca(^tBu-BIM){N(SiMe₃)₂}(THF)] **5c** in C₆D₆ at 293 K.

the additional nitrogen substituent and their modular synthesis; variation in the N–R substituent occasions a shift of the equilibrium position, and has a concomitant impact on the catalytic performance, although not on the stereocontrol offered by the ligand. We are undertaking further studies in this regard to ensure that redistribution processes are more fully understood, in order that a rational design of calcium complexes for catalytic applications may be achieved.

We thank the EPSRC (EP/H012109), the Royal Society, and the Leverhulme Trust (F/00 407/BL) for financial support.

Notes and references

‡ 42 μmol [Ca(R-BIM){N(SiMe₃)₂}(THF)] **5**, 0.42 mmol substrate, C₆D₆, rt. Reaction progress monitored by ¹H NMR spectroscopy. Enantiomeric excesses determined by ¹H NMR spectroscopy after the addition of R(-)-*O*-acetylmandelic acid.¹⁸

- Recent reviews: (a) M. Westerhausen, *Z. Anorg. Allg. Chem.*, 2009, **635**, 13; (b) S. Harder, *Chem. Rev.*, 2010, **110**, 3852; (c) M. Westerhausen, *Coord. Chem. Rev.*, 2008, **252**, 1516; (d) J. D. Smith, *Angew. Chem., Int. Ed.*, 2009, **48**, 6597.
- (a) M. R. Crimmin, I. J. Casely and M. S. Hill, *J. Am. Chem. Soc.*, 2005, **127**, 2042; (b) S. Datta, H. W. Roesky and S. Blechert, *Organometallics*, 2007, **26**, 4392; (c) A. G. M. Barrett, M. R. Crimmin, M. S. Hill, P. B. Hitchcock, G. Kociok-Köhn and P. A. Procopiu, *Inorg. Chem.*, 2008, **47**, 7366; (d) J. R. Lachs, A. G. M. Barrett, M. R. Crimmin, G. Kociok-Köhn, M. S. Hill, M. F. Mahon and P. A. Procopiu, *Eur. J. Inorg. Chem.*, 2008, 4173; (e) A. G. M. Barrett, C. Brinkmann, M. R. Crimmin, M. S. Hill, P. A. Hunt and P. A. Procopiu, *J. Am. Chem. Soc.*, 2009, **131**, 12906; (f) M. Arrowsmith, M. S. Hill and G. Kociok-Köhn, *Organometallics*, 2009, **28**, 1730; (g) P. Horriillo-Martinez and K. C. Hultzs, *Tetrahedron Lett.*, 2009, **50**, 2054.
- M. H. Chisholm, J. Gallucci and K. Phomphrai, *Inorg. Chem.*, 2004, **43**, 6717.
- F. Buch and S. Harder, *Z. Naturforsch. B*, 2008, **63**, 169.
- S. R. Neal, A. Ellern and A. D. Sadow, *J. Organomet. Chem.*, 2011, **696**, 228.
- J. S. Wixey and B. D. Ward, *Chem. Commun.*, 2011, **47**, 5449.
- D. Seyferth, *Organometallics*, 2009, **28**, 1598.
- M. Crimmin, M. Arrowsmith, A. G. M. Barrett, I. J. Casely, M. S. Hill and P. A. Procopiu, *J. Am. Chem. Soc.*, 2009, **131**, 9670.
- S. Bhor, G. Anilkumar, M. K. Tse, M. Klawonn, C. Döbler, B. Bitterlich, A. Grotevandt and M. Beller, *Org. Lett.*, 2005, **7**, 3393.

-
- 10 H. Liu and D. Du, *Adv. Synth. Catal.*, 2009, **351**, 489.
- 11 T. Arai, N. Yokoyama and A. Yanagisawa, *Chem.–Eur. J.*, 2008, **14**, 2052.
- 12 D. Akalay, G. Dürner, J. W. Bats, M. Bolte and M. W. Göbel, *J. Org. Chem.*, 2007, **72**, 5618.
- 13 B. Ramalingam, M. Neuburger and A. Pfaltz, *Synthesis*, 2007, **4**, 572.
- 14 J. S. Alexander and K. Ruhlandt-Senge, *Eur. J. Inorg. Chem.*, 2002, 2761.
- 15 D. C. Bradley, M. B. Hursthouse, A. A. Ibrahim, K. M. A. Malik, M. Motevalli, R. Mösele, H. Powell, J. D. Runnacles and A. C. Sullivan, *Polyhedron*, **9**, 2959.
- 16 S. Chadwick, U. Englich and K. Ruhlandt-Senge, *Angew. Chem. Int. Ed.*, 1998, **37**, 3007.
- 17 S. Hong, S. Tian, M. V. Metz and T. J. Marks, *J. Am. Chem. Soc.*, 2003, **125**, 14783.
- 18 G. Zi, F. Zhang, L. Xiang, Y. Chen, W. Fang and H. Song, *Dalton Trans.*, 2010, **39**, 4048.